Treatment-induced sculpting of melanoma phenotype and immunogenicity – Impact on resistance to CD8 T cells

Cumulative Dissertation
for
the doctoral degree of

Dr. rer. nat.

from the Faculty of Biology
University of Duisburg-Essen
Germany

Submitted by

Beatrice Thier

Born in Dorsten, Germany

May 2022

The experiments underlying the present work were conducted in the Group of Molecular Tumor Immunology at the Department of Dermatology at the University Hospital Essen, Germany.

DOI: 10.17185/duepublico/77123
URN: urn:nbn:de:hbz:465-20221125-104851-5

1. Examiner: Prof. Dr. rer. nat. Annette Paschen

2. Examiner: Prof. Dr. rer. nat. Wiebke Hansen

3. Examiner: Prof. Dr. rer. nat. Stefan Eichmüller

Chair of the Board of Examiners: Prof. Dr. rer. nat. Stefanie Flohé

Date of the oral examination: October 24th, 2022

Acknowledgments

I would like to thank a lot of people without whom this work would not have been possible: First and foremost, I would like to express my special thanks of gratitude to Prof. Dr. rer. nat. Annette Paschen. I am grateful to have carried out my PhD studies under your supervision and mentorship. I enjoyed being part of various projects and having the opportunity to participate in scientific conferences. During our lively and fruitful discussions, you have always set the right impulses that let me think further and broader throughout the projects. Thank you for supporting me during this special time and giving me your trust.

I would like to thank the Group of Molecular Tumor Immunology. It is my pleasure to work in such a supportive and warm-hearted environment. I appreciate our coffee and lunch breaks, as well as the fun times together. Special thanks go to Fang Zhao. You inspired me with your passion for science and forwarded your expertise. Furthermore, I thank Sonia Leonardelli and Natalia Pieper. You lay the foundation of important lab skills and emphasized to me, when to be hypercritically and when small issues are no problem. Simone Stupia and Alicia Brüggemann, thank you for our fun times, discussions, supportive environment, and (wo)manpower!

Special thanks go to Vicky Peller and Nadine Stadtler. I am grateful for having you in my life as some of my closest friends. I know I can always count on you in any situation that life throws at me. Thank you, girls, for your motivation, your shoulder to lay on, laughs, and wine nights! Additionally, I would like to thank Fabienne Maaßen and Maike Giesing. You both accompanied me during our whole incredible journey starting in Bonn with our Bachelor studies and continuing in Essen until now. I appreciate the strong friendship and the mutual support over the past (almost) 10 years! I am looking forward to sharing more special moments with you. I want to thank Luiza Martins Nascentes Melo. Thank you for your helpful advice and honesty. I appreciate our close friendship that made our journey together special. Further, I would like to thank Renata Varaljai for her honest assessment and helpful input. A big thank you goes to you.

Mein größter Dank gilt den wichtigsten Menschen in meinem Leben, meiner Familie. Ihr seid das Fundament, auf das ich immer bauen kann. Euer Glaube an mich gibt mir unentwegt neue Kraft. Danke, dass ihr immer für mich da seid und mich in jeder Lebenslage unterstützt. Ich bin sehr stolz und dankbar, eine so wunderbare Familie zu haben. Mein tiefster Dank gilt dabei insbesondere meinem Freund Martin für seine liebevolle Unterstützung. Danke für deine starke Schulter, die Geborgenheit und dein Vertrauen, das du mir schenkst.

Für meine Oma Lucie

Table of Contents

1 Preface

I present a cumulative thesis consisting of two published and one accepted for publication peer-reviewed original articles.

The work presented in this thesis was carried out between November 2017 and May 2022 under the supervision of Prof. Dr. rer. nat. Annette Paschen, principal investigator of the Group Molecular Tumor Immunology at the Department of Dermatology, University Hospital Essen, Germany.

I hereby declare that this thesis submitted for the consideration of Dr. rer. nat. award has been composed by me.

2 Summary

The landscape of melanoma treatment has tremendously changed over the last two decades with the implementation of immune checkpoint blockade (ICB). However, long-term beneficial effects are still limited to a minority of patients due to primary or acquired resistance. Tumor-cell intrinsic therapy resistance can be established by genetic alterations or non-genetic phenotypic adaptation. The latter can be associated with a switch from a differentiated towards a dedifferentiated cell state. Genetic, as well as non-genetic mechanisms, frequently establish resistance of melanoma cells to cytotoxic CD8 T cells. Those lymphocytes become activated upon recognition of tumor antigens presented on cognate HLA class I (HLA-I) molecules. The clinical efficacy of ICB is critically dependent on the anti-tumor activity of CD8 T cells. Thus, it is of importance to understand the diverse tumor-cell intrinsic resistance mechanisms to overcome those barriers and improve patient outcomes. Using different melanoma patient models consisting of tumor tissue, corresponding cell lines, and autologous cytotoxic CD8 T cells from tumor tissue or peripheral blood, we demonstrate (i) therapeutic targeting of the cytosolic innate immune receptor RIG-I in melanoma cells could be a strategy to overcome specific resistance to CD8 T cells and (ii) that phenotypic alterations induced by RIG-I signaling in melanoma cells do not protect from CD8 T-cell recognition.

In longitudinal tumor samples from patient-derived metastases, we detected an evolutionary pattern of resistance to cytotoxic CD8 T cells. Melanoma cells from late metastases evaded the anti-tumor activity of T cell-derived interferon-gamma (IFN-γ) by acquiring genetic defects in JAK1, a kinase of the IFN signaling pathway. In addition, some JAK1-mutant melanoma cells silenced the expression of HLA-I genes resulting in loss of immunogenicity and total evasion from CD8 T-cell surveillance. Interestingly, targeting of the innate immune receptor RIG-I restored HLA-I antigen presentation in those JAK1-mutant cells in an IFN-independent manner and resensitized the melanoma cells to cytotoxic CD8 T cells. Importantly, combinations of RIG-I agonists with immune checkpoint inhibitors showed synergistic effects on anti-tumor CD8 T-cell responses (article Such et al., JCI, 2020, in this thesis).

Besides enhancing antigen presentation, RIG-I activation in melanoma cells induced the switching from a differentiated towards a non-proliferative dedifferentiated cell state lacking expression of melanoma differentiation markers. The observed RIG-I-induced dedifferentiation was JAK-dependent and reversible as receptor signaling declined (article Thier et al., JITC, 2022, in this thesis). Importantly, transition into more dedifferentiated cell states has repeatedly

been associated with resistance to targeted therapy. In fact, our own studies on MAPK inhibitors (MAPKi) demonstrated that prolonged MAPKi treatment dynamically changes the melanoma cell phenotype (article Harbers et al., JID, 2021, in this thesis). In the course of this, distinct tumor cell states were found to be tightly linked to CD8 T-cell activity, as recognition of dedifferentiated melanoma cells by CD8 T cells was impaired. In contrast, upon RIG-I stimulation we found dedifferentiated melanoma cells to be still efficiently recognized by CD8 T cells as enhanced melanoma immunogenicity was preserved in those dedifferentiated cells. Hence, a dedifferentiated cell state does not necessarily imply resistance to CD8 T cells.

Overall, our findings suggest that the therapeutic context and the concomitant changes in the immunogenicity are decisive for the T-cell stimulatory capacity of melanoma cells. Moreover, targeting RIG-I strongly enhances melanoma immunogenicity and is a promising approach to overcome T-cell resistance in melanoma. The discoveries of this thesis provide rationals for future treatment options and may help to improve treatment protocols and thus melanoma patient outcomes.

3 Zusammenfassung

Die Landschaft der Melanom-Behandlung hat sich in den letzten zwei Jahrzehnten mit der Einführung der Immun-Checkpoint-Blockade (ICB) stark verändert. Aufgrund von primärer oder erworbener Resistenz bleiben jedoch langfristige positive Wirkungen nach wie vor auf eine Minderheit von Patienten beschränkt. Die intrinsische Therapieresistenz von Tumorzellen kann durch genetische Veränderungen oder nicht-genetische phänotypische Anpassung entstehen. Letztere kann mit einem Übergang von einem differenzierten zu einem dedifferenzierten Zellzustand verbunden sein. Sowohl genetische als auch nicht-genetische Mechanismen führen häufig zu einer Resistenz der Melanom-Zellen gegenüber zytotoxischen CD8-T-Zellen. Diese Lymphozyten werden durch die Erkennung von Tumorantigenen aktiviert, die auf kognitiven HLA-Klasse-I-Molekülen (HLA-I) präsentiert werden. Die klinische Wirksamkeit von ICB hängt entscheidend von der Anti-Tumor-Aktivität der CD8-T-Zellen ab. Daher ist es wichtig, die verschiedenen intrinsischen Resistenzmechanismen der Tumorzellen zu verstehen, um diese Barriere zu überwinden und die Behandlungsergebnisse der Patienten zu verbessern. Wir zeigen anhand verschiedener Melanom-Patientenmodellen, die aus Tumorgewebe, entsprechenden Zelllinien und autologen zytotoxischen CD8-T-Zellen aus Tumorgewebe oder peripherem Blut bestehen, dass (i) die therapeutische zielgerichtete Aktivierung des zytosolischen angeborenen Immunrezeptors RIG-I in Melanom-Zellen eine Strategie zur Überwindung der spezifischen Resistenz gegenüber CD8-T-Zellen sein könnte und (ii) dass phänotypische Veränderungen, die durch die RIG-I-Signalgebung in Melanom-Zellen ausgelöst werden, nicht vor der Erkennung durch CD8-T-Zellen schützen.

In longitudinalen Tumorproben von Patienten-Metastasen haben wir ein evolutionäres Muster einer Resistenzausbildung gegenüber zytotoxischen CD8-T-Zellen festgestellt. Melanom-Zellen aus späten Metastasen entzogen sich der Anti-Tumor-Aktivität von durch T-Zellen-freigesetztem Interferon-gamma (IFN-γ), indem sie genetische Defekte in JAK1, einer Kinase des IFN-Signalweges, erwarben. Darüber hinaus haben einige JAK1-mutierte Melanom-Zellen die Expression von HLA-I-Genen herabreguliert, was zu dem Verlust der Immunogenität und zur völligen Umgehung der CD8-T-Zellüberwachung führt. Interessanterweise wurde durch die gezielte Aktivierung des angeborenen Immunrezeptors RIG-I die HLA-I-Antigenpräsentation in diesen JAK1-Mutanten auf IFN-unabhängige Weise wiederhergestellt und eine Resensibilisierung der Melanom-Zellen für zytotoxische CD8-T-Zellen erreicht. Von Bedeutung ist, dass Kombinationen von RIG-I-Agonisten und Immun-

Checkpoint-Inhibitoren synergistische Effekte auf die anti-tumorale CD8-T-Zellantworten zeigten (Artikel Such et al., JCI, 2020, in dieser Arbeit).

Neben der Verstärkung der Antigenpräsentation führte die RIG-I-Aktivierung in Melanom-Zellen zu einem Wechsel von einem differenzierten zu einem nicht-proliferativen dedifferenzierten Zellzustand, in welchem die Expression von Melanom-Differenzierungsmarkern fehlt. Die beobachtete RIG-I-induzierte Dedifferenzierung war JAK-abhängig und reversibel, wenn die Rezeptor-Signalgebung nachließ (Artikel Thier et al., JITC, 2022). Hervorzuheben ist, dass der Übergang in einen stärker dedifferenzierten Zellzustand wiederholt mit einer Resistenz gegenüber einer zielgerichteten Therapie in Verbindung gebracht wurde. Unsere eigenen Studien zu MAPK-Inhibitoren (MAPKi) ergaben, dass sich der Phänotyp von Melanom-Zellen bei längerer MAPKi-Behandlung dynamisch verändert. Dabei zeigte sich, dass unterschiedliche Tumorzellzustände eng mit der CD8-T-Zellaktivität verknüpft sind und die Erkennung von dedifferenzierten Melanom-Zellen durch CD8-T-Zellen beeinträchtigt war (Harbers et al., JID, 2021). Im Gegensatz dazu konnten wir feststellen, dass dedifferenzierte Melanom-Zellen nach einer RIG-I-Stimulation immer noch effizient von CD8-T-Zellen erkannt werden, da die erhöhte Melanom-Immunogenität in diesen dedifferenzierten Zellen erhalten blieb. Diese Beobachtungen legen nahe, dass ein dedifferenzierter Zellzustand nicht zwingend mit einer Resistenz gegenüber CD8-T-Zellen einhergeht.

Insgesamt deuten unsere Ergebnisse darauf hin, dass der therapeutische Kontext und die damit verbundene Veränderung der Immunogenität entscheidend für die T-Zell-stimulierende Kapazität von Melanom-Zellen sind. Darüber hinaus steigert die zielgerichtete Aktivierung von RIG-I die Immunogenität des Melanoms und ist ein vielversprechender Ansatz zur Überwindung einer T-Zell-Resistenz. Die Entdeckungen dieser Arbeit liefern Anhaltspunkte für künftige Behandlungsmöglichkeiten und könnten dazu beitragen, die Behandlungsprotokolle und damit die Erfolge für Melanom-Patienten zu verbessern.

4 Introduction

4.1 Cancer immunosurveillance and immunoediting

The field of cancer immunology and immunotherapy evolved around the concept of "cancer immunosurveillance", which envisaged the immune system's capability to identify and eliminate malignant cells specifically.[1,2] Different pre-clinical and clinical observations supported the idea of immunosurveillance in cancer control. Experiments in mice lacking immune effector cells demonstrated the linkage between immune deficiency and tumor development.[3] In line with this, immunocompromised patients, for instance, after organ transplantation or with acquired immune deficiency syndrome (AIDS), have an increased cancer risk over the general population.[4–6] Inversely, spontaneous regression of tumors from immunocompetent patients is considered as an immune-related event that occurs in the absence of any therapeutic intervention. This phenomenon was observed in various cancer entities, such as melanoma, renal cell carcinoma, and neuroblastoma.[7] Furthermore, the presence and density of tumor-infiltrating lymphocytes (TILs) within the tumor lesion serve as prognostic values for good clinical outcomes of patients with melanoma, head and neck, breast, bladder, lung, and colorectal cancer.[8–10]

The indispensability of lymphocytes and the pro-inflammatory cytokine interferon-gamma (IFN-γ) is well established in protecting against tumor development. However, anti-tumor immune responses can lead to the selection of less immunogenic tumor cells that escape from immune recognition and favor tumor outgrowth.[3] Therefore, the capacity of the immune system to shape tumor immunogenicity refined the concept of immunosurveillance to the "immunoediting" hypothesis.[11–13] Cancer immunoediting is a dynamic process that comprises three phases. The *elimination* phase represents the concept of immunosurveillance and thus tumor elimination by the innate and adaptive immune system.[13] However, some tumor cell variants survive the elimination phase and enter a dynamic *equilibrium*, in which adaptive immune cells control further tumor growth and shape tumor cell immunogenicity. The equilibrium is the most prolonged phase, possibly explaining the latency between initial tumor formation and clinically detectable malignant disease.[13,14] In this phase, some residual tumor cells remain in a quiescent cell state characterized by immune-controlled proliferation arrest. These cells accumulate mutations under selective immune pressure, giving rise to new tumor-cell variants with immunoevasive properties.[13–15] In the *escape* phase, these tumor-cell variants progressively proliferate in an immunologically unrestricted fashion and establish tumors.

The immunological escape can be achieved by mechanisms at the tumor cell level (see chapter 4.5) or by the establishment of an immunosuppressive tumor microenvironment.[13,14,16]

4.1.1 Tumor-CD8 T-cell interaction

Anti-cancer immunity involves various effector cells from the innate and adaptive immune system, such as NK cells and T lymphocytes (T cells), respectively. Especially, cytotoxic tumor-infiltrating T lymphocytes play an essential role due to their high destructive potential. Their indispensability in cancer control was demonstrated in different tumor growth studies of carcinogen-induced malignancies in lymphocyte-depleted mice and a spontaneous lymphoma model depleted for T-cell-derived perforin.[3,17,18]

CD8 T cells, the main mediators of cytotoxic adaptive immunity, can recognize and eliminate infected or malignant cells specifically. Via their T cell receptor (TCR) in cooperation with the CD8 co-receptor, they recognize distinct tumor-antigen epitopes presented on the major histocompatibility complex class I (MHC-I) molecules on the surface of the target cell. In humans, the MHC-I is termed human leukocyte antigen class I (HLA-I). Additionally, T cell function requires secondary signals for self or non-self-discrimination, which can either promote (co-stimulatory) or inhibit (co-inhibitory) T cell activation.[19,20] Examples of co-stimulatory receptors on T cells are CD28, ICOS, 4-1BB, and CD40, which bind to their respective ligands on antigen-presenting cells (APCs) and tumor cells.[21–25] The most well-studied co-inhibitory receptors on T cells are CTLA-4 (cytotoxic T lymphocyte antigen-4) and PD-1 (programmed cell death-1), which can block T-cell function by binding to their corresponding ligand on the target cell.[21,26,27] Both so-called immune checkpoints are upregulated upon T cell activation and provide a negative feedback loop to prevent excessive immune responses and preserve self-tolerance.[28]

As CD8 T cells become activated, they use different cytotoxic mechanisms to kill infected or cancerous cells.[29,30] One mechanism to induce programmed cell death of the direct target cell is granule-dependent exocytosis. In doing so, activated CD8 T cells release the content of cytolytic granules, like perforins, granzymes, and granulysin, into the T cell-target cell interface (immunological synapse). Perforin polymerizes at the target cell's membrane and forms transmembrane pores. The latter pave the way for granzymes and granulysin to enter the target cell and allow ionic influx causing osmotic stress that results in cell death.[31,32] Additionally, granzymes induce apoptosis by caspase-dependent and -independent pathways.[31,33,34] Another mechanism is the Fas/FasL-mediated apoptosis induction, whereby Fas ligands (FasL) on

activated T cell binds to the Fas receptor expressed on tumor cells. The initiation of receptor-dependent apoptosis pathways requires recruitment of Fas-associated death domain (FADD) proteins, subsequent caspase-cascade activation, followed by cell death.[35–37] The tumor cell-destructive capacity of activated CD8 T cells implies also the production and release of pro-inflammatory cytokines, such as tumor necrosis factor-alpha (TNF-α) and IFN-γ which activate several apoptosis pathways in tumor cells.[35,38–43] The relevance of cytokines in tumor control was demonstrated in a thymoma mouse model, in which contact-dependent killing alone by cytotoxic T cells was insufficient for tumor regression.[44] Notably, T cell-secreted cytokines are not restricted to only act on the target cell but also on bystander cells.[45] A recent study imaged the long-distance spreading of IFN-γ throughout the tumor lesion modulating remote tumor cells, even in case of antigen-loss variants and at low frequencies of tumor-specific CD8 TILs.[46]

4.1.2 Role of interferons in cancer control

IFNs play a pivotal role in cancer control. Specifically, type I IFN (IFN-I, e.g., α, -β) and type II IFN (-γ) are principal mediators of anti-tumor immunity by facilitating crosstalk between tumor and immune cells. IFN-I are produced by both immune cells and infected cells and act autocrine and paracrine.[47] As part of the defense mechanism against pathogens, IFN-I are produced and released by infected cells upon sensing danger signals, such as DAMPs or PAMPs (damage/pathogen-associated molecular patterns), by pattern recognition receptors (PRRs).[48] In contrast, IFN-γ is mainly secreted by activated T lymphocytes and NK cells.[47,49] Binding of IFN-I to the IFN-α/-β receptor (IFNAR1/2) and IFN-γ to the IFN-γ receptor (IFNGR1/2) leads to the activation of distinct JAK (Janus kinase)-STAT (Signal transducer and activator of transcription) signaling pathways, which share specific components. Association of either JAK1/TYK2 or JAK1/2 to the receptor complex initiates tyrosine phosphorylation of STAT molecules, which are translocated to the nucleus as homo- or heterodimers driving expression of primary interferon-stimulated genes (ISGs). Many ISGs are transcription factors, such as interferon-regulatory factor 1 (IRF1), promoting secondary effector gene expression.[49–53]

The effects of IFNs are pleiotropic as they act either directly on tumor cells or indirectly via effective anti-tumor immune responses. Accordingly, IFNs can affect tumor cell proliferation, differentiation, apoptosis, and immunogenicity.[43,47] Particularly, the latter is increased due to the upregulation of HLA-I molecules on the cell surface via JAK-STAT signaling.[43,54–57] Likewise, IFNs modulate the activity, migration, differentiation, and survival of immune cells.[47,58] The contribution of treatment-induced IFN-I in tumor control has been studied in a melanoma mouse model showing delayed tumor outgrowth and prolonged survival,

which was even enhanced in the presence of a PD-1 inhibitor.[59] Recent studies demonstrated the indispensability of type II IFN for T-cell-based immunotherapy, as expression data analysis of patient-derived melanoma biopsies revealed that IFN-γ-related gene expression signature predicts clinical response.[60,61] Although IFNs are essential in cancer control, they exhibit immunomodulatory and pro-tumorigenic functions inducing an immunosuppressive microenvironment by, for instance, upregulation of PD-L1/2 and indoleamine 2,3-dioxygenase 1 (IDO1), promoting tumor immune evasion.[62,63]

4.1.3 HLA-I-restricted antigen presentation

IFNs can enhance tumor immunogenicity and thus T cell-mediated tumor killing by upregulating genes involved in HLA-I antigen presentation.[55–57] The antigen processing and presentation machinery (APM) coordinates a highly complex multistep process involving numerous interacting components (Figure 1). A key element is the proteasome, which enzymatically degrades cellular proteins into short fragments. The central proteolytic machine is the constitutive 26S proteasome consisting of a catalytic 20S core and two 19S regulatory caps. The 20S core possesses two pairs of outer α-rings and two pairs of β-rings with seven subunits each. Furthermore, the β-subunits β1, β2, and β5 have enzyme-like activities and represent the catalytic center. The 19S regulatory complex functions as a gatekeeper recognizing ubiquitinated proteins and facilitating their access to the active site of the proteasome. [64–67] Notably, exposure to IFNs induces the evolvement of an immunoproteasome, in which the catalytic β-subunits are replaced with the more efficient subunits LMP2 (PSMB9), MECL-1 and LMP7 (PSMB8), and the 19S regulatory complex with the proteasome-associated activator PA28. The accompanied elevated proteolytic functions promote increased efficacy of HLA-I antigen presentation on the cell surface.[66,68–71]

As precursor peptide fragments exit the proteasome they are eventually further processed by cytosolic peptidases and subsequently transported into the endoplasmic reticulum (ER) via ATP-dependent transporters TAP1 and TAP2 (transporter associated with antigen processing).[72] Here, they may be proteolytically processed by ER-resident aminopeptidases ERAP1 and ERAP2 to an optimal 8-10 amino acid length.[73,74] In the ER lumen, newly-synthesized HLA-I heavy chains are stabilized by the chaperons BiP (binding of immunoglobulin protein) and calnexin protecting the chains from degradation and facilitating their folding for the dimerization with the β2-microglobulin (β2m) light chain.[75–77] The loading of processed peptides onto the HLA-I/β2m dimer requires a large protein assembly, known as the protein loading complex (PLC). It consists of the TAP1/2 dimers, the chaperons Tapasin

(TAPBP) and calreticulin, and the thiol oxidoreductase ERp57.[77–80] As soon as the peptide is bound to the HLA-I molecule, the complex dissociates from the PLC and translocated via the Golgi apparatus to the cell surface for antigen presentation.[81,82]

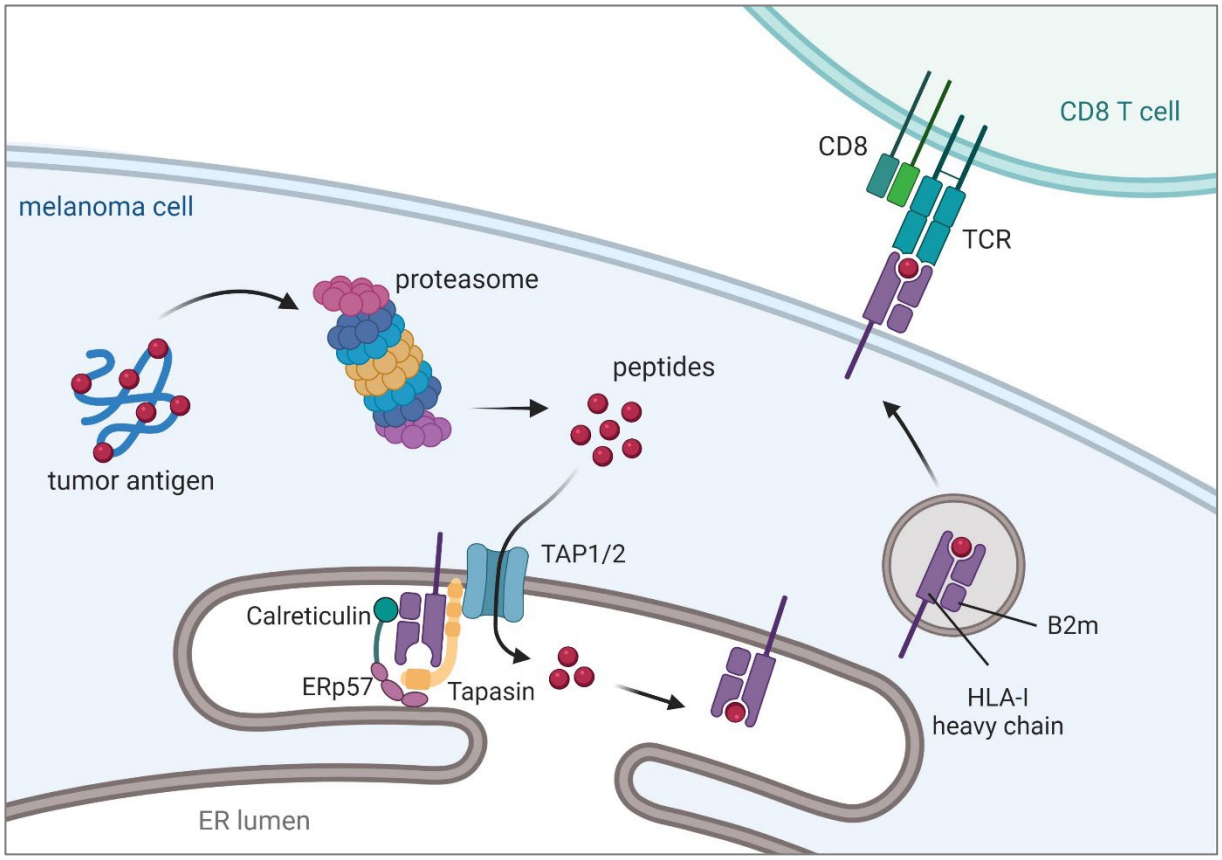

Figure 1: HLA-I antigen processing and presentation machinery. Created in BioRender.com.

In the past 30 years, many HLA-I-restricted tumor antigens recognized by cytotoxic T cells have been described. According to their tumor specificity and molecular characteristics, they can be categorized into different groups. Several tumor antigens are shared between patients, different cancers, and tissues (shared antigens). One example is cancer-germline antigens, for instance, the Melanoma-associated antigen (MAGE) family and NY-ESO-1.[83,84] They are aberrantly expressed in tumor cells but not in normal tissues except for germline and trophoblastic cells, that lack HLA-I surface expression. Therefore cancer-germline antigens are highly tumor-specific and represent an attractive target for T cell-based immunotherapy.[84,85] Further shared antigens are differentiation antigens that are derived from proteins expressed in tumor cells and their corresponding healthy tissue. In melanoma, many melanocyte-lineage antigens participate in melanin production, such as tyrosinase, tyrosinase-related protein-1/2

(TRP1/2), glycoprotein 100 (gp100), and Melan-A/MART-1, of which all are recognized by CD8 T cells.[86–88] In some melanoma patients, spontaneous T-cell responses towards differentiation antigens can cause vitiligo, a plaque-patterned depigmentation of healthy skin. Nevertheless, this adverse event is associated with a good prognosis.[85,89]

The most highly tumor-specific antigens are neoantigens generated by tumor-specific non-synonymous mutations or chromosomal alterations. Due to their unique expression in malignant cells, neoantigen-specific CD8 T cells are unaffected by negative selection in the thymus (central tolerance) and enrich a tumor-specific T-cell repertoire. Certain cancer entities with high mutation rates, such as melanoma and lung carcinoma, are expected to be more immunogenic due to their enriched putative neoantigen load.[90–93]

4.2 Cutaneous malignant melanoma

Malignant melanoma is one of the most highly immunogenic tumors due to the high level of antigens potentially recognized by immune cells, as previously mentioned. The high mutational load of cutaneous melanoma is predominantly caused by ultraviolet (UV) light-induced DNA damage.[93–95] Under normal conditions, the pigment melanin produced by skin-resident melanocytes serves as a protectant from UV light-induced DNA damages for melanocytes themselves and neighboring keratinocytes by scattering and absorbing UV radiation. However, sun exposure and subsequent sunburns, especially in early childhood and adolescence, result in irreversible genetic alterations contributing to melanomagenesis. Based on this, light-skinned and fair-haired individuals having low melanin content are more prone to develop melanoma. Additional genetic and environmental determinants of melanoma risk are personal or family predisposition, presence of melanocytic or dysplastic nevi, age, chronic immunosuppression, and socioeconomic and lifestyle factors.[96–100]

According to the GLOBOCAN 2020 cancer estimate, melanoma is the 6th most common newly-diagnosed malignant disease across all ages and genders in Europe.[101] The incidence of cutaneous melanoma steadily increased since the 1970s, reaching 324.635 cases (1.7 % of all new cancer cases) and accounting for 57.043 cancer deaths (0.6 % of all cancer deaths) in 2020, worldwide. Notably, the incidence and mortality rates differ strongly between countries due to geographic locations, ethnic origin, health education, and primary cancer prevention.[99,102–104] Among all types of skin cancer, melanoma is the most aggressive and lethal form due to its early metastatic spread. Different studies demonstrated that melanoma cells from primary

tumors disseminate very early in parallel to local and distant sites via lymphatic and vascular routes, respectively.[96,105,106]

The cellular properties and invasive behavior of melanoma cells are well-founded in their origin and biology. They emerge from melanocytes in the skin, iris, or mucosa undergoing a stepwise malignant transformation. At baseline, melanocytes are low proliferative; however, they start to divide more frequently with increased genetic alterations.[107] During the malignant transformation of melanocytes, certain genetic mutations lead to dysregulation of key cellular pathways resulting in unbalanced cell fate determination towards increased cell survival and reduced cell death. The different melanoma subtypes are classified according to the cumulative sun damage, which correlates with distinct oncogenic driver mutations.[108] This thesis focuses on cutaneous malignant melanoma, in which the central and most prevalent mutated signaling pathway is the mitogen-activated protein kinase (MAPK) pathway. Mutations in the v-Raf murine sarcoma viral oncogene homolog B (*BRAF*) encoding for a serine/threonine kinase, or other MAPK pathway components are early oncogenic events promoting cell proliferation. Around 50 % of cutaneous melanomas harbor an activation mutation in BRAF, most commonly the V600E (valine to glutamate) mutation. The accompanying constitutive activation of the MAPK pathway leads to uncontrolled proliferation despite any extrinsic growth signal. Of note, benign nevi often possess an activating BRAF mutation only that does not result in unrestricted cell proliferation. Further less frequent mutations occur in the neuroblastoma RAS viral oncogene homolog (*NRAS*; around 25 %), and the negative RAS regulator *NF1* (around 15 %). In general, cutaneous melanomas can be categorized based on their genetic makeup as BRAF, NRAS, NF1 mutant, or triple-wildtype (wt).[99,109,110]

4.3 Cellular plasticity of melanoma

The most critical step in melanoma progression is the transition of melanoma cells to become invasive. Besides irreversible genetic alterations, phenotypic changes in melanoma cells can provide metastatic potential and therapy resistance. In response to signals in the microenvironment, specific gene expression programs deeply anchored in their cell origin can drive the process of phenotype switching in a reversible fashion. Therefore, the invasive potential of melanoma arises from the intrinsic migratory nature of the melanocyte precursors melanoblasts. The property of cell motility is essential in melanocyte development when melanoblasts derived from pluripotent neural crest stem cells migrate dorsolaterally from the neural crest to the basal layer of the epidermis. At their final destination in the skin, they

undergo lineage-specific differentiation tightly governed by the microphthalmia-associated transcription factor (MITF), the master regulator of genes engaged in melanocytic differentiation.[111–114] In melanoma cells, MITF controls a variety of cellular processes by regulating the expression of genes involved in, for instance, cell proliferation and survival (CDK2, CDK4, $p27^{KIP1}$, BCL2), differentiation, and pigmentation (Melan-A/MART-1, gp100, tyrosinase), and invasion (Dia1, c-Met).[115–121]

Besides the development of melanocytes, MITF activity defines the phenotype of melanoma cells. Based on the MITF level, two distinct transcriptional subtypes have been initially described, the $MITF^{high}$ and $MITF^{low}$ phenotype. While higher expression levels of MITF characterize a proliferative and differentiated cell state, low MITF-expressing cells are more invasive, mesenchymal, and dedifferentiated.[113,122] To explain the diverse roles of MITF activity in melanoma cell cycle and invasiveness, Carreira et al. proposed the rheostat model, which implies the high dynamic and reversibility of phenotype switching concerning MITF expression influenced by the tumor microenvironment.[117,123,124] However, recent gene expression analyses revealed further MITF intermediate cell states refining the initial concept of the rheostat model by discrete gene regulatory networks that provide a highly complex and diverse landscape of melanoma cell states (Figure 2).[122,125–128] Besides MITF, distinct phenotypes are assigned to the expression of other specific molecules, such as the receptor

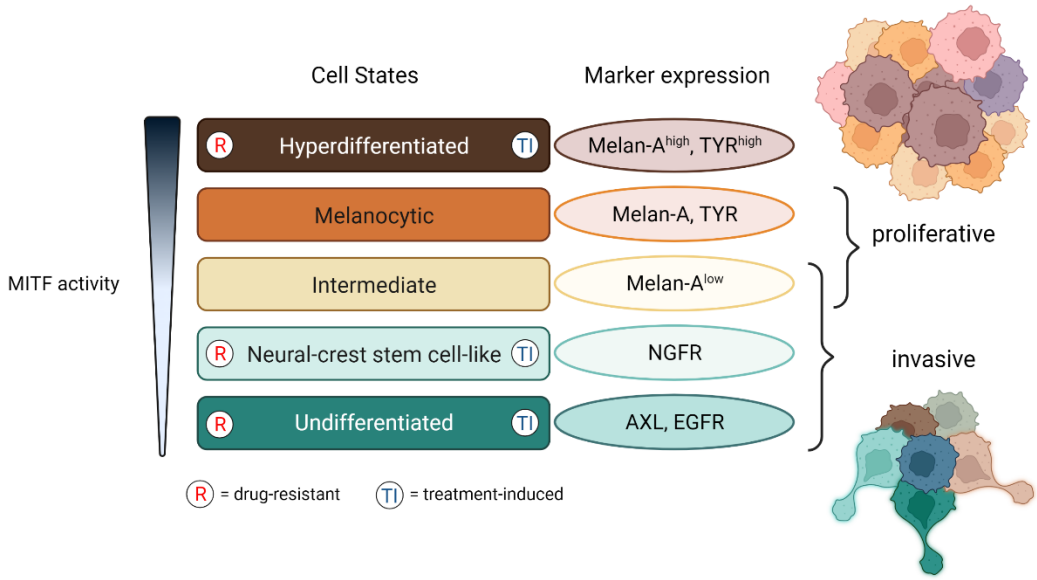

Figure 2: Distinct melanoma cell states. Classification according to the MITF activity level and simplified marker expression profile. Illustration adapted from Rambow et al.[135] and created in BioRender.com.

tyrosine kinase (RTK) AXL and the neural-crest stem cell marker NGFR (CD271), which describe distinct invasive melanoma cell states.[126,129,130]

The tumor microenvironment can direct melanoma cells towards certain cell states in response to stresses, including hypoxia, limited nutrient and amino acid supply, and inflammatory signaling.[131–133] Importantly, melanoma cells profit from their extraordinary plasticity and undergo phenotype switching to adapt to inflammation and therapeutic interventions.[134,135] The aspect of phenotype switching in the context of escape from therapeutic interventions will be explained in a later chapter (4.5).

4.4 Current treatment options for melanoma and prospectives

Therapeutic decisions highly depend on the melanoma subtype, the stage of the disease, and the patient's physical condition. In the case of localized or cutaneous metastatic tumors, surgical excision of the lesion is the primary treatment option. Early detection and complete surgical removal can be highly curable for primary melanomas, whereas 5-year overall survival rapidly declines for patients with regional or distant metastases.[136] Therefore, patients with metastasized melanoma require other treatments to prevent disease recurrence and further metastatic spread.[99,110] Ten years ago, the gold standard of care for the management of metastatic melanoma was chemotherapy with dacarbazine. However, it failed to have significant therapeutic benefit with only complete responses in about 5 % of patients due to the insensitivity of melanoma cells to the cytotoxic effects of chemotherapeutics.[137,138] But prognosis and survival of patients with advanced melanoma dramatically improved with the implementation of new therapeutic strategies, based on small molecule inhibitors targeting oncogenic MAPK signaling and antibody-based immunotherapies.

4.4.1 Targeted therapy

The knowledge about the impact of molecular alterations in melanoma development led to the discovery of small-molecule inhibitors selectively targeting the mutated BRAF V600 protein.[139,140] Vemurafenib and dabrafenib were the first two BRAF V600 inhibitors receiving approval by the US Food and Drug Administration (FDA) and the European Medicine Agency (EMA) to treat patients with BRAF-mutated unresectable or metastatic melanoma in 2011 and 2013, respectively.[141,142] As first-line treatment, both BRAF inhibitors showed superior response rates, representing 48 % for vemurafenib and 50 % for dabrafenib compared to chemotherapy with dacarbazine (5-6 %).[143,144] However, the duration of response to BRAF

inhibitor monotherapy was limited in most patients, who only benefited from a median progression-free survival of about five months.[143,144] The rapid tumor progression was due to the development of acquired resistance to BRAF inhibition, for instance, by mutation-mediated MAPK pathway reactivation.[145,146] To decrease MAPK-driven acquired resistance, BRAF inhibitor monotherapy was replaced by combinational treatment with BRAF inhibitor plus MEK inhibitor (vemurafenib+cobimetinib; dabrafenib+trametinib) acting on the mitogen-activated protein kinase kinase (MEK) downstream of BRAF. Simultaneous administration of both inhibitors resulted in longer response durations, better response rates, and comparable rates of adverse events to monotherapy.[146–148]

In 2018, the second-generation MAPK inhibitors were approved by the FDA.[149] In contrast to first-generation inhibitors, the BRAF inhibitor encorafenib has distinct pharmacological modifications improving pharmacodynamics and thus efficacy and tolerability.[150] In the COLUMBUS phase III clinical trial, encorafenib monotherapy and a combination of encorafenib with the MEK inhibitor binimetinib showed improved progression-free survival compared to vemurafenib monotherapy for the treatment of BRAF-mutant advanced melanomas.[151,152] Even though the discovery and advances of targeted therapies improved tremendously in the past ten years, acquired resistance to combinational therapy with BRAF and MEK inhibitors is still a major obstacle in the management of metastatic melanoma. Thus, other therapeutic approaches are needed to prolong patient outcomes.

4.4.2 Systemic immunotherapies

Immunotherapies were developed to boost the patient's immune system to fight against cancer cells and achieve robust anti-tumor responses with long-lasting immunity.[153] In the 1990s, two immunotherapy approaches using high-dose IFN-α and interleukin-2 (IL-2) were developed for adjuvant treatment of resected high-risk melanoma.[154,155] These early immunotherapies were non-specific exhibiting pleiotropic effects accompanied by severe toxicities when used in high doses.[153,156] Nevertheless, the clinical application of cytokines set a milestone in cancer therapy, paving the way for the intense development of new immunotherapeutic strategies in the last decades.

A revolutionary breakthrough in the systemic treatment of advanced melanoma was the discovery of immune checkpoint blockade (ICB), e.g., antibodies targeting the co-inhibitory receptors CTLA-4 and PD-1 on T cells that impair T-cell activation. Both receptors modify distinct spatiotemporal events during immune responses. CTLA-4 restricts the co-stimulation

of naïve T cells during the priming phase in the lymph nodes, whereas PD-1 prevents T-cell activation in the effector phase, predominantly in peripheral tissue.[157] Tumor cells exploit these peripheral tolerance mechanisms to evade the immune system by, for instance, PD-L1 expression on their cell surface. Blocking the inhibitory receptor-ligand interaction releases T cells from the inhibitory break, which results in elevated T-cell activation and tumor-cell killing.[28] In the last ten years, four monoclonal antibodies either targeting CTLA-4 (ipilimumab), PD-1 (nivolumab, pembrolizumab), or PD-L1 (atezolizumab) were approved by the FDA for the treatment of melanoma.[158] In the CheckMate 067 phase III clinical trial (NCT01844505), the combination of nivolumab with ipilimumab demonstrated superior clinical efficacy compared to each monotherapy as a first-line treatment for metastatic melanoma.[159,160] Within the 5-year follow-up, the median overall survival of patients, who received combined nivolumab and ipilimumab, was still unreached, accounting for a survival rate of 52 %, followed by 44 % for nivolumab alone and 26 % for ipilimumab alone. In general, the overall and progression-free survival and the objective response rates were higher in the groups receiving either combinational treatment or nivolumab alone than in the ipilimumab group.[161] Besides the remarkable clinical success, 59 % of patients treated with the combination suffered from high-grade immune-related adverse events, which were much less frequent in the nivolumab and ipilimumab monotherapy groups accounting for 23 % and 28 %, respectively.[161] Around 40 % of patients with advanced melanoma, who received combinational therapy, needed to discontinue the treatment because of high-grade adverse events. Nevertheless, a retrospective analysis of phase II and III clinical trials revealed beneficial effects of combination treatment even after discontinuation. The efficacy outcome was similar to patients who did not discontinue.[162]

Despite the improved therapeutic landscape of advanced melanoma targeting PD-1 and CTLA-4, primary and acquired resistance to immune checkpoint blocking inhibitors limit patient outcomes.[163] For this reason, further immune checkpoints have been recently identified, which seem promising targets for cancer therapy. Lately in March 2022, relatlimab, an immune checkpoint blocking antibody against LAG-3 (Lymphocyte activation gene-3), in combination with nivolumab received FDA approval for the treatment of patients with unresectable or metastatic melanoma.[164] Further potential ICBs, such as TIM-3 (T cell immunoglobulin and mucin-domain containing-3), and TIGIT (T cell immunoglobulin and ITIM domain) are under investigation in combination with anti-PD-1 antibodies for the treatment of melanoma and other solid tumors (NCT03743766, NCT04139902, NCT02913313).[165] Nowadays, the immunotherapeutic standard of care for patients with metastatic melanoma is either PD-1

inhibitor monotherapy or a combination of nivolumab and ipilimumab.[99] To improve patient outcomes, there is growing interest in the intratumoral application of immune-stimulatory agents to boost anti-tumor immune responses, also combination with immune checkpoint blocking antibodies.

4.4.3 RIG-I agonists in intratumoral immunotherapy

The goal of intralesional administration of immune-stimulatory agents is to enhance a local tumor-specific immune response and to generate systemic and durable clinical responses. This strategy is based on the local delivery of highly concentrated agents into the tumor lesions, thereby diminishing toxicities associated with systemic delivery and facilitating the use of multiple synergistic combinations.[166] In the last several years, immune-stimulatory agents for intratumoral administration gained great attention resulting in various therapeutic interventions with different modes of action, such as oncolytic and non-oncolytic viruses, engineered immune cells, pattern recognition receptor agonists, and immune-stimulatory mRNAs.[167] Several immune-stimulatory agents have successfully entered clinical trials, demonstrating encouraging results in combination with immune checkpoint blocking antibodies. This chapter will focus on agonists targeting the innate immune receptor RIG-I, which are under intense investigation for the treatment of metastatic melanoma.

RIG-I-like receptors (RLRs) belong to a group of intracellular pattern recognition receptors (PRRs), key players in innate immune activation. They are the first line of defense against pathogens by sensing cytosolic viral or endogenous double-stranded RNAs (dsRNAs). To date, three members of intracellular RLRs are known: RIG-I (retinoid acid-inducible gene I), MDA5 (melanoma differentiation-associated factor 5), and LGP2 (laboratory of genetics and physiology 2).[168,169] They are ubiquitously expressed but at low basal levels. Their expression can be strongly enhanced upon viral infection or exposure to IFN-I.[168,170] RIG-I and MDA5 share structural and functional similarities. Both receptors possess two N-terminal caspase activation and recruitment domains (CARD), followed by DExD/H box RNA helicase containing an ATPase domain and a C-terminal regulatory domain, which is essential for RNA binding and autoregulation.[169] Nevertheless, RIG-I specifically recognizes short dsRNA fragments possessing a 5'triphosphate end (3pRNA) that enables non-self discrimination. The triphosphate residue is required for RIG-I activation to its full potential. Therefore, synthetic 3pRNA serves as a valuable immune-stimulatory agent.[171]

Upon binding of its ligand, RIG-I multimerizes and interacts with the mitochondrial antiviral signaling protein MAVS (also known as IPS-1/VISA/Cardif) via the CARD domains (Figure 3). This interaction subsequently results in MAVS oligomerization and the formation of a signalosome that requires the recruitment of tumor necrosis factor receptor-associated factor (TRAF) proteins. The recruited proteins trigger two distinct signaling pathways: On the one hand, phosphorylation of the transcription factors IRF-3 and IRF-7 induce expression of type I and III IFNs, and on the other hand, phosphorylation of the transcription factor NFκB to activate the gene transcription of pro-inflammatory cytokines.[168,169] In tumor cells, RIG-I activation can be achieved upon transfection with synthetic 3pRNA which triggers various effects, such as production and release of IFN-I and other pro-inflammatory cytokines and induction of tumor cell apoptosis.[172–174] Importantly, IFN-I drive a feed-forward loop by autocrine and paracrine binding to IFNARs, leading to JAK-STAT signaling activation in the target and neighboring cells. This feed-forward loop amplifies pro-inflammatory cytokine production and the induction of proteins involved in antiviral activity, such as antigen presentation, RLR signaling, IRFs, and immune cell recruitment.[168,175,176]

Different studies showed striking effects of RIG-I activation on the tumor microenvironment. Upon RIG-I activation, cancer cell-released chemokines and IFN-I enrich immune-cell infiltration into the tumor lesion and enhance dendritic cell-mediated cross-presentation of tumor antigens to CD8 T cells, respectively.[173,174,177,178] Furthermore, uptake of RIG-I agonists by immune cells can lead to their activation, as shown for NK cells and dendritic cells.[179,180] These promising effects gave rise to combinational pre-clinical studies with immune checkpoint inhibitors. In mice, therapeutic targeting of RIG-I combined with anti-CTLA-4 inhibitors led to the control of locally 3pRNA-injected melanomas and distant, non-injected lesions.[178] Currently, RIG-I agonists are tested for the anti-tumor effects also in clinical settings. In a first-in-human phase I/II clinical trial (NCT03065023), the RIG-I activator MK-4621 (RGT100) was evaluated as safe and tolerable, showing antitumor activity in patients with advanced or recurrent tumors.[181,182] In keeping with this, intralesional application of MK-4621 is currently tested in combination with systemic PD-1 inhibition in a phase I clinical trial (NCT03739138) to assess therapeutic effects, safety, tolerability, and drug pharmacokinetics.[182,183] Another RNA-based agonist CV8102, targeting Toll-like receptor (TLR-) 7/-8 and RIG-I, demonstrated synergistic effects in combination with anti-PD-1 antibodies in mice reasoning the translation into a clinical trial (NCT03291002). This phase I study evaluates the efficacy, safety, and tolerability of CV8102 as monotherapy or in combination with PD-1 inhibition, including patients with melanoma and cutaneous squamous

cell carcinoma.[182,184–186] Detailed results of the studies mentioned above on both RIG-I stimulators are still awaited.

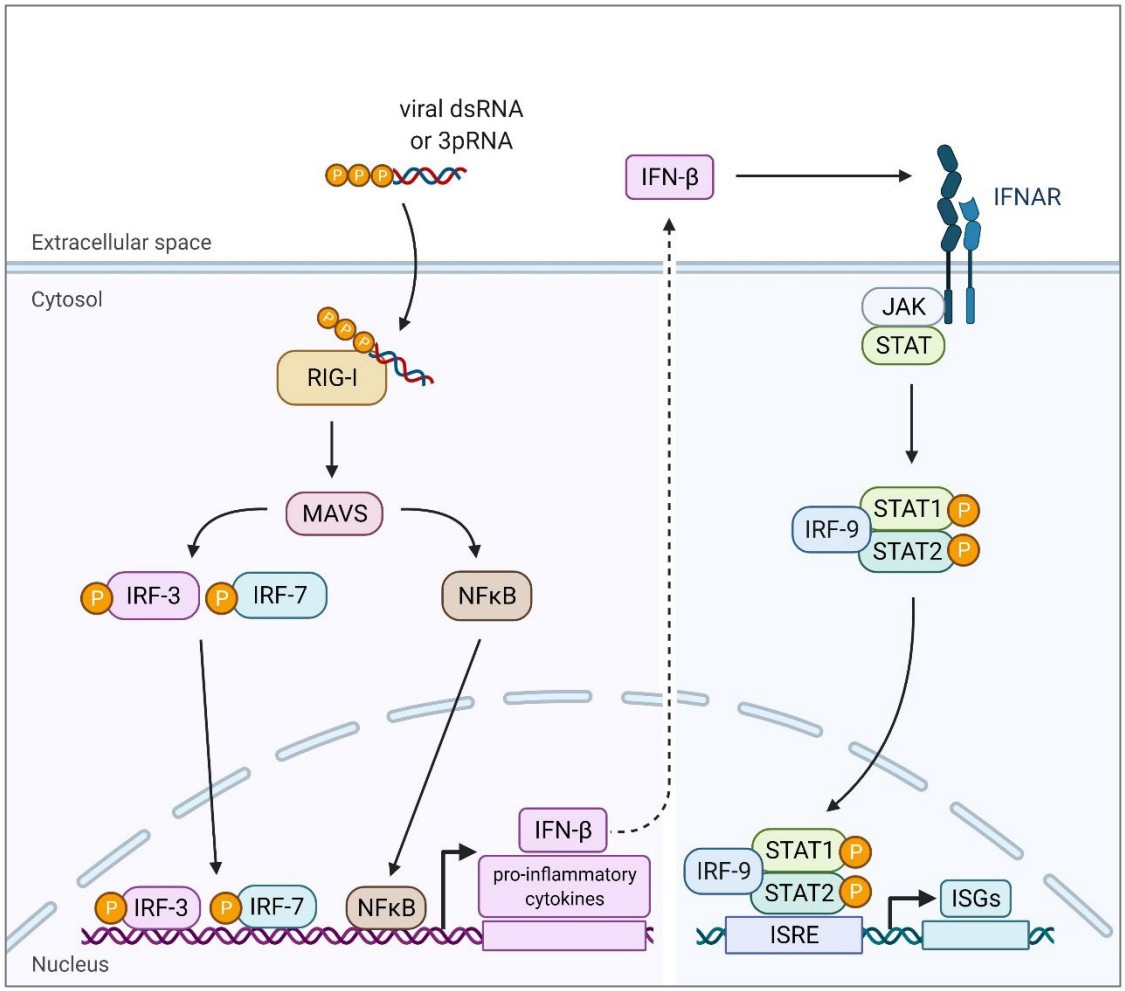

Figure 3: RIG-I signaling pathway. Adapted from "Innate Immune Antagonism by SARS CoV", by BioRender.com (2022). Retrieved from https://app.biorender.com/biorender-templates.

4.5 Tumor cell-intrinsic resistance to therapies

The field of melanoma therapy improved to a broad landscape of treatment options for patients with advanced or inoperable lesions. However, durable response rates to any approved therapy are still limited due to primary (intrinsic) and secondary (acquired) resistance. An important contributor to therapy resistance is the intratumoral heterogeneity of melanoma, which mainly emerges from genetic and phenotypic modifications during tumor progression. The high intratumoral diversity of cell subpopulations with distinct properties can confer tolerance towards therapeutic agents by selecting cell clones with survival advantages and elimination of others.[127,187] It is still unclear whether the selective pressure caused by drug treatment or inflammatory processes gives rise to tolerant tumor cells from pre-existing

resistant subclones, via newly-acquired mutations. Also, phenotypic adaptation has to be considered.[188] In the last decade, various resistance mechanisms to both targeted therapies and immunotherapies have been discovered. Nevertheless, it is an urgent need to extend the knowledge of how melanoma cells can escape from therapeutic intervention to improve long-term patient outcomes.

4.5.1 Escape mechanisms from targeted therapy

Elucidating molecular mechanisms leading to MAPKi resistance has been of tremendous interest. Early acquired resistance is a major obstacle to the efficacy of targeted therapy and limits long-term benefits. BRAFi-mutated melanoma cells mainly circumvent MAPKi effects by reactivation of the MAPK pathway and sustained ERK activation implying a solid dependency on this signaling pathway.[189] Genetic mechanisms conferring BRAFi and MEKi resistance are BRAF V600E amplifications, gain-of-function mutations in NRAS and MEK1/2, and loss of NF1.[189–194] Non-genetic bypass of BRAF inhibition includes aberrant BRAF V600E splice variants, expression of CRAF, and elevated levels of the kinase COT that activates ERK signaling by MEK-dependent mechanisms.[195–197] Additionally, cell proliferation, and survival can be maintained by alternative pathway activation, such as the PI3K-AKT-mTOR pathway, frequently activated in drug-resistant cells. Dysregulation of the PI3K pathway by loss of its negative regulator PTEN contributes to cell survival by suppressing pro-apoptotic BIM in BRAFi-resistant melanoma cells.[198] Overexpression of RTKs, such as AXL, epithelial growth factor receptor (EGFR), platelet-derived growth factor receptor beta (PDGFRβ), and insulin growth factor-1 receptor (IGF-1R) can lead to reactivation of the MAPK and the PI3K pathways conferring to MAPKi resistance.[192,199,200] Furthermore, Miller and colleagues demonstrated that proteolytic shedding of RTKs, predominantly AXL and MET, from the cell surface is impaired under MAPKi treatment in melanoma mouse models. Consequently, reduced proteolytic shedding of surface receptors protects the cells from negative feedback loops on signaling network activity and augments bypass signaling that adds to other pathways of resistance. Melanoma patients treated with combined BRAFi+MEKi that rapidly progressed showed decreased levels of shedded circulating RTKs in the blood serum.[201]

Within the last several years, epigenetic mechanisms received growing appreciation as drivers of adaptive plasticity facilitating melanoma phenotypic drug evasion. The accompanying cell state transition impacts on cell cycle progression, differentiation, and metabolic rewiring.[202] A comparative large-scale transcriptomic and methylomic study of melanoma patient biopsies prior to MAPKi therapy and during disease progression revealed

high recurrence and frequency of transcriptomic and epigenetic alterations that contribute to intra-patient and intratumoral heterogeneity.[203] Moreover, Konieczkowski and colleagues described distinct transcriptional profiles in BRAFi/MEKi-sensitive and -resistant BRAF-mutant melanoma biopsies. Accordingly, drug-sensitive tumors exhibited high levels of MITF, whereas drug-resistant possessed low MITF but high NFκB and AXL expression.[199] The $MITF^{low}/AXL^{high}$ phenotype has been described as a predictor of early resistance to MAPKi.[129] With the implementation of single-cell approaches, multiple drug-tolerant states were discovered to coexist in melanoma. Rambow and colleagues demonstrated the high complexity and dynamic of phenotypic heterogeneity in melanoma patient-derived xenograft mouse models upon BRAFi/MEKi treatment.[127] Different cell states with distinct MITF-transcriptional activities were identified, which can be therapy-induced and mediate drug tolerance (see Figure 2).[127,135] Beyond the classical proliferative $MITF^{high}$ and invasive $MITF^{low}$ phenotype, these additional intermediate cell states possess discrete gene regulatory networks that may co-emerge within the same lesion.[127,128,135] Several studies demonstrated the adaptive trajectories of melanoma cells under BRAFi treatment. Upon short-term BRAFi exposure, an initial upregulation of MITF towards a more hyperdifferentiated cell state was observed, following a transition into a dedifferentiated, slow-proliferative and neural crest stem cell-like ($NGFR^{high}$) phenotype.[204–207] Moreover, in both drug-tolerant melanoma cells and BRAFi-resistant melanoma patient biopsies, high expression of NGFR was associated with drug resistance and disease progression, respectively.[127,205] Notably, prolonged exposure to MAPKi can convert a transient-transcriptional, drug-tolerant cell state into a stably resistant state by epigenetic reprogramming.[206] The emergence of phenotypic resistance mechanisms to therapies demands for new therapeutic avenues to counteract adaptive cell state transition and therapy resistance.

4.5.2 Escape mechanisms from immunotherapy

The key purpose of cancer immunotherapy is to support and elevate tumor cell elimination by the host's immune system. As in a previous chapter described, the immune system exerts selective pressure that can lead to immunoediting by shaping tumor cell immunogenicity and promoting tumor escape from immune control. Several tumor cell-intrinsic mechanisms that enable melanoma cells to evade T cell-mediated surveillance have been described. The absence of HLA-I antigen presentation caused by mutational loss or silencing of HLA-I APM components protects tumor cells from recognition by cytotoxic T cells. Multiple lines of evidence demonstrated that mutations in the *B2M* gene result in loss

of HLA-I surface expression in melanoma.[208–211] Clinical relevance of *B2M* loss in resistance to immunotherapy was outlined by a study by Sade-Feldman et al., who found loss of heterozygosity of *B2M* in almost 30 % of non-responding melanoma patients under anti-CTLA-4 and anti-PD-1 blocking therapy.[212] Alternatively, resistance to T cells can be achieved by genetic alterations affecting HLA-I genes.[210,213] Besides these irreversible genetic defects in HLA-I that are unrestorable by IFN signaling, HLA-I expression is often downregulated by epigenetic silencing of HLA genes or APM components.[214,215] Transcriptional HLA-I downregulation can occur via promotor-associated DNA hypermethylation and histone hypoacetylation of APM genes. Inhibiting involved epigenetic modifiers can restore HLA-I surface expression and resensitize tumor cells to cytotoxic T cells in different cancer entities, including melanoma.[214,216–218] Importantly, pharmacological inactivation of the histone methyltransferase EZH2 could reverse the HLA-I downregulation and synergize with anti-CTLA-4 blocking therapy in a melanoma mouse model.[217]

Another way to evade immune cell recognition is the absence of tumor antigens, resulting from phenotype switching induced by T cell-derived pro-inflammatory cytokines. Adoptive T cell transfer (ACT) studies in mice and one clinical case report showed that T cell-derived TNF-α induces a reversible loss of differentiation antigens, causing resistance to differentiation antigen-specific cytotoxic T cells in melanoma. Hence, inflammation-induced dedifferentiation by TNF-α is associated with resistance to ACT therapy.[133,219] Strikingly, inflammatory signaling by IFN-γ and TNF-α during immunotherapy can induce melanoma dedifferentiation.[125,133,220] However, gene expression analysis of on-therapy biopsies from melanoma patients receiving anti-PD-1 therapy revealed an association of an IFN-γ-driven dedifferentiation signature with initial therapy response.[220] NGFR, another key player in phenotype switching, is upregulated upon pro-inflammatory signaling and desensitizes melanoma cells to the cytotoxic effects of T cell-derived cytokines.[59,220,221] Different studies demonstrated that the dedifferentiated NGFR^{high} melanoma phenotype confers cross-resistance to both targeted and immunotherapy.[203,204,221,222]

Defects in the IFN-γ pathway play a critical role in resistance to T cell-mediated anti-tumor immunity and thus to immune checkpoint inhibitors. Genetic defects in the IFN-γ signaling pathway facilitate resistance to ICB therapy. Loss-of-function mutations in JAK1/JAK2 impair IFN signaling and impede IFN-γ-induced PD-L1 upregulation on melanoma cells. Consequently, the lack of reactive PD-L1 on the tumor cells drives resistance to anti-PD-1 therapy.[223] Furthermore, melanoma cells with JAK1/2 deficiency are insensitive to the anti-tumor activity of IFN-γ, giving rise to T cell-resistant metastatic lesions.[43]

Several studies outlined the impact of primary and acquired mutations in IFN-γ signaling components in clinical ICB resistance.[211,223,224] Consistently, unbiased genetic screens revealed the indispensability of intact IFN-γ signaling for the effectiveness of immunotherapy.[225,226] The clinical relevance of this pathway was underpinned by Ayers and colleagues, who identified IFN-γ-related gene signatures as potential biomarkers for ICB responses in melanoma patients.[61] Nevertheless, further uncovering of resistance mechanisms to immunotherapy is needed to find strategies to overcome therapy resistance and prolong clinical responses of melanoma patients.

5 Objectives

The landscape of melanoma therapy changed tremendously over the last two decades by implementing MAPK small molecule inhibitors and immune checkpoint blocking antibodies and increased therapeutic options for patients diagnosed with advanced melanoma. However, intrinsic and acquired therapy resistance still limits durable outcomes for the majority of patients. The overarching objectives of this thesis were to deeper understand the non-genomic resistance mechanisms of melanoma cells towards targeted therapy and immunotherapy, with a specific focus on mechanisms establishing insensitivity to tumor-reactive cytotoxic CD8 T cells. These mechanisms include the invisibility of tumor cells to T cells by silenced HLA-I molecules and phenotype switching in response to therapeutic interventions. Knowledge of these mechanisms can be exploited to optimize or develop novel treatment protocols that might delay or overcome therapy resistance. To achieve this goal, different melanoma patient models consisting of tumor tissue, corresponding cell lines, and autologous T cells from tissue or peripheral blood were used to investigate the following:

1) Discovering therapeutic strategies to overcome T-cell resistance, also in IFN-insensitive melanoma,
2) Assessing the dynamic transition of melanoma phenotypic cell states under prolonged MAPK pathway inhibition and their effects on CD8 TILs, and
3) Elucidating RIG-I-mediated melanoma cell state switching and its impact on CD8 T-cell stimulation.

6 Articles

The presented doctoral thesis consists of the following three original articles:

1) **Targeting the innate immunoreceptor RIG-I overcomes melanoma-intrinsic resistance to T cell immunotherapy**

Lina Such, Fang Zhao, Derek Liu, Beatrice Thier[#], Vu Thuy Khanh Le-Trilling, Antje Sucker, Christoph Coch, Natalia Pieper, Sebastian Howe, Hilal Bhat, Halime Kalkavan, Cathrin Ritter, Robin Brinkhaus, Selma Ugurel, Johannes Köster, Ulrike Seifert, Ulf Dittmer, Martin Schuler, Karl S. Lang, Thomas A. Kufer, Gunther Hartmann, Jürgen C. Becker, Susanne Horn, Soldano Ferrone, David Liu, Eliezer M. Van Allen, Dirk Schadendorf, Klaus Griewank, Mirko Trilling, and Annette Paschen

Published in: Journal of Clinical Investigation (2020); 130(8):4266-4281

https://doi.org/10.1172/JCI131572

2) **Melanoma differentiation trajectories determine sensitivity towards pre-existing CD8+ tumor-infiltrating lymphocytes**

Franziska Noelle Harbers, Beatrice Thier[#], Simone Stupia, Si Zhu, Marion Schwamborn,Vicky Peller, Heike Chauvistré, Pietro Crivello, Katharina Fleischhauer, Alexander Roesch, Antje Sucker, Dirk Schadendorf, Yong Chen, Annette Paschen, Fang Zhao

Published in: Journal of Investigative Dermatology (2021); 141(10):2480-2489

https://doi.org/10.1016/j.jid.2021.03.013

3) **Innate immune receptor signaling induces transient melanoma dedifferentiation while preserving immunogenicity**

Beatrice Thier[#], Fang Zhao, Simone Stupia, Alicia Brüggemann, Susanne Horn, Christoph Coch, Gunther Hartmann, Antje Sucker, Dirk Schadendorf, Annette Paschen

Published in: Journal for Immunotherapy of Cancer (2022); 10:e003863

http://doi.org/10.1136/jitc-2021-003863

[#]ORCID iD: https://orcid.org/0000-0003-4869-0787

6.1 Article I

Targeting the innate immunoreceptor RIG-I overcomes melanoma-intrinsic resistance to T cell immunotherapy

Lina Such[1,2], Fang Zhao[1,2], Derek Liu[3,4], Beatrice Thier[1,2], Vu Thuy Khanh Le-Trilling[5], Antje Sucker[1,2], Christoph Coch[6], Natalia Pieper[1,2], Sebastian Howe[5], Hilal Bhat[7], Halime Kalkavan[2,7,8,9], Cathrin Ritter[2,10,11], Robin Brinkhaus[1,2], Selma Ugurel[1,2], Johannes Köster[12], Ulrike Seifert[13], Ulf Dittmer[5], Martin Schuler[2,8,14], Karl S. Lang[7], Thomas A. Kufer[15], Gunther Hartmann[6], Jürgen C. Becker[2,10,11], Susanne Horn[1,2,16], Soldano Ferrone[17], David Liu[3,4], Eliezer M. Van Allen[3,4], Dirk Schadendorf[1,2,14], Klaus Griewank[1,2], Mirko Trilling[5], and Annette Paschen[*1,2]

[1]Department of Dermatology, University Hospital Essen, University of Duisburg-Essen, Essen, Germany.

[2]German Cancer Consortium (DKTK), University Hospital Essen, Essen, Germany.

[3]Department of Medical Oncology, Dana-Farber Cancer Institute, Boston, Massachusetts, USA.

[4]Broad Institute of MIT and Harvard, Cambridge, Massachusetts, USA.

[5]Institute for Virology, University Hospital Essen, University of Duisburg-Essen, Essen, Germany.

[6]Institute of Clinical Chemistry and Clinical Pharmacology, University of Bonn, Bonn, Germany.

[7]Institute of Immunology, and

[8]Department of Medical Oncology, University Hospital Essen, University of Duisburg-Essen, Essen, Germany.

[9]Department of Immunology, St Jude Children's Research Hospital, Memphis, Tennessee, USA.

[10]Department of Translational Skin Cancer Research, University Hospital Essen, University of Duisburg-Essen, Essen, Germany.

[11]German Cancer Research Center (DKFZ), Heidelberg, Germany.

[12]Institute of Human Genetics, University Hospital Essen, University of Duisburg-Essen, Essen, Germany.

[13]Friedrich Loeffler Institute for Medical Microbiology, University Medicine Greifswald, Greifswald, Germany.

[14]West German Cancer Center, University Hospital Essen, University of Duisburg-Essen, Essen, Germany.

[15]Institute of Nutritional Medicine, Department of Immunology, University of Hohenheim, Stuttgart, Germany.

[16]Rudolf Schönheimer Institute of Biochemistry, University of Leipzig, Leipzig, Germany.

[17]Department of Surgery, Massachusetts General Hospital, Harvard Medical School, Boston, Massachusetts, USA.

[*]Corresponding author.

Published in: Journal of Clinical Investigation (2020); 130(8):4266-4281

https://doi.org/10.1172/JCI131572

Received: July 8, 2019 / Accepted: May 7, 2020 / Published: July 13, 2020

Contribution to present publication (Article I):

- Conception: 0 %
- Experimental work: 10 %
- Data analysis: 20 %
- Species identification: N/A
- Statistical analysis: 5 %
- Writing the manuscript: 10 %
- Revising the manuscript: 25 %

I hereby certify that Beatrice Thier contributed to the experimental design of this article. She performed experiments and data analysis on the patient model UKE-Mel-154 depicted in figure 8 (B, F, G, I, J), as well as in supplementary figure 5A-C. She was responsible for planning, execution, analysis, and illustration of depicted results. Furthermore, she contributed to the adjustment of figures and supplementary material, and the review and revision of the manuscript.

The above-listed contributions of Beatrice Thier to the publication are correct.

Essen, _____ _____

Annette Paschen

Essen, _____ _____

Beatrice Thier

The Journal of Clinical Investigation RESEARCH ARTICLE

Targeting the innate immunoreceptor RIG-I overcomes melanoma-intrinsic resistance to T cell immunotherapy

Lina Such,[1,2] Fang Zhao,[1,2] Derek Liu,[3,4] Beatrice Thier,[1,2] Vu Thuy Khanh Le-Trilling,[5] Antje Sucker,[1,2] Christoph Coch,[6] Natalia Pieper,[1,2] Sebastian Howe,[5] Hilal Bhat,[7] Halime Kalkavan,[2,7,8,9] Cathrin Ritter,[2,10,11] Robin Brinkhaus,[1,2] Selma Ugurel,[1,2] Johannes Köster,[12] Ulrike Seifert,[13] Ulf Dittmer,[5] Martin Schuler,[2,8,14] Karl S. Lang,[7] Thomas A. Kufer,[15] Gunther Hartmann,[6] Jürgen C. Becker,[2,10,11] Susanne Horn,[1,2,16] Soldano Ferrone,[17] David Liu,[3,4] Eliezer M. Van Allen,[3,4] Dirk Schadendorf,[1,2,14] Klaus Griewank,[1,2] Mirko Trilling,[5] and Annette Paschen[1,2]

[1]Department of Dermatology, University Hospital Essen, University of Duisburg-Essen, Essen, Germany. [2]German Cancer Consortium (DKTK), University Hospital Essen, Essen, Germany. [3]Department of Medical Oncology, Dana-Farber Cancer Institute, Boston, Massachusetts, USA. [4]Broad Institute of MIT and Harvard, Cambridge, Massachusetts, USA. [5]Institute for Virology, University Hospital Essen, University of Duisburg-Essen, Essen, Germany. [6]Institute of Clinical Chemistry and Clinical Pharmacology, University of Bonn, Bonn, Germany. [7]Institute of Immunology, and [8]Department of Medical Oncology, University Hospital Essen, University of Duisburg-Essen, Essen, Germany. [9]Department of Immunology, St Jude Children's Research Hospital, Memphis, Tennessee, USA. [10]Department of Translational Skin Cancer Research, University Hospital Essen, University of Duisburg-Essen, Essen, Germany. [11]German Cancer Research Center (DKFZ), Heidelberg, Germany. [12]Institute of Human Genetics, University Hospital Essen, University of Duisburg-Essen, Essen, Germany. [13]Friedrich Loeffler Institute for Medical Microbiology, University Medicine Greifswald, Greifswald, Germany. [14]West German Cancer Center, University Hospital Essen, University of Duisburg-Essen, Essen, Germany. [15]Institute of Nutritional Medicine, Department of Immunology, University of Hohenheim, Stuttgart, Germany. [16]Rudolf Schönheimer Institute of Biochemistry, University of Leipzig, Leipzig, Germany. [17]Department of Surgery, Massachusetts General Hospital, Harvard Medical School, Boston, Massachusetts, USA.

Understanding tumor resistance to T cell immunotherapies is critical to improve patient outcomes. Our study revealed a role for transcriptional suppression of the tumor-intrinsic HLA class I (HLA-I) antigen processing and presentation machinery (APM) in therapy resistance. Low HLA-I APM mRNA levels in melanoma metastases before immune checkpoint blockade (ICB) correlated with nonresponsiveness to therapy and poor clinical outcome. Patient-derived melanoma cells with silenced HLA-I APM escaped recognition by autologous CD8$^+$ T cells. However, targeted activation of the innate immunoreceptor RIG-I initiated de novo HLA-I APM transcription, thereby overcoming T cell resistance. Antigen presentation was restored in interferon-sensitive (IFN-sensitive) but also immunoedited IFN-resistant melanoma models through RIG-I–dependent stimulation of an IFN-independent salvage pathway involving IRF1 and IRF3. Likewise, enhanced HLA-I APM expression was detected in *RIG-I*^{hi} (*DDX58*^{hi}) melanoma biopsies, correlating with improved patient survival. Induction of HLA-I APM by RIG-I synergized with antibodies blocking PD-1 and TIGIT inhibitory checkpoints in boosting the antitumor T cell activity of ICB nonresponders. Overall, the herein-identified IFN-independent effect of RIG-I on tumor antigen presentation and T cell recognition proposes innate immunoreceptor targeting as a strategy to overcome intrinsic T cell resistance of IFN-sensitive and IFN-resistant melanomas and improve clinical outcomes in immunotherapy.

Introduction

Cytotoxic CD8$^+$ T cells are critical mediators of clinical responses in tumor immunotherapy, killing cancer cells upon recognition of HLA class I (HLA-I) tumor antigen peptide complexes. Antigen processing and presentation requires the interplay of a complex cellular machinery involving components for antigen peptide generation (proteasome subunits LMP2, LMP7), transport (TAP1, TAP2), and loading (TAPBP) onto presenting HLA-I complexes (B2M-associated HLA-A, -B, and -C heavy chains). Genetic alterations in distinct components of the HLA-I antigen processing and presentation machinery (APM) of cancer cells can impair T cell recognition (1–10) and have recently been linked to primary and acquired resistance in immune checkpoint blockade (ICB) and adoptive T cell therapy (ACT) (4–7, 9). In contrast to genomic alterations, nongenetic mechanisms impairing HLA-I APM expression and their role in therapy resistance are still poorly understood.

Previous studies applying immunohistochemistry or proteomics revealed low HLA-I tissue expression in melanoma and other cancer types (11–13) and found it associated with poor clinical

Conflict of interest: AP reports research grant support and provision of reagents from Bristol-Myers Squibb (BMS). EMVA reports advisory relationships and consulting with Tango Therapeutics, Genome Medical, Invitae, Illumina, and Ervaxx; research support from Novartis and BMS; equity in Tango Therapeutics, Genome Medical, Syapse, Ervaxx, and Microsoft; and travel reimbursement from Roche and Genentech. JCB has received speaker honoraria, advisory board honoraria, and/or research funding from Alcedis Amgen, Boehringer Ingelheim, BMS, CureVac, eTheRNA, IQVIA, Merck Serono, Novartis, Pfizer, Sanofi, ReProTher, and 4SC. GH is a cofounder of Rigontec GmbH. KSL is a cofounder of Abalos Therapeutics. DL reports funding by a postdoctoral fellowship from the Society for Immunotherapy of Cancers, which is funded in part by an educational grant from BMS. DS declares grants, personal fees, and/or nonfinancial support from BMS, Roche, Novartis, Regeneron, Sanofi, Merck Sharp & Dohme (MSD), Amgen, 4SC, Merck-EMD, Array, Pierre-Fabre, Philogen, Incyte, and Pfizer. MS has received speaker honoraria, advisory board honoraria, and/or research funding from AstraZeneca, BMS, Boehringer Ingelheim, MSD, Novartis, Pierre Fabre, Roche, and Takeda. AS reports personal fees from Novartis Adboard. SU declares research support, speaker honoraria, advisory board honoraria, and/or travel support from BMS, Merck Serono, MSD, Novartis, and Roche.

Submitted: July 8,
Reference information: *J Clin Invest*.
https://doi.org/10.1172/JCI131572.

outcome (12, 13). This strongly suggests that patients would benefit from strategies enhancing tumor cell–intrinsic HLA-I antigen processing and presentation (14). Type I IFN (IFN-I, IFN-α/β) and type II IFN (IFN-II, IFN-γ) vigorously promote HLA-I APM gene expression via the JAK/STAT signaling pathway (15–17). Viral infections stimulate de novo IFN-I expression. This response is initiated by different innate pattern recognition receptors including the ubiquitous cytosolic RIG-I–like helicases (RLHs) RIG-I and MDA-5, both of them sensing discrete types of virus-derived double-stranded RNA (18–21). Upon ligand binding, RLHs undergo conformational changes and multimerization allowing them to associate with the adaptor protein MAVS. The latter in turn stimulates different pathways which finally activate several transcription factors including NF-κB and IRF3 (22). As a result, expression and release of IFN-β and other proinflammatory cytokines as well as chemokines are initiated, which orchestrate innate and adaptive immune responses. In tumor cells, RLHs can be activated by transfection with mimetics of viral RNA, polyI:C, and 3pRNA as ligands of MDA-5 and RIG-I, respectively (22). Intratumoral injection of synthetic RLH ligands enhances antitumor immune responses by IFN-I release in different preclinical models (23, 24). Thus, RLH activation could be a strategy to induce HLA-I APM expression in tumor cells by autocrine and paracrine IFN-I signaling. However, growing evidence suggests that melanoma as well as other tumor types acquire IFN resistance by downregulation or mutational inactivation of genes encoding crucial components of the JAK/STAT pathway, thereby avoiding antiproliferative and proapoptotic cytokine effects (4, 25–29). Recently, inactivation of IFN signaling turned out as a key mechanism in primary and acquired resistance to immune checkpoint blocking tumor therapies (4, 27–29). Moreover, it was demonstrated that JAK-STAT signaling–defective tumor cells acquire a stable T cell–resistant phenotype through HLA-I APM gene silencing (29), calling for IFN-independent strategies restoring HLA-I antigen presentation.

Here, we demonstrate that coordinated transcriptional suppression of HLA-I APM genes in melanoma is associated with primary resistance to ICB and poor clinical outcome. However, targeted activation of the immunoreceptor RIG-I overcomes HLA-I APM silencing and resensitizes melanoma cells toward autologous $CD8^+$ T cells. RIG-I triggers an IFN-independent salvage pathway allowing for de novo HLA-I APM expression even in IFN-resistant JAK-STAT signaling–defective melanoma cells. Therefore, synthetic RIG-I agonists represent a valuable therapeutic tool to enhance the susceptibility of IFN-sensitive and IFN-resistant tumors to T cell–based immunotherapies.

Results

Nonresponsiveness to anti–CTLA-4 therapy and poor clinical outcome correlate with low HLA-I APM expression in melanoma. The role of genetic defects in HLA-I APM components in resistance to immunotherapy is well accepted, while that of nongenetic abnormalities remains to be defined. Analysis of the TCGA melanoma data set (n = 462) revealed an association of shortened overall survival (OS) with low expression of HLA-I antigen processing (*LMP2*, *LMP7*, *TAP1*, *TAP2*, *TAPBP*) and presentation (*B2M*, *HLA-A*, *HLA-B*, *HLA-C*) components (Figure 1, A and B). Based on this observation, we hypothesized that melanoma cells evade T cell surveillance by coordinated transcriptional suppression of the different HLA-I APM genes, which in turn accelerates disease progression and impairs immunotherapy efficacy. To address the role of HLA-I APM downregulation in resistance to immunotherapy we performed an integrative analysis on published transcriptomic data from melanoma biopsies (n = 42) taken before anti–CTLA-4 treatment and related clinical data (30). The study cohort included 14 responders and 23 nonresponders (30). As shown in Figure 1C, tumors from ICB responders expressed higher levels of HLA-I APM components compared with nonresponders. Significant differences were observed for *B2M*, *TAP1*, and *LMP2* (*PSMB9*). None of the individual genes passed multiple hypothesis correction (Supplemental Table 1; supplemental material available online with this article; https://doi.org/10.1172/JCI131572DS1), however, all HLA-I APM genes clearly trended toward higher expression in clinical responders compared with nonresponders (2-tailed binomial P value = 0.0039). Moreover, progression-free survival (PFS) and OS were significantly prolonged in the HLA-I APM^{hi} melanoma group (Figure 1D). Overall, these data argue in favor of a functional role for transcriptional HLA-I APM suppression in ICB nonresponders, suggesting patient outcome could be improved by strategies enhancing tumor cell–intrinsic HLA-I APM expression.

Seeking such strategies, we took advantage of short-term–cultured melanoma cell lines established from consecutive biopsies of the anti–CTLA-4 nonresponder UKE-Mel-105 (Figure 1E). Tumor cells (UKE-Mel-105b, UKE-Mel-105c) were treated either with clinically applied type I IFN (IFNα-2b) or transfected with a synthetic ligand (3pRNA) of the pattern recognition receptor RIG-I. We assumed that RLH activation, as elicited in the course of a viral infection, could boost HLA-I antigen presentation. As shown in Figure 1F, IFNα-2b modestly increased HLA-I expression on UKE-Mel-105b and UKE-Mel-105c cells whereas RIG-I activation strongly enhanced HLA-I levels. Superiority of RIG-I signaling in HLA-I upregulation compared with IFN-I signaling was confirmed using different melanoma cell lines (Figure 1G).

Tumor cell–intrinsic RIG-I activation enhances HLA-I–dependent $CD8^+$ T cell recognition. To mechanistically address the effect of RIG-I signaling on HLA-I APM component expression and determine its functional significance, we applied the patient model Ma-Mel-86, consisting of Ma-Mel-86c melanoma cells, expressing the tyrosinase antigen, and autologous tyrosinase–specific CD8 T cells (3). We detected elevated levels of HLA-I and the adhesion molecule ICAM-1 (CD54) on 3pRNA-transfected Ma-Mel-86c cells in comparison to control cells treated with nonstimulatory control RNA (Figure 2, A and B). Similar results were obtained upon RIG-I activation in melanoma cells from distinct patient metastases (Supplemental Figure 1, A–C), suggesting a broader applicability of our findings.

Analysis of HLA-I APM component expression in 3pRNA-treated Ma-Mel-86c cells revealed a strong increase in *B2M*, *HLA-A*, *LMP2*, *TAP1*, *TAP2*, and *TAPBP* mRNA (Figure 2C). Upregulation of selected HLA-I APM proteins such as HLA-I heavy chains, TAP1, and LMP2 was confirmed by immunoblot. Knockdown of RIG-I before 3pRNA transfection abrogated this effect (Figure 2D). To demonstrate the functional relevance of HLA-I APM upregulation, we exposed 3pRNA- and control RNA–transfected Ma-Mel-86c cells to autologous tyrosinase–specific $CD8^+$ T cells.

The Journal of Clinical Investigation RESEARCH ARTICLE

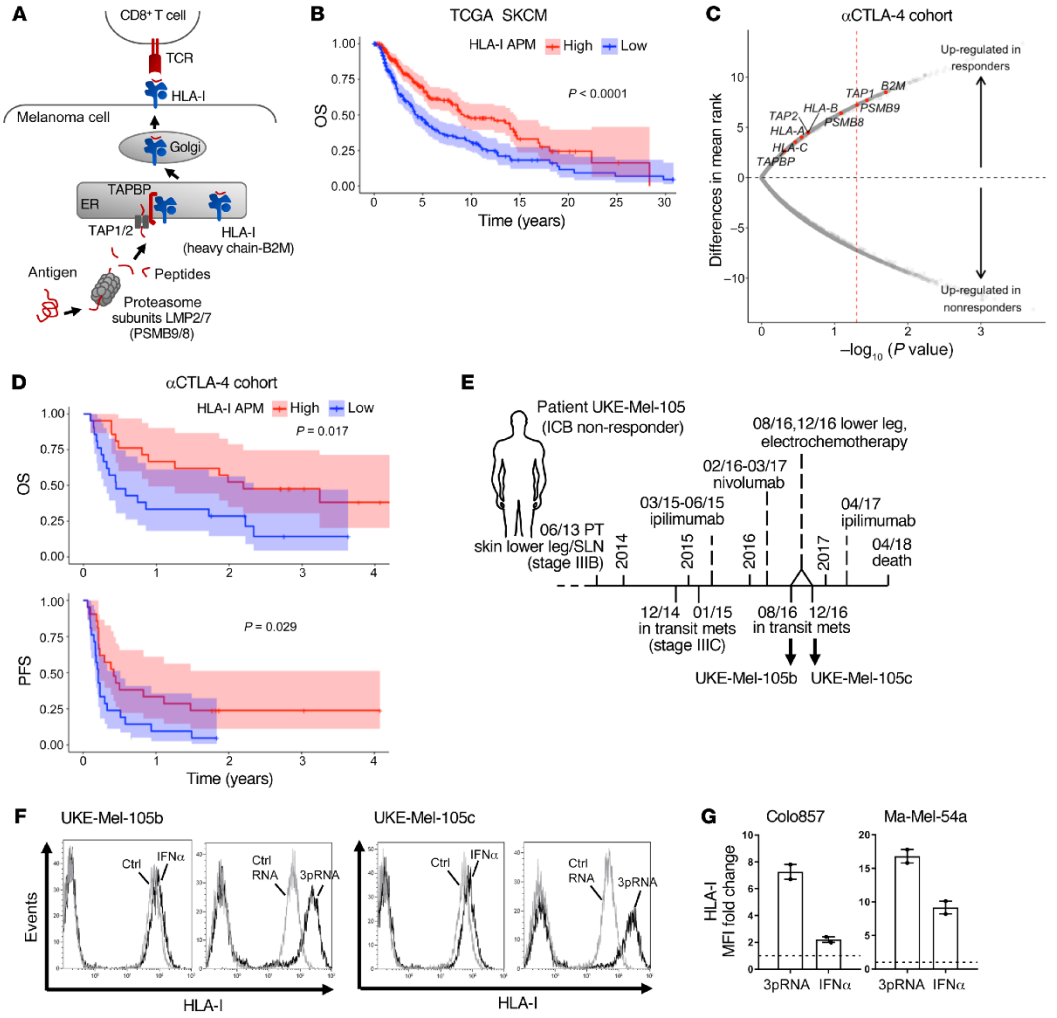

Figure 1. Low HLA-I APM expression correlates with nonresponsiveness to anti–CTLA-4 therapy and poor clinical outcome. (**A**) Schematic representation of HLA-I APM components. (**B**) Overall survival (OS) in the TCGA SKCM cohort (n = 462) stratified by high and low HLA-I APM (*HLA-A*, *HLA-B*, *HLA-C*, *B2M*, *LMP2*, *LMP7*, *TAP1*, *TAP2*, *TAPBP*) expression relative to the median, log-rank test. (**C** and **D**) Clinical relevance of altered HLA-I APM expression in an anti–CTLA-4–treated (αCTLA-4–treated) patient cohort (30). (**C**) Volcano plot showing overall upregulation of HLA-I APM genes in clinical responders (n = 14) versus nonresponders (n = 23) in the αCTLA-4–treated cohort. The x axis is the negative $\log_{10}$ value of the Mann-Whitney U P value; the y axis is the difference in mean rank between response groups. Red vertical dashed line, unadjusted P value of 0.05. (**D**) Kaplan-Meier survival curves of OS and PFS of high (n = 21) and low (n = 21) HLA-I APM expression groups, log-rank test. High and low expression groups were classified relative to the median HLA-I APM expression level in the entire cohort. (**E**) Clinical history of melanoma patient UKE-Mel-105 (ICB nonresponder). Horizontal line, time axis; above: diagnosis, therapeutic regimens, death; below: metastases development; arrows indicate cell lines established from metastases UKE-Mel-105b and UKE-Mel-105c. (**F** and **G**) Melanoma cells were transfected with 3pRNA, control (ctrl) RNA, or treated with IFNα-2a (IFNα) and subjected to further analysis following an incubation of 20 to 24 hours. HLA-I surface expression was measured by flow cytometry. (**F**) Representative histograms for UKE-Mel-105b and UKE-Mel-105c cells from 3 independent experiments. (**G**) HLA-I expression on Colo857 and Ma-Mel-54a melanoma cells. Relative MFI given as mean plus SEM, 2 independent experiments.

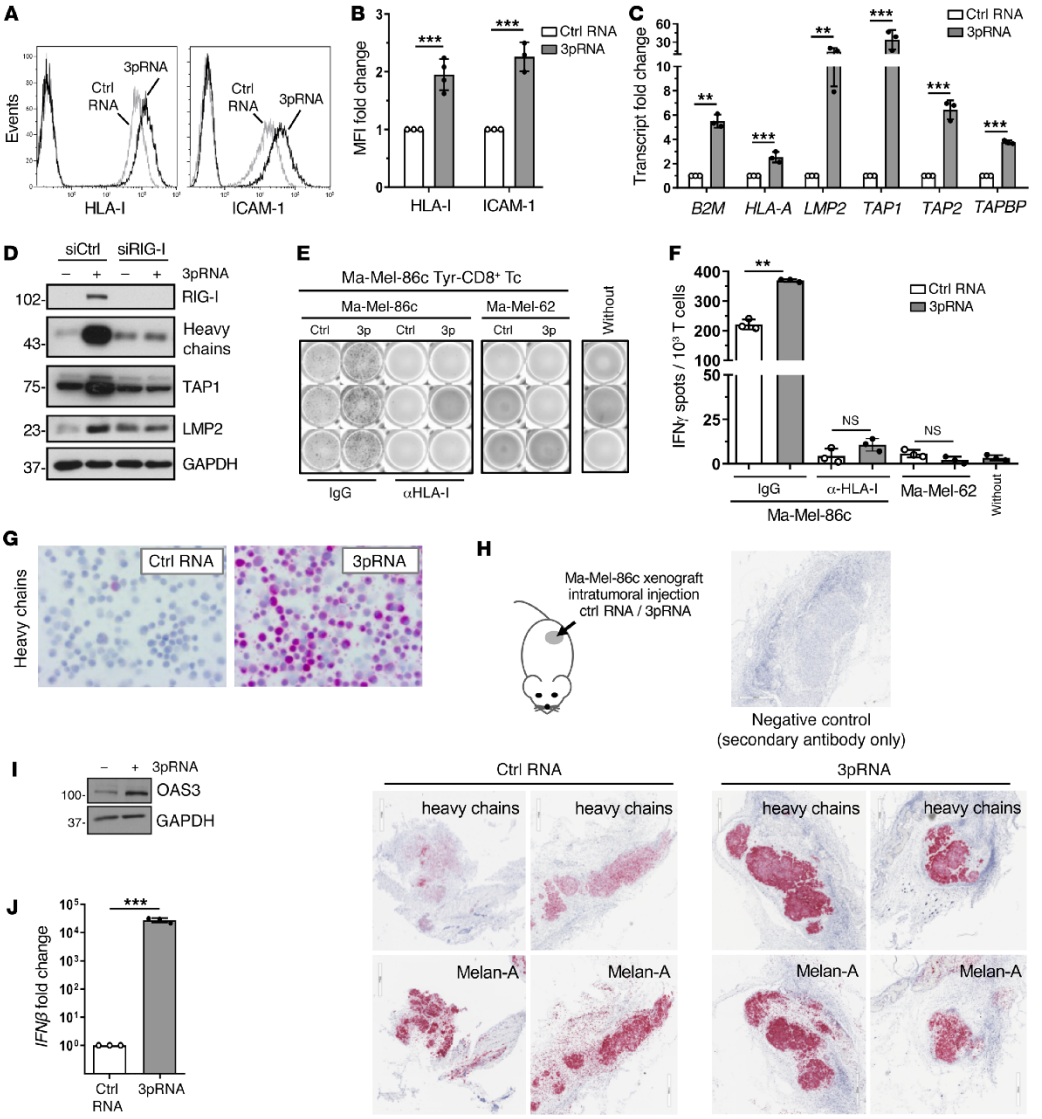

Figure 2. Targeted RIG-I activation enhances HLA-I APM expression and CD8⁺ T cell recognition of melanoma cells. (**A**–**G**, **I** and **J**) Melanoma Ma-Mel-86c cells were transfected with 3pRNA or control (ctrl) RNA and subjected to further analyses following an incubation of 20 to 24 hours. (**A** and **B**) HLA-I and ICAM-1 surface expression measured by flow cytometry. (**A**) Representative histograms, (**B**) relative MFI given as mean plus SEM from 3 independent experiments. (**C**) HLA-I APM component expression determined by qPCR. Relative expression given as mean plus SEM from 3 independent experiments. (**D**) Ma-Mel-86c cells were transfected with RIG-I (siRIG-I) or control (siCtrl) siRNA 24 hours before 3pRNA or ctrl RNA transfection and subsequently analyzed for APM component expression by immunoblot. GAPDH, loading control. Representative data from 3 independent experiments. (**E** and **F**) 3pRNA- and ctrl RNA–transfected Ma-Mel-86c cells, preincubated with blocking anti–HLA-I mAb W6/32 or control IgG, were cocultured with an autologous tyrosinase–specific CD8⁺ T cell clone (Tyr-CD8⁺ Tc). T cell activation by autologous Ma-Mel-86c and allogenic HLA-I–mismatched Ma-Mel-62 cells was determined by IFN ELISpot assay. (**E**) Representative ELISpot results and (**F**) mean IFN-γ spots (+ SEM) from 3 independent experiments. Without, T cells without tumor cells. (**G**) Representative immunocytochemical staining of Ma-Mel-86c cells for HLA-I heavy chains from 3 independent experiments. (**H**) Ma-Mel-86c tumors grown subcutaneously on NOD/SCID mice were injected once with ctrl RNA ($n = 4$) or 3pRNA ($n = 4$). After 24 hours, tumors were excised and analyzed by immunohistochemistry for expression of HLA-I heavy chains and melanoma marker Melan-A. Representative staining, original magnification ×20. (**I**) OAS3 expression analyzed by immunoblot. GAPDH, loading control. Representative data from 3 independent experiments. (**J**) *IFNβ* mRNA expression determined by qPCR. Relative expression given as mean plus SEM from 3 independent experiments. Significantly different experimental groups: $^{**}P < 0.01$, $^{***}P < 0.005$ by 2-tailed paired *t* test.

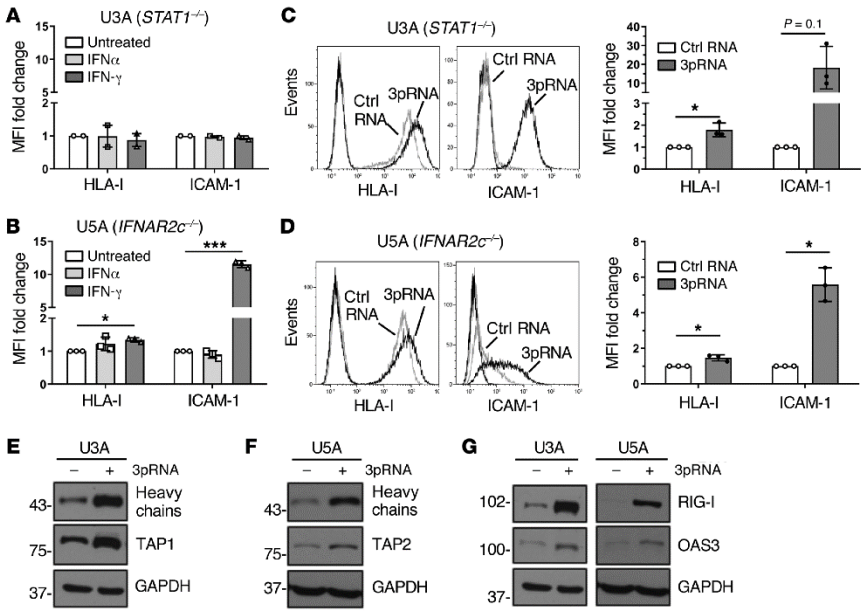

Figure 3. RIG-I upregulates HLA-I APM expression in IFN-I–resistant tumor cells. (**A** and **B**) Human fibrosarcoma cells U3A (*STAT1*$^{-/-}$) (**A**) and U5A (*IFNAR2c*$^{-/-}$) (**B**) were treated with IFNα or IFN-γ for 20 to 24 hours. Controls were left untreated. HLA-I and ICAM-1 surface expression was determined by flow cytometry. Relative MFI given as mean plus SEM of 2 (**A**) and 3 (**B**) independent experiments. (**C**–**G**) U3A and U5A cells were transfected with 3pRNA or control (ctrl) RNA and subjected to further analyses following an incubation of 20 to 24 hours. (**C** and **D**) HLA-I and ICAM-1 surface expression of U3A (**C**) and U5A (**D**) cells measured by flow cytometry. Left, representative histogram; right, relative MFI given as mean plus SEM from 3 independent experiments. (**E** and **F**) HLA-I APM component expression in U3A (**E**) and U5A (**F**) cells analyzed by immunoblot. GAPDH, loading control. Representative data from 3 independent experiments. (**G**) RIG-I and OAS3 expression in U3A and U5A cells determined by immunoblot. GAPDH, loading control. Representative data from 3 independent experiments. Significantly different experimental groups: $^{*}P < 0.05$, $^{***}P < 0.005$ by 2-tailed paired *t* test.

Cytokine release by T cells was strongly increased in the presence of 3pRNA-transfected melanoma cells (Figure 2, E and F). Studies in an independent autologous tumor T cell model confirmed this result (Supplemental Figure 2A). Enhanced T cell stimulation was HLA-I– and T cell receptor–dependent, as it was abrogated in the presence of anti–HLA-I blocking antibodies and, accordingly, could not be induced by allogenic HLA-I–mismatched 3pRNA-transfected Ma-Mel-62 melanoma cells (Figure 2, E and F; Supplemental Figure 2B).

By immunocytochemistry we confirmed the pronounced upregulation of HLA-I heavy chains in 3pRNA-transfected Ma-Mel-86c cells (Figure 2G). To determine the impact of RIG-I activation on HLA-I heavy chain expression in vivo, we transplanted Ma-Mel-86c cells subcutaneously onto immunodeficient NOD/SCID mice. On day 9, palpable melanomas were injected with 3pRNA complexed with a polyethylenimine-based carrier system already used in clinical trials for intratumoral 3pRNA administration (NCT03065023, NCT03739138). Melanomas were explanted 24 hours after treatment and analyzed for HLA-I heavy chain expression by immunohistochemistry. As shown in Figure 2H, 3pRNA-treated melanomas strongly expressed HLA-I heavy chains in contrast to tumors subjected to control RNA. Both 3pRNA and control RNA–treated Ma-Mel-86c tumors expressed comparable levels of the melanoma marker Melan-A (Figure 2H), indicating a specific effect of RIG-I activation on HLA-I heavy chains.

Aside from HLA-I APM components, RIG-I stimulation triggered its own expression (Figure 2D) and upregulated OAS3, a member of the interferon-stimulated gene (ISG) family (Figure 2I). Consistent with the observed ISG induction, de novo *IFNB* expression was detected in 3pRNA-transfected Ma-Mel-86c cells (Figure 2J), raising the question of what extent IFN-β release and subsequent autocrine IFN-I signaling contributed to the upregulation of ICAM-1 and HLA-I APM components. Indeed, treatment of Ma-Mel-86c cells with recombinant IFNα-2b increased HLA-I antigen surface expression but only slightly affected ICAM-1 levels (Supplemental Figure 2C).

RIG-I activation upregulates HLA-I APM, even in IFN-I signaling–defective tumor cells. To determine whether immunogenicity enhancement critically relies on IFN signaling, we examined the effects of RIG-I activation in IFN-I–resistant, JAK-STAT signaling–defective tumor cells, playing a key role also in primary and acquired melanoma resistance to ICB as recently demonstrated by us and others (4, 27–29).

In normal cells, IFN-I binds to the heterodimeric IFNAR1/IFNAR2 receptor complex, leading to the activation of the receptor-associated kinases TYK2 and JAK1 that in turn phosphorylate

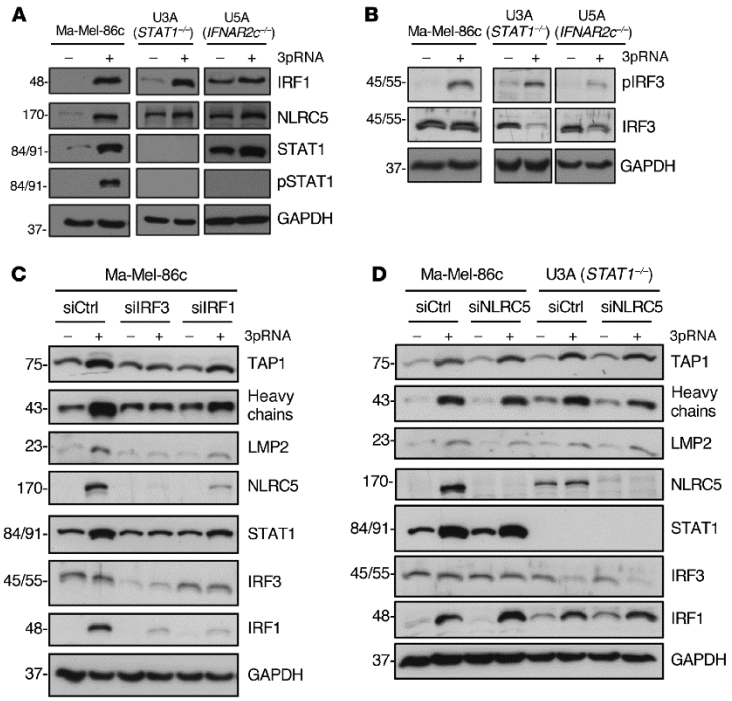

Figure 4. IRF1 and IRF3 mediate IFN-independent HLA-I APM upregulation upon RIG-I activation. (**A**–**D**) Melanoma cells Ma-Mel-86c and fibrosarcoma cells U3A (*STAT1*$^{-/-}$) and U5A (*IFNAR2c*$^{-/-}$) were transfected with 3pRNA (+) or control RNA (–) and subjected to further analysis following an incubation of 20 to 24 hours. (**A** and **B**) Representative (p)STAT1 (**A**), IRF1 (**A**), (p)IRF3 (**B**), and NLRC5 (**A**) immunoblots from 3 independent experiments. GAPDH, loading control. (**C** and **D**) Ma-Mel-86c and U3A cells were transfected with siRNA targeting IRF3 (siIRF3) (**C**), IRF1 (siIRF1) (**C**), NLRC5 (siNLRC5) (**D**), or control siRNA (siCtrl) (**C** and **D**) 24 hours before 3pRNA (+) or control RNA (–) transfection. Protein expression was analyzed by immunoblot. GAPDH, loading control. Representative data from 3 independent experiments.

STAT1 and STAT2 proteins. Phosphorylated STAT1/STAT2 heterodimers associate with IRF9, forming the DNA-binding ISGF3 complex that recruits the transcriptional machinery to initiate expression of numerous ISGs (16). To decipher the role of the JAK-STAT signaling pathway in 3pRNA-induced enhancement of HLA-I antigen presentation, we took advantage of the STAT1-deficient U3A and the IFNAR2-deficient U5A fibrosarcoma cells (31, 32). As expected, U3A (*STAT1*$^{-/-}$) cells did not respond to IFN-I (IFNα-2b) or to IFN-II (IFN-γ) treatment in terms of enhanced HLA-I and ICAM-1 expression (Figure 3A), whereas U5A (*IFNAR2c*$^{-/-}$) cells responded to IFN-II but not IFN-I (Figure 3B). Upon transfection with 3pRNA, both U3A (Figure 3C) and U5A (Figure 3D) cells upregulated HLA-I and ICAM-1 surface expression. The increase in HLA-I heavy chain and TAP1/2 protein expression was confirmed by immunoblot (Figure 3, E and F). Similarly, protein levels of OAS3 and RIG-I were enhanced by 3pRNA transfection (Figure 3G). Taken together, these data demonstrate that 3pRNA is capable of stimulating the expression of HLA-I APM and ISGs despite defective interferon signaling.

RIG-I signaling triggers HLA-I APM expression by IRF1 and IRF3. To gain insight into the molecular mechanism(s) underlying HLA-I APM upregulation, we focused our analysis on transcription factors known to be activated in response to RIG-I signaling, including IRF1, IRF3 (22, 33), and the activator of HLA-I genes, NLRC5 (34, 35). RIG-I activation led to an upregulation of IRF1, phospho-IRF3 (pIRF3), and NLRC5 in IFN-sensitive Ma-Mel-86c as well as IFN-resistant STAT1- and IFNAR-defective U3A and U5A cells, respectively, indicating the existence of a STAT1-independent RIG-I–induced signaling pathway (Figure 4, A and B).

To define the role of IRF transcription factors in HLA-I APM induction, we transfected Ma-Mel-86c cells with IRF1- or IRF3-specific siRNA before treatment with 3pRNA. IRF1 and IRF3 knockdown abrogated HLA-I APM upregulation as shown by immunoblot (Figure 4C). Furthermore, silencing of IRF1 or IRF3 blocked NLRC5 induction, suggesting a direct involvement of IRF1 and IRF3 upstream of *NLRC5* transcription. Interestingly, NLRC5 downregulation by specific siRNA did not significantly affect 3pRNA-mediated HLA-I APM upregulation in IFN-sensitive Ma-Mel-86c and IFN-resistant U3A cells, arguing against NLRC5 as a critical HLA-I APM regulator under these conditions (Figure 4D). Taken together, our data indicate an essential role for IRF1 and IRF3 in the RIG-I signaling cascade, upregulating HLA-I APM components in IFN-sensitive and IFN-resistant tumor cells.

Targeted RIG-I activation induces de novo HLA-I APM expression in IFN-resistant melanoma cells and overcomes T cell resistance. As mentioned, mutations abrogating IFN signaling in melanoma cells mediate primary and acquired resistance to T cell immunotherapy (4, 27–29). To determine the effect of RIG-I activation on HLA-I APM expression in IFN-resistant melanoma cells, we took advantage of patient model Ma-Mel-61 consisting of a set of short-term cultured melanoma cell lines (Ma-Mel-61b, Ma-Mel-61g, Ma-Mel-61h) established from consecutive metastases collected over a period of 2 years, with the latest ones, Ma-Mel-61g and Ma-Mel-61h, being JAK1 deficient (Figure 5A) (29). Accord-

The Journal of Clinical Investigation RESEARCH ARTICLE

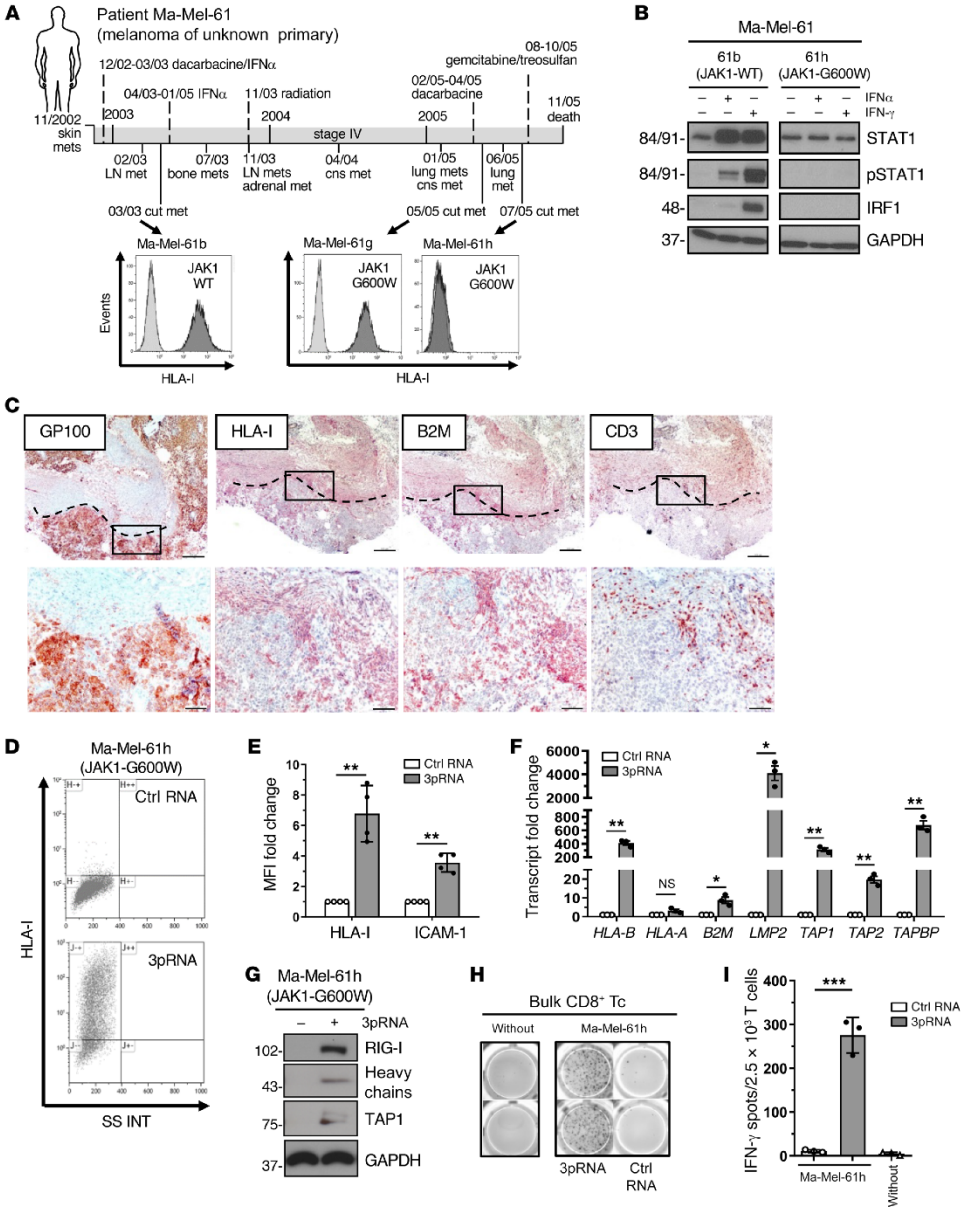

Figure 5. Targeted RIG-I activation overcomes HLA-I APM silencing in IFN-I–resistant melanoma cells and restores T cell sensitivity. (**A**) Clinical history of melanoma patient Ma-Mel-61. Horizontal line, time axis; above: diagnosis, therapeutic regimens, death; below: metastases development; arrows indicate cell lines established from metastases Ma-Mel-61b (JAK1-wildtype, JAK1-WT), Ma-Mel-61g (JAK1-mutant, JAK1-G600W) and Ma-Mel-61h (JAK1-mutant, JAK1-G600W). HLA-I surface expression on cell lines established from corresponding lesions was determined by flow cytometry. Representative histograms from 3 independent experiments. (**B**) Cell lines treated with IFNα-2b or IFN-γ for 48 hours were analyzed for (p) STAT1 and IRF1 expression by immunoblot. GAPDH, loading control. Representative data from 3 independent experiments. (**C**) Immunohistochemical staining of serial cryostat tissue sections from metastasis Ma-Mel-61g for melanoma marker GP100, HLA-I, B2M, and CD3. Top, tumor margin indicated by the dotted line; bottom, higher magnification of boxed regions; original magnifications: ×2.5 (top), ×10 (bottom). (**D–I**) Ma-Mel-61h cells were transfected with 3pRNA or control (ctrl) RNA and subjected to further analysis following an incubation of 20 to 24 hours. (**D** and **E**) HLA-I and ICAM-1 surface expression measured by flow cytometry. (**D**) Representative HLA-I dot plot and (**E**) relative MFI given as mean plus SEM from 3 independent experiments. (**F**) mRNA expression of APM components analyzed by qPCR. Relative expression given as mean plus SEM from 3 independent experiments. (**G**) Expression of indicated proteins analyzed by immunoblot. GAPDH, loading control. Representative data from 3 independent experiments. (**H** and **I**) Activation of autologous $CD8^+$ T cells by Ma-Mel-61h cells determined by IFN-γ ELISpot assay. (**H**) Representative ELISpot, (**I**) mean IFN-γ spots (+ SEM) from 3 independent experiments. without, incubation of T cells without tumor cells. Significantly different experimental groups: $^*P < 0.05$, $^{**}P < 0.01$, $^{***}P < 0.005$ by 2-tailed paired *t* test.

ingly, IFN signaling was intact only in early Ma-Mel-61b but not in immunoedited JAK1-G600W mutant Ma-Mel-61g and Ma-Mel-61h cells (Figure 5B, Supplemental Figure 3A). Aside from defective IFN signaling, Ma-Mel-61h cells lacked HLA-I surface expression (Figure 5A) due to the coordinated silencing of HLA-I APM genes (29). Previous analyses of corresponding tumor tissue by immunohistochemistry found IHLA-I–negative melanoma cells to be present in both metastasis Ma-Mel-61h and Ma-Mel-61g (29), and tissue staining for B2M confirmed in vivo silencing of distinct HLA-I APM genes in IFN-resistant melanoma cells from patient Ma-Mel-61 (Figure 5C).

We concluded that loss-of-function mutation of *JAK1* enabled Ma-Mel-61h cells to preserve their immune-evasive HLA-I–negative phenotype in the presence of interferons (Supplemental Figure 3B) (29). Strikingly, targeted activation of RIG-I restored IHLA-I expression in IFN-resistant Ma-Mel-61h cells (Figure 5, D and E). Quantification of HLA-I APM component expression by qPCR revealed de novo transcription of genes including *HLA-B*, *B2M*, *LMP2*, *TAP1*, *TAP2*, and *TAPBP* (Figure 5F). De novo expression of HLA heavy chains and TAP1 was further confirmed at the protein level (Figure 5G). Restoration of HLA-I antigen presentation in response to 3pRNA transfection resensitized Ma-Mel-61h cells toward autologous CD8 T cells (Figure 5, H and I), indicating tumor cell–intrinsic RIG-I signaling bypassed defective IFN signaling to overcome HLA-I APM silencing and T cell resistance.

RIG-I activation enhances $CD8^+$ T cell recruitment. Previous studies demonstrated that IHLA-I–negative melanoma lesions lack T cell infiltrates (36). Accordingly, $CD3^+$ T cells were primarily located within HLA-I–positive regions of metastasis Ma-Mel-61g, while HLA-I–negative areas were largely devoid of T cells (Figure 5C). Since RLH signaling induces expression of T cell–recruiting chemokines (37, 38), we asked to which extent chemokine release was retained in IFN-resistant Ma-Mel-61g cells. Besides enhanced HLA-I APM expression (Figure 6A, Supplemental Figure 4A), 3pRNA-transfected Ma-Mel-61g cells induced de novo transcription of *IFNβ* (Supplemental Figure 4B) and specific chemokine genes (*CCL2*, *CCL4*, *CCL5*, *CXCL10*) (Figure 6B). The strongest enhancement was observed for *CCL5* and *CXCL10*, and their release was confirmed by ELISA (Figure 6C). Accordingly, conditioned media (CM) of 3pRNA-transfected Ma-Mel-61g cells, in contrast to CM of control RNA-transfected cells, led to enhanced migration of autologous $CD8^+$ T cells in a Boyden chamber assay (Supplemental Figure 4, C and D), indicating that functionally relevant chemokine release could be induced by 3pRNA even if melanoma cells lost their IFN signaling competence.

To study the recruitment of autologous T cells in an in vivo model, we transplanted Ma-Mel-86c cells onto the chorioallantoic membrane (CAM) of fertilized chicken eggs (Figure 6D). Melanoma cells were applied on 2 distant sites of each CAM. Tumors formed within 4 days were treated with jetPEI-complexed 3pRNA or control RNA. Autologous $CD8^+$ T cells were injected into the blood vessels of the embryo on the following day (Figure 6D). As shown in Figure 6E, 3pRNA-treated Ma-Mel-86c tumors showed marked HLA-I upregulation and enhanced $CD8^+$ T cell infiltration in contrast to tumors treated with control RNA.

Taken together, the significant and biologically relevant upregulation and even de novo induction of HLA-I APM components by 3pRNA in an IFNAR2-, JAK1-, and STAT1-independent but RIG-I–dependent manner indicates the existence of an IFN-independent salvage pathway capable of restoring melanoma immunogenicity and inducing T cell recruitment.

Correlation of RIG-I expression with improved antigen presentation and T cell activation in melanoma tissues. The striking effect of RIG-I activation on antigen presentation, T cell recognition, and T cell recruitment in different IFN-sensitive and IFN-resistant patient-derived melanoma models prompted us to extend our investigations to melanoma tissue samples. Analyzing transcriptomic data of the TCGA SKCM cohort ($n = 462$), we found HLA-I APM genes (*HLA-B*, *HLA-C*, *TAP1*, *TAP2*, *TAPBP*, *B2M*, *PSMB8*, *PSMB9*) to be differentially expressed in *RIG-I*^{hi} (*DDX85*^{hi}) and *RIG-I*^{lo} (*DDX58*^{lo}) tumors (Figure 7A). In addition to HLA-I APM components, *RIG-I* (*DDX58*) levels strongly correlated with T cell–recruiting chemokines (*CCL5*, *CXCL10*), markers of T cell infiltration (*CD8A*), and T cell cytotoxicity (*GZMA*, *GZMB*, *PRF1*) (Table 1). Integrative analyses of transcriptomic and annotated clinical data revealed a significant improvement in overall survival for patients with *RIG-I*^{hi} (*DDX58*^{hi}) tumors compared with *RIG-I*^{lo} (*DDX58*^{lo}) tumors (Figure 7B). The impact on survival was even more pronounced when tumors were segregated based on high and low expression of *RIG-I* (*DDX58*) pathway genes (*DDX58*, *IRF1*, *IRF3*) (Figure 7B). Overall, these data demonstrate a linkage between HLA-I APM expression and *RIG-I* (*DDX58*) expression in melanoma patient tumors, confirming our in vitro findings and favoring RIG-I as a valuable druggable therapeutic target to restore melanoma immunogenicity.

Targeted RIG-I activation synergizes with ICB in T cell stimulation. Finally, we addressed the effect of combined ICB and

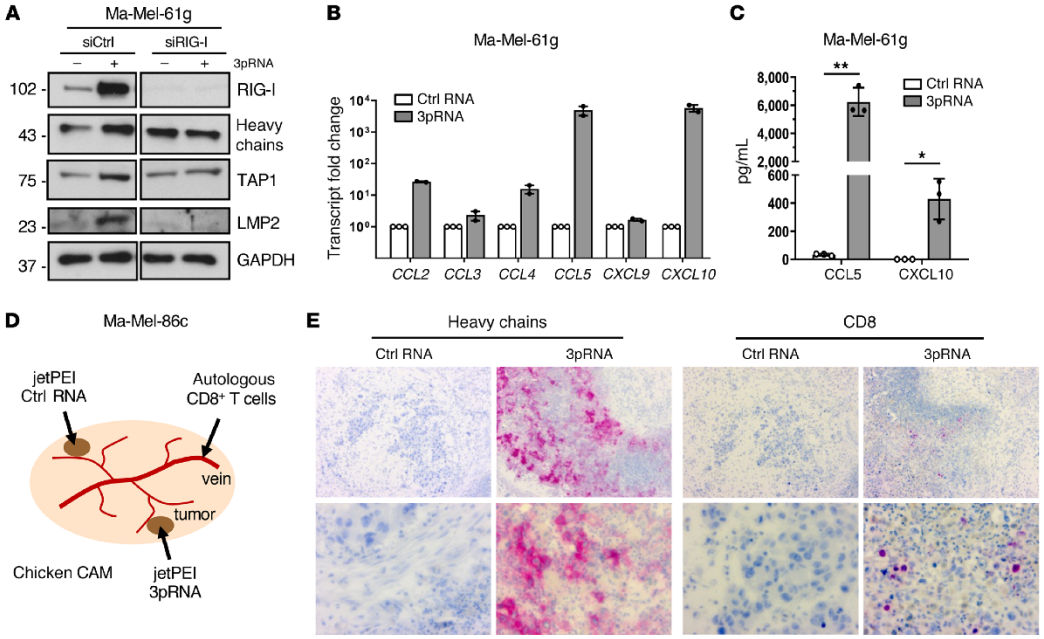

Figure 6. IFN-I–independent chemokine release and CD8⁺ T cell recruitment in response to RIG-I signaling. (**A**–**C**) Ma-Mel-61g cells were transfected with 3pRNA or control (ctrl) RNA and subjected to further analyses following an incubation of 20 to 24 hours. (**A**) Ma-Mel-61g cells were transfected with RIG-I siRNA (siRIG-I) or control siRNA (siCtrl) 24 hours before 3pRNA or ctrl RNA transfection and subsequently analyzed for protein expression by immunoblot. GAPDH, loading control. Representative data from 3 independent experiments. (**B**) Chemokine mRNA expression determined by qPCR. Relative expression given as mean plus SEM from 2 independent experiments. (**C**) Cell culture supernatants were analyzed for CCL5 and CXCL10 content by ELISA. Chemokine levels given as mean plus SEM from 3 independent experiments. Significantly different experimental groups: $^{*}P < 0.05$, $^{**}P < 0.01$ by 2-tailed paired *t* test. (**D**) Schematic representation of the chicken CAM model. Ma-Mel-86c cells transplanted onto 2 distant sites of each CAM, autologous tumor–reactive CD8⁺ T cells injected into accessible vein. (**E**) Human Ma-Mel-86c tumors grown on chicken CAM were analyzed by immunohistochemistry. The 2 tumors on each CAM were treated with either 3pRNA ($n = 4$) or ctrl RNA ($n = 4$) on 2 consecutive days. At 24 hours after RNA application, autologous T cells were injected into the blood vessels of the embryo. Tumors were harvested 20 hours after T cell injection. Representative CD8 and HLA-I heavy chain staining shown for each group; original magnifications: ×10 (top), ×40 (bottom).

RIG-I–driven HLA-I APM upregulation on T cell reactivity toward autologous melanoma cells. Here, we took advantage of patient model UKE-Mel-154, a nonresponder to anti–PD-1 therapy (Figure 8A). Tumor cells (UKE-Mel-154c) from a lymph node metastasis of this patient, excised before anti–PD-1 treatment, showed a HLA-I^{lo} phenotype (Figure 8B), suggesting impaired antigen presentation contributed to primary ICB resistance. Consistent with this finding, we observed an association between transcriptional HLA-I APM suppression and therapy resistance in a cohort of melanoma patients receiving anti–PD-1 ICB ($n = 121$) (39). Analyses of the recently published transcriptomic data from pre–anti-PD-1 melanoma biopsies revealed a trend toward lower HLA-I APM component expression in anti–PD-1 nonresponders ($n = 62$) compared with responders ($n = 37$) (2-tailed binomial P value = 0.039) (Figure 8C; Supplemental Table 2), similar to anti–CTLA-4 ICB (Figure 1C). In biopsies of both the anti–PD-1 and anti–CTLA-4 patient cohorts, we detected a strong correlation between expression of *RIG-I* (*DDX58*) pathway genes and HLA-I APM genes (rho = 0.81 for anti–CTLA-4, rho = 0.815 for anti–PD-1; Figure 8, D and E), nominating 3pRNA as a drug to overcome HLA-I APM downregulation. In line with this, tumor cells from ICB nonresponder UKE-Mel-154 acquired a HLA-I^{hi}/ICAM-1^{hi} phenotype upon 3pRNA transfection (Figure 8B; Supplemental Figure 5A). Messenger RNA levels of the distinct HLA-I APM components and *IFNβ* followed the same response pattern (Supplemental Figure 5, B and C). In addition to enhanced HLA-I antigen presentation, we detected a strong upregulation of PD-L1 (Figure 8, F and G). Interestingly, phenotype analyses of corresponding autologous CD8⁺ tumor infiltrating lymphocytes (TILs) revealed positivity not only for PD-1 but also for TIGIT (Figure 8, A and H), another inhibitory checkpoint of tumor antigen–specific T cells currently targeted with blocking antibodies in different clinical trials (40). The TIGIT ligand CD155 (PVR) was highly expressed on UKE-Mel-154c cells and remained stable upon 3pRNA transfection (Figure 8, F and G).

Based on these data, we examined the influence of combined 3pRNA/anti–PD-1 ICB and 3pRNA/anti-TIGIT ICB on CD8⁺ TIL reactivity toward UKE-Mel-154c cells. To this end, TILs were coincubated with 3pRNA- and control RNA–treated melanoma cells

Table 1. Differentially expressed HLA-I APM and immune effector genes in high versus low *RIG-I* (*DDX58*) expression groups of the TCGA SKCM cohort

Gene	Log fold change	Adjusted *P* value
HLA-B	1.71	5.16×10^{-37}
HLA-C	1.32	4.53×10^{-45}
B2M	1.45	2.44×10^{-36}
TAP1	1.36	5.54×10^{-26}
PSMB8	1.08	6.80×10^{-45}
PSMB9	1.62	5.21×10^{-30}
CCL5	1.98	3.71×10^{-21}
CXCL10	3.40	2.97×10^{-40}
CD8A	2.31	2.08×10^{-18}
CD8B	2.48	1.71×10^{-20}
GZMA	2.30	3.79×10^{-23}
GZMB	2.16	1.74×10^{-18}
PRF1	1.83	8.23×10^{-16}

Groups were defined relative to median *RIG-I* (*DDX58*) expression in the TCGA SKCM cohort.

in the absence or presence of anti–PD-1 and anti-TIGIT blocking antibodies. After 4 hours of incubation, intracellular cytokine staining (ICS) showed a strong increase in $CD8^+$ T cell activation in the presence of 3pRNA-transfected UKE-Mel-154c cells compared with control RNA–treated tumor cells (Figure 8I). TIL responses toward 3pRNA-treated UKE-Mel-154c cells could be significantly enhanced when blocking anti–PD-1 and anti-TIGIT antibodies were added, indicating a synergistic effect of targeted RIG-I activation and ICB (Figure 8I). Improvement of T cell activation by anti–PD-1 ICB was achieved only in the presence of 3pRNA- but not control RNA–transfected tumor cells (Figure 8I), most likely attributable to the strong upregulation of PD-L1 upon RIG-I activation (Figure 8, F and G). In contrast, anti-TIGIT ICB significantly improved $CD8^+$ T cell activation under both conditions (Figure 8I), due to constant high CD155 expression on UKE-Mel-154c cells (Figure 8, F and G).

In addition to concurrent treatment, we tested a sequential protocol of ICB and targeted RIG-I activation (Figure 8J). Initially, TILs were cocultured with irradiated UKE-Mel-154c cells in the absence or presence of anti–PD-1 and anti-TIGIT blocking antibodies. After an incubation period of 7 days, T cells were harvested and analyzed for their reactivity toward 3pRNA- and control RNA–transfected melanoma cells. Again, we observed a strong T cell activation only in the presence of 3pRNA- but not control RNA–transfected UKE-Mel-154c cells. Preincubation with anti–PD-1 and anti-TIGIT blocking antibodies clearly increased the fraction of TILs responding to 3pRNA-treated tumor cells, though significance was achieved only in the 3pRNA/anti-TIGIT setting (Figure 8J).

In summary, studies in the anti–PD-1 nonresponder melanoma model clearly demonstrated synergistic effects of HLA-I APM restoration by targeted RIG-I activation and ICB on antitumor T cell responses, suggesting combination therapy could improve clinical outcomes.

Discussion

Loss-of-function genetic alterations affecting tumor antigen presentation (4, 6, 7, 9) and IFN-γ signaling (4, 27–29) have recently been identified as key resistance mechanisms to ICB in different cancers. Studies applying CRISPR/Cas9 for tumor genome editing recapitulated those findings in mouse melanoma models, demonstrating that the efficacy of T cell–based therapy critically depends on intact antigen presentation and IFN-γ signaling (41, 42). Here, we provide evidence that, aside from genetic alterations, resistance of melanoma to ICB and T cells can be attributed to the coordinated transcriptional suppression of a gene set involved in antigen peptide generation (*LMP2*, *LMP7*), transport (*TAP1*, *TAP2*), and loading (*TAPBP*) onto presenting HLA-I complexes (*HLA-A*, *HLA-B*, *HLA-C*, *B2M*). We introduce tumor cell–intrinsic activation of the pattern recognition receptor RIG-I as a strategy to restore antigen processing and presentation and overcome T cell resistance independent of IFN signaling.

The association of low HLA-I APM mRNA levels and poor patient survival in melanoma prompted us to investigate the role of HLA-I APM downregulation in the outcome of immunotherapy. Analyzing a cohort of anti–CTLA-4–treated melanoma patients, we found low HLA-I APM levels associated with primary therapy resistance and shortened PFS and OS, indicating initial and durable clinical responses to this therapy require intact antigen processing and presentation. In line with our observation, a prior immunohistochemistry study correlated loss of melanoma membrane HLA-I expression with resistance in anti–CTLA-4 therapy (43). Moreover, we found the HLA-I APM^{lo} tumor cell phenotype involved in primary resistance to anti–PD-1 therapy. Analysis of recently published transcriptomic data from pretreatment biopsies of a patient cohort receiving anti–PD-1 ICB revealed lower expression of HLA-I APM components in nonresponders compared with responders.

Aside from primary resistance, acquired resistance in adoptive T cell therapy (ACT) of melanoma (44) and anti–PD-1 ICB/ACT of Merkel cell carcinoma (45, 46) has recently been linked to the downregulation of single or multiple HLA-I APM components. Though the latter studies comprised only single patients, the total data suggest a cancer-overarching relevance of nongenetic HLA-I APM alterations in resistance to different types of T cell–based therapy.

Taking advantage of different melanoma patient models, we provide evidence for the functional relevance of transcriptional HLA-I APM suppression. Our data show that patient-derived melanoma cells with silenced HLA-I APM are resistant toward cognate autologous $CD8^+$ T cells. Seeking counteracting mechanisms, we demonstrated that tumor cell–intrinsic activation of the immunoreceptor RIG-I by its synthetic ligand 3pRNA induces de novo transcription of HLA-I APM genes, thereby overcoming T cell resistance. Consistently, a remarkable increase in HLA-I surface expression of 3pRNA-treated tumor cells going along with a strong enhancement in T cell activation was detected in different patient models. The HLA-I^{lo} to HLA-I^{hi} phenotypic switch could also be induced in vivo upon 3pRNA injection into human melanomas subcutaneously grown on NOD/SCID mice, using a clinical applied carrier system for dsRNA delivery.

Since RIG-I triggers IFN-I release, we initially expected the restoration of antigen presentation to be dependent on autocrine and

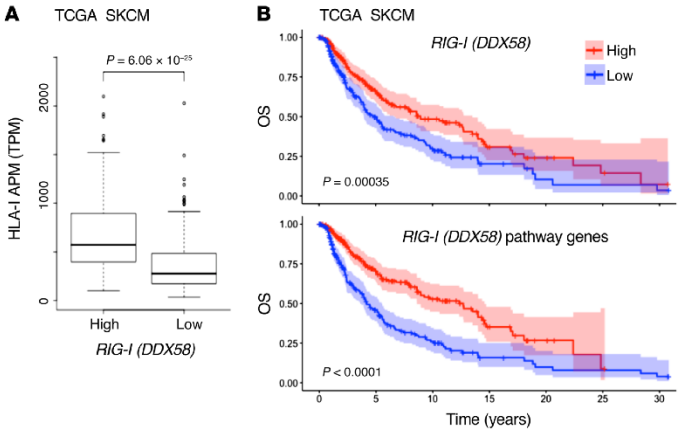

Figure 7. *RIG-I* (*DDX58*) expression in melanoma correlates with HLA-I APM expression and patient survival. (**A**) HLA-I APM expression in high and low *RIG-I* (*DDX58*) expression groups relative to the median *RIG-I* (*DDX58*) expression level in the TCGA SKCM cohort. Mann-Whitney *U* *P* value is shown. (**B**) Overall survival in the TCGA SKCM cohort (n = 462) stratified by high and low expression of *RIG-I* (*DDX58*) (top) and *RIG-I* (*DDX58*) pathway genes (bottom) relative to the median. Log-rank *P* value shown.

paracrine IFN-I signaling in melanoma cells. Strikingly, RIG-I activation also allowed for de novo HLA-I APM transcription in IFN-I–resistant JAK1-deficient melanoma cells, indicating RLH-dependent stimulation of an IFN-I–independent salvage pathway, which resensitized tumor cells to T cells. In addition to demonstrating activation of the salvage pathway in JAK1 mutants, we also demonstrated activation of the salvage pathway in IFNAR2- and STAT1-deficient tumor cells. Previous studies, including our own, showed that a subset of melanomas acquires inactivating genetic alterations in different IFN-I and IFN-II signaling pathway components, contributing to primary and acquired ICB resistance (4, 27–29). Here, we demonstrate that IFN-I/IFN-II–resistant melanomas can still be forced to upregulate HLA-I APM expression in order to enhance responsiveness to immunotherapy.

To unravel the underlying mechanism we screened IFN-sensitive and IFN-resistant cell lines for RIG-I–controlled transcription factors and found IRF1, IRF3, and NLRC5 to be upregulated in all cases. NLRC5 is a known transcriptional activator of *HLA-I*, *TAP*, and *LMP* genes (34, 35) and its loss has been associated with cancer immune evasion (47). In the course of viral infection, RIG-I activation induces NLRC5 expression, mediating HLA-I upregulation (35). In our experimental setting however, siRNA knockdown of NLRC5 had no major impact on HLA-I APM upregulation by 3pRNA. In contrast, ablation of IRF1 or IRF3 by siRNA abrogated the effect. While activation of IRF3 downstream of RIG-I/MAVS signaling is well established, the connection to IRF1 is less studied (22, 33, 48). Both IRF1 and IRF3 have been implicated in the IFN-I–independent induction of virus defense genes (33, 49). Our study now extends this mechanistic link to genes coding for HLA-I APM components and T cell activation in tumor cells. Also, de novo expression of chemokines, attracting $CD8^+$ T cells into transplanted autologous tumors in a chicken CAM model, efficiently occurred in a RIG-I–dependent but IFN-I–independent manner.

Consistent with our observations from distinct in vivo and patient models, we detected enhanced expression of chemokines, HLA-I APM genes, and markers of T cell activation in *RIG-I*^{hi} (*DDX58*^{hi}) melanomas of the TCGA sample collection, further emphasizing the clinical relevance of our findings. Moreover, melanoma biopsies from anti–PD-1– and anti–CTLA-4–treated patient cohorts showed a strong correlation between expression of *RIG-I* (*DDX58*) pathway genes and HLA-I APM genes, nominating RIG-I as a druggable therapeutic target. Recent mouse model studies demonstrated that targeted RLH activation in the tumor microenvironment can transform a T cell–deficient melanoma metastasis into a T cell–inflamed lesion and enhance the efficacy of anti–CTLA-4 and anti–PD-1 therapies (23, 50–52). Notably, HLA-I APM^{lo} patient tumors lack T cell infiltrates (11, 36) and absence of T cells in melanoma lesions has been described as a primary resistance mechanism in ICB (53, 54). Thus, injection of synthetic RIG-I ligands into accessible lesions of cancer patients could be a promising strategy to achieve both an increased infiltration of T cells into tumors and enhanced T cell recognition of tumor cells, which could improve clinical responses in ICB. In fact, we demonstrated that HLA-I APM upregulation by 3pRNA and checkpoint blocking antibodies synergistically enhanced the reactivity of $CD8^+$ TILs toward autologous melanoma cells in an anti–PD-1 nonresponder model. Synergism was observed not only for combined 3pRNA/anti–PD-1 but also 3pRNA/anti-TIGIT treatment, in line with the positivity of TILs for PD-1 and TIGIT and with the expression of their ligands on melanoma cells. These findings provide a strong rational for already ongoing clinical trials combining intratumoral injection of synthetic RLH ligands (NCT03739138, NCT02828098, NCT02423863) with anti–PD-1 or anti–PD-L1 antibodies.

Recent studies demonstrated RLH activation by dsRNA derived from human endogenous retrovirus (hERV) transcripts, reexpressed in different cancers and associated with improved patient outcome (55–57). Our data from analyses on patient-derived tumor cells and melanoma biopsies indicate a clear benefit from direct targeting of RIG-I by optimized synthetic ligands in order to achieve efficient HLA-I APM induction. So far, RLH ligands are complexed with specific carrier systems and injected into accessible patient lesions, which induces not only local but also systemic immune responses (58). However, therapy efficacy would benefit from delivery of dsRNA to distant (micro)metastases, clearly demanding for the development targeted carrier systems such as antibody-coupled nanoparticles (59, 60).

Overall, our study links transcriptional HLA-I APM suppression in melanoma to primary resistance in anti–CTLA-4 and anti–PD-1 therapy. Tumor cell–intrinsic activation of the innate immune receptor RIG-I restores antigen processing and presentation and overcomes resistance to autologous $CD8^-$ T cells. Though HLA-I APM upregulation is generally thought to be IFN-dependent, RIG-I efficiently induces de novo HLA-I APM expression even in IFN-resistant tumor cells. Our findings, which demonstrate synergistic effects on antitumor T cell responses of combined RIG-I activation and ICB, suggest that targeted tumor cell–intrinsic RLH activation presents a potent strategy to enhance the efficacy of immunotherapies in metastasized IFN-sensitive and IFN-resistant melanoma and other neoplasia.

Methods

Tumor cells. Melanoma cell lines were established at the Department of Dermatology (University Hospital Essen, Essen, Germany) from surgically resected, mechanically dissected tumor tissues, as previously described (3, 29). Melanoma cells (Ma-Mel-47, Ma-Mel-54a, Ma-Mel-61b, Ma-Mel-61g, Ma-Mel-61h, Ma-Mel-62, Ma-Mel-66b, Ma-Mel-86c, UKE-Mel-105b, UKE-Mel-105c, UKE-Mel-154c) were authenticated by genetic profiling on genomic DNA at the Institute for Forensic Medicine (University Hospital Essen) using the AmpFLSTR-Profiler Plus kit (Applied Biosystems). Fibrosarcoma cell lines U3A and U5A (31, 32) and melanoma cells were cultured in RPMI1640 medium or DMEM (Gibco) with glutamine and confirmed to be mycoplasma-free in monthly intervals. Both media were supplemented with 10% (vol/vol) fetal calf serum (PAA Laboratories), 100 U/mL penicillin, and 100 μg/mL streptomycin. All cells were maintained at 5% CO_2, 37°C.

T cells. Tumor-reactive bulk $CD8^+$ T cells and tumor antigen–specific CD8 T cell clones from peripheral blood of patients Ma-Mel-86 and Ma-Mel-61 were established as previously described (3, 29). TILs were isolated from tumor single-cell suspensions of lymph node metastasis UKE-Mel-154c using the gentleMACS Dissociator (Miltenyi Biotec) for tumor digestion. $CD8^+$ TILs were positively selected from single-cell suspension using anti-CD8 beads (Miltenyi Biotec). Selected TILs (10^6 cells/well of 24-well plate) were cocultured with irradiated (100 Gy) autologous UKE-Mel-154c melanoma cells (10^5 cells/well) in 2 mL AIM-V medium (Gibco-BRL) supplemented with 10% (vol/vol) human AB serum (complete medium). Interleukin-2 (IL-2) was added on day 3 at 250 IU/mL (Chiron Corporation). TILs (10^6 cells/well) were restimulated in weekly intervals with 10^5 irradiated tumor cells in IL-2–supplemented complete medium. All cells were maintained at 5% CO_2, 37°C.

Mice. Ma-Mel-86c cells (2×10^6 cells) were injected subcutaneously into the left flank of 6- to 12-week-old NOD/SCID mice (Jackson Laboratory). On day 9 after inoculation, tumors with a volume of approximately 50 mm^3 were injected with 50 μg control RNA or 3pRNA complexed with in vivo-jetPEI (Polyplus), according to the manufacturer's protocol. After 24 hours, mice were sacrificed and tumors were collected, formalin-fixed, and paraffin-embedded for subsequent analysis by immunohistochemistry.

IFN treatment. Tumor cells (1×10^5 to 2×10^5 cells/well) were seeded in 6-well culture plates 16 to 20 hours before treatment with IFNα-2b (1000 IU/mL Roferon-A, Roche) or IFN-γ (500 IU/mL Imukin, Boehringer Ingelheim). Control cells were left untreated. Following an incubation of 20 to 24 hours at 37°C, cells were subjected to further analyses.

Synthesis of 3pRNA. For generation of DNA template–dependent in vitro–transcribed RNA (3pRNA), the T7-promoter region 5′-CAGTAATACGACTCACTATAG-3′ was hybridized with the promoter + template strand (5′-TTGTAATACGACTCACTATAGGGACGCTGACCCAGAAGATCTACTAGAAATAGTAGATCTTCTGGGTCAGCGTCCC) and directly used as a template for in vitro transcription reactions. 3pRNA was provided by Christoph Coch and Gunther Hartmann, (Institute of Clinical Chemistry and Clinical Pharmacology, University of Bonn, Bonn, Germany). Nonstimulatory control RNA (5′-CACACACACACACACACA-3) was purchased from Biomers.

3pRNA and siRNA transfection. Tumor cells (1×10^5 to 2×10^5 cells/well) were seeded in 6-well culture plates 16 to 20 hours before transfection with 100–200 ng/mL 3pRNA or control (ctrl) RNA, using Lipofectamine 2000 (Invitrogen). Where indicated, tumor cells were transfected with siRNA (10 nM) specific for IRF1, IRF3, NLRC5, or control siRNA (Dharmacon) using Viromer blue (Lipocalyx) 20 to 24 hours before 3pRNA or ctrl RNA (200 ng/mL) treatment. All transfections were performed according to the manufacturer's instructions. Cells were subjected to further analyses following an incubation of 20 to 24 hours at 37°C.

Antibodies for immunoblot, immunocytochemistry, and immunohistochemistry. The following anti-human antibodies were used for immunoblot: mouse anti-STAT1 (clone 9H12), rabbit anti-phospho STAT1 (Y701) (clone 58D6), rabbit anti-phospho IRF3 (S396) (clone 4D4G), rabbit anti-GAPDH (clone 14C10), rabbit anti–RIG-I (clone D14G6) were purchased from Cell Signaling; rabbit anti-IRF1 (clone H-205), rabbit anti-IRF3 (clone FL-425), rabbit anti-OAS3 (clone M-190) were obtained from Santa Cruz. TAP1 was detected with mouse mAb NOB-1 (61) and LMP2 with mouse mAb SY-1 (61). Both antibodies were provided by Soldano Ferrone (Department of Surgery, Massachusetts General Hospital, Harvard Medical School, Boston, Massachusetts, USA). NLRC5 was detected with rat mAb 3H8 (62), provided by Thomas A. Kufer (Institute of Nutritional Medicine, Department of Immunology, University of Hohenheim, Stuttgart, Germany). Mouse mAb HC10 (recognizing an epitope on specific B2M-free HLA-A and all B2M-free HLA-B and -C heavy chains) from Nordic-MUbio was used for immunoblots, immunocytochemistry, and staining of formalin-fixed paraffin-embedded (FFPE) tissue sections. Mouse anti-human Melan-A/MART-1 (clone M2-7C10) for FFPE tissue staining was purchased from von Zytomed. Additionally, cryostat tissue sections were stained with mouse antibodies specific for GP100 (clone HMB-45, Dako), HLA-I antigen complexes (clone W6/32, Dianova), B2M (clone BBM.1, Abcam), CD3 (clone HIT3a, BD Pharmingen).

Immunoblot. Tumor cells were lysed in RIPA buffer for protein isolation. Proteins (10–50 μg) were separated by SDS-PAGE, electroblotted onto nitrocellulose membranes, and probed with the indicated primary anti-human antibodies. After washing, membranes were incubated with the appropriate secondary antibodies linked to horseradish peroxidase (HRP). Antibody binding was visualized using the ECL chemiluminescence system (Thermo Fisher Scientific). GAPDH levels served as loading control in all experiments.

Immunocytochemistry. For immunocytochemistry, cells (1.5×10^4) were placed onto glass slides using the cytospin cytocentrifuge universal 30F (Hettich Zentrifugen). Cells were fixed with aceton for 15 minutes and slides were allowed to air-dry before storing at –20°C. Staining of fixed cells was carried out on the AutostainerLink48 (Dako) using the Real Detection System Alkaline Phosphatase/RED Rabbit/

The Journal of Clinical Investigation RESEARCH ARTICLE

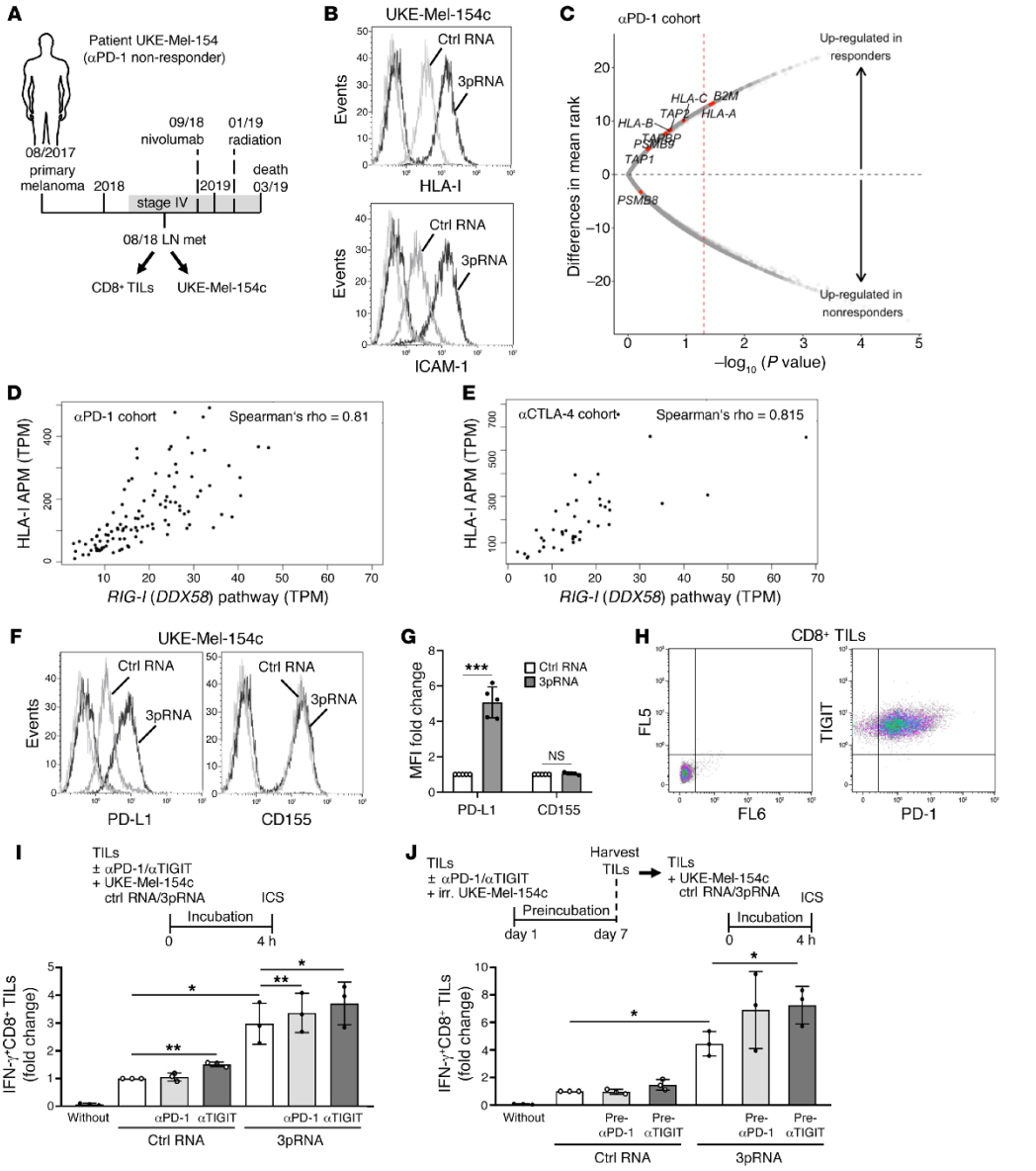

Figure 8. Combination of 3pRNA and ICB improves TIL reactivity toward autologous melanoma cells. (**A**) Clinical history of melanoma patient UKE-Mel-154. Horizontal line, time axis; above: diagnosis, therapeutic regimens, death; below: UKE-Mel-154c melanoma cell and $CD8^+$ TILs obtained from lymph node (LN) metastasis. (**B**) HLA-I and ICAM-1 surface expression on 3pRNA- and ctrl RNA–transfected UKE-Mel-154c cells. Representative histograms from 3 independent experiments. (**C**) Volcano plot showing overall upregulation of HLA-I APM genes in clinical responders (n = 57) versus nonresponders (n = 62) in the αPD-1–treated cohort (39). The x axis is the negative $\log_{10}$ value of the Mann-Whitney U P value; the y axis is the difference in mean rank between response groups. Red vertical dashed line, unadjusted P value of 0.05. (**D** and **E**) Scatterplot of *RIG-I* (*DDX58*) pathway expression against HLA-I APM expression across all samples in the αPD-1 (n = 121) and αCTLA-4 (n = 42) cohort. (**F** and **G**) PD-L1 and CD155 surface expression on 3pRNA- or ctrl RNA–transfected UKE-Mel-154c cells. (**F**) Representative histograms, (**G**) relative MFI given as mean plus SEM from 3 independent experiments. (**H**) Representative PD-1 and TIGIT surface expression on TILs from 3 independent experiments. (**I** and **J**) Combination of targeted RIG-I activation and ICB enhances TIL reactivity toward autologous melanoma cells. (**I**) Concurrent treatment. TIL activation after 4-hour coincubation with 3pRNA- or ctrl RNA–treated UKE-Mel-154c cells in the presence of PD-1 or αTIGIT antibodies, by intracellular cytokines staining (ICS). (**J**) Sequential treatment. After 7-day preincubation with irradiated (irr.) UKE-Mel-154c cells in the absence or presence of αPD-1 or αTIGIT antibodies, TILs were harvested and activation was measured after 4-hour coincubation with 3pRNA- or ctrl RNA–treated UKE-Mel-154c cells. (**I** and **J**) Mean plus SEM fold change in frequency of IFN-γ$^+$$CD8^+$ T cells stimulated by ctrl RNA–transfected UKE-Mel-154c cells from 3 independent experiments. (**G**, **I**, and **J**) Significantly different experimental groups: $^*P < 0.05$, $^{**}P < 0.01$, $^{***}P < 0.005$ by 2-tailed paired t test.

Mouse and EnVision FLEX Hematoxylin (Dako). Images of stained sections were acquired with the Axio Observer.Z1 microscope (Zeiss).

Immunohistochemistry. Serial cryostat tissue sections were stained with indicated primary antibodies in combination with a polymer kit containing an AP-coupled secondary antibody (ZytoChem-Plus AP Polymer Kit, Zytomed). Serial FFPE sections were stained using the Real Detection System Alkaline Phosphatase/RED Rabbit/Mouse and EnVision FLEX Hematoxylin (Dako).

Quantitative real-time PCR (qPCR). Total mRNA was isolated from tumor cells using the RNeasy plus Mini Kit (Qiagen), in combination with RNAse-free DNase Set (Qiagen) according to the manufacturer's instructions. Reverse transcription, TaqMan-based real-time PCR and calculation of relative expression were performed as previously described (29). In all experiments, the amount of specific mRNA was normalized to endogenous *GAPDH* mRNA levels.

Flow cytometry. Cells were stained for surface marker expression with either directly labeled or nonlabeled antibodies in combination with a secondary PE-conjugated goat anti-mouse F(ab')2 (IgG (H+L) polyclonal) (Dianova). Background fluorescence was defined based on unstained cells or cells stained with or secondary antibody only. After fixation, cells were analyzed employing Gallios flow cytometer (Beckman Coulter) and Kaluza software. Surface expression was determined as mean fluorescence intensity (MFI), normalized to background MFI (unstained or secondary antibody only). Mouse antibodies used in flow cytometry were as follows: anti–CD54-PE (clone 84H10) from Beckman Coulter; anti–PD-L1-PE (clone 29E2A3), anti-CD155(PVR)-APC (clone SKIL4), anti–CD3-BV42 (clone UCHT1), anti–CD8-APC/Cy7 (clone SK1), anti–PD-1–APC (clone EH12.2H7) and anti–TIGIT-PE/Cy7 (clone A15153G) from BioLegend; anti-β2m–associated HLA class heavy chains (clone W6/32) from eBioscience.

T cell activation assays. IFN-γ release by $CD8^+$ T cells in the presence of 3pRNA- or control RNA–transfected melanoma cells was quantified by ELISpot assay as follows: 2×10^4 T cells were coincubated with 2×10^4 melanoma cells per well (96-well plate) at 37°C. Following an incubation of 24 hours, IFN-γ release was detected using anti–human IFN-γ capture mAb (clone 1-D1K), biotinylated detection mAb (clone 7-6B-1) (Mabtech), and ExtrAvidin alkaline phosphatase (MilliporeSigma). Where indicated, tumor cells were preincubated with anti–HLA-I blocking mAb W6/32 or isotype-matched control IgG (50 μg/mL).

Intracellular IFN-γ staining was performed to determine TIL reactivity toward autologous tumor cells under combined 3pRNA/ICB treatment in 2 different settings. Initially, 1×10^5 $CD8^+$ TILs were incubated with anti–PD-1 (nivolumab [1 μg/mL], Bristol Myers Squibb [BMS]) or anti-TIGIT (BMS-986207 [1 μg/mL], BMS) antibodies in the presence of autologous control RNA– or 3pRNA-transfected tumor cells (1×10^5) in AIM-V complete medium containing 10 μg/mL Brefeldin A (MilliporeSigma). After 4 hours, cells were subjected to the Fixation/Permeabilization Concentrate and Diluent kit (eBioscience) followed by staining with an antibody cocktail containing anti–human CD3-BV421 (clone UCHT1), CD8-APC/Cy7 (clone SK1) and IFN-γ–PE (clone B27) antibodies (BioLegend). Gallios flow cytometer and Kaluza software were used for cell analyses and data processing, respectively (Beckman Coulter). In a second sequential approach, $CD8^+$ TILs were preincubated with anti-TIGIT (BMS-986207 [1 μg/mL], BMS) or anti–PD-1 (nivolumab [1 μg/mL], BMS) antibodies in the presence of irradiated autologous tumor cells. After 7 days, 1×10^5 T cells were stimulated for 4 hours with the control RNA– or 3pRNA-transfected tumor cells (1×10^5) in AIM-V complete medium containing 10 μg/mL Brefeldin A (MilliporeSigma), followed by intracellular cytokine staining as described above.

ELISA. Supernatants from 3pRNA- and control RNA–transfected melanoma cells were harvested and analyzed for the content of CCL5 and CXCL10 by ELISA (BioLegend) following the manufacturer's instructions.

Migration assay. $CD8^+$ T cell migration was determined in a Boyden chamber assay, using 5.0-μm pore size polycarbonate membrane Transwells (Corning). The lower chamber of the Transwell plates was filled with 500 μL conditioned medium (CM) from 3pRNA- or control RNA–transfected Ma-Mel-61g cells. RPMI medium containing 10–100 ng/mL recombinant CCL5 or CXCL10 was used as positive control. A quantity of 2×10^5 $CD8^+$ T cells was resuspended in RPMI and then loaded to the upper side of the chamber (200 μL/well). After 4 hours, migration was stopped with 0.5 M EDTA and migrated cells were counted in a Neubauer chamber.

Chicken chorioallantoic membrane (CAM) assay. Fertilized chicken eggs were obtained from Sörries-Trockels. Upon arrival, eggs were incubated in a thermostat under rotation at 37.5°C and 70% humidity for 3 days. For ex ovo culture fertilized eggs were cleaned with 3% Incidin on day 4 of embryonic development and cracked into sterile plastic reservoirs (63). The reservoirs were incubated at 37.5°C and 70% humidity without movement for 6 days to enable development of the embryos. For generation of on-plants on embryonic day 10, Ma-Mel-86c cells (3×10^6) were resuspended in 30 μL culture medium and transferred onto a 3 mm^3 gelatin sponge (SMI AG). After the cell solution had been entirely absorbed, 2 cell-soaked sponges were trans-

ferred on distant sites of each chicken CAM and subsequently incubated for 4 days until solid tumors had formed. The 2 tumors on the same embryo were treated with either 10 μg 3pRNA or control RNA complexed with in vivo-jetPEI (Polyplus), every 24 hours for 2 consecutive days. Tumors were enclosed with a silicon ring to form a reservoir to constrain the 3pRNA or control RNA solution at the tumor side. A quantity of 1×10^5 T cells (autologous to Ma-Mel-86c) was injected with an omnican insulin syringe (Braun) into the blood vessels of each embryo. Twenty hours after T cell injection the tumors were harvested together with the attached CAM and fixed in 10% formalin.

TCGA melanoma data set. Harmonized RNA-Seq data for TCGA SKCM (skin cutaneous melanoma) samples (n = 462) were obtained using the TCGAbiolinks package (64) in R (queried on 12/28/2018; project = "TCGA-SKCM", data.category = "Transcriptome Profiling", data.type = "Gene Expression Quantification", workflow.type = "HTSeq - FPKM"). FPKM counts were then converted to TPM (transcript per million) normalized counts. HLA-I APM expression was defined as the geometric mean of the TPM expression for *HLA-A*, *HLA-B*, *HLA-C*, *TAP1*, *TAP2*, *TAPBP*, *B2M*, *LMP2* (*PSMB9*), and *LMP7* (*PSMB8*). *RIG-I* (*DDX58*) and *RIG-I* (*DDX58*) pathway gene expression was defined as geometric mean of the TPM (transcript per million) expression for *DDX58* and *DDX58*, *IRF1*, *IRF3*, respectively.

Anti–CTLA-4– and anti–PD-1–treated patient cohorts. Tumor pretreatment RNA-Seq data from the anti–CTLA-4–treated (n = 42) (30) and anti–PD-1–treated (n= 121) (39) patient cohorts were analyzed for differential expression of HLA-I APM genes. As previously described, clinical response was defined using both Response Evaluation Criteria In Solid Tumors (RECIST) and OS criteria. Briefly, clinical responders were defined as patients with a complete or partial response as well as patients with stable disease and OS of at least 1 year. Clinical nonresponders were defined as patients with progressive disease as best response as well as patients with stable disease and OS less than 1 year. As previously described, the long-survival group (n = 5) of the anti–CTLA-4 cohort (30) and 2 samples with a mixed RECIST response in the anti–PD-1 clinical cohort (39) were excluded from differential expression analysis.

Statistics. For analyses of TCGA RNA-Seq data, high and low HLA-I APM expression groups were defined relative to median expression in the TCGA SKCM cohort. Differences in expression and survival between high and low expression groups were tested using the Mann-Whitney U test and the log-rank test, respectively. For analyses of RNA-Seq data from anti–CTLA-4– and anti–PD-1–treated patient cohorts, statistical testing for differential expression was performed using the Mann-Whitney U test. For survival analyses, high and low HLA-I APM expression groups were defined relative to the median TPM expression across the entire cohort. The difference in survival between high and low expression groups was tested using the log-rank test. For experimental data analyses, data from independent experiments were plotted as means plus standard error of the mean. For comparison between experimental groups, the 2-tailed paired t test was carried out using the GraphPad Prism 5.03 software (GraphPad). Experimental groups were considered to be significantly different at levels of less than P less than 0.05.

Study approval. Patient samples, including tumor tissue and peripheral blood cells, were collected after written informed consent. Studies on human material were approved by the institutional review board (Ethikkommission, Universitätsklinikum Essen; vote SCABIO_114715). Animal experiments were approved by the Veteriäramt Nordrhein Westfalen (Düsseldorf, Germany) and performed in accordance with the German law for animal protection.

Author contributions

LS conducted experiments, acquired and analyzed data, and wrote the manuscript. FZ, BT, VTKLT, NP, S Howe, HB, HK, CR, and RB performed experiments and acquired and analyzed data. S Horn and JK conducted bioinformatic data analyses. Derek Liu and David Liu performed bioinformatic and statistical data analyses and reviewed the manuscript. CC, TAK, GH, and SF provided critical reagents. AS, SU, and DS collected clinical samples, annotated clinical data, and reviewed the manuscript. US, UD, MS, KSL, JCB, and EMVA reviewed the manuscript. KG and MT edited the manuscript and contributed to experimental design. AP designed the study, reviewed data, and wrote the manuscript.

Acknowledgments

This work was partly funded by the Deutsche Krebshilfe (DKH, German Cancer Aid; Translational Oncology 70113455) and the Deutsche Forschungsgemeinschaft (DFG, German Research Foundation; BE 1394/12-1, HO 6389/2-1, PA 2376/1-1, SCHA 422/17-1 [KFO 337]).

Address correspondence to: Annette Paschen, Department of Dermatology, University Hospital Essen, Hufelandstrasse 55, 45122 Essen, Germany. Phone: 49.201.723.2406; Email: annette.paschen@uk-essen.de.

1. Sucker A, et al. Genetic evolution of T-cell resistance in the course of melanoma progression. *Clin Cancer Res*. 2014;20(24):6593–6604.
2. Rooney MS, Shukla SA, Wu CJ, Getz G, Hacohen N. Molecular and genetic properties of tumors associated with local immune cytolytic activity. *Cell*. 2015;160(1–2):48–61.
3. Zhao F, et al. Melanoma lesions independently acquire T-cell resistance during metastatic latency. *Cancer Res*. 2016;76(15):4347–4358.
4. Zaretsky JM, et al. Mutations associated with acquired resistance to PD-1 blockade in melanoma. *N Engl J Med*. 2016;375(9):819–829.
5. Tran E, et al. T-cell transfer therapy targeting mutant KRAS in cancer. *N Engl J Med*. 2016;375(23):2255–2262.
6. Gettinger S, et al. Impaired HLA class I antigen processing and presentation as a mechanism of acquired resistance to immune checkpoint inhibitors in lung cancer. *Cancer Discov*. 2017;7(12):1420–1435.
7. Sade-Feldman M, et al. Resistance to checkpoint blockade therapy through inactivation of antigen presentation. *Nat Commun*. 2017;8(1):1136.
8. McGranahan N, et al. Allele-specific HLA loss and immune escape in lung cancer evolution. *Cell*. 2017;171(6):1259–1271.e11.
9. Chowell D, et al. Patient HLA class I genotype influences cancer response to checkpoint blockade immunotherapy. *Science*. 2018;359(6375):582–587.
10. Grasso CS, et al. Genetic mechanisms of immune evasion in colorectal cancer. *Cancer Discov*. 2018;8(6):730–749.
11. Perea F, et al. The absence of HLA class I expression in non-small cell lung cancer correlates with the tumor tissue structure and the pattern of T cell infiltration. *Int J Cancer*. 2017;140(4):888–899.
12. Pedersen MH, Hood BL, Beck HC, Conrads TP, Ditzel HJ, Leth-Larsen R. Downregulation of antigen presentation-associated pathway proteins is linked to poor outcome in triple-negative breast cancer patient tumors. *Oncoimmunology*. 2017;6(5):e1305531.
13. Anichini A, et al. Association of antigen-processing machinery and HLA antigen phenotype of melanoma cells with survival in American Joint Committee on Cancer stage III and IV melanoma

patients. *Cancer Res*. 2006;66(12):6405–6411.
14. Garrido F, Aptsiauri N, Doorduijn EM, Garcia Lora AM, van Hall T. The urgent need to recover MHC class I in cancers for effective immunotherapy. *Curr Opin Immunol*. 2016;39:44–51.
15. Leone P, Shin EC, Perosa F, Vacca A, Dammacco F, Racanelli V. MHC class I antigen processing and presenting machinery: organization, function, and defects in tumor cells. *J Natl Cancer Inst*. 2013;105(16):1172–1187.
16. González-Navajas JM, Lee J, David M, Raz E. Immunomodulatory functions of type I interferons. *Nat Rev Immunol*. 2012;12(2):125–135.
17. Megger DA, Philipp J, Le-Trilling VTK, Sitek B, Trilling M. Deciphering of the human interferon-regulated proteome by mass spectrometry-based quantitative analysis reveals extent and dynamics of protein induction and repression. *Front Immunol*. 2017;8:1139.
18. Yoneyama M, et al. The RNA helicase RIG-I has an essential function in double-stranded RNA-induced innate antiviral responses. *Nat Immunol*. 2004;5(7):730–737.
19. Gitlin L, et al. Essential role of mda-5 in type I IFN responses to polyriboinosinic:polyribocytidylic acid and encephalomyocarditis picornavirus. *Proc Natl Acad Sci USA*. 2006;103(22):8459–8464.
20. Kato H, et al. Length-dependent recognition of double-stranded ribonucleic acids by retinoic acid-inducible gene-I and melanoma differentiation-associated gene 5. *J Exp Med*. 2008;205(7):1601–1610.
21. Schlee M, et al. Recognition of 5' triphosphate by RIG-I helicase requires short blunt double-stranded RNA as contained in panhandle of negative-strand virus. *Immunity*. 2009;31(1):25–34.
22. Loo YM, Gale M. Immune signaling by RIG-I-like receptors. *Immunity*. 2011;34(5):680–692.
23. Bald T, et al. Immune cell-poor melanomas benefit from PD-1 blockade after targeted type I IFN activation. *Cancer Discov*. 2014;4(6):674–687.
24. Yu X, et al. Activation of the MDA-5-IPS-1 viral sensing pathway induces cancer cell death and type I IFN-dependent antitumor immunity. *Cancer Res*. 2016;76(8):2166–2176.
25. Pansky A, et al. Defective Jak-STAT signal transduction pathway in melanoma cells resistant to growth inhibition by interferon-alpha. *Int J Cancer*. 2000;85(5):720–725.
26. Respa A, et al. Association of IFN-gamma signal transduction defects with impaired HLA class I antigen processing in melanoma cell lines. *Clin Cancer Res*. 2011;17(9):2668–2678.
27. Gao J, et al. Loss of IFN-γ pathway genes in tumor cells as a mechanism of resistance to anti-CTLA-4 therapy. *Cell*. 2016;167(2):397–404.e9.
28. Shin DS, et al. Primary resistance to PD-1 blockade mediated by JAK1/2 mutations. *Cancer Discov*. 2017;7(2):188–201.
29. Sucker A, et al. Acquired IFNγ resistance impairs anti-tumor immunity and gives rise to T-cell-resistant melanoma lesions. *Nat Commun*. 2017;8:15440.
30. Van Allen EM, et al. Genomic correlates of response to CTLA-4 blockade in metastatic melanoma. *Science*. 2015;350(6257):207–211.
31. McKendry R, John J, Flavell D, Müller M, Kerr IM, Stark GR. High-frequency mutagenesis of human cells and characterization of a mutant unresponsive to both alpha and gamma interferons. *Proc Natl Acad Sci USA*. 1991;88(24):11455–11459.
32. Lutfalla G, et al. Mutant U5A cells are complemented by an interferon-alpha beta receptor subunit generated by alternative processing of a new member of a cytokine receptor gene cluster. *EMBO J*. 1995;14(20):5100–5108.
33. Dixit E, et al. Peroxisomes are signaling platforms for antiviral innate immunity. *Cell*. 2010;141(4):668–681.
34. Meissner TB, et al. NLR family member NLRC5 is a transcriptional regulator of MHC class I genes. *Proc Natl Acad Sci USA*. 2010;107(31):13794–13799.
35. Guo X, et al. Respiratory syncytial virus infection upregulates NLRC5 and major histocompatibility complex class I expression through RIG-I induction in airway epithelial cells. *J Virol*. 2015;89(15):7636–7645.
36. Al-Batran SE, et al. Intratumoral T-cell infiltrates and MHC class I expression in patients with stage IV melanoma. *Cancer Res*. 2005;65(9):3937–3941.
37. Ducwell P, et al. Targeted activation of melanoma differentiation-associated protein 5 (MDA5) for immunotherapy of pancreatic carcinoma. *Oncoimmunology*. 2015;4(10):e1029698.
38. Engel C, et al. RIG-I resists hypoxia-induced immunosuppression and dedifferentiation. *Cancer Immunol Res*. 2017;5(6):455–467.
39. Liu D, et al. Integrative molecular and clinical modeling of clinical outcomes to PD1 blockade in patients with metastatic melanoma. *Nat Med*. 2019;25(12):1916–1927.
40. Chauvin JM, et al. TIGIT and PD-1 impair tumor antigen-specific CD8+ T cells in melanoma patients. *J Clin Invest*. 2015;125(5):2046–2058.
41. Manguso RT, et al. In vivo CRISPR screening identifies Ptpn2 as a cancer immunotherapy target. *Nature*. 2017;547(7664):413–418.
42. Patel SJ, et al. Identification of essential genes for cancer immunotherapy. *Nature*. 2017;548(7669):537–542.
43. Rodig SJ, et al. MHC proteins confer differential sensitivity to CTLA-4 and PD-1 blockade in untreated metastatic melanoma. *Sci Transl Med*. 2018;10(450):eaar3342.
44. Donia M, et al. Acquired immune resistance follows complete tumor regression without loss of target antigens or IFNγ signaling. *Cancer Res*. 2017;77(17):4562–4566.
45. Ugurel S, et al. MHC class-I downregulation in PD-1/PD-L1 inhibitor refractory Merkel cell carcinoma and its potential reversal by histone deacetylase inhibition: a case series. *Cancer Immunol Immunother*. 2019;68(6):983–990.
46. Paulson KG, et al. Acquired cancer resistance to combination immunotherapy from transcriptional loss of class I HLA. *Nat Commun*. 2018;9(1):3868.
47. Yoshihama S, et al. NLRC5/MHC class I transactivator is a target for immune evasion in cancer. *Proc Natl Acad Sci USA*. 2016;113(21):5999–6004.
48. Odendall C, et al. Diverse intracellular pathogens activate type III interferon expression from peroxisomes. *Nat Immunol*. 2014;15(8):717–726.
49. Hasan M, et al. Trex1 regulates lysosomal biogenesis and interferon-independent activation of antiviral genes. *Nat Immunol*. 2013;14(1):61–71.
50. Nagato T, Lee YR, Harabuchi Y, Celis E. Combinatorial immunotherapy of polyinosinic-polycytidylic acid and blockade of programmed death-ligand 1 induce effective CD8 T-cell responses against established tumors. *Clin Cancer Res*. 2014;20(5):1223–1234.
51. Elion DL, et al. Therapeutically active RIG-I agonist induces immunogenic tumor cell killing in breast cancers. *Cancer Res*. 2018;78(21):6183–6195.
52. Heidegger S, et al. RIG-I activation is critical for responsiveness to checkpoint blockade. *Sci Immunol*. 2019;4(39):eaau8943.
53. Taube JM, et al. Association of PD-1, PD-1 ligands, and other features of the tumor immune microenvironment with response to anti-PD-1 therapy. *Clin Cancer Res*. 2014;20(19):5064–5074.
54. Tumeh PC, et al. PD-1 blockade induces responses by inhibiting adaptive immune resistance. *Nature*. 2014;515(7528):568–571.
55. Chiappinelli KB, et al. Inhibiting DNA methylation causes an interferon response in cancer via dsRNA including endogenous retroviruses. *Cell*. 2015;162(5):974–986.
56. Smith CC, et al. Endogenous retroviral signatures predict immunotherapy response in clear cell renal cell carcinoma. *J Clin Invest*. 2018;128(11):4804–4820.
57. Cañadas I, et al. Tumor innate immunity primed by specific interferon-stimulated endogenous retroviruses. *Nat Med*. 2018;24(8):1143–1150.
58. Kyi C, et al. Therapeutic immune modulation against solid cancers with intratumoral poly-ICLC: a pilot trial. *Clin Cancer Res*. 2018;24(20):4937–4948.
59. Rosenblum D, Joshi N, Tao W, Karp JM, Peer D. Progress and challenges towards targeted delivery of cancer therapeutics. *Nat Commun*. 2018;9(1):1410.
60. Adams BD, Parsons C, Walker L, Zhang WC, Slack FJ. Targeting noncoding RNAs in disease. *J Clin Invest*. 2017;127(3):761–771.
61. Wang X, et al. A method to generate antigen-specific mAb capable of staining formalin-fixed, paraffin-embedded tissue sections. *J Immunol Methods*. 2005;299(1–2):139–151.
62. Neerincx A, et al. A role for the human nucleotide-binding domain, leucine-rich repeat-containing family member NLRC5 in antiviral responses. *J Biol Chem*. 2010;285(34):26223–26232.
63. Deryugina EI, Quigley JP. Chapter 2. Chick embryo chorioallantoic membrane models to quantify angiogenesis induced by inflammatory and tumor cells or purified effector molecules. *Meth Enzymol*. 2008;444:21–41.
64. Colaprico A, et al. TCGAbiolinks: an R/Bioconductor package for integrative analysis of TCGA data. *Nucleic Acids Res*. 2016;44(8):e71.

Such et al., Supplemental Material

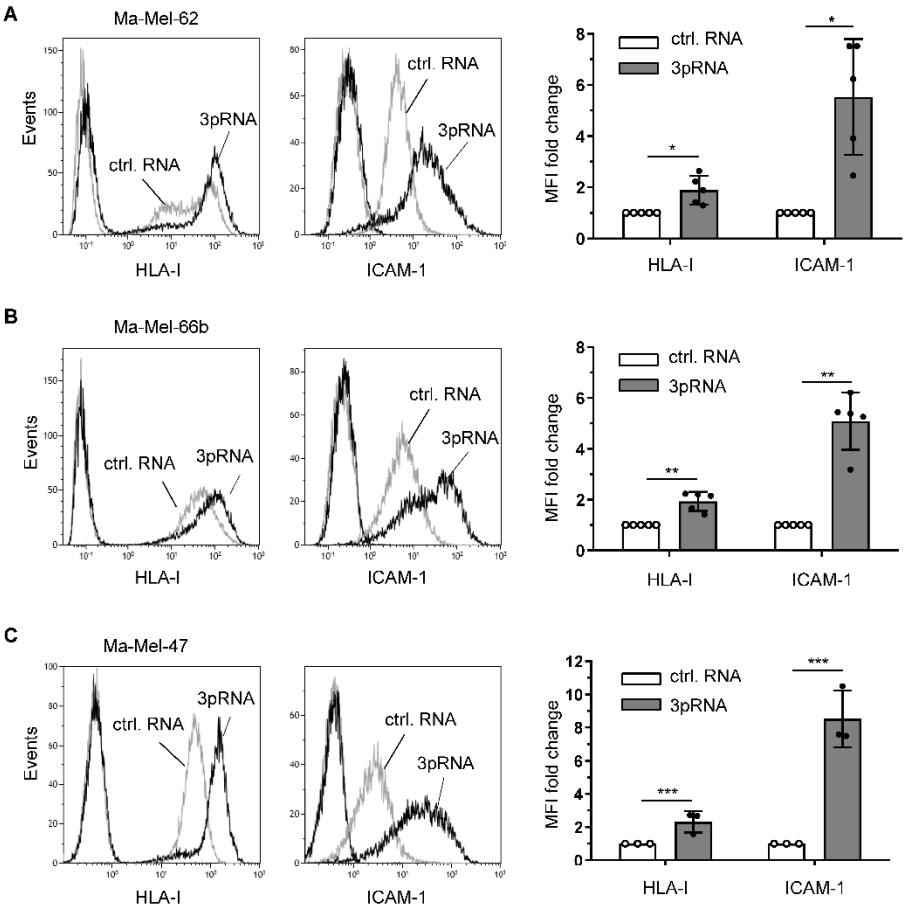

Supplemental Figure 1. RIG-I activation upregulates HLA-I expression in different melanoma patient models. (**A-C**) Melanoma cell lines established from metastases of patients Ma-Mel-62 (**A**), Ma-Mel-66b (**B**) and Ma-Mel-47 (**C**) were transfected with 3pRNA or control (ctrl.) RNA. Following an incubation of 20-24 h, cells were analyzed for HLA-I and ICAM-1 surface expression by flow cytometry. Left, representative histograms; right, relative MFI given as mean (+ SEM) of n ≥ 3 independent experiments. Significantly different experimental groups: *p<0.05, **p<0.01, ***p<0.001, 2-tailed paired t-test.

Such et al., Supplemental Material

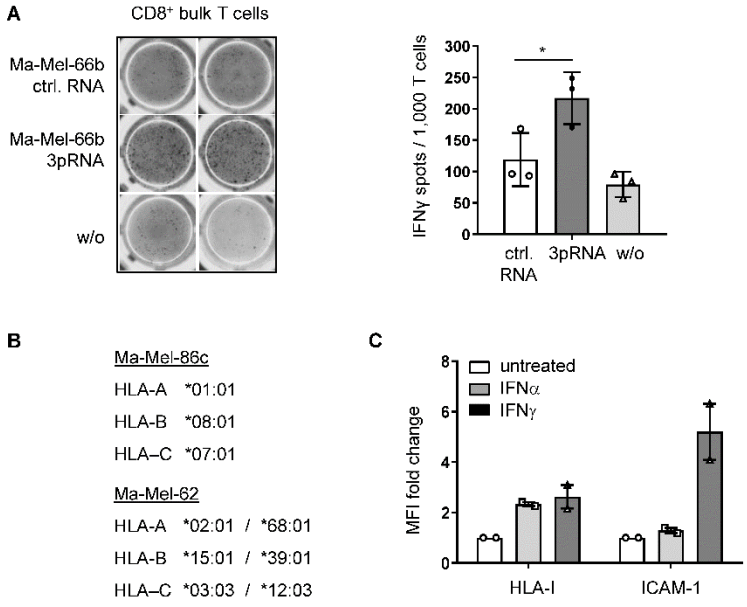

Supplemental Figure 2. RIG-I activation in melanoma cells enhances recognition by autologous CD8⁺ T cells. (**A**) Melanoma cells Ma-Mel-66b were transfected with 3pRNA or control (ctrl.) RNA following an incubation of 20-24 h. Activation of bulk CD8⁺ T cells by autologous melanoma cells was determined by IFNγ ELISpot assay. w/o, incubation of T cells without tumor cells. Left, representative IFNγ ELISpot result; right, mean IFNγ spots (+ SEM) of n = 3 independent experiments. Significantly different experimental groups: *p<0.05, 2-tailed paired t-test. (**B**) HLA-I genotypes of indicated cell lines.(**C**) Ma-Mel-86c cells were treated with IFNα or IFNγ for 20-24 h. Controls were left untreated. HLA-I and ICAM-1 surface expression was measured by flow cytometry. Relative MFI given as mean (+ SEM) of n = 2 independent experiments.

Such et al., Supplemental Material

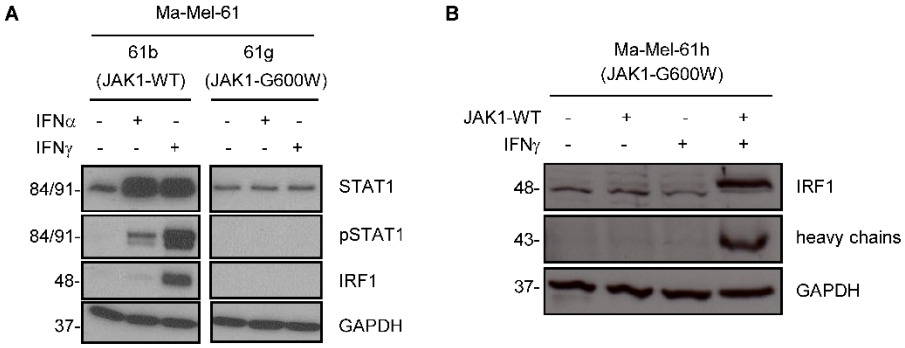

Supplemental Figure 3. Mutant JAK1-G600W abrogates IFN signaling in Ma-Mel-61g and Ma-Mel-61h melanoma cells. (**A**) Ma-Mel-61b and Ma-Mel-61g cells, treated with IFNα-2b or IFNγ for 48 h, were analyzed for (p)STAT1 and IRF1 expression by immunoblot; GAPDH, loading control. Representative data of n = 3 independent experiments. (**B**) Mutant JAK1-G600W Ma-Mel-61h cells, transfected with an expression plasmid encoding wild-type JAK1 followed by treatment with IFNγ for 48 h, were analyzed for expression of the indicated proteins. Representative data from n = 3 independent experiments.

Such et al., Supplemental Material

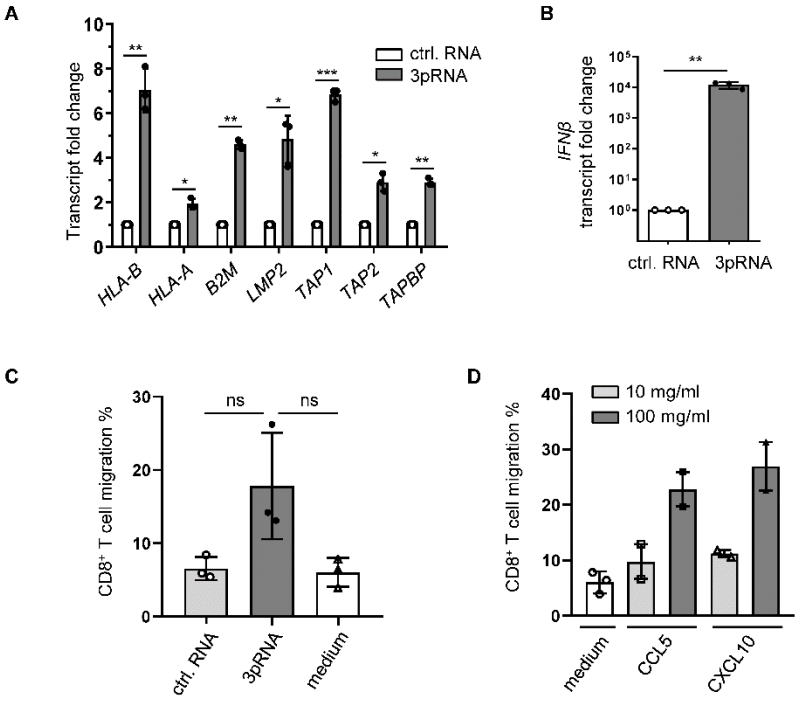

Supplemental Figure 4. RIG-I activation enhances HLA-I antigen presentation in IFN-resistant Ma-Mel-61g melanoma cells. (**A-C**) Ma-Mel-61g cells were transfected with 3pRNA or control (ctrl.) RNA and subjected to further analyses following an incubation of 20-24 h. (**A** and **B**) HLA-I APM (**A**) and *IFNβ* (**B**) mRNA expression analyzed by qPCR. Relative expression given as mean (+ SEM) of n = 3 independent experiments. Significantly different experimental groups: *p<0.05, **p<0.01, ***p<0.001, 2-tailed paired t-test. (**C**) Migration of $CD8^+$ T cells towards conditioned medium from 3pRNA- or ctrl. RNA-transfected Ma-Mel-61g cells measured in transwell-assays after an incubation of 4 h. Representative results of n = 3 independent experiments. ns, not significant; 2-tailed paired t-test. (**D**) Chemokine-induced $CD8^+$ T cell migration. Migration of $CD8^+$ T cells towards medium supplemented with recombinant CCL5 or CXCL10 was determined in transwell-assays after 4 h of incubation. Representative results of n = 2 independent experiments.

Such et al., Supplemental Material

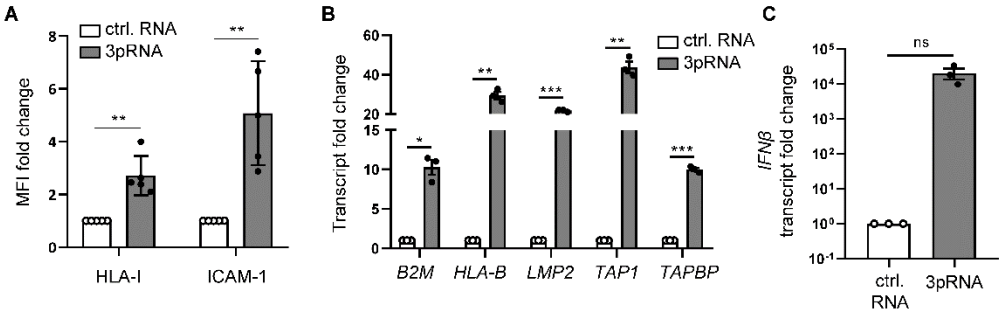

Supplemental Figure 5. RIG-I activation enhances HLA-I antigen presentation in 3pRNA-treated UKE-Mel-154c cells. (**A**-**C**) UKE-Mel-154c cells were transfected with 3pRNA or control (ctrl.) RNA and subjected to further analyses following an incubation of 20-24 h. (**A**) HLA-I and ICAM-1 surface expression measured by flow cytometry. Relative MFI given as mean (+ SEM) of n ≥ 3 independent experiments. (**B** and **C**) HLA-I APM component (**B**) and *IFNβ* (**C**) mRNA expression was quantified by qPCR. Relative expression given as mean (+ SEM) of n = 3 independent experiments. Significantly different experimental groups: *p<0.05, **p<0.01, ***p<0.001; ns, not significant; 2-tailed paired t-test.

Such et al., Supplemental Material

Supplemental Table 1: Differential expression analysis results for HLA-I APM genes in the anti-CTLA-4-treated cohort. Mann-Whitney U test p-values and FDR-corrected q-values are shown for the comparison of individual HLA-I APM gene expression in clinical responders vs. non-responders.

Gene	P-value	Q-value
HLA-A	0.284	0.365
HLA-B	0.231	0.347
HLA-C	0.344	0.387
TAP1	0.036	0.148
TAP2	0.231	0.347
TAPBP	0.486	0.486
B2M	0.020	0.148
PSMB9	0.049	0.148
PSMB8	0.082	0.185

Supplemental Table 2: Differential expression analysis results for HLA-I APM genes in the anti-PD-1-treated cohort. Mann-Whitney U test p-values and FDR-corrected q-values are shown for the comparison of individual HLA-I APM gene expression in clinical responders vs. non-responders.

Gene	P-value	Q-value
HLA-A	0.038	0.172
HLA-B	0.195	0.339
HLA-C	0.111	0.333
TAP1	0.458	0.515
TAP2	0.186	0.339
TAPBP	0.226	0.339
B2M	0.034	0.172
PSMB9	0.441	0.515
PSMB8	0.604	0.604

6.2 Article II

Melanoma differentiation trajectories determine sensitivity towards pre-existing CD8+ tumor-infiltrating lymphocytes

Franziska Noelle Harbers[1], Beatrice Thier[1], Simone Stupia[1], Si Zhu[1], Marion Schwamborn[1],Vicky Peller[1], Heike Chauvistré[1], Pietro Crivello[2], Katharina Fleischhauer[2], Alexander Roesch[1], Antje Sucker[1], Dirk Schadendorf[1], Yong Chen[3], Annette Paschen[1,4], Fang Zhao[*1]

[1]Department of Dermatology, University Hospital Essen, University Duisburg-Essen and German Cancer Consortium (DKTK), Partner Site Essen/Düsseldorf, Essen, Germany

[2]Institute for Experimental Cellular Therapy, University Hospital Essen, Essen, Germany

[3]Department of Musculoskeletal Oncology, Fudan University Shanghai Cancer Center, Fudan University, Shanghai, China

[4]Senior author

[*]Corresponding author.

Published in: Journal of Investigative Dermatology (2021); 141(10):2480-2489

https://doi.org/10.1016/j.jid.2021.03.013

Received: October 5, 2020 / Accepted: March 16, 2021 / Available online: March 30, 2021

Contribution to present publication (Article II):

- Conception: 0 %
- Experimental work: 5 %
- Data analysis: 5 %
- Species identification: N/A
- Statistical analysis: 0 %
- Writing the manuscript: 0 %
- Revising the manuscript: 10 %

I hereby certify that Beatrice Thier contributed to this article by execution of cell culture experiments and Western Blots. During the experimental phase of this work, she helped the first author and provided her methodological expertise. Furthermore, she contributed to the review and revision of the manuscript.

The above-listed contributions of Beatrice Thier to the publication are correct.

Essen, _____ _____

Annette Paschen

Essen, _____ _____

Beatrice Thier

ORIGINAL ARTICLE

Melanoma Differentiation Trajectories Determine Sensitivity toward Pre-Existing CD8$^+$ Tumor-Infiltrating Lymphocytes

Franziska Noelle Harbers[1], Beatrice Thier[1], Simone Stupia[1], Si Zhu[1], Marion Schwamborn[1], Vicky Peller[1], Heike Chauvistré[1], Pietro Crivello[2], Katharina Fleischhauer[2], Alexander Roesch[1], Antje Sucker[1], Dirk Schadendorf[1], Yong Chen[3], Annette Paschen[1,4] and Fang Zhao[1]

The highly plastic nature of melanoma enables its transition among diverse cell states to survive hostile conditions. However, the interplay between specific tumor cell states and intratumoral T cells remains poorly defined. With MAPK inhibitor–treated BRAF^{V600}-mutant tumors as models, we linked human melanoma state transition to CD8$^-$ T cell responses. Repeatedly, we observed that isogenic melanoma cells could evolve along distinct differentiation trajectories on single BRAF inhibitor (BRAFi) treatment or dual BRAFi/MEKi treatment, resulting in BRAFi–induced hyperdifferentiated and BRAFi/MEKi–induced dedifferentiated resistant subtypes. Taking advantage of patient-derived autologous CD8$^+$ tumor-infiltrating lymphocytes (TILs), we demonstrate that progressive melanoma cell state transition profoundly affects TIL function. Tumor cells along the hyperdifferentiation trajectory continuously gained sensitivity toward tumor-reactive CD8$^+$ TILs, whereas those in the dedifferentiation trajectory acquired T cell resistance in part owing to the loss of differentiation antigens. Overall, our data reveal the tight connection of MAPKi–induced temporary (drug-tolerant transition state) and stable (resistant state) phenotype alterations with T cell function and further broaden the current knowledge on melanoma plasticity in terms of sculpting local antitumor immune responses, with implications for guiding the optimal combination of targeted therapy and immunotherapy.

Journal of Investigative Dermatology (2021) **141,** 2480–2489; doi:10.1016/j.jid.2021.03.013

INTRODUCTION

Melanoma is known for its high phenotypic plasticity, switching between different transcriptional programs to survive when threatened by external cues (Arozarena and Wellbrock, 2019; Bai et al., 2019). Marked by the level of MITF (master regulator of melanocytic lineage), two main transcriptional subtypes have initially been observed across melanoma cultures and patient biopsies: the MITF^{high} proliferative and MITF^{low} invasive phenotypes (Hoek et al., 2006; Sensi et al., 2011; Tirosh et al., 2016). Recently, increasing evidence points out the existence of additional intermediate cell states with discrete gene regulatory landscapes apart from those of classical proliferative and invasive phenotypes (Rambow et al., 2019; Wouters et al., 2020).

[1]*Department of Dermatology, University Hospital Essen, University Duisburg-Essen and German Cancer Consortium (DKTK), Partner Site Essen/Düsseldorf, Essen, Germany;* [2]*Institute for Experimental Cellular Therapy, University Hospital Essen, Essen, Germany; and* [3]*Department of Musculoskeletal Oncology, Fudan University Shanghai Cancer Center, Fudan University, Shanghai, China*

[4]*Senior author.*

Correspondence: Fang Zhao, Department of Dermatology, University Hospital Essen, Hufelandstrasse 55, 45122 Essen, Germany. E-mail: fang.zhao@uk-essen.de

Abbreviations: BRAFi, BRAF inhibitor; DDR, double drug–resistant; MAPKi, MAPK inhibitor; MD, melanoma differentiation; MEKi, mitogen-activated protein kinase kinase inhibitor; MITF, microphthalmia-associated transcription factor; SDR, single drug–resistant; TIL, tumor-infiltrating lymphocyte

Received 5 October 2020; revised 23 February 2021; accepted 16 March 2021; accepted manuscript published online 30 March 2021; corrected proof published online 25 August 2021

In response to stresses, melanoma cells may transit into an alternative state for adaptation. Taking MAPK inhibition in BRAF^{V600}-mutant tumors as a paradigm, besides genetic resistance mechanisms such as *RAS* mutation, *BRAF* amplification, or alternative splicing (Shi et al., 2014; Van Allen et al., 2014), the MITF-regulated gene network substantially contributes to the nongenetic drug-resistance mechanisms (Arozarena and Wellbrock, 2019; Meierjohann, 2017). We and others demonstrated that MITF^{high} melanoma cells dynamically changed their phenotype under prolonged MAPK inhibitor (MAPKi) treatment before acquiring a stable drug-resistant MITF^{low}-dedifferentiated cell state (Pieper et al., 2018; Smith et al., 2016; Su et al., 2017; Tsoi et al., 2018). Moreover, by comprehensively analyzing the effect of MAPKi on human melanoma differentiation trajectories, Rambow and colleagues showed that different drug-tolerant cell states may even coevolve within the same lesion and exhibit distinct MITF activities (Rambow et al., 2018).

Another clinic-relevant aspect of melanoma plasticity is its role in mediating resistance to immunotherapies, such as adoptive cell transfer or immune checkpoint inhibition. By means similar to BRAF inhibitor (BRAFi) resistance, melanoma may escape T cell surveillance through a transition into a dedifferentiated state (Hugo et al., 2016; Landsberg et al., 2012; Mehta et al., 2018; Tsoi et al., 2018).

However, the extent to which cell state dynamics may affect surrounding host T cells remains largely undefined, particularly at the functional level. Previously, we demonstrated that upon single BRAFi or combined BRAFi and MEKi treatment, melanoma cells could acquire a dedifferentiated

drug-resistant phenotype associated with cross-resistant to $CD8^+$ T cells (Pieper et al., 2018). In this study, we sought to gain deeper insights into the impact of MAPKi-induced fluctuating cell states on tumor recognition by $CD8^-$ tumor-infiltrating lymphocytes (TILs). Using multiple $BRAF^{V600}$-mutant melanoma patient models, our precise kinetic analysis revealed that isogenic tumor cells can move along distinct differentiation trajectories and acquire opposing resistance phenotypes in a treatment-dependent manner. Divergent phenotype evolution under single and combined drug treatment was detectable already in the drug-tolerant phase and was sensed by $CD8^+$ TILs, demonstrating that the real-time state of melanoma cells under MAPKi treatment could profoundly affect T cell responses. Taken together, our data point out that melanoma phenotype plasticity shapes local antitumor T cell response and highlight the need for further analyses on its generality to other phenotype modulators.

RESULTS

Characterization of melanoma cells resistant to single BRAFi and combined BRAFi and MEKi treatment

Melanoma cells alter their differentiation states in the course of developing resistance to MAPKi treatment. Previously, two main resistance phenotypes were described: a dedifferentiated $MITF^{low}$ phenotype and a differentiated phenotype with $MITF^{high}$ expression (Müller et al., 2014). In this study, we sought to determine the impact of different treatment strategies, i.e. single BRAFi versus dual BRAFi and MEKi, on resistance phenotypes. To induce drug resistance, we exposed $BRAF^{V600E}$-mutant Ma-Mel-80d melanoma cells continuously to BRAFi (vemurafenib) at a concentration of 0.5 μM, defined as half maximal inhibitory concentration (IC50, Supplementary Figure S1). Then, a reported BRAFi:MEKi ratio of 10:1 was applied for combination treatment (Hong et al., 2018; Tirosh et al., 2016). As shown in Figure 1a, drug-tolerant tumor cells (treated for 3–21 days) presented senescence-like features, showing elongated and/or flattened morphology and enhanced β-galactosidase activity. After 2–5 months, proliferative single drug–resistant (SDR) and double drug–resistant (DDR) sublines evolved, remaining alive in the presence of BRAFi and combined BRAFi and MEKi, respectively (Figure 1b and Supplementary Figure S2). However, on drug withdrawal, DDR cells showed drug addiction indicated by significantly increased apoptotic cells, whereas survival of SDR cells was not affected (Figure 1c), suggesting that SDR and DDR cells exploited different mechanisms to overcome MAPK inhibition.

Next, we studied the differentiation states of drug-resistant cells. In comparison to parental counterparts (drug sensitive, S) with intermediate MITF levels ($MITF^{intermediate}$), SDR cells exhibited enhanced MITF expression, whereas DDR cells displayed a dedifferentiated phenotype with decreased MITF level (Figure 1d). According to the role of MITF as a transcriptional activator of melanoma differentiation genes (Supplementary Figure 3a), tyrosinase and melan-A were no longer detectable in $MITF^{low}$ DDR cells but increased in the $MITF^{high}$ SDR group (Figure 1d). Regarding other tested cell state–related markers such as NGFR, AXL, and EGFR (Fallahi-Sichani et al., 2017; Müller et al., 2014; Sun et al., 2014; Tsoi et al., 2018), SDR cells completely lacked NGFR and AXL expression, in line with their $MITF^{high}$ phenotypes, whereas both molecules were expressed in drug-sensitive as well as in DDR cells (Figure 1e). EGFR was not detectable in all the groups analyzed (data not shown). Collectively, we observed that isogenic melanoma cells could acquire distinct resistant phenotypes on BRAFi or combined BRAFi and MEKi treatment.

To analyze the clinical significance of our findings, we screened transcriptomic data of a MAPKi-treated melanoma patient cohort ($n = 29$) for expression of MITF and multiple melanoma differentiation (MD) genes (Hugo et al., 2015). The latter was summarized as an MD gene signature, composed of *MLANA* (encoding melan-A); *TYR* (encoding tyrosinase); *PMEL* (encoding glycoprotein 100/gp100); *TYRP1* (encoding TRP1); and *DCT* (encoding dopachrome tautomerase/TRP2). We observed a significant correlation between MITF and MD signature across all the samples, including both baseline and resistant tumors (Supplementary Figure S4), confirming MITF as a master regulator of melanoma differentiation also in the context of MAPKi therapy. Intriguingly, serial drug-resistant lesions from the same patient could display distinct MITF levels, and similar to our in vitro finding, both $MITF^{high}$ BRAFi–resistant and $MITF^{low}$ BRAFi/MEKi–resistant lesions were recurrently found in this cohort (Figure 1f).

Treatment-specific differentiation trajectories determine TIL activation

To understand whether the different states of SDR and DDR Ma-Mel-80d tumor cells were the consequences of distinct differentiation trajectories, we monitored cell state changes on drug exposure over time. Meanwhile, single MEKi treatment was performed to decipher its role in the drug combination. Compared with the parental $MITF^{intermdiate}$ cell state, treatment with BRAFi, MEKi, or combined BRAFi and MEKi led to a hyperdifferentiated drug-tolerant state till day 14, indicated by enhanced MITF, tyrosinase, and melan-A expression (Figure 2a). On day 21, only the persisters exposed to single BRAFi or MEKi treatment remained hyperdifferentiated, whereas the combined BRAFi and MEKi–treated group appeared to revert MITF to a similar level as drug-naive cells, suggesting that dual inhibition enforced melanoma dedifferentiation in this model.

To precisely track the dynamic drug response at a single-cell level, we performed multicolor flow cytometry (Supplementary Figure S5a), taking the advantages of NGFR and melan-A as robust phenotype indicators (Fallahi-Sichani et al., 2017; Su et al., 2017). Three phases were selected in this time-course analysis: brief drug-exposure phase (3 and 7 days), prolonged drug-exposure phase (21 days), and established drug-resistant phase. Overall, we observed a two-dimensional mode of phenotypic changes, indicating the treatment effectiveness and the highly plastic nature of Ma-Mel-80d cells (Figure 2b). Summarized in Figure 2c, BRAFi as well as combined BRAFi and MEKi treatments enhanced the melan-A^{pos}/$NGFR^{pos}$ population (quadrant Q2) within 3 days, followed by the appearance of melan-A^{neg}/$NGFR^{low}$ (quadrant Q4) within 7 days. After prolonged inhibition,

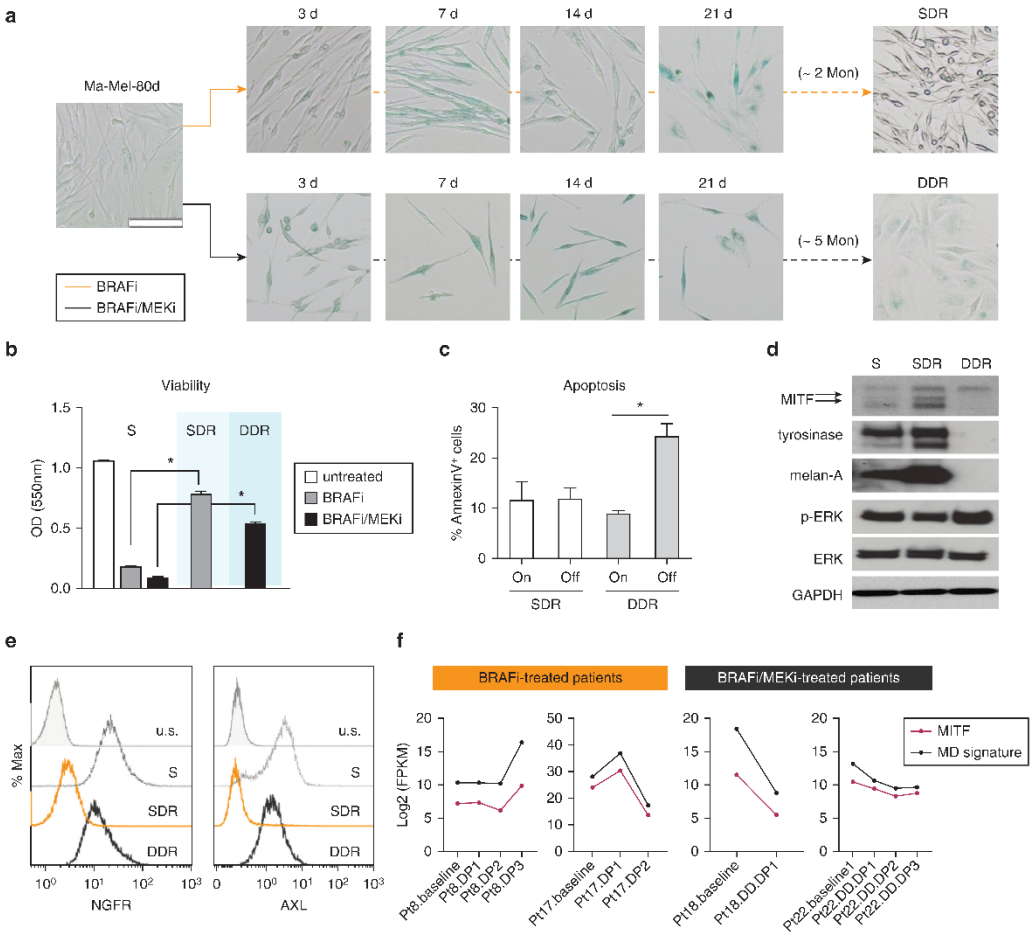

Figure 1. Characterization of melanoma cells resistant to single BRAFi and combined BRAFi–MEKi treatments. (a) Morphological changes of Ma-Mel-80d cells visualized by SA-β-Gal assay. BRAFi, 0.5 μM; BRAFi/MEKi, 0.5 μM/50 nM. Bar = 100 μm. **(b)** Cell viability in S (⊥ MAPKi, 6 d), SDR and/or DDR cells. Quantified crystal violet assay (see Supplementary Materials and Methods). **(c)** Percentage apoptosis (Annexin-V$^+$) in drug-resistant cells treated with (On) or without (Off) corresponding inhibitors (7 d). **(d)** Protein expression determined by Western blot. GAPDH served as the loading control. **(e)** Protein expression was determined by flow cytometry. **(f)** Changes of MITF and MD signature in serial tumor lesions from individual Pts (Hugo cohort, see Supplementary Materials and Methods). **(a, d, e)** Representative data from three independent experiments. **(b)** and **(c)** n = 3 mean + SEM. *, $P < 0.05$. DDR, double drug–resistant; d, day; DD.DP, double drug–treated disease progression; DP, disease progression; ERK, extracellular signal–regulated kinase; Max, maximum; MD, melanoma differentiation; MEK, mitogen-activated protein kinase kinase; Mon, month; OD, optical density; p-ERK, phosphorylated ERK; Pt, patient; S, drug-sensitive; SA-β-Gal, senescence-associated β-galactosidase assay; SDR, single drug–resistant; u.s., unstained control.

trajectory differences became noticeable. When comparing between treatment groups on day 21, melan-A^{pos}/NGFR^{low} cells (quadrant Q3) in the BRAFi trajectory and melan-A^{neg}/NGFR^{high} cells (quadrant Q1) in the BRAFi and MEKi trajectory were significantly enriched, which proceeded into major populations in the drug-resistant sublines, respectively. Altogether, both bulk analysis and single-cell profiling revealed that single BRAFi and combined BRAFi and MEKi treatments guided Ma-Mel-80d cells into divergent differentiation trajectories.

Considering the importance of pre-existing intratumoral T cells in BRAFi therapy (Cooper et al., 2013), we used patient-derived TILs to investigate the association of phenotype evolution with tumor sensitivity toward CD8$^+$ T cells. To model the basal antitumor response, drug-naive tumor cells were applied as antigen-presenting cells to expand autologous CD8$^-$ TILs in vitro. Afterward, the T cell stimulation capacity of drug-treated tumor cells was assessed by testing the numbers of IFN-γ$^-$ T cells after a 4-hour tumor/T cell coincubation (Supplementary Figure S6). Setting drug-naive

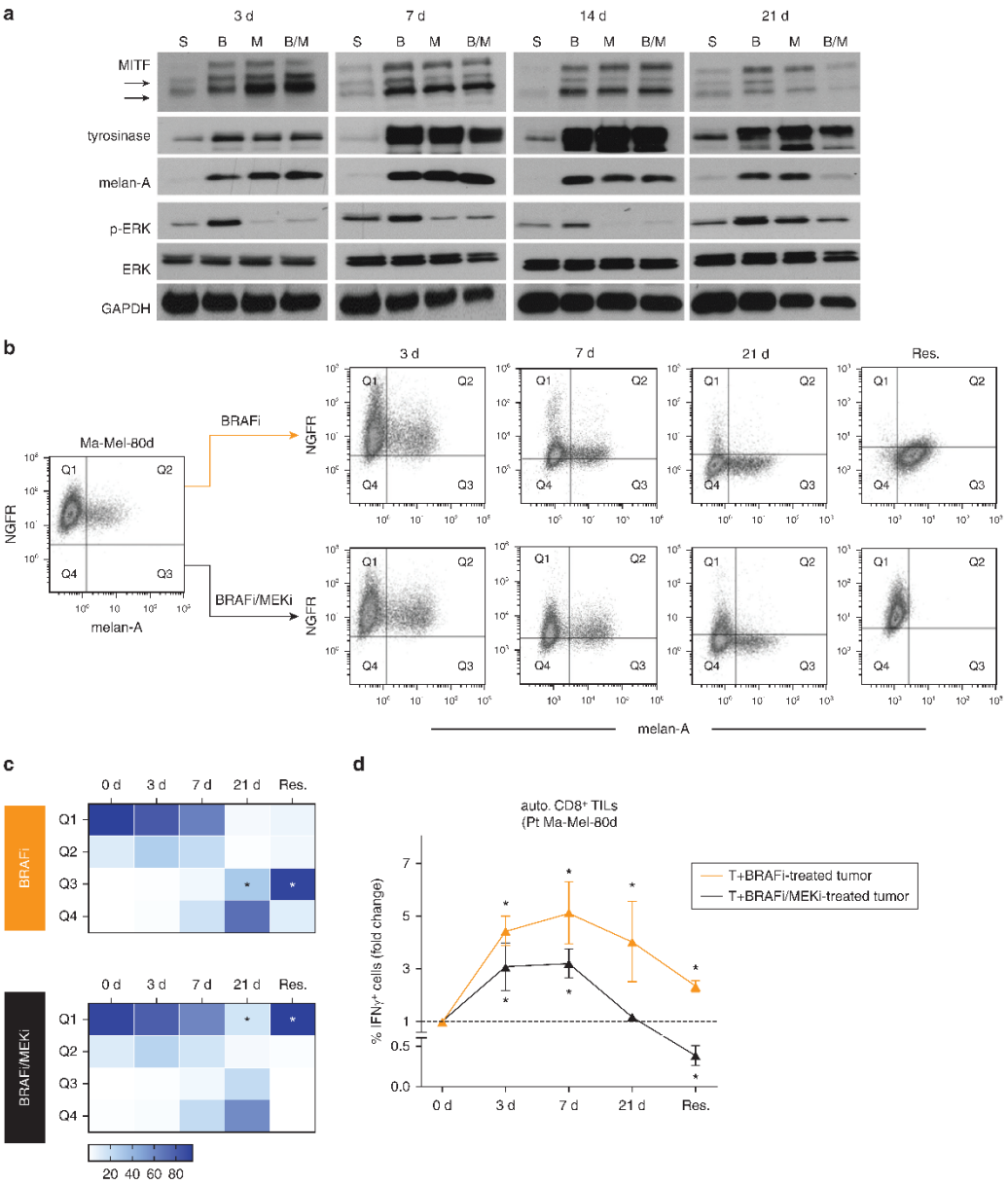

Figure 2. CD8$^+$ TILs monitor distinct cell state transitions driven by single B and combined B and M treatment. **(a)** Expression of the indicated proteins in Ma-Mel-80d cells under treatment (3−21 d) with B (0.5 μM), M (50 nM), or combined B and M (0.5 μM/50 nM). GAPDH served as the loading control. **(b)** Flow cytometry–based single-cell phenotype profiling of drug-treated Ma-Mel-80d cells in drug-tolerant phase (3/7/21 d) and Res. Qs are defined on the basis of autofluorescence in unstained cells. **(c)** Summarized mean percent for the indicated quadrants from **b**. n = 3. *$P < 0.05$ for B versus B and M. **(d)** Fold change of IFN-γ$^+$ CD8$^+$ TILs after stimulation by B- or combined B and M–treated tumor cells relative to stimulation by untreated tumor cells. n = 3. mean ± SEM. *$P <$ 0.05 for drug-treated versus −untreated cells. **(a, b)** Representative data from three independent experiments. B, BRAF inhibitor; d, day; ERK, extracellular signal–regulated kinase; M, MAPK/extracellular signal–regulated kinase kinase inhibitor; p-ERK, phosphorylated extracellular signal–regulated kinase; Pt, patient; Q, quadrant; Res., drug-resistant state; S, untreated controls; T, T cells; TIL, tumor-infiltrating lymphocyte.

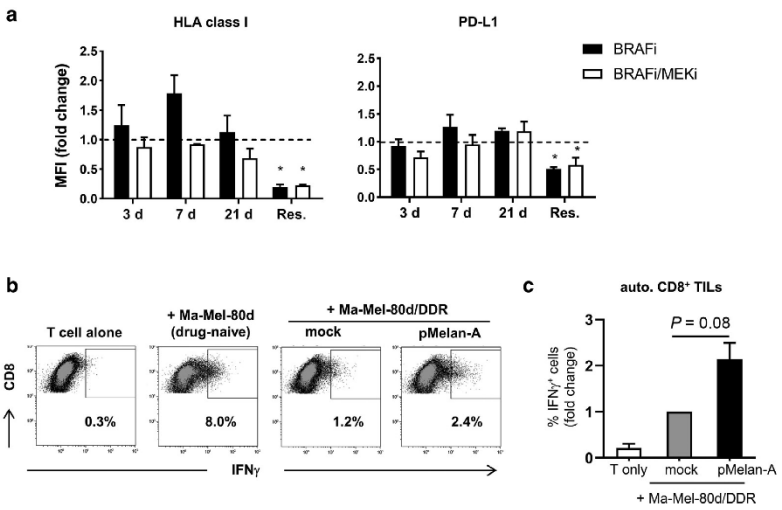

Figure 3. Dedifferentiation of DDR Ma-Mel-80d cells impairs T-cell activation. (a) Surface HLA class I and PD-L1 expressions on Ma-Mel-80d cells in the course of MAPKi treatment measured by flow cytometry. MFI is depicted as fold change relative to that of the untreated controls (mean + SEM, n = 3). *$P < 0.05$ for drug-treated or drug-resistant versus untreated group. **(b)** Double drug–resistant Ma-Mel-80d cells (Ma-Mel-80d/DDR) transiently transfected with a pMelanA were cocultured with $CD8^-$ TILs. Drug-sensitive and mock-transfected cells served as controls. Numbers in dot plots indicate the percentage of IFN-γ^+ cells within $CD8^-$ cells. Representative data are from three independent experiments. **(c)** Fold change in IFN-γ^+ $CD8^+$ TILs after being stimulated by transfected Ma-Mel-80d/DDR cells relative to those by mock-transfected control cells. n = 3, mean + SEM. auto., autologous; d, day; DDR, double drug–resistant; MAPKi, MAPK inhibitor; MFI, mean fluorescence intensity; pMelanA, melan-A expression plasmid; Res., drug-resistant state; TIL, tumor-infiltrating lymphocyte.

tumor cell–induced activation as the baseline, significantly increased IFN-γ–producing CD8 TILs were detected after being cocultured with tumor cells of BRAFi trajectory (Figure 2d and Supplementary Figure S7). In contrast, only melanoma cells from the early phase in BRAFi and MEKi track (3 and 7 days) showed enhanced T cell-stimulatory capacity, which diminished when drug exposure was prolonged (21 days to resistance).

In summary, $CD8^+$ TILs may follow distinct melanoma differentiation trajectories on MAPK inhibition, sensing temporary (drug-tolerant transition state) and stable (resistance state) phenotype alterations.

Antigen loss mediates tumor escape from $CD8^+$ TILs

Considering the role of tumor HLA class I and PD-L1 in tuning T cell activation, we investigated whether their expressions could be differentially regulated by BRAFi or combined BRAFi and MEKi treatment. Compared with untreated cells, HLA class I and PD-L1 expression on single or double drug-treated cells remained unchanged until day 21, followed by significant downregulation on drug-resistant cells (Figure 3a). However, the similar levels of HLA class I and PD-L1 between single BRAFi- and combined BRAFi plus MEKi–treated cells excluded a contribution of their biased expression to the different T cell-stimulatory capacities of single or double drug-treated tumor cells.

Considering the well-defined intratumoral presence of tyrosinase and melan-A antigen-specific T cells in patients with melanoma (Andersen et al., 2012; Kawakami et al., 2000) and the association of hyperdifferentiation with enhanced T cell activation in Ma-Mel-80d patient (Figure 2a and d), we hypothesized that re-expressing differentiation antigens into DDR tumor cells could improve their recognition by TILs. To test this, Ma-Mel-80d/DDR cells transiently transfected with melan-A or tyrosinase expression plasmids (Supplementary Figure S8a) were cocultured with autologous TILs. Whereas no effect of tyrosinase re-expression could be observed (Supplementary Figure S8b and 8c), melan-A overexpression in DDR cells clearly trended toward an improved capacity to stimulate $CD8^+$ TILs in comparison with that in mock-transfected controls ($P = 0.08$) (Figure 3b and c), demonstrating the functional relevance of differentiation antigen loss in tumor escape from T-cell surveillance.

Common T cell response pattern toward melanoma cell state transition

To test the broader applicability of our findings, we applied a single versus combined MAPKi treatment strategy to the second $BRAF^{V600E}$-mutant melanoma patient model Ma-Mel-61a (Supplementary Figure S1) and again observed the differential effects of BRAFi and combined BRAFi and MEKi treatments on cell state transition. As shown in Figure 4a, drug-sensitive tumor cells acquired resistance (SDR and DDR) on continuous drug exposure after an intermediate drug-tolerant senescence-like phase. Like in the Ma-Mel-80d model, drug withdrawal led to significant apoptosis in addicted DDR cells, whereas no change was observed in SDR cells (Supplementary Figure S9). Kinetic analysis on differentiation antigen expression in drug-tolerant cells revealed a steady upregulation of tyrosinase

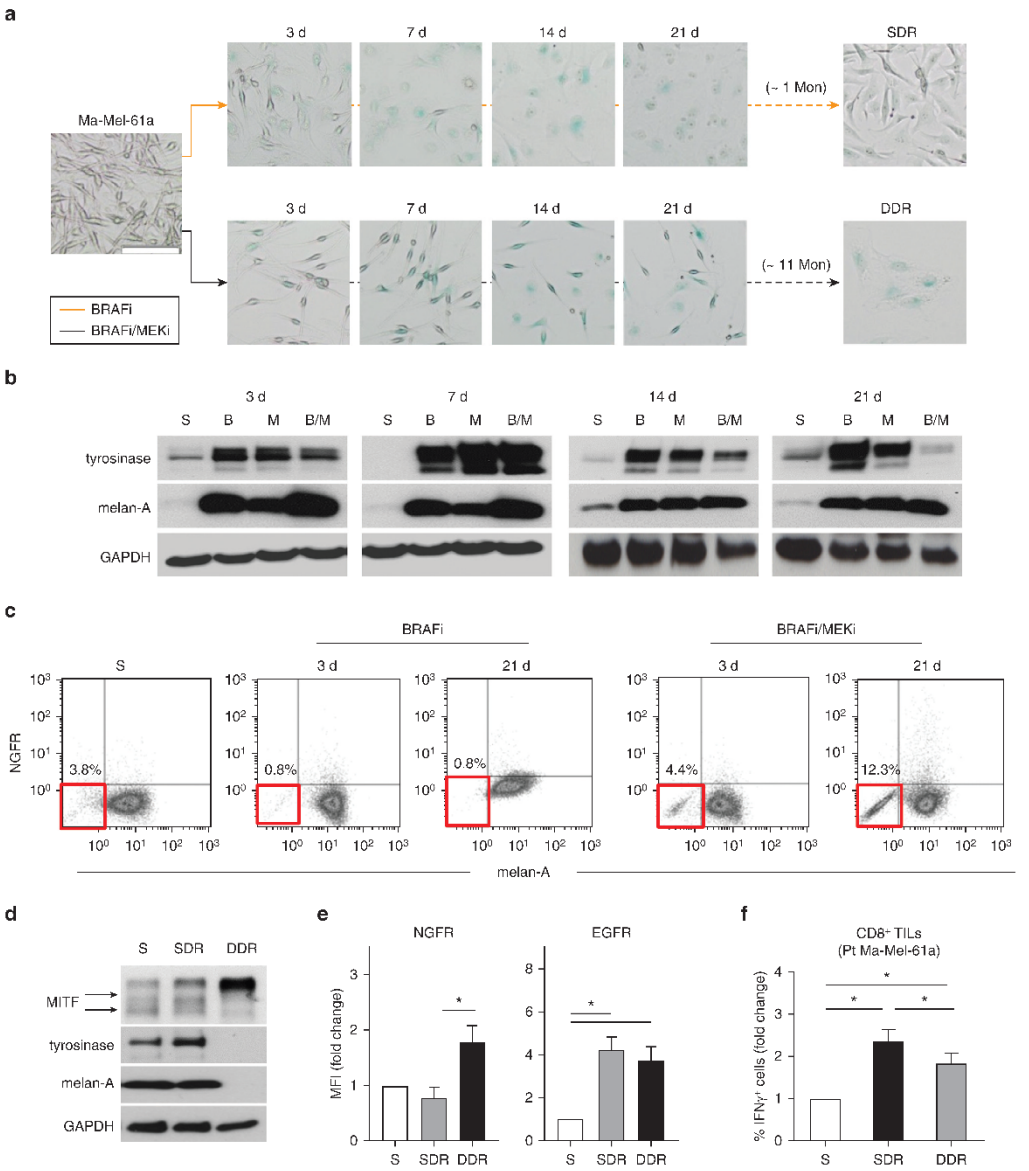

Figure 4. The common pattern of T-cell responsiveness toward B- or combined B and M–resistant melanoma cells. (a) SA β-Gal staining of Ma-Mel-61a cells on prolonged drug exposure. Bar = 100 μm. **(b)** Protein expression was determined by western blot. GAPDH was used as the loading control. **(c)** Phenotypic profiling of S and B- and combined B and M–treated Ma-Mel-61a cells through flow cytometry. **(d)** MITF, tyrosinase, and melan-A expressions were determined by western blot. GAPDH was sued as the loading control. **(e)** NGFR and EGFR expression determined by flow cytometry, depicted as MFI relative to that of the S cells. **(f)** Activation of $CD8^1$ TILs by S, SDR, or DDR Ma-Mel-61a cells, depicted as fold change of IFN-γ $CD8^1$ TILs stimulated by resistance relative to that of the sensitive tumor cells. **(a, b, c, d)** Representative data are from three independent experiments. n = 3 for **e** and f. mean + SEM. $*P < 0.05$. B, BRAF inhibitor; d, day; DDR, double drug–resistant; M, MAPK/extracellular signal–regulated kinase kinase inhibitor; MFI, mean fluorescence intensity; Mon, month; Pt, patient; S, untreated control cell; SA β-Gal, senescence-associated β-galactosidase assay; SDR, single drug–resistant

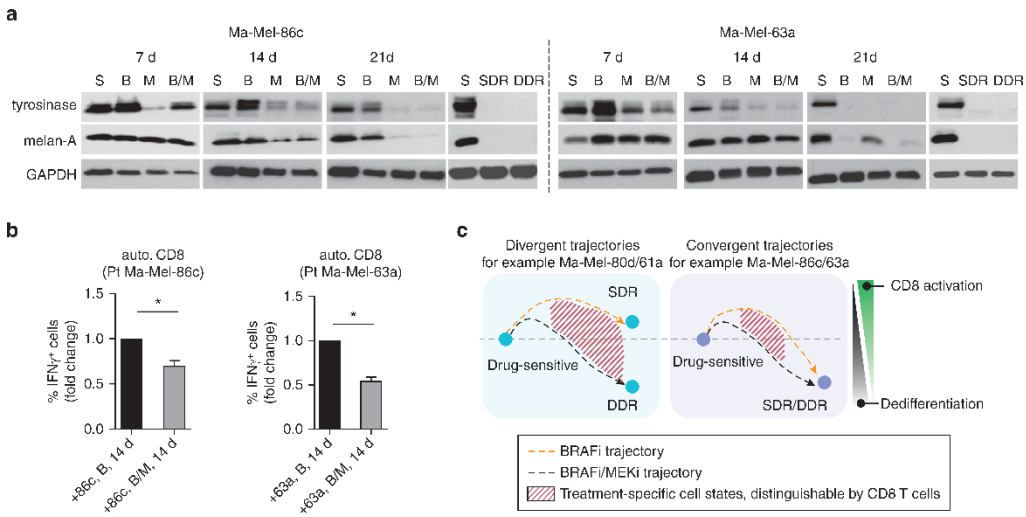

Figure 5. T-cell responses toward temporary distinct cell states and graphic summary of the investigated models. (a) Expression of the indicated proteins in Ma-Mel-86c and Ma-Mel-63a cells under treatment (7–21 d) with B, M, combined B and M, or S and matched drug-resistant (SDR and DDR) cells. GAPDH served as the loading control. Representative data are from three independent experiments. **(b)** Fold change of IFN-γ$^+$ CD8 T cells stimulated by combined B and M–treated (14 d) tumor cells relative to those by B-treated cells (B, 14 d) in Ma-Mel-86c and Ma-Mel-63a patient models. n = 3. mean + SEM. *$P < 0.05$. **(c)** Schematic summary of distinct differentiation trajectories under MAPK inhibition in isogenic melanoma models and their association with CD8$^+$ T-cell activation. auto., autologous; B, BRAF inhibitor; C, untreated control cell; d, day; DDR, double drug–resistant; M, MAPK/extracellular signal–regulated kinase kinase inhibitor; Pt, patient; S, drug-sensitive; SDR, single drug–resistant.

and melan-A on single BRAFi treatment over time, supporting a BRAFi-induced hyperdifferentiation trajectory (Figure 4b). In the combined BRAFi and MEKi treatment setting, tyrosinase expression was temporarily increased until day 14, followed by a downregulation on day 21. Single-cell profiling by flow cytometry unraveled a progressive accumulation of melan-A^{neg}/NGFR^{low} cells only in BRAFi plus MEKi– but not in BRAFi-treated cells (Figure 4c). Along the corresponding differentiation trajectories, tyrosinase and melan-A were no longer detectable in MITF^{low} DDR cells but increased or remained the same in the MITF^{high} SDR group (Figure 4d). Moreover, NGFR expression was significantly upregulated in DDR cells compared with that in SDR cells, whereas EGFR was comparably increased in both SDR and DDR cells (Figure 4e). AXL was not detectable at all (data not shown).

The limited number of TILs from this patient allowed us to study T cell responses only toward SDR and DDR cells. Again, T cell activation by MITF^{high} SDR tumor cells was superior to parental or DDR counterparts (Figure 4f). In addition, the killing of Ma-Me-61a SDR cells by autologous CD8$^+$ T cells was most effective (Supplementary Figure S10). Altogether, two melanoma models indicated that isogenic melanoma cells can move along distinct differentiation trajectories for adaption to different treatments, which in turn affects their recognition by surrounding tumor-infiltrating T cells.

However, divergent phenotype evolution is not the only response pattern toward different MAPKi treatments in melanoma. Previously, we observed a convergent manner of phenotype evolution in other patient models Ma-Mel-86c and Ma-Mel-63a. Both single BRAFi and combined BRAFi and MEKi treatments eventually gave rise to dedifferentiated drug-resistant cells (Pieper et al., 2018). But additional side-by-side kinetic studies on the drug-tolerant state revealed that combined BRAFi and MEKi treatment initiated melanoma dedifferentiation at earlier time points (day 7) than BRAFi alone (day 21) (Figure 5a). To prove whether T cells could distinguish between the temporarily distinct cell states, we coincubated drug-pretreated Ma-Mel-86c and Ma-Mel-63a cells (BRAFi or combined BRAFi and MEKi, 14 days) with corresponding autologous T cells. Indeed, in both models, significantly enhanced T cell activation was detected after stimulation by BRAFi-treated tumor cells compared with that by BRAFi plus MEKi–treated tumor cells (Figure 5b).

Collectively, our results support the model of an active cross-talk between tumor and host cells in the course of MAPKi treatment and reveal the capability of CD8$^-$ TILs to distinguish diverse melanoma differentiation states in temporary (transition state) and stable (resistant state) conditions (Figure 5c).

DISCUSSION

The highly plastic melanoma cells are capable of shifting between various cell states to persist upon microenvironmental dangers (Ahmed and Haass, 2018; Arozarena and Wellbrock, 2019; Bai et al., 2019). In the context of BRAF^{V600}-targeted therapy, drug exposure can lead to the rewiring of the gene network governed by MITF, the master transcriptional regulator of melanocyte lineage (Kemper

et al., 2014; Zipser et al., 2011). However, the situation is complex. Both MITF^{high} and MITF^{low} cell states can confer melanoma survival advantages and contribute to therapy resistance (Meierjohann, 2017; Wellbrock and Arozarena, 2015). Consistent with other studies (Smith et al., 2016; Su et al., 2017; Tsoi et al., 2018), our previous work showed that melanoma cells exposed to BRAFi or combined BRAFi and MEKi treatment transiently upregulate MITF-driven melanocyte-lineage program in the drug-tolerant phase, followed by dedifferentiation in drug-resistant cells (Pieper et al., 2018). Strikingly, this study further complements our understanding of melanoma plasticity in the course of MAPKi treatment. In two patient models, we showed that isogenic melanoma cells treated with single BRAFi evolved toward a MITF^{high} drug–resistant state, whereas the same bulk population lost MITF on combined BRAFi and MEKi treatment. So far, the underpinning molecular mechanisms guiding such divergent differentiation trajectories in this condition are undefined and are currently under investigation. Recent single-cell RNA-sequencing analysis revealed that melanoma lesions exposed to MAPKi can move along distinct differentiation trajectories, with retinoid X receptor (RXR) signaling driving the emergence of a dedifferentiated resistance-conferring population (Rambow et al., 2018).

Taking advantage of autologous TIL/tumor models to mimic tumor-T cell interaction within the tumor microenvironment of individual patients, we observed that hyperdifferentiated melanoma cell state showed enhanced sensitivity to T cells, whereas the dedifferentiated phenotype favored resistance. These findings may hold clinical implications, arguing against immunotherapy as a salvage strategy for patients with dedifferentiated MAPKi-resistant tumors. Indeed, retrospective studies indicate that patient outcomes of immune checkpoint blockade therapy after MAPKi resistance are poor (Ackerman et al., 2014; Puzanov et al., 2020). Whether simultaneous treatment with MAPKi and immunotherapy could be more efficient in tumor elimination is being actively tested, with multiple ongoing clinical trials exploring patient responses to concomitant or subsequent administration of BRAFi+MEKi therapy and immunotherapy using anti–PD-(L)1 antibodies (www.clinicaltrials.gov). Preliminary clinical results suggest that first-line combination therapy (anti–PD-(L)1 + BRAFi + MEKi) may significantly increase long-lasting antitumor responses and patient survival (Gutzmer et al., 2020; Ribas et al., 2019; Sullivan et al., 2019).

Furthermore, in-depth analyses of tumor antigen alterations during cell state transition may improve our understanding regarding the precise influence of melanoma plasticity on tumor immunogenicity. Here, we provide evidence that loss of melanoma differentiation antigens contributes to immune escape of drug-resistant tumor cells (Figure 3c and Supplementary Figure S3b). Because the BRAF–MEK-extracellular signal–associated kinase axis is upstream of multiple signaling pathways that control the expression of numerous target genes, the broad impact of MAPK inhibition on the tumor transcriptome would potentially result in alterations of the tumor antigen landscape in drug-treated tumors. Previously, we showed that not only differentiation antigens but also other tumor antigens can be affected by MAPKi treatment, including shared melanoma antigen CSPG4 and private neoantigens (Pieper et al., 2018). Consistently, Oh et al. recently showed that the inhibition of receptor tyrosine kinase ALK and RET by modulating the MAPK pathway led to large quantitative and qualitative changes on HLA-presented peptides in human lymphoma cells (Oh et al., 2019).

Besides MAPKi, other conditions such as hypoxia, nutrient limitation, and inflammation can induce melanoma cell state transition (Ravindran Menon et al., 2015), suggesting a constant impact of various tumor microenvironmental cues on T cell responses. For instance, regional glutamine deficiency can promote melanoma dedifferentiation accompanied by increased NGFR expression (Pan et al., 2016). Recently, Boshuizen and colleagues showed that NGFR^{hi} melanoma is in a T-cell–resistant state and is poorly infiltrated by CD8^{+} T cells (Boshuizen et al., 2020). In the future, comprehensive studies are needed to unravel how tumor cell state transition sculpts antitumor T cell responses in both biological and therapeutical conditions and to identify druggable targets for guiding tumor transition toward T cell-stimulatory states.

MATERIALS AND METHODS

Patient samples

Samples from patients with melanoma were collected after approval by the institutional review board (Ethics committee, University Hospital Essen [Germany]; vote SCABIO_114715), and participants gave their written informed consent. For cell line establishment (one line per lesion), mechanically dissected tumor tissues were cultured in RPMI1640 medium (Gibco, Waltham, MA) supplemented with 10% fetal calf serum (GE Healthcare, Chicago, IL), 100 U/ml penicillin, and 100 μg/ml streptomycin (both from PAN-Biotech, Aidenbach, Germany) at 37 °C in a 5% carbon dioxide atmosphere. After approximately 6–8 weeks, proliferative bulk cell lines were confirmed for their melanoma origin by targeted sequencing of melanoma-associated driver mutations (*BRAF, NRAS, NF1,* and *KIT)* and qPCR testing for differentiation markers (*MLANA; TYR; PMEL; TYRP1;* and *DCT*). Melanoma cell lines (Supplementary Table S1) were monthly controlled for mycoplasma negativity and authenticated by genomic DNA profiling at the Institute for Forensic Medicine (University Hospital Essen) using AmpFlSTR-Profiler Plus kit (Applied Biosystems, Foster City, CA).

For TIL culture, cell suspension from mechanically dissociated tumor tissue was expanded in AIM-V medium (Thermo Fisher Scientific, Waltham, MA) supplemented with 10% human serum and 500 IU/ml recombinant human IL-2 (Chiron Corporation, Emeryville, CA) for 2–5 weeks. CD8^{+} T cells were then positively selected using CD8 MicroBeads (Miltenyi Biotec, Bergisch Gladbach, Germany) and restimulated weekly with irradiated drug-naive tumor cells, serving as tumor antigen-presenting cells, in 250 IU/ml IL-2–supplemented AIM-V/10% human serum medium.

Senescence-associated β-galactosidase assay

On the day of experiment termination, drug-persistent tumor cells were fixed with 37% formaldehyde and incubated overnight in previously described staining solution (Dimri et al., 1995). Cell morphology was photographed using light microscopy.

Crystal violet-based viability assay

Melanoma cells preseeded into six-well plates (1×10^5 cells per well) were cultured in different conditions for 6 days. Afterward,

adherent cells were fixed with 4% formaldehyde and stained with 0.5% crystal violet (AppliChem, Darmstadt, Germany) diluted in 20% ethanol. For quantification, crystal violet solubilized in 100% ethanol was measured by absorbance at 550 nm.

Inhibitor treatment

Preseeded drug-naive melanoma cells were treated with 0.5 μM BRAFi (vemurafenib, Selleckchem, Houston, TX), 50 nM MEKi (cobimetinib, Selleckchem), or in combination. Inhibitors were added twice per week, together with the medium exchange. On drug exposure, some treatment-naïve melanoma cells underwent apoptosis, while the remaining switched into a nonproliferative drug-tolerant state. In this phase, cells were kept in the presence of the inhibitors without passaging. Once drug-tolerant cells started to proliferate, they were passaged whenever they reached 80–90% confluence and cultured continuously in the presence of corresponding inhibitors. Drug-naive cells were cultured as controls side by side (Supplementary Figure S6).

Flow cytometry

Antibodies, such as anti–NGFR-APC-Fire (intracellular, clone ME20.4, BioLegend, San Diego, CA), anti–melan-A FITC (intracellular, clone A103, Santa Cruz Biotechnology, Dallas, TX), anti-HLA class-I APC (surface, clone W6/32, eBiosciences, San Diego, CA), and anti-PD-L1 phycoerythrin (PE) antibodies (surface, clone 29E2A3, BioLegend) were used for tumor staining. Annexin-V-APC (BD Biosciences, Heidelberg, Germany) was used to determine tumor cell apoptosis. Background fluorescence was determined by unstained samples. Cells were measured in a Gallios flow cytometer, and the Kaluza software was used for data analysis (Beckman-Coulter, Krefeld, Germany). The gating strategy for intracellular NGFR and melan-A staining is shown in Supplementary Figure S5a.

Western blot

Lysates were prepared by lysing cell pellets in 1 × Cell Lysis buffer (Cell Signaling Technology, Danvers, MA) supplemented with 1 mM phenylmethylsulfonyl fluoride and then centrifuged at 13,000 r.p.m. at 4 °C for 15 minutes. Proteins separated by 10% SDS-PAGE were electroblotted onto nitrocellulose membranes and probed with the following primary antibodies: anti-MITF (clone C5, Sigma-Aldrich, Darmstadt, Germany), anti-tyrosinase (T311, Santa Cruz Biotechnology), anti–melan-A (clone M2-7C10, Zytomed Systems, Berlin, Germany), anti-phosphorylated ERK (Cell Signaling Biotechnology), and anti-GAPDH (Cell Signaling Biotechnology). After washing, membranes were incubated with the appropriate secondary antibodies linked to horseradish peroxidase. Antibody binding was visualized with the ECL chemiluminescence system (Thermo Fisher Scientific, Waltham, MA).

Intracellular cytokine staining

A total of 1×10^5 TILs were coincubated for 4 hours with the indicated autologous tumor cells (1×10^5 cells) in AIM-V complete medium containing 10 μg/ml brefeldin A (Sigma-Aldrich). Cells were then fixed and permeabilized using the Fixation/Permeabilization Concentrate and Diluent kit (eBioscience) followed by staining with an antibody cocktail containing antihuman CD3-Brilliant-Violet-421, CD8-APC-Cy7, TNFα-PE-Cy7, and IFN-γ-PE antibodies (BioLegend). Cells were analyzed on a Gallios flow cytometer, and the Kaluza software was used for data analysis, Gating strategy is shown in Supplementary Figure S5b.

Statistical analysis

For comparison between experimental groups, the two-tailed student's *t*-test was performed using the GraphPad Prism software (GraphPad Software, San Diego, CA). Significance was considered as $P < 0.05$ and marked with asterisks (*).

Data availability statement

No datasets were generated during this study.

ORCIDs

Franziska Noelle Harbers: http://orcid.org/0000-0003-1487-0552
Beatrice Thier: http://orcid.org/0000-0003-4869-0787
Simone Stupia: http://orcid.org/0000-0002-0961-5736
Si Zhu: http://orcid.org/0000-0002-2897-2341
Marion Schwamborn: http://orcid.org/0000-0001-6515-8333
Vicky Peller: http://orcid.org/0000-0001-8748-7613
Heike Chauvistré: http://orcid.org/0000-0002-7703-1054
Pietro Crivello: http://orcid.org/0000-0001-9668-5013
Katharina Fleischhauer: http://orcid.org/0000-0002-5827-8000
Alexander Roesch: http://orcid.org/0000-0002-0773-6067
Antje Sucker: http://orcid.org/0000-0002-2753-9626
Dirk Schadendorf: http://orcid.org/0000-0003-3524-7858
Yong Chen: http://orcid.org/0000-0002-7188-4566
Annette Paschen: http://orcid.org/0000-0003-1651-1262
Fang Zhao: http://orcid.org/0000-0002-2746-9242

CONFLICTS OF INTEREST

AP reports research grant support from Bristol-Myers Squibb. AR received travel grants and honoraria from Roche, TEVA, Bristol-Myers Squibb, Merck Sharp & Dohme, Amgen, and Novartis and research grants from Novartis and Bristol-Myers Squibb. DS is an advisory board member for Roche, Genentech, Novartis, Amgen, GlaxoSmithKline, Bristol-Myers Squibb, Boehringer Ingelheim, and Merck Sharp & Dohme. The remaining authors state no conflict of interest.

ACKNOWLEDGMENTS

This work was supported by grants from the Hiege-Stiftung gegen Hautkrebs to FZ and the Else Kröner-Promotionskolleg under Else Kröner-Fresenius-Stiftung to FNH and VP, and was partly funded by the Deutsche Forschungsgemeinschaft (German Research Foundation) (PA 2376/1-1, RO 3577/7-1, and SCHA 422/17-1 [KFO 337]). PC received funding from the Deutsche Knochenmarkspenderdatei (DKMS-SLS-MHG-2018-01). AP is considered the senior author of this paper.

AUTHOR CONTRIBUTIONS

Conceptualization: FZ, AP; Formal Analysis: FNH, BT, SS, SZ; Funding Acquisition: FZ, AP, AR, DS, PC; Investigation: FNH, BT, SS, SZ, MS; Methodology: SS, HC, PC, YC; Resources: AS, DS, KF, AR, YC, AP; Supervision: FZ; Validation: SS, SZ, VP; Visualization: FNH, FZ; Writing - Original Draft Preparation: FNH, FZ; Writing - Review and Editing: FZ, AP

SUPPLEMENTARY MATERIAL

Supplementary material is linked to the online version of the paper at www.jidonline.org, and at https://doi.org/10.1016/j.jid.2021.03.013.

REFERENCES

Ackerman A, Klein O, McDermott DF, Wang W, Ibrahim N, Lawrence DP, et al. Outcomes of patients with metastatic melanoma treated with immunotherapy prior to or after BRAF inhibitors. Cancer 2014;120:1695–701.

Ahmed F, Haass NK. Microenvironment-driven dynamic heterogeneity and phenotypic plasticity as a mechanism of melanoma therapy resistance. Front Oncol 2018;8:173.

Andersen RS, Thrue CA, Junker N, Lyngaa R, Donia M, Ellebæk E, et al. Dissection of T-cell antigen specificity in human melanoma. Cancer Res 2012;72:1642–50.

Arozarena I, Wellbrock C. Phenotype plasticity as enabler of melanoma progression and therapy resistance. Nat Rev Cancer 2019;19:377–91.

Bai X, Fisher DE, Flaherty KT. Cell-state dynamics and therapeutic resistance in melanoma from the perspective of MITF and IFNgamma pathways. Nat Rev Clin Oncol 2019;16:549–62.

Boshuizen J, Vredevoogd DW, Krijgsman O, Ligtenberg MA, Blankenstein S, de Bruijn B, et al. Reversal of pre-existing NGFR-driven tumor and immune therapy resistance. Nat Commun 2020;11:3946.

Cooper ZA, Frederick DT, Ahmed Z, Wargo JA. Combining checkpoint inhibitors and BRAF-targeted agents against metastatic melanoma. Oncoimmunology 2013;2:e24320.

Dimri GP, Lee X, Basile G, Acosta M, Scott G, Roskelley C, et al. A biomarker that identifies senescent human cells in culture and in aging skin in vivo. Proc Natl Acad Sci USA 1995;92:9363–7.

Fallahi-Sichani M, Becker V, Izar B, Baker GJ, Lin JR, Boswell SA, et al. Adaptive resistance of melanoma cells to RAF inhibition via reversible induction of a slowly dividing de-differentiated state. Mol Syst Biol 2017;13:905.

Gutzmer R, Stroyakovskiy D, Gogas H, Robert C, Lewis K, Protsenko S, et al. Atezolizumab, vemurafenib, and cobimetinib as first-line treatment for unresectable advanced $BRAF^{V600}$ mutation-positive melanoma (IMspire150): primary analysis of the randomised, double-blind, placebo-controlled, phase 3 trial. Lancet 2020;395:1835–44.

Hoek KS, Schlegel NC, Brafford P, Sucker A, Ugurel S, Kumar R, et al. Metastatic potential of melanomas defined by specific gene expression profiles with no BRAF signature. Pigment Cell Res 2006;19:290–302.

Hong A, Moriceau G, Sun L, Lomeli S, Piva M, Damoiseaux R, et al. Exploiting drug addiction mechanisms to select against MAPKi-resistant melanoma. Cancer Discov 2018;8:74–93.

Hugo W, Shi H, Sun L, Piva M, Song C, Kong X, et al. Non-genomic and immune evolution of melanoma acquiring MAPKi resistance. Cell 2015;162:1271–85.

Hugo W, Zaretsky JM, Sun L, Song C, Moreno BH, Hu-Lieskovan S, et al. Genomic and transcriptomic features of response to anti-PD-1 therapy in metastatic melanoma. Cell 2016;165:35–44.

Kawakami Y, Dang N, Wang X, Tupesis J, Robbins PF, Wang RF, et al. Recognition of shared melanoma antigens in association with major HLA-A alleles by tumor infiltrating T lymphocytes from 123 patients with melanoma. J Immunother 2000;23:17–27.

Kemper K, de Goeje PL, Peeper DS, van Amerongen R. Phenotype switching: tumor cell plasticity as a resistance mechanism and target for therapy. Cancer Res 2014;74:5937–41.

Landsberg J, Kohlmeyer J, Renn M, Bald T, Rogava M, Cron M, et al. Melanomas resist T-cell therapy through inflammation-induced reversible dedifferentiation. Nature 2012;490:412–6.

Mehta A, Kim YJ, Robert L, Tsoi J, Comin-Anduix B, Berent-Maoz B, et al. Immunotherapy resistance by inflammation-induced dedifferentiation. Cancer Discov 2018;8:935–43.

Meierjohann S. Crosstalk signaling in targeted melanoma therapy. Cancer Metastasis Rev 2017;36:23–33.

Müller J, Krijgsman O, Tsoi J, Robert L, Hugo W, Song C, et al. Low MITF/AXL ratio predicts early resistance to multiple targeted drugs in melanoma. Nat Commun 2014;5:5712.

Oh CY, Klatt MG, Bourne C, Dao T, Dacek MM, Brea EJ, et al. ALK and RET inhibitors promote HLA Class I antigen presentation and unmask new antigens within the tumor immunopeptidome. Cancer Immunol Res 2019;7:1984–97.

Pan M, Reid MA, Lowman XH, Kulkarni RP, Tran TQ, Liu X, et al. Regional glutamine deficiency in tumours promotes dedifferentiation through inhibition of histone demethylation. Nat Cell Biol 2016;18:1090–101.

Pieper N, Zaremba A, Leonardelli S, Harbers FN, Schwamborn M, Lübcke S, et al. Evolution of melanoma cross-resistance to CD8 T cells and MAPK inhibition in the course of BRAFi treatment. Oncoimmunology 2018;7:e1450127.

Puzanov I, Ribas A, Robert C, Schachter J, Nyakas M, Daud A, et al. Association of BRAF V600F/K mutation status and prior BRAF/MEK inhibition with pembrolizumab outcomes in advanced melanoma: pooled analysis of 3 clinical trials. JAMA Oncol 2020;6:1256–64.

Rambow F, Marine JC, Goding CR. Melanoma plasticity and phenotypic diversity: therapeutic barriers and opportunities. Genes Dev 2019;33:1295–318.

Rambow F, Rogiers A, Marin-Bejar O, Aibar S, Femel J, Dewaele M, et al. Toward minimal residual disease-directed therapy in melanoma. Cell 2018;174:843–55.e19.

Ravindran Menon D, Das S, Krepler C, Vultur A, Rinner B, Schauer S, et al. A stress-induced early innate response causes multidrug tolerance in melanoma. Oncogene 2015;34:4448–59.

Ribas A, Lawrence D, Atkinson V, Agarwal S, Miller WH Jr, Carlino MS, et al. Combined BRAF and MEK inhibition with PD-1 blockade immunotherapy in BRAF-mutant melanoma. Nat Med 2019;25:936–40.

Sensi M, Catani M, Castellano G, Nicolini G, Alciato F, Tragni G, et al. Human cutaneous melanomas lacking MITF and melanocyte differentiation antigens express a functional Axl receptor kinase. J Invest Dermatol 2011;131:2448–57.

Shi H, Hugo W, Kong X, Hong A, Koya RC, Moriceau G, et al. Acquired resistance and clonal evolution in melanoma during BRAF inhibitor therapy. Cancer Discov 2014;4:80–93.

Smith MP, Brunton H, Rowling EJ, Ferguson J, Arozarena I, Miskolczi Z, et al. Inhibiting drivers of non-mutational drug tolerance is a salvage strategy for targeted melanoma therapy. Cancer Cell 2016;29:270–84.

Su Y, Wei W, Robert L, Xue M, Tsoi J, Garcia-Diaz A, et al. Single-cell analysis resolves the cell state transition and signaling dynamics associated with melanoma drug-induced resistance. Proc Natl Acad Sci USA 2017;114:13679–84.

Sullivan RJ, Hamid O, Gonzalez R, Infante JR, Patel MR, Hodi FS, et al. Atezolizumab plus cobimetinib and vemurafenib in BRAF-mutated melanoma patients. Nat Med 2019;25:929–35.

Sun C, Wang L, Huang S, Heynen GJ, Prahallad A, Robert C, et al. Reversible and adaptive resistance to BRAF(V600E) inhibition in melanoma. Nature 2014;508:118–22.

Tirosh I, Izar B, Prakadan SM, Wadsworth MH 2nd, Treacy D, Trombetta JJ, et al. Dissecting the multicellular ecosystem of metastatic melanoma by single-cell RNA-seq. Science 2016;352:189–96.

Tsoi J, Robert L, Paraiso K, Galvan C, Sheu KM, Lay J, et al. Multi-stage differentiation defines melanoma subtypes with differential vulnerability to drug-induced iron-dependent oxidative stress. Cancer Cell 2018;33:890–04.e5.

Van Allen EM, Wagle N, Sucker A, Treacy DJ, Johannessen CM, Goetz EM, et al. The genetic landscape of clinical resistance to RAF inhibition in metastatic melanoma. Cancer Discov 2014;4:94–109.

Wellbrock C, Arozarena I. Microphthalmia-associated transcription factor in melanoma development and MAP-kinase pathway targeted therapy. Pigment Cell Melanoma Res 2015;28:390–406.

Wouters J, Kalender-Atak Z, Minnoye L, Spanier KI, De Waegeneer M, Bravo González-Blas C, et al. Robust gene expression programs underlie recurrent cell states and phenotype switching in melanoma. Nat Cell Biol 2020;22:986–98.

Zipser MC, Eichhoff OM, Widmer DS, Schlegel NC, Schoenewolf NL, Stuart D, et al. A proliferative melanoma cell phenotype is responsive to RAF/MEK inhibition independent of BRAF mutation status. Pigment Cell Melanoma Res 2011;24:326–33.

Supplementary Information

Supplementary Materials and Methods

Cell viability assay

Presto-Blue based: Melanoma cells were seeded at the density of 8000 cells per well in 96-well plates on day 0. After an overnight incubation in culture medium, cells were treated with increasing concentrations of BRAFi/vemurafenib in triplicates (0.5 μM, 1 μM, 3 μM, 5 μM, 10 μM, 10 μM or 40 μM) on day 1. Metabolic activity of treated cells was measured 72 hours later on day 4 using PrestoBlue reagents (ThermoFisher Scientific, United States). Briefly, a working solution containing 1 unit volume of reagent was freshly prepared by diluting the 10x stock solution with PBS. The medium was removed from the wells and replaced with 200 μL of PrestoBlue working solution, followed by a further incubation at 37°C. After 2 to 3 hours, absorbance at 570 nm was measured with an automated microplate fluorometer (Tecan, Switzerland) with signals at 600 nm as reference. The background signal was determined by medium in the absence of cells in the experimental conditions. Data is analyzed as following:

$$\text{Cell viability} = \frac{\text{Abs (drug-treated wells}^{570\text{nm-}600\text{nm}} - \text{medium}^{570\text{nm-}600\text{nm}})}{\text{Abs (DMSO-treated wells}^{570\text{nm-}600\text{nm}} - \text{medium}^{570\text{nm-}600\text{nm}})} \times 100\%$$

Analysis of MAPKi-treated patient cohort

RNAseq data from the Hugo cohort (Hugo et al., 2015) were analyzed for differential expression of MITF and multiple melanoma differentiation genes. Briefly, a log2 transformation was applied to FPKM values (GSE65185), followed by normalization to the tumor purity for each individual sample. Gene signature was calculated by averaging the Log2 (FPKM) values of included genes for the melanoma differentiation signature, including *MLANA, TYR, PMEL, TYRP1* and *DCT*.

Plasmids transfection

To overexpress MITF, melan-A, or tyrosinase expression in the corresponding experiment, melanoma cells pre-seeded in 6-well plates were transiently transfected with respective plasmids using Lipofectamine 2000 (ThermoFisher scientific, United States) for 48 h or 72 h. Mock or empty-vector transfected cells were used as negative controls.

Quantitative real-time PCR (qPCR)

Total mRNA from tumor cells was isolated using the RNeasy plus Mini Kit (Qiagen, Germany) and reverse transcribed into cDNA using High Capacity cDNA Reverse Transcription Kit (Applied Biosystems, United States) following the instructions of the manufacturers. Afterwards, qPCR was carried out with specific TaqMan Gene Expression assays. Relative RNA expression was calculated by the $2^{-\Delta\Delta Ct}$ method after normalizing expression levels of investigated mRNA to endogenous *GAPDH* mRNA levels.

Tumor killing assay

The impedance-based assay was performed on xCELLigence system (Agilent technologies, United States) to validate T cell-mediated tumor killing (Erskine et al., 2012). Briefly, tumor cells were pre-seeded into a 96 well-formatted xCELLigence E-plate for adhesion for roughly 20 hours, followed by adding T cells into the well at a 1:1 Effector-To-Target ratio for another 5 hours. As the impedance reading, reported as cell index (CI), is associated with numbers of adherent tumor cells, the following formula was used to determine percent of tumor lysis:

$(CI^{\text{tumor only}} - (CI^{\text{tumor + T cells}})) / (CI^{\text{tumor only}}) \times 100.$

Supplementary Figures

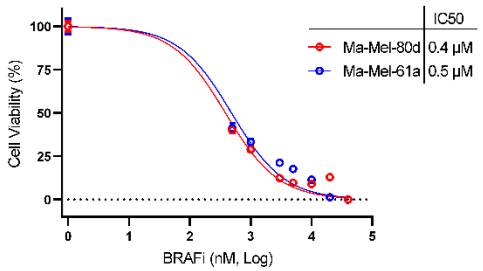

Supplementary Figure 1. Dose-dependent growth inhibition of melanoma cells by BRAFi.

PrestoBlue-based cell viability assay performed on indicated melanoma cell lines after a 3 day-treatment with increasing concentrations of BRAFi (0 - 40 µM). Representative viability curve of 2 independent experiments. Mean IC50 indicated on the upper right corner.

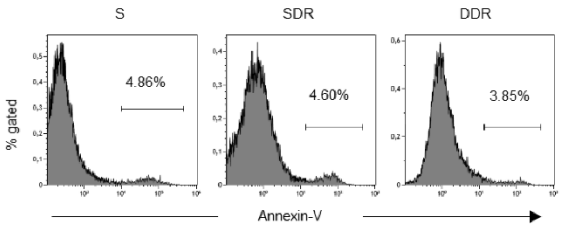

Supplementary Figure 2. Comparable spontaneous apoptosis of drug-sensitive (S), SDR, and DDR cell culture determined by Annexin-V staining.

Representative histogram of 3 independent experiments.

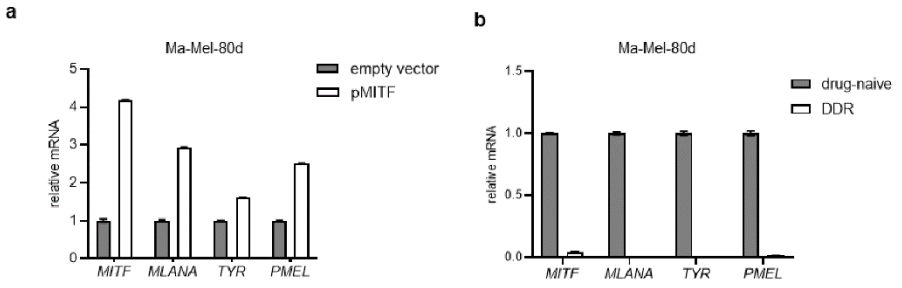

Supplementary Figure 3. Expression of MITF and its target genes in Ma-Mel-80d cells.

(a) Transient transfection of Ma-Mel-80d cells with a MITF expression plasmid (pMITF). After 72-hour incubation, mRNA levels of indicated genes were quantified by qPCR. Expression levels are depicted relative to the expression in empty vector-transfected cells. n=2. mean + SEM.

(b) mRNA levels of indicated molecules in drug-naïve and DDR Ma-Mel-80d cells determined by qPCR. Expression levels are depicted relative to the expression in drug-naive cells. n=2. mean + SEM.

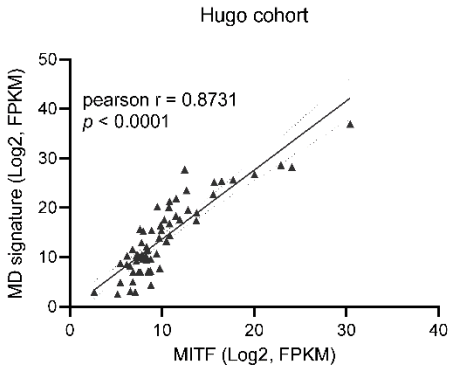

Supplementary Figure 4. Association of MITF and melanoma differentiation (MD) genes in tumor biopsies of MAPKi-treated patients.

Scatterplot of MITF compared to MD signature (*MLANA, TYR, PMEL, TYRP1,* and *DCT*) in tumor lesions from a published MAPKi-treated patient cohort (Hugo et al., 2015). Correlation: pearson's r.

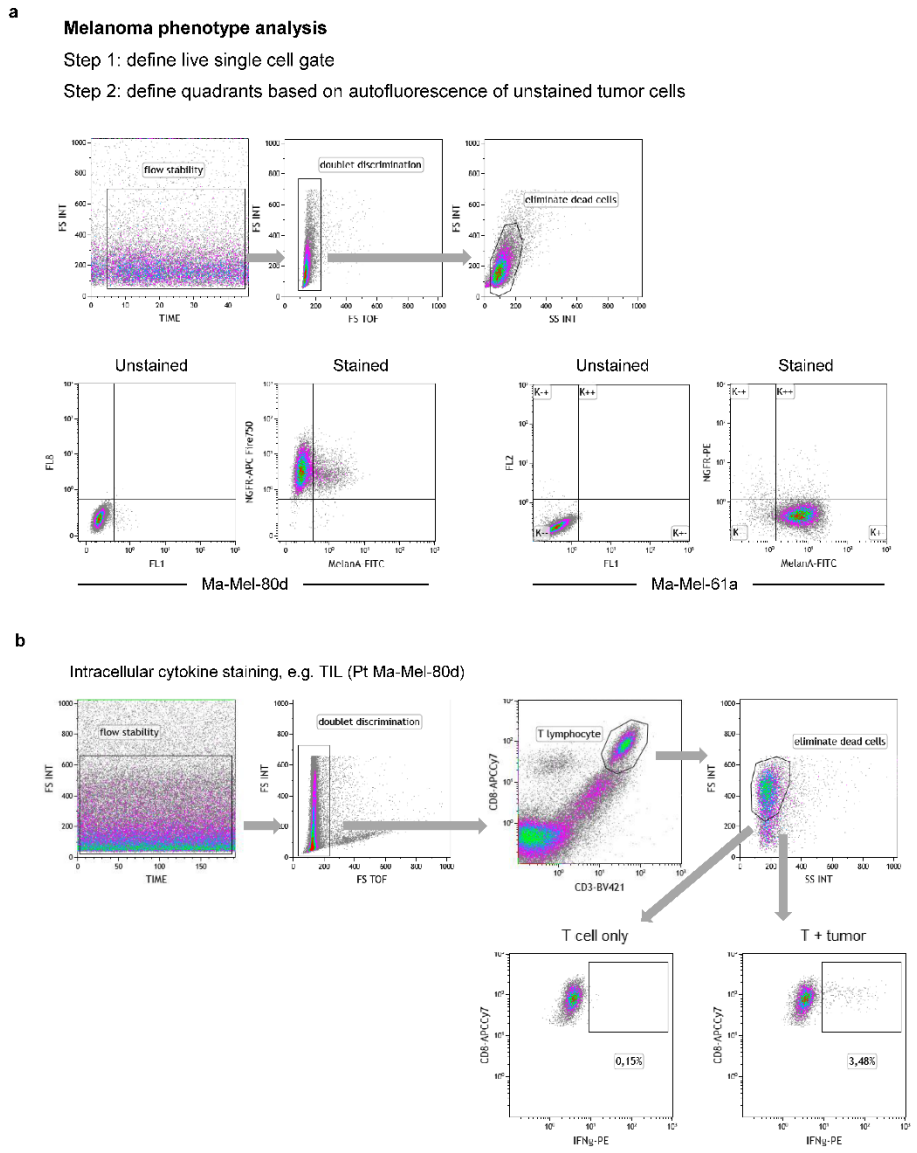

Supplementary Figure 5. Exemplary gating strategy of flow cytometric analysis for tumor cells (panel a) and TILs (panel b).

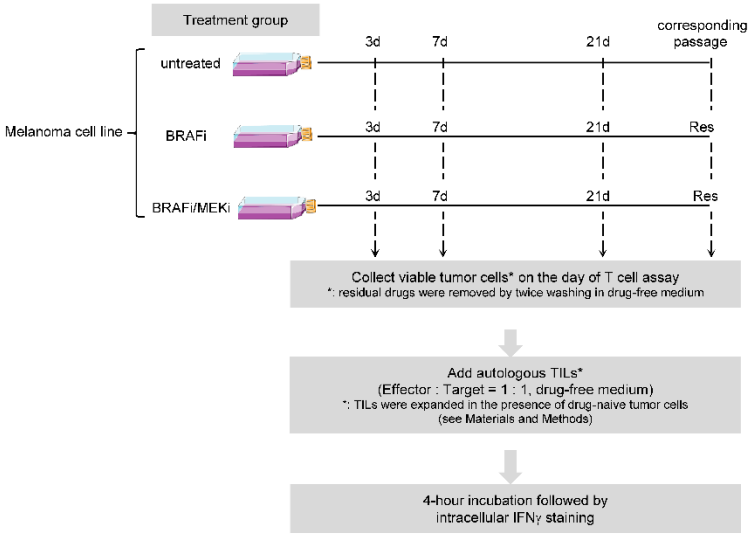

Supplementary Figure 6. Schematic of experimental setup showing drug-treatment on tumor cells and the follow-up T cell activation analysis.

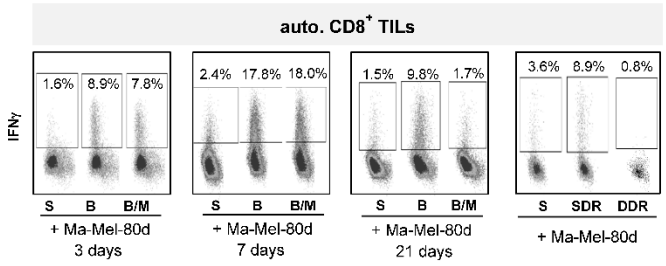

Supplementary Figure 7. Representative dot plots of IFNγ production by TILs in patient Ma-Mel-80d model.

Ma-Mel-80d cells untreated (C) or treated for indicated time periods with BRAFi (B, 0.5 μM), or combined BRAFi/MEKi (B/M, 0.5 μM/50 nM) were cocultured with autologous (auto.)

CD8$^+$ TILs. After 4-hour coincubation, T cells were stained for intracellular IFNγ. Numbers in dot plots indicate % IFNγ$^+$ cells within the CD8$^+$ cell population.

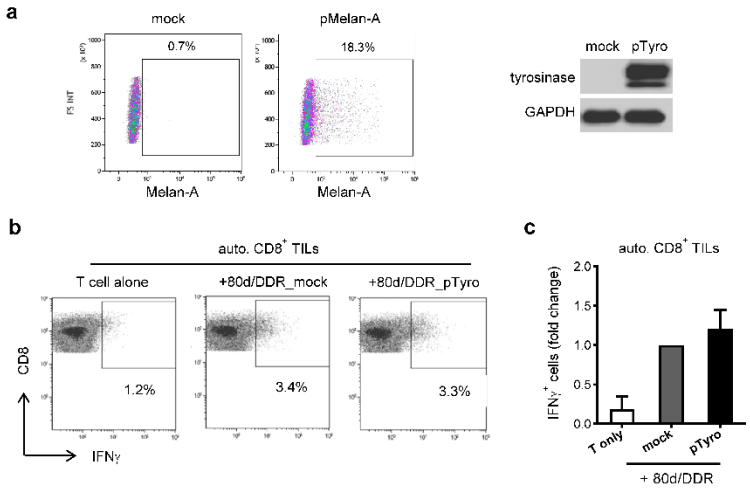

Supplementary Figure 8. Re-expresssion of differentiation antigens in Ma-Mel-80d/DDR cells and its impact on T cell activity

(a) Detection of melan-A and tyrosinase expression by flow cytometry and Western blot, respectively, in double drug-resistant Ma-Mel-80d (DDR) cells after 48-hour transient transfection with corresponding expression plasmids (pMelan-A, pTyro). Representative data of 2 independent experiments.

(b) Double drug-resistant Ma-Mel-80d cells (80d/DDR), transiently transfected with expression plasmids encoding tyrosinase (pTyro), were cocultured with autologous (auto.) CD8 TILs. Mock transfected 80d/DDR cells served as control. After 4-hour coincubation, T cells were stained for intracellular IFNγ. Numbers in dot plots indicate % IFNγ$^+$ cells within the CD8$^+$ cell population.

(c) Fold change in IFNγ$^+$ CD8$^+$ TILs stimulated by transfected 80d/DDR cells relative to mock-transfected control cells. n=3. mean + SEM.

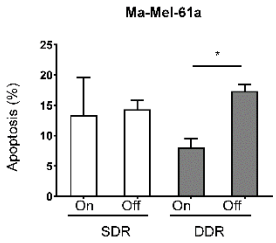

Supplementary Figure 9. Effect of drug-withdrawal on survival of MAPKi-resistant Ma-Mel-61a cells.

Apoptosis in SDR or DDR Ma-Mel-61a cells cultured with (On) or without (Off) corresponding inhibitors for 7 days detected by Annexin-V staining in flow cytometry. Apoptotic cells: Annexin-V^+. n=3. mean + SEM. *, $p < 0.05$.

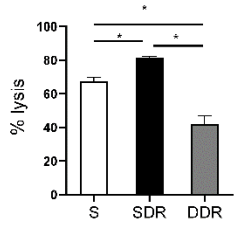

Supplementary Figure 10. Killing of Ma-Mel-61a cells by autologous $CD8^+$ T cells.

Lysis of drug-sensitive (S), single drug-resistant (SDR), or double drug-resistant (DDR) Ma-Mel-61a cells by autologous peripheral blood $CD8^-$ T cells after 5-hour coincubation. Formula for calculating T cell-mediated tumor lysis is described in Supplementary Materials and Methods. Representative result from 2 independent experiments. mean + SEM. *, $p < 0.05$.

.

Supplementary Table 1. Melanoma-associated driver mutations in investigated cell lines sequenced on the MiSeq platform

Gene Targets	Ma-Mel-80d	Ma-Mel-61a	Ma-Mel-86c	Ma-Mel-63a
BRAF	V600E	V600E	V600E	V600E
NRAS	WT	WT	WT	WT
NF1	WT	WT	WT	WT
KIT	WT	WT	WT	WT

References:

Erskine CL, Henle AM, Knutson KL. Determining optimal cytotoxic activity of human Her2neu specific CD8 T cells by comparing the Cr51 release assay to the xCELLigence system. J Vis Exp 2012(66):e3683.

Hugo W, Shi H, Sun L, Piva M, Song C, Kong X, et al. Non-genomic and Immune Evolution of Melanoma Acquiring MAPKi Resistance. Cell 2015;162(6):1271-85.

6.3 Article III

Innate immune receptor signaling induces transient melanoma dedifferentiation while preserving immunogenicity

Beatrice Thier[1], Fang Zhao[1], Simone Stupia[1], Alicia Brüggemann[1], Johannes Koch[2], Nina Schulze[2], Susanne Horn[3], Christoph Coch[4,5], Gunther Hartmann[5], Antje Sucker[1], Dirk Schadendorf[1,6], Annette Paschen[*1]

[1]Department of Dermatology, University Hospital Essen, University Duisburg-Essen and

German Cancer Consortium (DKTK), Partner Site Essen/Düsseldorf, Essen, Germany

[2]Imaging Center Campus Essen (ICCE), Center of Medical Biotechnology (ZMB), University of Duisburg-Essen, Essen, Germany

[3]Rudolf Schönheimer Institute of Biochemistry, University of Leipzig, Leipzig, Germany;

[4]Institute of Clinical Chemistry and Clinical Pharmacology, University of Bonn, Bonn, Germany;

[5]nextevidence GmbH, Grünwald, Germany;

[6]West German Cancer Center, University Hospital Essen, University of Duisburg-Essen, Essen, Germany

[*]Corresponding author.

Published in: Journal for ImmunoTherapy of Cancer (2022)

http://doi.org/10.1136/jitc-2021-003863

Received: September 15, 2021 / Accepted: May 13, 2022/ Available online: June 13, 2022

Letter of Acceptance

Thier, Beatrice

Von:	Journal for ImmunoTherapy of Cancer <onbehalfof@manuscriptcentral.com>
Gesendet:	Samstag, 14. Mai 2022 00:34
An:	Paschen, Annette
Betreff:	Your submission to Journal for ImmunoTherapy of Cancer has been accepted

13-May-2022
jitc-2021-003863.R2 - Innate immune receptor signaling induces transient melanoma dedifferentiation while preserving immunogenicity

Dear Dr. Paschen:

We are pleased to accept your article for publication in Journal for ImmunoTherapy of Cancer.

Within 2-3 working days, you will receive an email with payment options and instructions from BMJ's e-commerce partner, Copyright Clearance Center. You will be able to choose either to pay by credit card or invoice. If you are not making the payment yourself, you may forward the email to the person or organisation that will be paying on your behalf. Your article will not be processed by production until you have paid the article processing charge or requested an invoice. For more details on open access publication please visit our Author Hub: https://portal.uk-essen.de/enqsig/link?id=BCAAAABGd7m3lfMOLOIhx3uNR_1Qav4Ffx8-jQB0torD82ts_IAAAABHDbI5-Wl2J840X4GI7WUGKMdhZb8DTr2rv-0QaOZirXbneuq7N4821xHi0KkI0sGp_d0gNac4gXa4YKL7IVkYJ0xcG38YMEUAj5q-AHdeSS4TITKaUIhIu2IqZyLRd7DDMf3VwIHeACLgbzHF0NvONJ1g05BgJEjNdJWaSJmOZw2 .

Please note, that if your institution is part of one of BMJ's Publish and Read or prepay agreements your request for funding will be automatically processed based on this acceptance and you will only receive an email accepting or denying your funding request. To find out if your institution is part of a Publish and Read or prepay agreement visit BMJ's open access agreements page: https://portal.uk-essen.de/enqsig/link?id=BCAAAABGd7m3lfMOLOIhx3uNR_1Qav4Ffx8-jQB0torD82ts_JgAAAABM-CjoBcjBylXnh4D7zvqJZdHiVKV8gZDjETSePpKWYkIKCW2G52RJpk4Xcuw_F5CjO50MeLPTxhPZ2HCc1QAilgxASzEa6N1Tw3xl51qRMhdDlwjC19dlfWMzoAf2b8aOZmEaitrHbCiWWhhVH5zgZvtffzahuInurmagVaGF82WyNRaeAwDafg_Zqh-42SD2pEsR2r0mA2 .

Once payment is confirmed and your article is sent to Production, copyediting and typesetting will be completed. We will email you a proof to check via our online tool usually within 10-15 days of this time; please check your junk mail folder.

The proof is your opportunity to check for typesetting errors and the completeness and accuracy of the text; including author names and affiliations, tables and figures; including legends, numerical, mathematical, or other scientific expressions. We ask that you only make minor corrections at this stage. Please provide any comments within 48 hours. There will be no further opportunities to make corrections prior to publication.

See https://portal.uk-essen.de/enqsig/link?id=BCAAAABGd7m3lfMOLOIhx3uNR_1Qav4Ffx8-jQB0torD82ts_I4AAAAkaxJiDqFYxxQj1pWYhVu62iiDcejg8GLC-Fqj4JwU3H20g7wFMa6ue9z6dfTzrVm6RqJMzUaNYb_k2MzRMMH2P2CNf8L-KLz4ox88icTz1HpN60lNXlqn8zsdyk5_aEzzO8sVrDsmLgUq1uYsGIlR3NdZ9Ki_uP5tQTyN4f8pwn0CAY9PoAz9_LvH1lxr0 for more information about what to expect once your article has been accepted.

We publish most articles online in their final form around three weeks after acceptance. See https://portal.uk-essen.de/enqsig/link?id=BCAAAABGd7m3lfMOLOIhx3uNR_1Qav4Ffx8-jQB0torD82ts_JgAAABvpOj6XiAqDJcli3e3LDSmHWdqqEA7BKVbTtaW-_VMli6XZzaroMcMdstqwYJkguPVHF3MpNYgORfAq8VTQBmohv33gev9HelJLKbw6x7LED7OpxiZegcY26yKHCSD7afiI59

q0JXi7iWPei0ziuxwLQzwUvxUDxNvNAwDt-PiHfwViA02G31htNCWXDNZfrYwQLFVEDQRXg2 for more information about online publication. BMJ will deposit your article in all indexes affiliated with the journal.

Any final comments from the reviewer(s) are included at the foot of this email. The comments are for your information only, but in the case of minor requests (e.g. typos) these can be corrected when you receive your proof.

If your article is selected for press release by BMJ's Press Office you will be informed as soon as possible.

If you have any questions, please contact the Editorial Office.

Thank you for your contribution, and we hope that you will continue to submit to the journal in future.

Kind regards,

Pedro J. Romero, MD
Editor-in-Chief
Journal for ImmunoTherapy of Cancer

https://portal.uk-essen.de/enqsig/link?id=BCAAAABGd7m3IfMOLOIhx3uNR_1Qav4Ffx8-jQB0torD82ts_HEAAADy1_1TaXnaqMPYa9kKq4yxl00RiCXUfFjQCm_AYW490TxZmoSqwRWW3-aWSMPouq2jBBthUBEVYkFC47Ldjfc7ZHRmBPFb8F3Gn6axTo38IB-wMJt4NFI_NIJQOIJGaaJCzWo1IZICLsj8BtbuIHjnNw2

Editor(s)' Comments to Author (if any):

The authors have provided new data that significantly strengthens the conclusions of the manuscript. They have responded to the reviewer's concerns.

Contribution to present publication (Article III):

- Conception: 40 %
- Experimental work: 90 %
- Data analysis: 90 %
- Species identification: N/A
- Statistical analysis: 90 %
- Writing the manuscript: 80 %
- Revising the manuscript: 70 %

I hereby certify that Beatrice Thier was the main contributor to the concept and experimental design of this manuscript. She was the principal scientist in the planning and execution of the experiments. She wrote the original draft, visualized the results, and contributed to the review and revision of the manuscript. She performed and analyzed all experiments shown, except for figures 4A, 6C-D (right), 7N, and supplementary figures S4, S5B-D, S9A, S11, and cell sorting of Ma-Mel-47.

The above-listed contributions of Beatrice Thier to the publication are correct.

Essen, _____ _____

Annette Paschen

Essen, _____ _____

Beatrice Thier

Innate immune receptor signaling induces transient melanoma dedifferentiation while preserving immunogenicity

Beatrice Thier[1], Fang Zhao[2], Simone Stupia[3], Alicia Brüggemann[4], Johannes Koch[5], Nina Schulze[6], Susanne Horn[7], Christoph Coch[8], Gunther Hartmann[9], Antje Sucker[10], Dirk Schadendorf[11], Annette Paschen[12*]

[1]Department of Dermatology, University Hospital Essen; German Cancer Consortium (DKTK), Partner site University Hospital Essen; Hufelandstrasse 55, 45122 Essen, Germany; email: Beatrice.Thier@uk-essen.de

[2]Department of Dermatology, University Hospital Essen; German Cancer Consortium (DKTK), Partner site University Hospital Essen; Hufelandstrasse 55, 45122 Essen, Germany; email: Fang.Zhao@uk-essen.de

[3]Department of Dermatology, University Hospital Essen; German Cancer Consortium (DKTK), Partner site University Hospital Essen; Hufelandstrasse 55, 45122 Essen, Germany; email: Simone.Stupia@uk-essen.de

[4]Department of Dermatology, University Hospital Essen; German Cancer Consortium (DKTK), Partner site University Hospital Essen; Hufelandstrasse 55, 45122 Essen, Germany; email: Alicia.Brueggemann@uk-essen.de

[5]Imaging Center Campus Essen (ICCE), Center of Medical Biotechnology (ZMB), University of Duisburg-Essen, 45141 Essen, Germany;email: Johannes.Koch@uni-due.de

[6]Imaging Center Campus Essen (ICCE), Center of Medical Biotechnology (ZMB), University of Duisburg-Essen, 45141 Essen, Germany; email: Nina.Schulze@uni-due.de

[7]Rudolf Schönheimer Institute of Biochemistry, University of Leipzig, Johannisallee 30, 04103 Leipzig, Germany; email: Susanne.Horn@medizin.uni-leipzig.de

[8]Institute of Clinical Chemistry and Clinical Pharmacology, University of Bonn, Building 12, Venusberg-Campus 1, 53127 Bonn, Germany; nextevidence GmbH, Herrenwiesstrasse 12, 82031 Grünwald, Germany; email: Christoph.Coch@nextevidence.io

[9]Institute of Clinical Chemistry and Clinical Pharmacology, University of Bonn; Building 12, Venusberg-Campus 1, 53127 Bonn, Germany; email: Gunther.Hartmann@uni-bonn.de

[10]Department of Dermatology, University Hospital Essen; German Cancer Consortium (DKTK), Partner site University Hospital Essen; Hufelandstrasse 55, 45122 Essen, Germany; email: Antje.Sucker@uk-essen.de

[11]Department of Dermatology, University Hospital Essen; German Cancer Consortium (DKTK), Partner site University Hospital Essen; West German Cancer Center, University Hospital Essen, University of Duisburg-Essen; Hufelandstrasse 55, 45122 Essen, Germany; email: Dirk.Schadendorf@uk-essen.de

[12]Department of Dermatology, University Hospital Essen; German Cancer Consortium (DKTK), Partner site University Hospital Essen; Hufelandstrasse 55, 45122 Essen, Germany; email: Annette.Paschen@uk-essen.de

*Corresponding Author Annette Paschen
Department of Dermatology, University Hospital Essen
Hufelandstrasse 55, 45122 Essen, Germany
Tel. (+49) 201 723 2406, Fax (+49) 201 723 5171
email: annette.paschen@uk-essen.de

WORD COUNT: 6405

RUNNING TITLE: RIG-I-induced melanoma dedifferentiation

KEYWORDS: innate immune receptor agonists; RIG-I; 3pRNA; melanoma; plasticity and phenotype switching; cell state transition; dedifferentiation; CD8 T cells; intratumoral injection

ABSTRACT

Background: Immune-stimulatory agents, like agonists of the innate immune receptor RIG-I, are currently tested in clinical trials as an intratumoral treatment option for patients with unresectable melanoma, aiming to enhance anti-tumor T-cell responses. Switching of melanoma toward a dedifferentiated cell state has recently been linked to T-cell and therapy resistance. It remains to be determined whether RIG-I agonists affect melanoma differentiation, potentially leading to T-cell resistance.

Methods: Patient metastases-derived melanoma cell lines were treated with the synthetic RIG-I agonist 3pRNA and effects on tumor cell survival, phenotype and differentiation were determined. Transcriptomic data sets from cell lines and metastases were analyzed for associations between *RIG-I/DDX58* and melanoma differentiation markers and used to define signaling pathways involved in RIG-I-driven dedifferentiation. The impact of 3pRNA-induced melanoma dedifferentiation on CD8 T-cell activation was studied in autologous tumor-T cell models.

Results: RIG-I activation by 3pRNA induced apoptosis in a subpopulation of melanoma cells, while the majority of tumor cells switched into a non-proliferative cell state. Those persisters displayed a dedifferentiated cell phenotype, marked by downregulation of the melanocytic lineage transcription factor MITF and its target genes, including melanoma differentiation antigens (MDA). Transition into the $MITF^{low}/MDA^{low}$ cell state was JAK-dependent, with some cells acquiring Nerve Growth Factor Receptor (NGFR) expression. $MITF^{low}/MDA^{low}$ persisters switched back to the proliferative differentiated cell state when RIG-I signaling declined. Consistent with our *in vitro* findings, an association between melanoma dedifferentiation and high *RIG-I/DDX58* levels was detected in transcriptomic data from patient metastases. Notably, despite their dedifferentiated cell phenotype, 3pRNA-induced $MITF^{low}/MDA^{low}$ persisters were still efficiently targeted by autologous CD8 tumor-infiltrating T lymphocytes (TILs).

Conclusions: Our results demonstrate that RIG-I signaling in melanoma cells drives a transient phenotypic switch toward a non-proliferative dedifferentiated persister cell state. Despite their dedifferentiation, those persisters are highly immunogenic and sensitive toward autologous TILs, challenging the concept of melanoma dedifferentiation as a general indicator of T-cell resistance. In sum, our findings support the application of RIG-I agonists as a therapeutic tool for the generation of long-term clinical benefit in non-resectable melanoma.

Key Messages

- **What is already known on this topic** – Human melanoma is highly plastic and can adapt to environmental stresses by transition into dedifferentiated cell states, that have repeatedly been associated with T-cell resistance. Synthetic agonists of the innate pattern recognition receptor RIG-I are administered intratumorally to improve anti-tumor T-cell responses, though knowledge about their impact on the differentiation state of melanoma cells is lacking.
- **What this study adds** – Here, we demonstrate that in response to RIG-I activation subpopulations of melanoma cells switch into a non-proliferative dedifferentiated persister cell state, from which they escape when RIG-I signaling declines. Despite their JAK-STAT-dependent dedifferentiation, those persisters can be efficiently targeted by autologous tumor-infiltrating lymphocytes.
- **How this study might affect research, practice or policy** – RIG-I-induced melanoma dedifferentiation is not a barrier to effective anti-tumor T-cell responses, supporting the application of RIG-I agonists in tumor therapy and suggesting that melanoma dedifferentiation is not a general but rather context-dependent indicator of T-cell resistance.

BACKGROUND

Immune checkpoint blockade (ICB) has revolutionized the treatment of advanced melanoma, but clinical responses are still limited to a subgroup of patients. Cytotoxic CD8 T cells are central anti-tumor effectors in ICB. Accordingly, ICB resistance has been associated with metastases lacking CD8 T-cell infiltrates and expressing low levels of HLA class I (HLA-I) molecules presenting antigens to CD8 T cells [1–3]. To overcome resistance and improve clinical responses, innate pattern recognition receptors (PRRs) attracted attention as targets for combination ICB therapies.

Intratumoral application of PRR agonists can induce tumor cell death and orchestrate local innate and adaptive anti-tumor immune responses, potentially translating into systemic immunity [4–6]. This has also been demonstrated for mimetics of viral double-stranded RNA (dsRNA) binding to the ubiquitous cytosolic immune receptor retinoic acid-inducible gene I (RIG-I) [7,8]. Activation of RIG-I by its synthetic agonist 5'-triphosphate dsRNA (3pRNA) triggers the production of type I interferons (IFN-I) and T cell-attracting chemokines in melanoma cells [2,8]. Moreover, PRR signaling enhances melanoma cell immunogenicity by upregulation of the HLA-I antigen processing and presentation machinery (HLA-I APM) and has the capacity to overcome tumor cell-intrinsic resistance to T cells [2,9]. There is accumulating evidence also from preclinical studies that PRR signaling synergizes with ICB in boosting the anti-tumor activity of CD8 T cells in melanoma [2,10–12]. These findings and the clinical observation that patients with *RIG-I* (*DDX58*)-high melanomas show improved survival [2,11] provided a strong rational for clinical trials combining intratumoral injection of synthetic RIG-I ligands with anti-PD-1/-L1 antibodies.

Upon therapy, tumor cells are exposed to various environmental pressures that melanoma cells can adapt to and escape from via phenotype switching [13,14]. For instance, upon prolonged exposure to proinflammatory cytokines or inhibitors of oncogenic signaling pathways (MAPK

inhibitors, MAPKi), differentiated melanoma cells can stably switch into diverse dedifferentiated cell states [15–17]. Common to these cell states is the downregulation of the melanocytic lineage Microphthalmia-associated transcription factor (MITF) and its target gene network [15–17]. Of note, certain dedifferentiated cell states are characterized by the upregulation of specific phenotypic markers, such as receptor tyrosine kinase AXL or Nerve Growth Factor Receptor (NGFR/CD271) [14,18–21], the latter recently described as a regulator of melanoma phenotype switching [18].

Melanoma dedifferentiation is of highest clinical relevance, as it has repeatedly been observed in tumor biopsies derived from patients resistant to targeted inhibitor therapy or immunotherapy [3,22–24]. Therapy resistance of dedifferentiated melanomas has been attributed, at least partly, to the lower immunogenicity of dedifferentiated cells, lacking expression of melanoma differentiation antigens (MDA), such as Melan-A and tyrosinase [15–17,22].

Our previous studies demonstrated that short-term RIG-I activation in melanoma cells (up to 24 hours) immediately enhances their sensitivity towards autologous CD8 T cells [2]. However, tumor-T cell contacts might be delayed, in particular, when RIG-I agonists are injected into immune-cold lesions. Here, we demonstrate that upon prolonged RIG-I signaling, melanoma cells transiently switch into a dedifferentiated but highly immunogenic persister cell state, still sensitive to autologous CD8 T cells. Our findings suggest that despite induction of melanoma dedifferentiation, intratumoral injection of RIG-I agonists could be a valuable strategy for improvement of melanoma therapy.

MATERIALS AND METHODS

Patient samples

Tumor tissues were collected after written informed consent. Studies on human material were approved by the institutional review board. Melanoma cell lines (Ma-Mel-47, Ma-Mel-61a, Ma-Mel-63a, Ma-Mel-86c, UKE-Mel-164a) were established from metastatic lesions, as previously described [16,25,26]. Cells were confirmed to be mycoplasma-free in monthly intervals and authenticated by genetic profiling on genomic DNA at the Institute for Forensic Medicine (University Hospital Essen) using the AmpFLSTR-Profiler Plus kit (Applied Biosystems). Melanoma cell lines were cultured in RPMI1640 medium supplemented with 10 % (v/v) fetal calf serum (FCS) and penicillin/streptomycin except for UKE-Mel-164a, maintained in DMEM medium supplemented with 10 % FCS, penicillin/streptomycin, 1 % non-essential amino acids and 1 % sodium pyruvate. All cells were grown at 5 % CO_2, 37 °C.

Transfection of RIG-I agonists

The here used 3pRNA and non-stimulatory control (Ctrl) RNA were described previously [2]. High molecular weight poly(I:C) was purchased from Invivogen. Tumor cells were transfected with 100-200 ng/ml 3pRNA, Ctrl RNA or 50-100 ng/ml poly(I:C) using Lipofectamine 2000 (Invitrogen). All transfections were performed according to the manufacturer's instructions. Serum addition (Ma-Mel cells) or medium exchange (UKE-Mel-164a) was carried out 6-h post-transfection. Cells were incubated at 5 % CO_2, 37 °C, and subjected to further analyses at the indicated time points.

Transfection efficiency was estimated using a fluorescence-conjugated microRNA mimic (Dharmacon), resembling 3pRNA in structure (double-stranded) and size. Cells were transfected with 100-200 ng/ml microRNA according to the 3pRNA transfection protocol. After 24 hours, cells were harvested, washed at least three times, and subjected to fluorescence

measurement applying the Gallios flow cytometer (Beckman Coulter). Data analysis was carried out using Kaluza software (Beckman Coulter).

Inhibitor and cytokine treatment

Inhibitor treatment: Cells were seeded and transfected with 3pRNA or Ctrl RNA as described above. 6-h post-3pRNA-transfection, cells were treated with 0.5 or 2 µM JAK1/2 inhibitor (JAKi, Ruxolitinib; Selleckchem) for 3 days. Cytokine treatment: Cells were seeded and 24 h later exposed to IFN-γ (500 IU/ml; Imukin, Boehringer Ingelheim) or TNF-α (100 ng/ml; Boehringer Ingelheim) for the indicated time period. Control cells were left untreated.

Annexin V-Propidium iodide (PI) staining

On day 3 post-transfection, cells were harvested and washed with PBS. For staining, pellets were resuspended in binding buffer (10 mM HEPES, pH 7.4; 140 mM NaCl; 2.5 mM $CaCl_2$) containing Annexin V-APC (BD Pharmingen) and propidium iodide (PI; BD Pharmingen) and incubated at room temperature in the absence of light for 15 minutes. Afterward, PBS was added, and cells were immediately measured. Measurement and data processing were performed using the Gallios flow cytometer and Kaluza software, respectively (Beckman Coulter).

Western blot

Tumor cell lysates were obtained using 1x Cell Lysis Buffer (Cell Signaling). 15 µg protein/sample were separated on 8-12 % SDS-polyacrylamide gels, electroblotted onto nitrocellulose membranes, and probed with the following primary antibodies at 4 °C overnight: Anti-human rabbit antibodies anti-RIG-I (clone D14G6), anti-STAT1 (clone D1K9Y), anti-phospho (Tyr701) STAT1 (clone 58D6), anti-IRF1 (clone D5E4, XP), anti-CDK2 (clone 78B2), anti-p21 Waf1/Cip1 (clone 12D1), anti-p27 Kip (clone D69C12, XP), anti-AXL (clone

C89E7), c-jun (clone 60A8), phospho (Ser73) c-jun (clone D47G9), FRA1 (clone D80B4) and anti-GAPDH (clone 14C10) were purchased from Cell Signaling. Anti-human mouse antibodies used: anti-tyrosinase (clone T311, Santa Cruz), anti-MITF (clone C5, Sigma-Aldrich), anti-MART1/Melan-A (clone M2-7C10, Zytomed). After washing, membranes were incubated with the appropriate secondary antibody conjugated with horseradish peroxidase (HRP). Antibody binding was visualized using enhanced chemiluminescence (ECL) system (Thermo Scientific). In all experiments, GAPDH served as a loading control.

Quantitative real-time PCR (qPCR)

Total mRNA isolation, reverse transcription and TaqMan-based real-time PCR were performed as previously described [2,26]. The amount of specific mRNA was normalized to endogenous *GAPDH* (Ma-Mel-47) or *RPLP0* (Ma-Mel-61a) mRNA levels. Due to the instability of different house keeping genes in 3pRNA-transfected Ma-Mel-61a cells, specific mRNA levels of 3pRNA-treated Ma-Mel-61a cells were normalized to *RPLP0* mRNA levels of Ctrl RNA-transfected cells. Fold change in relative mRNA expression was calculated by normalizing the expression of treated cells to the corresponding controls.

Microscopy

Cell morphology and density were documented by light microscopy (Olympus CKX41) using the Olympus CellSens Standard software.

Real-time proliferation assay (xCELLigence)

Background was measured with 50 µl medium per well in an E-Plate 16 (Roche). Then 3 x 10^3 or 5 x 10^3 cells/well were seeded in 150 µl additional volume. Cell attachment was monitored with RTCA SP (Roche) instrument and the RTCA Software Version 1.2 (Roche) every 10 min. After 16-20 h, melanoma cells were transfected with 100-200 ng/ml 3pRNA or Ctrl RNA and

incubated for 10-15 days at 5 % CO_2, 37 °C. As additional controls, cells were treated with Lipofectamine 2000 only or left untransfected. 6-h post-transfection, 10 % FCS was added to Ma-Mel-86c and Ma-Mel-47 cells, the medium was exchanged entirely for UKE-Mel-164a cells. All experiments were carried out as triplicates. Changes in the electric impedance were given as a dimensionless cell index value derived from relative impedance changes corresponding to cellular coverage of the electrode sensors. The cell index was first normalized to the baseline impedance value of the background and then to the time point of transfection.

Flow cytometry

Melanoma cells were harvested at the indicated time points after transfection and once washed with PBS, followed by staining with live/dead stain kit (Invitrogen) and incubation at room temperature in the absence of light for 30 min. After washing, cells were split up for intracellular and surface staining. For surface staining, cells were incubated with the following antibodies: anti-AXL-SB436 (clone DS7HAXL, Invitrogen), anti-HLA-ABC-APC (clone W6/32, Invitrogen), anti-CD271(NGFR)-PE (clone ME20.4, BioLegend) and fixed with 4 % Paraformaldehyde. For intracellular staining, cells were fixed and permeabilized using Fixation/Permeabilization Kit (eBioscience) and stained with the following antibodies: anti-Melan-A-FITC (clone A103, Santa Cruz); anti-CD271(NGFR)-APC/Fire^{TM}750 (clone ME20.4, BioLegend). Fixed samples were measured using the Gallios flow cytometer (Beckman Coulter). Autofluorescence was determined by unstained samples, and Kaluza software (Beckman Coulter) was used for data analysis. Fold change in relative mean fluorescence intensity (MFI) was calculated by normalizing the MFI of treated cells to the corresponding controls.

Cell sorting

Ma-Mel-47 were transfected with 3pRNA or Ctrl RNA. On day 3 post-transfection, cells were stained with anti-CD271(NGFR)-APC/Fire™750 (clone ME20.4, BioLegend). Stained 3pRNA-transfected cells were separated into $NGFR^{high}$ and $NGFR^{low}$ subpopulations applying the BD FACSAria III cell sorter. Aliquots of sorted cells were analyzed for their differentiation status by intracellular Melan-A staining. The remaining cells were cultured until regrowth, followed by analyses of intracellular Melan-A and NGFR expression levels via flow cytometry, as described above.

CFSE proliferation assay

Ma-Mel-61a cells were transfected with 3pRNA or Ctrl RNA. On day 3 post-transfection, cells were stained with 10 µM CellTrace™ CFSE Cell Proliferation Kit (Invitrogen) according to the manufacturer's instructions. CFSE-labled cells were harvested and co-stained for intracellular NGFR at the indicated time points followed by flow cytometry analysis.

Expansion of autologous CD8 T cells

Tumor-reactive bulk CD8 T cells from peripheral blood of patient Ma-Mel-61 and CD8 TILs from patient Ma-Mel-86 were expanded following previously described protocols [16,26]. Expansion of tumor-reactive tumor-infiltrating lymphocytes (TILs) from patient UKE-Mel-164 was carried out as follows: Single-cell suspension from fresh tumor tissue was obtained using GentleMACS dissociation kit (Miltenyi Biotec). CD8 T cells were isolated using anti-CD8 MicroBeads (Miltenyi Biotec). Isolated T cells (1×10^6) were co-cultured in 24-well culture plates with irradiated autologous melanoma cells (1×10^5) in AIM-V medium (Gibco/BRL) supplemented with 10 % (v/v) human serum at 5 % CO_2, 37 °C. On day 3, recombinant human IL-2 (250 IU/ml) was added. In weekly intervals, 10^6 T cells were restimulated with 10^5 irradiated melanoma cells.

T-cell activation assay

Intracellular cytokine staining was performed to determine the activation of CD8 T cells by 3pRNA- and poly(I:C)-transfected autologous melanoma cells. The T-cell stimulatory capacity of 3pRNA-, poly(I:C)- or Ctrl RNA-treated melanoma cells was determined 24 hours and/or 3 days after transfection. For long-term 3pRNA- or Ctrl RNA-treatment, melanoma cells were transfected twice (day 0 and 6) and subjected to T cells 24 hours later (day 7). Briefly, T cells were stimulated with indicated autologous melanoma cells (1:1 ratio) for 4 hours in the presence of Brefeldin A (10 µg/ml; Sigma-Aldrich) at 5 % CO_2, 37°C. Afterward, cells were fixed and permeabilized using Fixation/Permeabilization Kit (eBioscience) and stained with an antibody cocktail containing anti-human CD3-BV421 (clone UCHT1, BioLegend); anti-human CD8-APC/Cy7 (clone SK1, BioLegend), anti-human IFN-γ-PE (clone B27, BioLegend) and anti-human TNF-α-PE/Cy7 (clone Mab11, BioLegend). For cell analysis and data processing, the Gallios flow cytometer and Kaluza software were used, respectively (Beckman Coulter).

Public RNA-seq data analyses

RNA sequencing (RNA-seq) data from human melanoma cell lines (Tsoi data set [27]) and patient samples (Gide cohort [28], Liu cohort [29]) were analyzed by dividing the cohorts into equally sized groups of samples with low and high expression of *RIG-I* (*DDX58*). Groups were compared for expression of *MLANA*, *MITF*, *DCT*, *TYR,* and *CD8A*. For the Gide cohort, gene expression was quantified from fastq files in transcripts per million mapped reads (TPM) per gene using kallisto [30]. The annotation of transcripts to genes was used as provided by kallisto in the Homo_sapiens.GRCh38.96.gtf from the isoform estimates. The data on gene expression from the other cohorts were used as published. Immune infiltrates were quantified applying the TIMER webtool [31] using the TPM expression values of the Gide and Liu cohorts with the SKCM cancer type selected [32].

285 **Enrichment Analysis**

286 For the enrichment analysis *RIG-I* (*DDX58*) co-regulated genes were determined using
287 Spearman correlation in RNA-seq data of the Tsoi melanoma cell line cohort [27]. The
288 conservative correction for the number of tests yielded Bonferroni-corrected q-values, and
289 FDR-corrected q-values were computed by applying p.adjust() in R using the FDR method.
290 Genes were then sorted by significance. The top 50 correlated genes were queried in enrichment
291 analysis using the Enrichr webtool [33] at https://maayanlab.cloud/Enrichr/. The resulting
292 enrichments were considered statistically significant if p-values were less than 0.05.

293 **Statistics**

294 Experimental data from three independent experiments are depicted as means plus standard
295 error of the mean (±SEM). For comparison of experimental groups, the two-tailed paired t-test
296 was applied using GraphPad Prism 8 software (GraphPad). For group comparisons of RNA-seq
297 data, the two-sided wilcoxon rank test was applied. Experimental groups were considered to be
298 significantly different at levels of p-value less than 0.05.

299

RESULTS

3pRNA-treated melanoma cells persist in a transient non-proliferative cell state

To study the effects of RIG-I signaling on melanoma cell states, we transfected various tumor cell lines, established from patient metastases, with 3pRNA or Ctrl RNA. Tumor cells were treated once, according to clinical trial protocols applying PRR agonists intratumorally in 3-week intervals [NCT03739138, NCT02828098]. Intact RIG-I signaling was confirmed by elevated RIG-I protein expression in 3pRNA-treated melanoma cells (figure 1A) and cytotoxic effects of the highly efficient transfection procedure were excluded (supplementary file 1, figure S1A-D).

Activation of RIG-I in tumor cells has been demonstrated to trigger apoptosis [34–36]. As shown in figure 1B by Annexin V-PI staining, we detected significantly enhanced cell death in all 3pRNA-treated melanoma cell lines (figure 1B,C). But, except for cell line Ma-Mel-63a, the majority of transfected cells (60-80 %) remained viable (figure 1C).

Analyzing the cells that persisted upon RIG-I activation, we recognized a more spindle-like mesenchymal cell shape of 3pRNA-treated melanoma cells compared to control cells (figure 2A). Moreover, persisters switched into a non-proliferative cell state, indicated by downregulation of the cell-cycle regulator CDK2 in four out of five 3pRNA-treated cell lines and upregulation of the CDK inhibitor p27 in Ma-Mel-61a, Ma-Mel-86c, and UKE-Mel-164a cells (figure 2B). We confirmed the strong inhibitory effect of RIG-I activation on Ma-Mel-86c and UKE-Mel-164a cells in real-time proliferation assays applying an impedance-based technology (figure 2C,D; supplementary file 1, figure S2A,B). Strikingly, on day 4 to 5 after 3pRNA transfection, melanoma cells resumed proliferation. Overall, these data demonstrated that prolonged RIG-I signaling in melanoma cells induced a transient non-proliferative cell state.

Persisting melanoma cells acquire a dedifferentiated phenotype

The lineage transcription factor MITF functions is a driver of melanoma cell proliferation [37]. As shown by Western blot in figure 3A, 3pRNA-induced non-proliferative persisters strongly downregulated the expression of MITF and its targets Melan-A and tyrosinase. Some cell lines (Ma-Mel-61a, Ma-Mel-47) appeared to even switch off differentiation marker expression. Considering that loss in melanoma differentiation can be accompanied by an upregulation of dedifferentiation markers, such as AXL or NGFR [14,21,38], we examined the expression of Melan-A, AXL, and NGFR in 3pRNA- and Ctrl RNA-treated cells by flow cytometry. Consistent with the Western blot analyses, a decrease in Melan-A was measured also by flow cytometry in all cell lines tested, with Ma-Mel-47 lacking protein expression in the majority of cells and Ma-Mel-61a displaying a nearly complete Melan-A loss. Among the 3pRNA-induced Melan-A-negative cells, we detected subpopulations of cells upregulating NGFR or AXL. An increase in the $NGFR^{high}$/$Melan\text{-}A^{neg}$ fraction (Q1) was observed in all investigated melanoma cell lines (figure 3B,C), while an enrichment of AXL-positive cells was detected only in two cases (figure. 3D; supplementary file 1, figure S3A,B). Thus, prolonged RIG-I signaling induced a non-proliferative dedifferentiated melanoma cell state.

To verify our finding that melanoma differentiation and RIG-I levels are inversely correlated, we analyzed public transcriptomic data from 53 patient-derived melanoma cell lines (Tsoi data set) [27]. Melanoma cell lines were divided into *RIG-I* (*DDX58*) low and high expression groups and compared for levels of *MITF* and its targets *MLANA*, *DCT,* and *TYR*. As shown in figure 3E, expression of each marker was significantly decreased in the *RIG-I*^{high} (*DDX58*^{high}) compared to *RIG-I*^{low} (*DDX58*^{low}) group, in line with our findings that elevated RIG-I protein expression (figure 1A) in melanoma cells is associated with dedifferentiation.

348 **RIG-I-induced melanoma dedifferentiation involves JAK-STAT signaling**

349 To decipher the mechanisms underlying 3pRNA-induced dedifferentiation, we performed
350 pathway analysis on the Tsoi transcriptome data set [27] and found genes involved in IFN and
351 JAK/STAT signaling strongly enriched in *RIG-I*^{high} (*DDX58*^{high}) melanoma cells (figure 4A;
352 supplementary file 1, figure S4; supplementary file 2, table S1A,B). Considering also our
353 previous observations of IFN-I expression by 3pRNA-treated tumor cells [2], we postulated the
354 involvement of JAK-STAT signaling in melanoma dedifferentiation. To analyze this, we
355 selected melanoma models Ma-Mel-47 and Ma-Mel-61a, showing strongest RIG-I-induced
356 dedifferentiation in terms of Melan-A downregulation (figure 3A-C), and treated those cells
357 with 3pRNA in the presence or absence of the JAK inhibitor (JAKi) Ruxolitinib. As shown for
358 Ma-Mel-47 in figure 4B, JAK-STAT signaling, triggered in response to RIG-I activation, was
359 strongly decreased in the presence of Ruxolitinib. The inhibitor also blocked Melan-A
360 downregulation by 3pRNA in a concentration-dependent manner (figure 4C-E). Similar effects
361 of JAKi were observed for 3pRNA-treated Ma-Mel-61a cells (figure 4F,G), indicating an
362 involvement of JAK-STAT signaling in RIG-I-induced melanoma dedifferentiation.
363 In addition to 3pRNA, JAK-STAT pathway activation and tumor-cell dedifferentiation were
364 induced also by poly(I:C), functioning as a RIG-I ligand upon transfection and demonstrating
365 that distinct synthetic RIG-I agonists trigger the same molecular and phenotypic alterations in
366 melanoma cells (supplementary file 1, figure S5A-D).
367

368 **Decline in RIG-I signaling reverses melanoma phenotype switching**

369 To address the transient nature of dedifferentiation, we harvested persisting Ma-Mel-47 cells
370 on day 3 and day 14 post-3pRNA-transfection. Time points were selected based on real-time
371 cell viability measurement (figure 5A), with day 3 corresponding to the non-proliferative cell
372 state and day 14 to the regrowth phase. As shown in figure 5B, on day 3 of RIG-I activation,
373 the majority of non-proliferative Ma-Mel-47 persisters lost Melan-A expression. In contrast,

when cells regained their proliferative capacity (day 14), the Melan-A-positive phenotype dominated (figure 5B-D). Consistent with a back-switch toward a differentiated phenotype, proliferative Ma-Mel-47 persisters showed a decrease in NGFR and AXL expression (figure 5B; supplementary file 1, figure S6E) and downregulation in JAK-STAT signaling (figure 5E). Similar time-dependent changes in the expression of differentiation and dedifferentiation markers were observed for 3pRNA-treated Ma-Mel-61a cells (supplementary file 1, figure S6A-E).

To stress the reversibility of RIG-I-driven phenotype switching and demonstrate that even highly dedifferentiated persisters can switch back to a differentiated proliferative cell state, we sorted 3pRNA-induced $NGFR^{high}$ Ma-Mel-47 cells from $NGFR^{low}$ cells (day 3 post-transfection) (figure 5F,G). Of the sorted $NGFR^{high}$ cells, more than 91 % showed a dedifferentiated Melan-A-negative phenotype compared to 57 % of the $NGFR^{low}$ population (figure 5G,H). Both, the $NGFR^{low}$ and $NGFR^{high}$ population resumed proliferation and switched back toward a differentiated phenotype similar to control cells (day 20 post-transfection) (figure 5G,H).

Notably, transition back to proliferation was observed also for 3pRNA-treated Ma-Mel-61a persisters, that consisted of up to 93 % dedifferentiated cells on day 3 post-transfection (figure 3B; supplementary file 1, figure S6E). To exclude that proliferative cells were exclusively derived from the small subpopulation of Ma-Mel-61a cells that preserved their differentiated phenotype under 3pRNA treatment (figure 3B; supplementary file 1, figure S6E), we monitored the reproliferation of CFSE-labeled persister in a short-term setting. Bulk adherent persister cells were stained with CFSE on day 3 post-3pRNA-transfection and fluorescence intensity was measured on day 3, day 6 and day 8. Flow cytometry analysis revealed a time-dependent gradual loss of CFSE signal intensity in total cells, associated with a reexpression of Melan-A (supplementary file 1, figure S7), clearly demonstrating that even

399 highly dedifferentiated persisters switched back toward a differentiated cell state and resumed
400 proliferation.
401 Taken together, our findings suggest that RIG-I signaling in melanoma cells induces a transient
402 non-proliferative dedifferentiated cell state via JAK-STAT pathway activation that tumor cells
403 escape from when RIG-I activation declines.
404
405 **Dedifferentiated *RIG-I*^{high} tumors show enhanced T-cell infiltration**
406 To address the clinical relevance of our findings, we studied *RIG-I/DDX58* and differentiation
407 marker expression in public transcriptomic data sets from melanoma tissues. Analysis of two
408 independent patient cohorts revealed a significant downregulation of differentiation genes
409 (*MITF*, *MLANA*, *TYR*, *DCT*) in *RIG-I*^{high} (*DDX58*^{high}) compared to *RIG-I*^{low} (*DDX58*^{low}) tumors
410 (figure 6A,B). Moreover, *RIG-I*^{high} (*DDX58*^{high}) melanomas showed elevated *CD8A* expression
411 (figure 6C,D). Applying the TIMER webtool, we estimated the CD8 T-cell infiltrates based on
412 the transcriptomic data and found them increased in *RIG-I*^{high} (*DDX58*^{high}) lesions
413 (figure 6C,D), consistent with the elevated *CD8A* expression. In summary, the tissue expression
414 data strengthened our *in vitro* findings, and the enhanced infiltration of *RIG-I*^{high} (*DDX58*^{high})
415 melanomas by CD8 T cells led us to ask for the reactivity of CD8 T cells toward 3pRNA-
416 induced dedifferentiated persister cells.
417
418 **CD8 T cells efficiently respond toward RIG-I-induced dedifferentiated persisters**
419 Recently, we demonstrated impaired recognition of MAPKi-induced dedifferentiated
420 melanoma cells by CD8 T cells [16,17]. To study T-cell responses toward 3pRNA-induced
421 persisters, we took advantage of various autologous CD8 T cell-melanoma cell models.
422 In patient model UKE-Mel-164, we analyzed the recognition of 3pRNA-induced persisters by
423 autologous TILs. To enhance RIG-I signaling and melanoma dedifferentiation, tumor cells were
424 transfected twice with 3pRNA. Compared to single transfection (figure 3A), we detected a

stronger downregulation of the differentiation antigen tyrosinase (figure 7A), but still, the majority of melanoma cells retained Melan-A expression (figure 7B). RIG-I signaling also triggered JAK-STAT pathway activation (figure 7C) and upregulation of HLA-I surface molecules (figure 7D). Strikingly, the amount of TILs producing IFN-γ and/or TNF-α was strongly increased in the presence of 3pRNA-induced persisters compared to Ctrl RNA-treated tumor cells (figure 7E,F).

With Ma-Mel-86c, we studied a second melanoma model, showing stronger dedifferentiation in response to RIG-I activation than UKE-Mel-164a (figure 3A, supplementary file 1, figure S8A,B). We confirmed JAK-STAT pathway activation and increased HLA-I expression in response to RIG-I signaling (supplementary file 1, figure S8C-E). 3pRNA treatment of Ma-Mel-86c cells triggered enhanced activation of autologous TILs at early time points (24 h) (supplementary file 1, figure S8F,H), in line with our previous study [2]. In contrast, persister cells showed T cell-stimulatory capacity similar to control cells (supplementary file 1, figure S8G-H).

So far, the functional data suggested that T-cell responses toward dedifferentiated persisters were not impaired but even enhanced. However, persisters from both patient models still contained subpopulations of partially differentiated cells, potentially contributing to T-cell activation. To overcome this limitation, we finally incorporated the melanoma model Ma-Mel-61 in our study. Tumor cells from this patient showed a complete loss of MITF, tyrosinase, and Melan-A protein expression on day 3 post-3pRNA-transfection (figure 3A, 7G), concurrent to JAK-STAT pathway activation and HLA-I upregulation (figure 7H-J). Despite total dedifferentiation, 3pRNA-induced persisters strongly activated autologous CD8 T cells in contrast to Ctrl RNA-treated melanoma cells (figure 7K,L). Thus, persisting Ma-Mel-61a cells showed enhanced immunogenicity and triggered T-cell activation by antigens other than the lost differentiation antigens. Similar to 3pRNA-induced persisters, also poly(I:C)-transfected

Ma-Mel-61a cells displayed improved T cell-stimulatory capacity (supplementary file 1, figure S9A-C).

3pRNA-induced persisters upregulate the HLA-I antigen presenting machinery similar to IFNγ-treated cells

Our previous study demonstrated increased expression of the HLA-I antigen processing and presentation machinery (HLA-I APM) by short-term 3pRNA-treated melanoma cells [2], suggesting that HLA-I APM upregulation could contribute also to the enhanced T-cell stimulatory capacity of 3pRNA-induced persisters. To estimate the level of HLA-I APM upregulation, we compared the expression of specific APM components in 3pRNA-induced persisters to IFN-γ- and TNF-α-treated melanoma cells. IFN-γ is known as potent HLA-I APM inducer and both IFN-γ and TNF-α have been described to trigger melanoma dedifferentiation [15,22,39]. In fact, each agent (3pRNA, IFN-γ, TNF-α) downregulated MITF and its target genes in our melanoma models (supplementary file 1, figure S10A,B). But, only 3pRNA and IFN-γ potently triggered JAK/STAT pathway activation linked to the induction of HLA-I APM genes, including *HLA-B, HLA-C, B2M* and *PSMB9* involved in antigen peptide presentation and processing, respectively (figure 7M,N). In line with this observation, HLA-I upregulation was strongest on 3pRNA-induced dedifferentiated $NGFR^{high}$ persisters (supplementary file 1, figure S11A-C), indicating their potent antigen-presenting capacity.

Overall, our data from the different melanoma models clearly demonstrate that, despite inducing dedifferentiation, RIG-I activation in melanoma cells preserves or even enhances the immunogenicity of persisting melanoma cells, enabling efficient anti-tumor T-cell responses.

DISCUSSION

The capacity of RIG-I agonists to enhance innate and adaptive anti-tumor immune responses has been demonstrated in various preclinical studies [2,11,40,41], leading to their implementation in clinical trial protocols. RIG-I ligands are applied intratumorally in a carrier-complexed format, thereby acting on stromal and tumor cells. Previous studies demonstrated that uptake of 3pRNA in tumor cells can induce mitochondrial apoptosis *in vitro* and *in vivo* [34–36]. Accordingly, in this study, we observed an increase in cell death in 3pRNA-treated patient-derived melanoma cell lines. However, the majority of melanoma cells remained viable upon 3pRNA treatment and persisted in a non-proliferative state. RIG-I-induced persisters downregulated the expression of melanocytic differentiation proteins, which led to the development of a $MITF^{low}/MDA^{low}$ tumor cell phenotype consistently detected in the distinct melanoma models studied. Transition into the $MITF^{low}/MDA^{low}$ cell state was induced not only by 3pRNA but also by the synthetic RIG-I agonist poly(I:C). Among the dedifferentiated persisters, subpopulations evolved showing an upregulation also of the dedifferentiation markers NGFR or AXL. Treatment with Ruxolitinib largely blocked switching toward the $MITF^{low}/MDA^{low}$ phenotype, suggesting an involvement of JAK-STAT signaling in RIG-I-induced cell state transition. In fact, 3pRNA treatment triggered phosphorylation of STAT1 and expression of IRF1 in melanoma cells. Activation of the JAK-STAT1-IRF1 pathway is also induced by interferons. IFN-γ has recently been described as a potent inducer of melanoma dedifferentiation, similar to TNF-α [15,22,39]. Both inflammatory cytokines have been demonstrated to induce a $Melan\text{-}A^{low}/NGFR^{high}$ tumor-cell phenotype. Accordingly, we detected downregulation of MITF and its target genes in our melanoma models not only in response to 3pRNA but also to IFN-γ and TNF-α treatment. It remains to be determined whether mechanisms eliciting melanoma dedifferentiation upon RIG-I signaling overlap with those triggered by IFN-γ or TNF-α. Moreover, it needs to be investigated whether other PRR ligands, currently tested in clinical trials, such as TLR agonists [42–44], have similar effects on the melanoma differentiation state.

Melanoma phenotype switching has repeatedly been associated with T-cell and therapy resistance [15–17,22,45]. Our own previous studies demonstrated that a subgroup of melanoma cells acquires resistance to MAPKi by transition into a dedifferentiated cell state that can confer cross-resistance to autologous tumor-reactive CD8 T cells [16,17]. Unlike those MAPKi-resistant melanoma cells, 3pRNA-induced dedifferentiated persisters can still be efficiently recognized by autologous CD8 TILs which could be due to distinct transcriptional and epigenetic programs triggered in response to the specific treatments. According to its role in innate immunity, RIG-I signaling elicits the expression of specific immune molecules to ensure detection and killing by cytotoxic CD8 T cells. This includes several HLA-I APM components [2], which might reshape the presented antigen repertoire and boost recognition by autologous CD8 TILs [46]. In fact, a recent study by Samuels and colleagues demonstrated that melanoma cells expressing subunits of the immunoproteasome display a distinct repertoire of HLA-I-bound tumor antigen peptides with stronger T-cell stimulatory capacity [47]. Expression of immunoproteasome subunits is induced in response to RIG-I signaling [2] and can be detected also in 3pRNA-induced persister cells. In this regard, 3pRNA-induced $MITF^{low}/MDA^{low}$ persisters very much resemble IFN-γ-induced $MITF^{low}/MDA^{low}$ melanoma cells, both showing JAK-STAT pathway activation linked to potent HLA-I APM upregulation. Tumor cell-intrinsic JAK-STAT signaling and HLA-I antigen presentation play a key role in response to immunotherapy [2,48]. Notably, while TNF-α signaling also elicited melanoma dedifferentiation, it did not trigger JAK-STAT pathway activation and HLA-I APM upregulation, suggesting lack of immunogenicity enhancement for TNF-α-treated cells which should be addressed in future studies.

Hence, the outcome of treatment-induced dedifferentiation on anti-tumor T-cell responses seems to be dependent on the agent that triggers melanoma dedifferentiation and the specific transcriptional program induced upon treatment. In line with our findings, Kim et al. recently demonstrated that melanoma biopsies from patients responding to ICB show a decrease in

melanocytic marker expression [39]. Based on this observation, the authors proposed melanoma dedifferentiation as an indicator for an initial response to anti-PD-1 therapy [39].

Though, data from our study and Kim et al. challenge the concept of melanoma dedifferentiation as a general T-cell and therapy resistance marker, we expect that the association still holds true for patients whose anti-tumor T-cell responses heavily rely on a MDA-specific T-cell repertoire, and for those receiving MDA-specific therapies, like adoptive transfer of MDA-specific T-cells.

Overall, we think that our study is of strong clinical significance. First, our findings support ongoing clinical trials combining intratumoral injection of RIG-I agonists with anti-PD-1 blocking antibodies as a treatment option for unresectable melanomas (NCT03739138, NCT02828098). Second, our data suggest that treatment-induced melanoma dedifferentiation should not be considered as a general T-cell and therapy resistance marker.

DECLARATIONS

Ethics approval and consent to participate

Specimens from melanoma patients were collected after written informed consent. Studies on human material were approved by the institutional review board (18-8269-BO). Biological samples and related data were provided by the Westdeutsche Biobank Essen (WBE/SCABIO, University Hospital Essen, University of Duisburg-Essen, Essen, Germany; approval no. SCABIO_114715).

Patient consent for publication

Not required.

548 **Availability of data and material**

549 Cell lines will be available on request.

550 **Competing interests**

551 AP reports research grant support and provision of reagents from Bristol-Myers Squibb (BMS)
552 and Merck Sharp & Dohme (MSD). AS reports personal fees from Novartis Adboard. GH is a
553 co-founder of Rigontec GmbH. DS declares grants, personal fees, and/or nonfinancial support
554 from BMS, Roche, Novartis, Regeneron, Sanofi, MSD, Amgen, 4SC, Merck-EMD, Array,
555 Pierre-Fabre, Philogen, Incyte, and Pfizer.

556 **Funding**

557 AP was supported by grants of the Deutsche Krebshilfe (DKH, German Cancer Aid;
558 Translational Oncology 70113455) and the Deutsche Forschungsgemeinschaft (DFG, German
559 Research Foundation) - SFB1430 - Project-ID 424228829 and KFO337 – Project-ID
560 405344257 [PA 2376/1-1]. DS was supported by grants of the Deutsche Krebshilfe (DKH,
561 German Cancer Aid; Translational Oncology 70113455) and the Deutsche
562 Forschungsgemeinschaft (DFG, German Research Foundation) KFO337 – Project-ID
563 405344257 [SCHA 422/17-1]. SH received funding from the Deutsche
564 Forschungsgemeinschaft (DFG, German Research Foundation) KFO337 – Project-ID
565 405344257 [HO 6389/2-1]. GH was supported by grants of the Deutsche
566 Forschungsgemeinschaft (DFG, German Research Foundation) of TRR259 and TRR237 and is
567 member of Germany's Excellence Strategy (EXC2151—390873048). NS was supported by the
568 Deutsche Forschungsgemeinschaft (DFG, German Research Foundation) - SFB1430 - Project-
569 ID 424228829.

570 **Author contributions**

571 BT conceptualized the study, conducted experiments, acquired and analyzed data, and wrote
572 the manuscript. FZ, SS and AB performed experiments, acquired and analyzed data, and
573 reviewed the manuscript. JK and NS performed experiments, acquired and analysed data. SH
574 provided software, conducted bioinformatics and statistical data analyses, and reviewed the
575 manuscript. CC and GH provided critical reagents. AS and DS collected clinical samples and
576 annotated clinical data. AP conceptualized and supervised the study, reviewed data, and wrote
577 the manuscript.

578 **Acknowledgments**

579 Cell sorting was performed at the Imaging Center Essen (IMCES), a Service Core Facility of
580 the Faculty of Medicine of the University Duisburg-Essen, Germany.

581 **LIST OF ABBREVIATIONS**

582 3pRNA: 5'triphosphorylated double-stranded RNA; CDK: cyclin-dependent kinase; control
583 RNA: Ctrl RNA; ECL: enhanced chemiluminescence; FCS: fetal calf serum; FDR: False
584 Discovery Rate; GAPDH: Glyceraldehyde 3-phosphate dehydrogenase; HLA-I: HLA class I;
585 HRP: horseradish peroxidase; ICB: Immune checkpoint blockade; ICS: intracellular cytokine
586 staining; IFN-I: type I interferons; JAK: Janus kinase; MAPKi: mitogen-activated protein
587 kinase inhibitor; IFN-γ: interferon-gamma; IL-2: interleukin-2; IRF1: interferon regulatory
588 factor 1; JAKi: JAK1/2 inhibitor; KEGG: Kyoto Encyclopedia of Genes and Genomes; MDA:
589 melanoma differentiation antigens; MFI: mean fluorescence intensity; MITF: Microphthalmia-
590 associated transcription factor; NGFR: Nerve Growth Factor Receptor; Lipo: Lipofectamine;
591 PBS: phosphate-buffered saline; PD-1: programmed cell death protein 1; PI: propidium iodide;
592 PRR: pattern recognition receptors; pSTAT1: phosphorylated (Y701) STAT1; RIG-I: retinoic

593 acid inducible gene I; RNA-seq: RNA sequencing; SEM: standard error of the mean; STING:
594 stimulator of interferon genes; STAT: signal transducer and activator of transcription; TILs:
595 tumor-infiltrating lymphocytes; TLR9: Toll like receptor 9; TNF-α: tumor necrosis factor
596 alpha; TPM: transcripts per million; untransf.: untransfected

597

598 **APPENDICES**

599 Supplementary file 1
600 Supplementary file 2

601 **FIGURE CAPTIONS**

602 **Figure 1: Enhanced melanoma cell death in response to 3pRNA-treatment.** (A-C)
603 Melanoma cells were transfected with 3pRNA (+) or Ctrl RNA (-) and subjected to further
604 analyses on day 3 post-transfection. (A) RIG-I expression analyzed by Western blot. GAPDH,
605 loading control. Representative data from three independent experiments. (B,C) Cells stained
606 for Annexin V/PI and analyzed by flow cytometry. (B) Representative dot plots, (C) percentage
607 of Annexin V-positive (Annexin V^+) cells shown as mean±SEM from three independent
608 experiments. Significantly different experimental groups: * $p < 0.05$, ** $p < 0.01$, *** $p < 0.005$
609 by two-tailed paired t-test.

610 **Figure 2: Induction of a transient non-proliferative melanoma cell state upon RIG-I**
611 **activation.** (A,B) Melanoma cells were transfected with 3pRNA (+) or Ctrl RNA (-) and
612 subjected to further analyses on day 3 post-transfection. (A) Microscopic analyses of cell
613 morphology and density (10x magnification). Representative images from three independent
614 experiments. (B) Expression of cell cycle regulators analyzed by Western blot. GAPDH,
615 loading control. Representative data from three independent experiments. (C,D) Real-time

proliferation of cell line Ma-Mel-86c (C) and UKE-Mel-164a (D) after 3pRNA (red) or Ctrl RNA (blue) transfection. Vertical grey lines indicate time point of transfection; grey arrow shows medium exchange. Representative data from three independent experiments.

Figure 3: Dedifferentiation of 3pRNA-induced persister cells. (A-D) Melanoma cells were transfected with 3pRNA (+) or Ctrl RNA (-) and subjected to further analyses on day 3 post-transfection. (A) Expression of differentiation markers analyzed by Western blot. GAPDH, loading control. Representative data of three independent experiments. (B,C) Single-cell phenotype profiling by flow cytometry. (B) Representative dot plots of NGFR and Melan-A expression. Numbers indicate the percentage of specific cell populations. Quadrants defined based on autofluorescence of unstained cells. (C) Heat map of the quadrant's median of three independent experiments. (D) Surface expression of AXL measured by flow cytometry. Percentage of AXL-positive (AXL^+) cells shown as mean±SEM of three independent experiments. Significantly different experimental groups: * $p < 0.05$, ** $p < 0.01$ by two-tailed paired t-test. (E) Analysis of Tsoi transcriptomic data set [27], comparing gene expression in patient-derived melanoma cell lines grouped by *RIG-I*^{low} (*DDX58*^{low}) and *RIG-I*^{high} (*DDX58*^{high}) (n=27 vs. n=27; threshold: 7 TPM). P-values calculated by two-sided wilcoxon rank tests.

Figure 4: JAK-dependent dedifferentiation of 3pRNA-induced persisters. (A) KEGG database pathways enriched for genes co-regulated with *DDX58* mRNA in the Tsoi transcriptomic data set [27]. (B) Ma-Mel-47 cells were transfected with 3pRNA or Ctrl RNA, incubated with or without 0.5 µM JAKi (Ruxolitinib) for 24 h. JAK-STAT signaling analyzed by Western blot. GAPDH, loading control. Representative data of two independent experiments. (C,D) Ma-Mel-47 cells were transfected with 3pRNA or Ctrl RNA, incubated with or without 0.5 µM JAKi (Ruxolitinib), and subjected to further analyses on day 3 post-transfection. Intracellular Melan-A expression determined by flow cytometry. (C) Representative histograms with dotted line representing unstained control and (D) fold change

of MFI given as mean±SEM of three independent experiments. (E) Melan-A expression in Ma-Mel-47 after 3pRNA transfection and incubation with different JAKi concentrations for 3 days; representative dot plots of two or three independent experiments. (F,G) Ma-Mel-61a cells were transfected with 3pRNA or Ctrl RNA, incubated with or without 0.5 µM JAKi (Ruxolitinib) for 3 days, and subjected to further analyses. Intracellular Melan-A expression determined by flow cytometry. (F) Representative histograms with dotted line representing unstained control and (G) fold change of MFI given as mean±SEM of three independent experiments. Significantly different experimental groups: ** $p < 0.01$ by two-tailed paired t-test.

Figure 5: Transient dedifferentiation upon RIG-I activation. (A-E) Ma-Mel-47 cells were transfected once with 3pRNA or Ctrl RNA and analyzed on day 3 (3 d) and 14 (14 d) post-transfection. (A, top) Real-time proliferation of Ma-Mel-47 after 3pRNA (red) or Ctrl RNA (blue) transfection. Vertical grey line indicates time point of transfection; grey arrows show medium exchange. Representative data of three independent experiments. (A, bottom) Morphology and cell density monitored microscopically (10x magnification). Representative images of three independent experiments. (B) Differentiation status determined by the expression of indicated proteins. GAPDH, loading control. Representative data of three independent experiments. (C,D) Melan-A expression determined by flow cytometry. (C) Representative histograms with dotted line representing unstained control and (D) fold change of MFI given as mean±SEM of three independent experiments. (E) RIG-I expression and JAK-STAT pathway activation analyzed by Western blot. GAPDH, loading control. Representative data of three independent experiments. (F-H) 3pRNA-transfected Ma-Mel-47 were sorted for NGFR expression on day 3 post-transfection and cultured until reproliferation (20 d). (F) Scheme of workflow. Illustration created with BioRender.com. (G, top) NGFR surface expression before cell sorting on day 3 post-transfection. (G, bottom) Melan-A and NGFR co-expression in melanoma cells analyzed by flow cytometry directly after cell sorting (3 d) and at the time point of reproliferation at day 20 post-transfection (20 d). Representative dot plots

667 with percentage of cells of two independent experiments. (H) Quantification of Melan-A
668 expression given as fold change of MFI from two independent experiments. Linked points
669 indicate results from the same experiment. Significantly different experimental groups: ** $p <$
670 0.01; *** $p < 0.005$ by two-tailed paired t-test.

671 **Figure 6: *RIG-I* (*DDX58*) expression in melanoma biopsies correlates with**
672 **dedifferentiation and T-cell infiltration.** Expression of melanoma differentiation markers
673 *MITF*, *MLANA*, *TYR*, and *DCT* (A,B), and T-cell marker *CD8A* (C,D, left) in *RIG-I*^{low}
674 (*DDX58*^{low}) and *RIG-I*^{high} (*DDX58*^{high}) expression groups from the published RNA-seq data
675 sets. (C,D, right) Calculated CD8 T-cell infiltrates in *RIG-I*^{low} (*DDX58*^{low}) and *RIG-I*^{high}
676 (*DDX58*^{high}) expression groups. Data sets of the Gide cohort [28] (A,C, n=45 vs n=46;
677 threshold: 11.1 TPM) and Liu cohort [29] (B,D; n=60 vs n=61; threshold: 7.7 TPM). P-values
678 from two-sided wilcoxon rank tests.

679 **Figure 7: Strong CD8 T-cell reactivity toward 3pRNA-induced dedifferentiated**
680 **persisters.** (A,B and D-F) UKE-Mel-164a cells were transfected twice with 3pRNA (+) or Ctrl
681 RNA (-) and subjected to further analyses on day 7 post-transfection. (A) Differentiation status
682 of UKE-Mel-164a determined by the expression of indicated proteins. GAPDH, loading
683 control. Representative data from three independent experiments. (B) Melan-A expression
684 determined by flow cytometry. Representative histogram from three independent experiments.
685 (C) RIG-I expression and JAK-STAT pathway activation analyzed 24 h post-transfection by
686 Western blot. GAPDH, loading control. Representative data from three independent
687 experiments. (D) HLA-I cell surface expression measured by flow cytometry. Representative
688 histogram from three independent experiments. (E,F) Activation of autologous TILs by UKE-
689 Mel-164a cells transfected with 3pRNA or Ctrl RNA analyzed by intracellular cytokine staining
690 in flow cytometry. (E) Representative dot plot and (F) quantification of IFN-γ^+ TNF-α^+ CD8$^+$
691 TILs. Fold change given as mean±SEM from three independent experiments. (G-J) Ma-Mel-

61a melanoma cells were transfected with 3pRNA (+) or Ctrl RNA (-) and subjected to further analyses on day 1 (H) or day 3 (G, I-L) post-transfection. (G) Melan-A expression analyzed by flow cytometry. Representative data from three independent experiments. (H) RIG-I expression and JAK-STAT pathway activation analyzed on day 1 post-transfection by Western blot. GAPDH, loading control. Representative data from three independent experiments. (I,J) HLA-I cell surface expression measured by flow cytometry. (I) Representative histogram and (J) fold change of MFI given as mean±SEM from three independent experiments. (K,L) Activation of autologous T cells by Ma-Mel-61a cells transfected with 3pRNA or Ctrl RNA analyzed by intracellular IFN-γ staining in flow cytometry. w/o: spontaneous cytokine release in the absence of target cells. (K) Representative dot plot and (L) quantification of IFN-γ^+ $CD8^+$ T cells. Fold change given as mean±SEM from two independent experiments. (M) RIG-I and JAK/STAT pathway activation analzyed 24 h post-transfection/post-treatment by Western Blot. GAPDH, loading control. Representative data from two independent experiments. (N) Relative mRNA expression of genes involved in antigen processing and presentation in Ma-Mel-47 and Ma-Mel-61a cells on day 3 post-3pRNA transfection or post-cytokine treatment. Fold change given as mean from two independent experiments. Significantly different experimental groups: * $p < 0.05$; **** $p < 0.001$ by two-tailed paired t-test.

REFERENCES

[1] Sharma P, Hu-Lieskovan S, Wargo JA, Ribas A. Primary, Adaptive, and Acquired Resistance to Cancer Immunotherapy. Cell 2017;168:707–23. https://doi.org/10.1016/j.cell.2017.01.017.

[2] Such L, Zhao F, Liu D, Thier B, Khanh Le-Trilling VT, Sucker A, et al. Targeting the innate immunoreceptor RIG-I overcomes melanoma-intrinsic resistance to T cell immunotherapy. J Clin Invest 2020;140:4266–81. https://doi.org/10.1172/JCI131572.

[3] Lee JH, Shklovskaya E, Lim SY, Carlino MS, Menzies AM, Stewart A, et al. Transcriptional downregulation of MHC class I and melanoma de- differentiation in

718 resistance to PD-1 inhibition. Nat Commun 2020;11:1–12.
719 https://doi.org/10.1038/s41467-020-15726-7.

720 [4] Middleton MR, Hoeller C, Michielin O, Robert C, Caramella C, Öhrling K, et al.
721 Intratumoural immunotherapies for unresectable and metastatic melanoma: current
722 status and future perspectives. Br J Cancer 2020;123:885–97.
723 https://doi.org/10.1038/s41416-020-0994-4.

724 [5] Melero I, Castanon E, Alvarez M, Champiat S, Marabelle A. Intratumoural
725 administration and tumour tissue targeting of cancer immunotherapies. Nat Rev Clin
726 Oncol 2021;18. https://doi.org/10.1038/s41571-021-00507-y.

727 [6] Bommareddy PK, Silk AW, Kaufman HL. Intratumoral Approaches for the Treatment
728 of Melanoma. Cancer J (United States) 2017;23:40–7.
729 https://doi.org/10.1097/PPO.0000000000000234.

730 [7] Hornung V, Ellegast J, Kim S, Brzózka K, Jung A, Kato H, et al. 5'-Triphosphate RNA
731 is the ligand for RIG-I. Science 2006;314:994–7.
732 https://doi.org/10.1126/science.1132505.

733 [8] Iurescia S, Fioretti D, Rinaldi M. The innate immune signalling pathways: Turning RIG-
734 I sensor activation against cancer. Cancers (Basel) 2020;12:1–26.
735 https://doi.org/10.3390/cancers12113158.

736 [9] Kalbasi A, Tariveranmoshabad M, Hakimi K, Kremer S, Campbell KM, Funes JM, et al.
737 Uncoupling interferon signaling and antigen presentation to overcome immunotherapy
738 resistance due to JAK1 loss in melanoma. Sci Transl Med 2020;12.
739 https://doi.org/10.1126/scitranslmed.abb0152.

740 [10] Torrejon DY, Abril-Rodriguez G, Champhekar AS, Tsoi J, Campbell KM, Kalbasi A, et
741 al. Overcoming Genetically Based Resistance Mechanisms to PD-1 Blockade. Cancer
742 Discov 2020;10:1140–57. https://doi.org/10.1158/2159-8290.CD-19-1409.

743 [11] Heidegger S, Wintges A, Stritzke F, Bek S, Steiger K, Koenig PA, et al. RIG-I activation
744 is critical for responsiveness to checkpoint blockade. Sci Immunol 2019;4.
745 https://doi.org/10.1126/sciimmunol.aau8943.

746 [12] Aznar MA, Planelles L, Perez-Olivares M, Molina C, Garasa S, Etxeberría I, et al.
747 Immunotherapeutic effects of intratumoral nanoplexed poly I:C. J Immunother Cancer

748 2019;7:1–16. https://doi.org/10.1186/s40425-019-0568-2.

749 [13] Boumahdi S, de Sauvage FJ. The great escape: tumour cell plasticity in resistance to
750 targeted therapy. Nat Rev Drug Discov 2020;19:39–56. https://doi.org/10.1038/s41573-
751 019-0044-1.

752 [14] Rambow F, Marine JC, Goding CR. Melanoma plasticity and phenotypic diversity:
753 Therapeutic barriers and opportunities. Genes Dev 2019;33:1295–318.
754 https://doi.org/10.1101/gad.329771.119.

755 [15] Landsberg J, Kohlmeyer J, Renn M, Bald T, Rogava M, Cron M, et al. Melanomas resist
756 T-cell therapy through inflammation-induced reversible dedifferentiation. Nature
757 2012;490:412–6. https://doi.org/10.1038/nature11538.

758 [16] Pieper N, Zaremba A, Leonardelli S, Harbers FN, Schwamborn M, Lübcke S, et al.
759 Evolution of melanoma cross-resistance to CD8+ T cells and MAPK inhibition in the
760 course of BRAFi treatment. Oncoimmunology 2018;7:1–9.
761 https://doi.org/10.1080/2162402X.2018.1450127.

762 [17] Harbers FN, Thier B, Stupia S, Zhu S, Schwamborn M, Peller V, et al. Melanoma
763 Differentiation Trajectories Determine Sensitivity toward Pre-Existing CD8+ Tumor-
764 Infiltrating Lymphocytes. J Invest Dermatol 2021;141:2480–9.
765 https://doi.org/10.1016/j.jid.2021.03.013.

766 [18] Restivo G, Diener J, Cheng PF, Kiowski G, Bonalli M, Biedermann T, et al. Low
767 Neurotrophin receptor CD271 regulates phenotype switching in Melanoma. Nat
768 Commun 2017;8. https://doi.org/10.1038/s41467-017-01573-6.

769 [19] Rambow F, Rogiers A, Marin-Bejar O, Aibar S, Femel J, Dewaele M, et al. Toward
770 Minimal Residual Disease-Directed Therapy in Melanoma. Cell 2018;174:843-855.e19.
771 https://doi.org/10.1016/j.cell.2018.06.025.

772 [20] Konieczkowski DJ, Johannessen CM, Abudayyeh O, Kim JW, Cooper ZA, Piris A, et
773 al. A melanoma cell state distinction influences sensitivity to MAPK pathway inhibitors.
774 Cancer Discov 2014;4:816–27. https://doi.org/10.1158/2159-8290.CD-13-0424.

775 [21] Müller J, Krijgsman O, Tsoi J, Robert L, Hugo W, Song C, et al. Low MITF/AXL ratio
776 predicts early resistance to multiple targeted drugs in melanoma. Nat Commun 2014;5.
777 https://doi.org/10.1038/ncomms6712.

778 [22] Mehta A, Kim YJ, Robert L, Tsoi J, Comin-Anduix B, Berent-Maoz B, et al.
779 Immunotherapy resistance by inflammation-induced dedifferentiation. Cancer Discov
780 2018;8:935–43. https://doi.org/10.1158/2159-8290.CD-17-1178.

781 [23] Hugo W, Shi H, Sun L, Piva M, Song C, Kong X, et al. Non-genomic and Immune
782 Evolution of Melanoma Acquiring MAPKi Resistance. Cell 2015;162:1271–85.
783 https://doi.org/10.1016/j.cell.2015.07.061.

784 [24] Hugo W, Zaretsky JM, Sun L, Song C, Moreno BH, Hu-Lieskovan S, et al. Genomic
785 and Transcriptomic Features of Response to Anti-PD-1 Therapy in Metastatic
786 Melanoma. Cell 2016;165:35–44. https://doi.org/10.1016/j.cell.2016.02.065.

787 [25] Zhao F, Sucker A, Horn S, Heeke C, Bielefeld N, Schrörs B, et al. Melanoma lesions
788 independently acquire t-cell resistance during metastatic latency. Cancer Res
789 2016;76:4347–58. https://doi.org/10.1158/0008-5472.CAN-16-0008.

790 [26] Sucker A, Zhao F, Pieper N, Heeke C, Maltaner R, Stadtler N, et al. Acquired IFNγ
791 resistance impairs anti-tumor immunity and gives rise to T-cell-resistant melanoma
792 lesions. Nat Commun 2017;8:15440. https://doi.org/10.1038/ncomms15440.

793 [27] Tsoi J, Robert L, Paraiso K, Galvan C, Sheu KM, Lay J, et al. Multi-stage Differentiation
794 Defines Melanoma Subtypes with Differential Vulnerability to Drug-Induced Iron-
795 Dependent Oxidative Stress. Cancer Cell 2018;33:890-904.e5.
796 https://doi.org/10.1016/j.ccell.2018.03.017.

797 [28] Gide TN, Quek C, Menzies AM, Tasker AT, Shang P, Holst J, et al. Distinct Immune
798 Cell Populations Define Response to Anti-PD-1 Monotherapy and Anti-PD-1/Anti-
799 CTLA-4 Combined Therapy. Cancer Cell 2019;35:238-255.e6.
800 https://doi.org/10.1016/j.ccell.2019.01.003.

801 [29] Liu D, Schilling B, Liu D, Sucker A, Livingstone E, Jerby-Amon L, et al. Integrative
802 molecular and clinical modeling of clinical outcomes to PD1 blockade in patients with
803 metastatic melanoma. Nat Med 2019;25:1916–27. https://doi.org/10.1038/s41591-019-
804 0654-5.

805 [30] Bray NL, Pimentel H, Melsted P, Pachter L. Near-optimal probabilistic RNA-seq
806 quantification. Nat Biotechnol 2016;34:525–7. https://doi.org/10.1038/nbt.3519.

807 [31] Li T, Fu J, Zeng Z, Cohen D, Li J, Chen Q, et al. TIMER2.0 for analysis of tumor-

808 infiltrating immune cells. Nucleic Acids Res 2020;48:W509–14.
809 https://doi.org/10.1093/nar/gkaa407.

810 [32] Sturm G, Finotello F, Petitprez F, Zhang JD, Baumbach J, Fridman WH, et al.
811 Comprehensive evaluation of transcriptome-based cell-type quantification methods for
812 immuno-oncology. Bioinformatics 2019;35:i436–45.
813 https://doi.org/10.1093/bioinformatics/btz363.

814 [33] Kuleshov M V, Jones MR, Rouillard AD, Fernandez NF, Duan Q, Wang Z, et al. Enrichr:
815 a comprehensive gene set enrichment analysis web server 2016 update. Nucleic Acids
816 Res 2016;44:W90-7. https://doi.org/10.1093/nar/gkw377.

817 [34] Besch R, Poeck H, Hohenauer T, Senft D, Häcker G, Berking C, et al. Proapoptotic
818 signaling induced by RIG-I and MDA-5 results in type I interferon-independent
819 apoptosis in human melanoma cells. J Clin Invest 2009;119:2399–411.
820 https://doi.org/10.1172/JCI37155.

821 [35] Kübler K, Gehrke N, Riemann S, Böhnert V, Zillinger T, Hartmann E, et al. Targeted
822 activation of RNA helicase retinoic acid - Inducible gene-I induces proimmunogenic
823 apoptosis of human ovarian cancer cells. Cancer Res 2010;70:5293–304.
824 https://doi.org/10.1158/0008-5472.CAN-10-0825.

825 [36] Duewell P, Steger A, Lohr H, Bourhis H, Hoelz H, Kirchleitner S V., et al. RIG-I-like
826 helicases induce immunogenic cell death of pancreatic cancer cells and sensitize tumors
827 toward killing by CD8(+) T cells. Cell Death Differ 2014;21:1825–37.
828 https://doi.org/10.1038/cdd.2014.96.

829 [37] Carreira S, Goodall J, Denat L, Rodriguez M, Nuciforo P, Hoek KS, et al. Mitf regulation
830 of Dia1 controls melanoma proliferation and invasiveness. Genes Dev 2006;20:3426–
831 39. https://doi.org/10.1101/gad.406406.

832 [38] Boshuizen J, Vredevoogd DW, Krijgsman O, Ligtenberg MA, Blankenstein S, de Bruijn
833 B, et al. Reversal of pre-existing NGFR-driven tumor and immune therapy resistance.
834 Nat Commun 2020;11:1–13. https://doi.org/10.1038/s41467-020-17739-8.

835 [39] Kim YJ, Sheu KM, Tsoi J, Abril-Rodriguez G, Medina E, Grasso CS, et al. Melanoma
836 dedifferentiation induced by IFN-γ epigenetic remodeling in response to anti–PD-1
837 therapy. J Clin Invest 2021;131. https://doi.org/10.1172/jci145859.

838 [40] Elion DL, Jacobson ME, Hicks DJ, Rahman B, Sanchez V, Gonzales-Ericsson PI, et al.
839 Therapeutically active RIG-I agonist induces immunogenic tumor cell killing in breast
840 cancers. Cancer Res 2018;78:6183–95. https://doi.org/10.1158/0008-5472.CAN-18-
841 0730.

842 [41] Jiang X, Muthusamy V, Fedorova O, Kong Y, Kim DJ, Bosenberg M, et al. Intratumoral
843 delivery of RIG-I agonist SLR14 induces robust antitumor responses. J Exp Med
844 2019;216:2854–68. https://doi.org/10.1084/jem.20190801.

845 [42] Ribas A, Medina T, Kummar S, Amin A, Kalbasi A, Drabick JJ, et al. Sd-101 in
846 combination with pembrolizumab in advanced melanoma: Results of a phase ib,
847 multicenter study. Cancer Discov 2018;8. https://doi.org/10.1158/2159-8290.CD-18-
848 0280.

849 [43] Ribas A, Medina T, Kirkwood JM, Zakharia Y, Gonzalez R, Davar D, et al. Overcoming
850 PD-1 Blockade Resistance With CpG-A Toll-Like Receptor 9 Agonist Vidutolimod in
851 Patients With Metastatic Melanoma. Cancer Discov 2021:candisc.0425.2021.
852 https://doi.org/10.1158/2159-8290.cd-21-0425.

853 [44] Márquez-Rodas I, Longo F, Rodríguez-Ruiz ME, Calles A, Ponce S, Jove M, et al.
854 Intratumoral nanoplexed poly I:C BO-112 in combination with systemic anti-PD-1 for
855 patients with anti-PD-1-refractory tumors. Sci Transl Med 2020;12.
856 https://doi.org/10.1126/scitranslmed.abb0391.

857 [45] Massi D, Mihic-Probst D, Schadendorf D, Dummer R, Mandalà M. Dedifferentiated
858 melanomas: Morpho-phenotypic profile, genetic reprogramming and clinical
859 implications. Cancer Treat Rev 2020;88. https://doi.org/10.1016/j.ctrv.2020.102060.

860 [46] Olsson N, Heberling ML, Zhang L, Jhunjhunwala S, Phung QT, Lin S, et al. An
861 Integrated Genomic, Proteomic, and Immunopeptidomic Approach to Discover
862 Treatment-Induced Neoantigens. Front Immunol 2021;12:1–17.
863 https://doi.org/10.3389/fimmu.2021.662443.

864 [47] Kalaora S, Lee JS, Barnea E, Levy R, Greenberg P, Alon M, et al. Immunoproteasome
865 expression is associated with better prognosis and response to checkpoint therapies in
866 melanoma. Nat Commun 2020;11:1–12. https://doi.org/10.1038/s41467-020-14639-9.

867 [48] Paschen A, Melero I, Ribas A. Central Role of the Antigen-Presentation and Interferon-

γ Pathways in Resistance to Immune Checkpoint Blockade. Annu Rev Cancer Biol 2022;6:85–102. https://doi.org/10.1146/annurev-cancerbio-070220-111016.

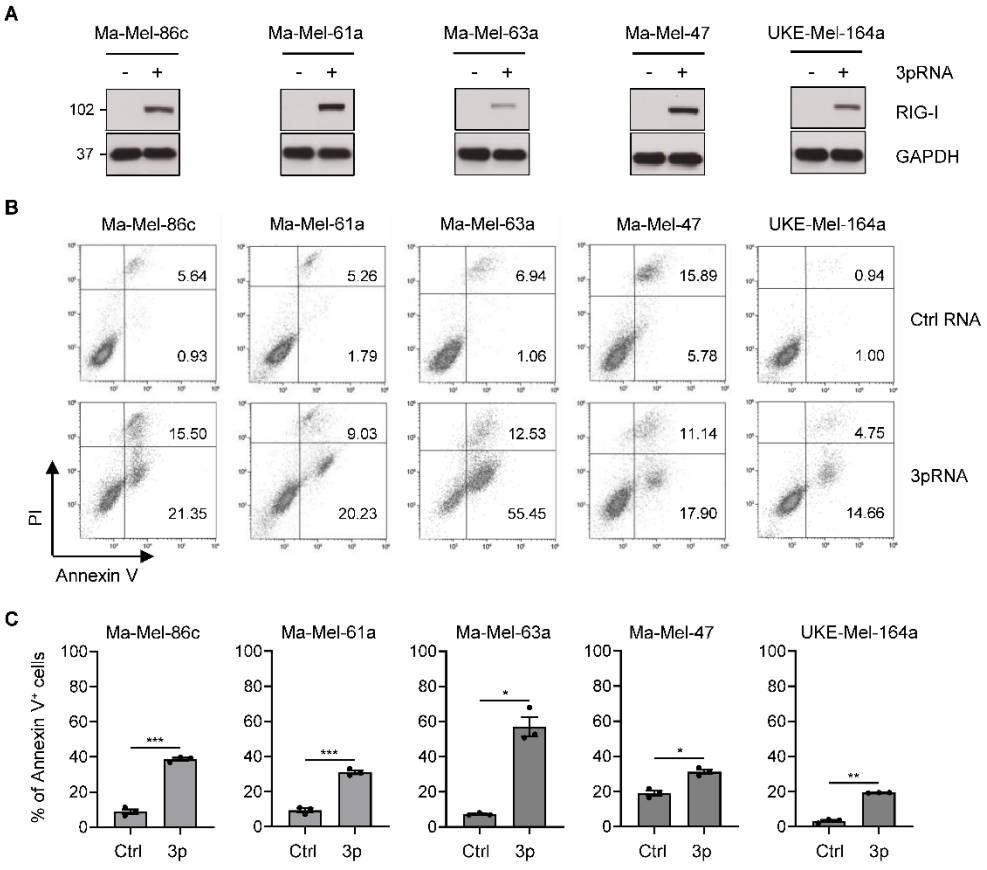
A
Ma-Mel-86c
Ma-Mel-61a
Ma-Mel-63a
Ma-Mel-47
UKE-Mel-164a
- +
3pRNA
102
37
RIG-I
GAPDH
B
Ctrl RNA
3pRNA
5.64
0.93
5.26
1.79
6.94
1.06
15.89
5.78
0.94
1.00
15.50
21.35
9.03
20.23
12.53
55.45
11.14
17.90
4.75
14.66
PI
Annexin V
C
% of Annexin V+ cells
Ctrl
3p

Figure 1

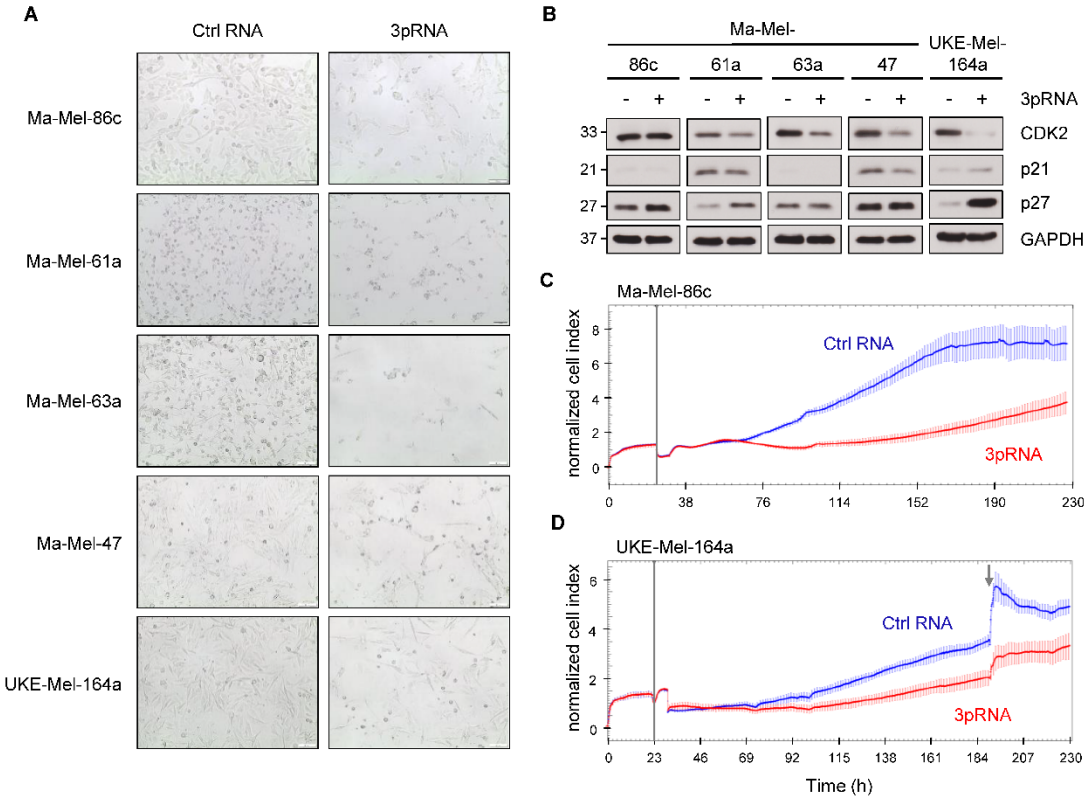
A
Ctrl RNA
3pRNA
Ma-Mel-86c
Ma-Mel-61a
Ma-Mel-63a
Ma-Mel-47
UKE-Mel-164a
B
Ma-Mel-
86c
61a
63a
47
UKE-Mel-
164a
- + - + - + - + - +
3pRNA
33
21
27
37
CDK2
p21
p27
GAPDH
C
Ma-Mel-86c
normalized cell index
Ctrl RNA
3pRNA
0 38 76 114 152 190 230
D
UKE-Mel-164a
normalized cell index
Ctrl RNA
3pRNA
0 23 46 69 92 115 138 161 184 207 230
Time (h)

Figure 2

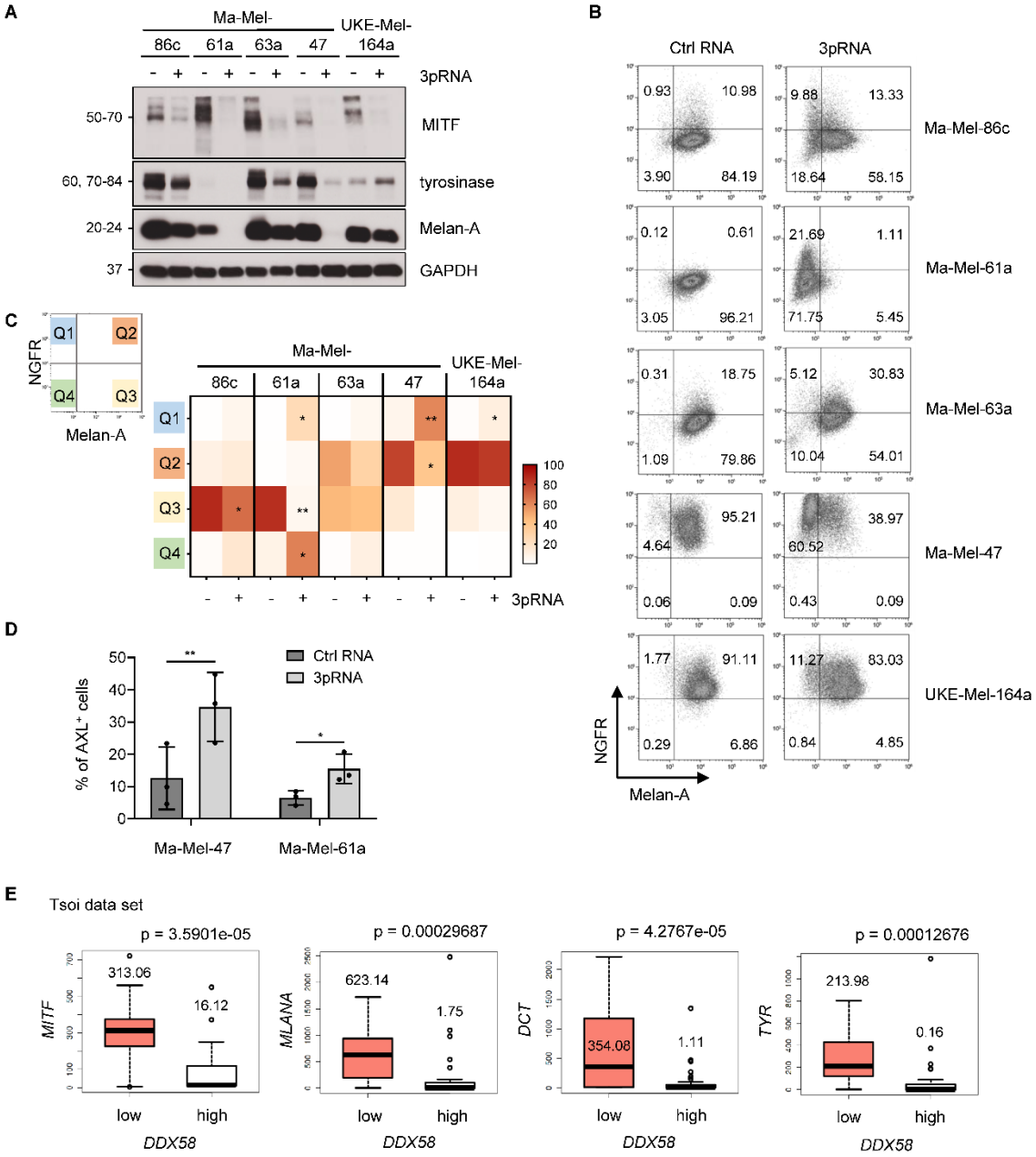
A
Ma-Mel-
86c
61a
63a
47
UKE-Mel-164a
3pRNA
50-70
MITF
60, 70-84
tyrosinase
20-24
Melan-A
37
GAPDH
B
Ctrl RNA
3pRNA
Ma-Mel-86c
Ma-Mel-61a
Ma-Mel-63a
Ma-Mel-47
UKE-Mel-164a
NGFR
Melan-A
C
NGFR
Melan-A
Q1
Q2
Q3
Q4
Ma-Mel-
UKE-Mel-164a
3pRNA
D
% of AXL+ cells
Ctrl RNA
3pRNA
Ma-Mel-47
Ma-Mel-61a
E
Tsoi data set
p = 3.5901e-05
p = 0.00029687
p = 4.2767e-05
p = 0.00012676
MITF
MLANA
DCT
TYR
low
high
DDX58

Figure 3

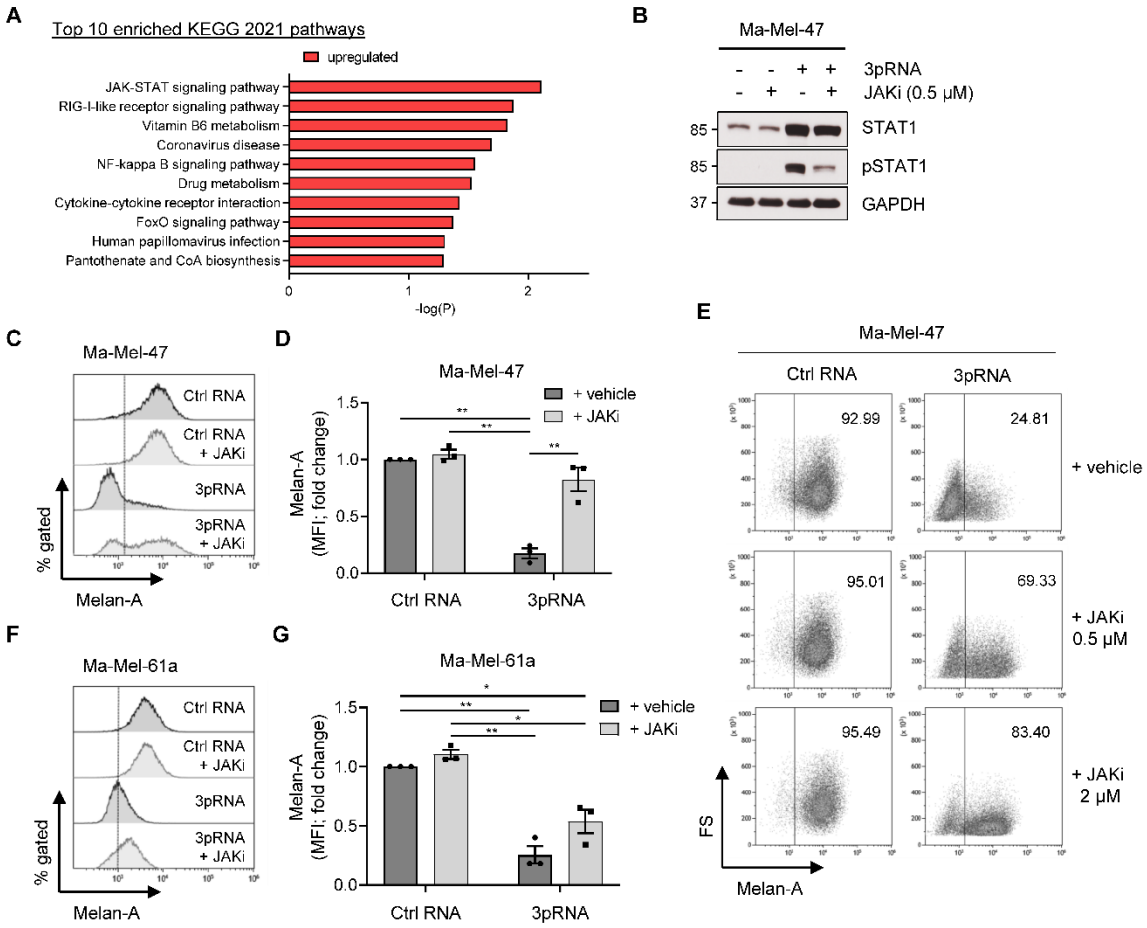
A
Top 10 enriched KEGG 2021 pathways
upregulated
JAK-STAT signaling pathway
RIG-I-like receptor signaling pathway
Vitamin B6 metabolism
Coronavirus disease
NF-kappa B signaling pathway
Drug metabolism
Cytokine-cytokine receptor interaction
FoxO signaling pathway
Human papillomavirus infection
Pantothenate and CoA biosynthesis
0
1
2
-log(P)
B
Ma-Mel-47
- - + + 3pRNA
- + - + JAKi (0.5 µM)
85
STAT1
85
pSTAT1
37
GAPDH
C
Ma-Mel-47
Ctrl RNA
Ctrl RNA + JAKi
3pRNA
3pRNA + JAKi
% gated
Melan-A
D
Ma-Mel-47
+ vehicle
+ JAKi
Melan-A (MFI; fold change)
1.5
1.0
0.5
0.0
**
**
**
Ctrl RNA
3pRNA
E
Ma-Mel-47
Ctrl RNA
3pRNA
92.99
24.81
+ vehicle
95.01
69.33
+ JAKi 0.5 µM
95.49
83.40
+ JAKi 2 µM
FS
Melan-A
F
Ma-Mel-61a
Ctrl RNA
Ctrl RNA + JAKi
3pRNA
3pRNA + JAKi
% gated
Melan-A
G
Ma-Mel-61a
+ vehicle
+ JAKi
Melan-A (MFI; fold change)
1.5
1.0
0.5
0.0
*
**
*
**
Ctrl RNA
3pRNA

Figure 4

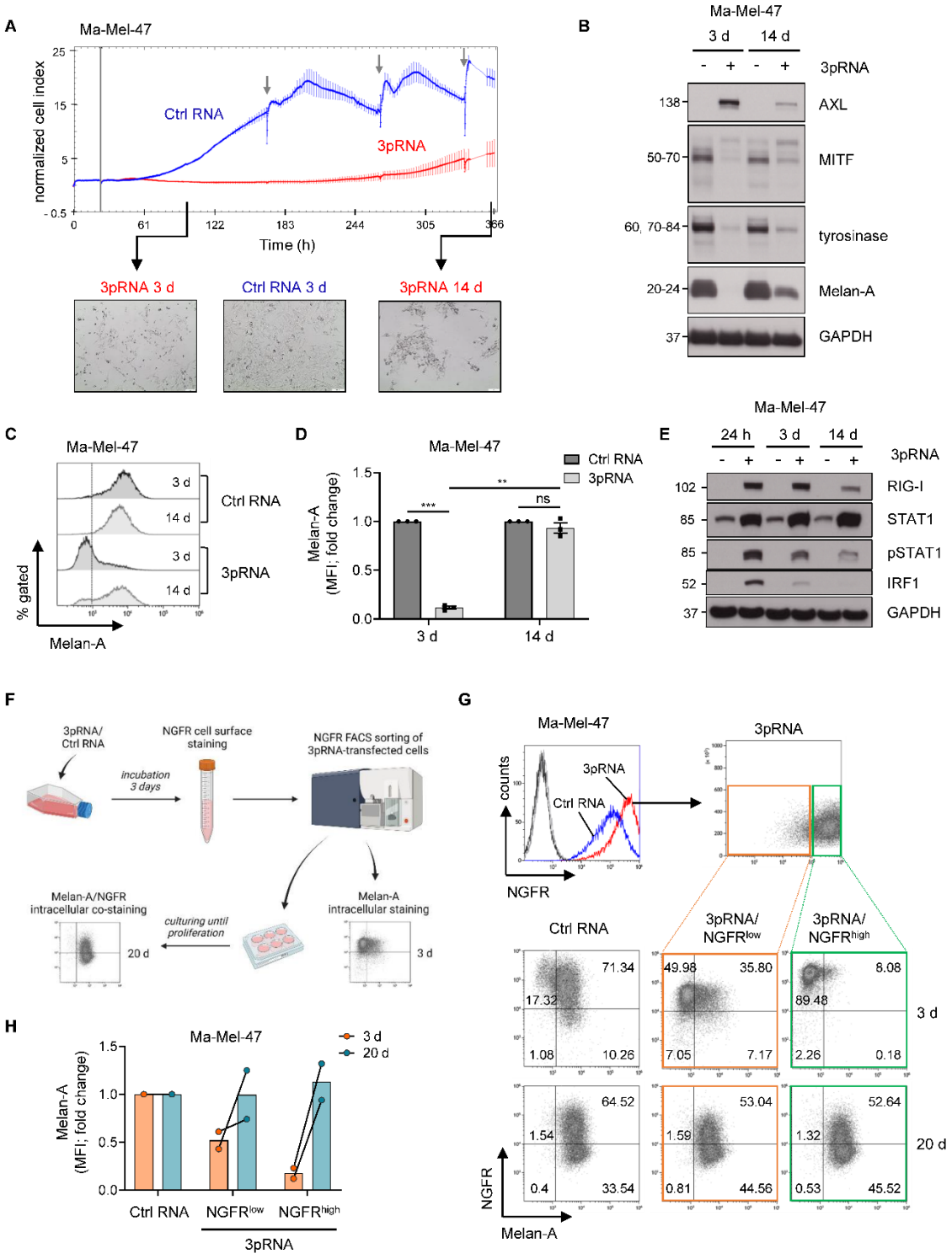
A
Ma-Mel-47
normalized cell index
Ctrl RNA
3pRNA
Time (h)
3pRNA 3 d
Ctrl RNA 3 d
3pRNA 14 d
B
Ma-Mel-47
3 d
14 d
3pRNA
AXL
MITF
tyrosinase
Melan-A
GAPDH
C
Ma-Mel-47
Ctrl RNA
3pRNA
% gated
Melan-A
D
Ma-Mel-47
Ctrl RNA
3pRNA
Melan-A (MFI; fold change)
ns
E
Ma-Mel-47
24 h
3 d
14 d
3pRNA
RIG-I
STAT1
pSTAT1
IRF1
GAPDH
F
3pRNA/ Ctrl RNA
incubation 3 days
NGFR cell surface staining
NGFR FACS sorting of 3pRNA-transfected cells
Melan-A/NGFR intracellular co-staining
culturing until proliferation
Melan-A intracellular staining
20 d
3 d
G
Ma-Mel-47
counts
3pRNA
Ctrl RNA
NGFR
3pRNA/ NGFRlow
3pRNA/ NGFRhigh
71.34
17.32
1.08
10.26
49.98
35.80
7.05
7.17
8.08
89.48
2.26
0.18
64.52
1.54
0.4
33.54
53.04
1.59
0.81
44.56
52.64
1.32
0.53
45.52
3 d
20 d
Melan-A
H
Ma-Mel-47
3 d
20 d
Melan-A (MFI; fold change)
Ctrl RNA
NGFRlow
NGFRhigh
3pRNA

Figure 5

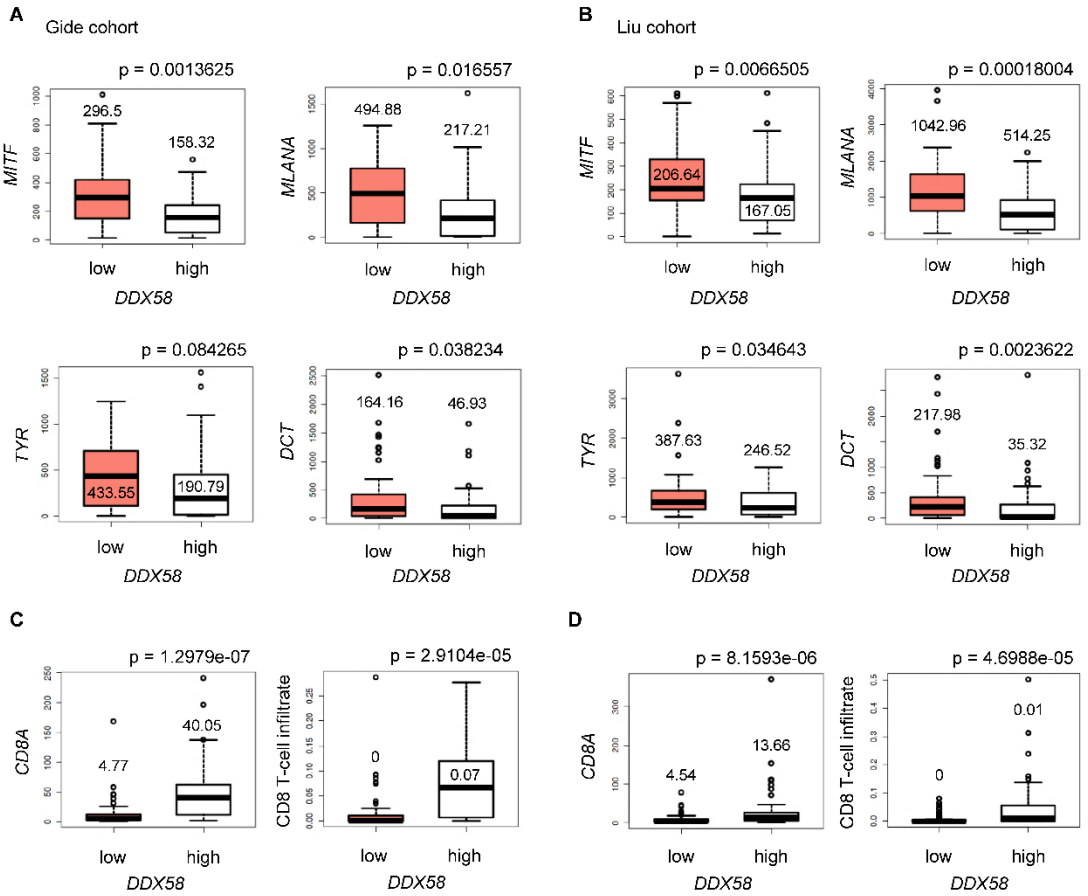
A
Gide cohort
B
Liu cohort
C
D
MITF
MLANA
TYR
DCT
CD8A
CD8 T-cell infiltrate
DDX58
low
high
p = 0.0013625
296.5
158.32
p = 0.016557
494.88
217.21
p = 0.0066505
206.64
167.05
p = 0.00018004
1042.96
514.25
p = 0.084265
433.55
190.79
p = 0.038234
164.16
46.93
p = 0.034643
387.63
246.52
p = 0.0023622
217.98
35.32
p = 1.2979e-07
4.77
40.05
p = 2.9104e-05
0
0.07
p = 8.1593e-06
4.54
13.66
p = 4.6988e-05
0
0.01

Figure 6

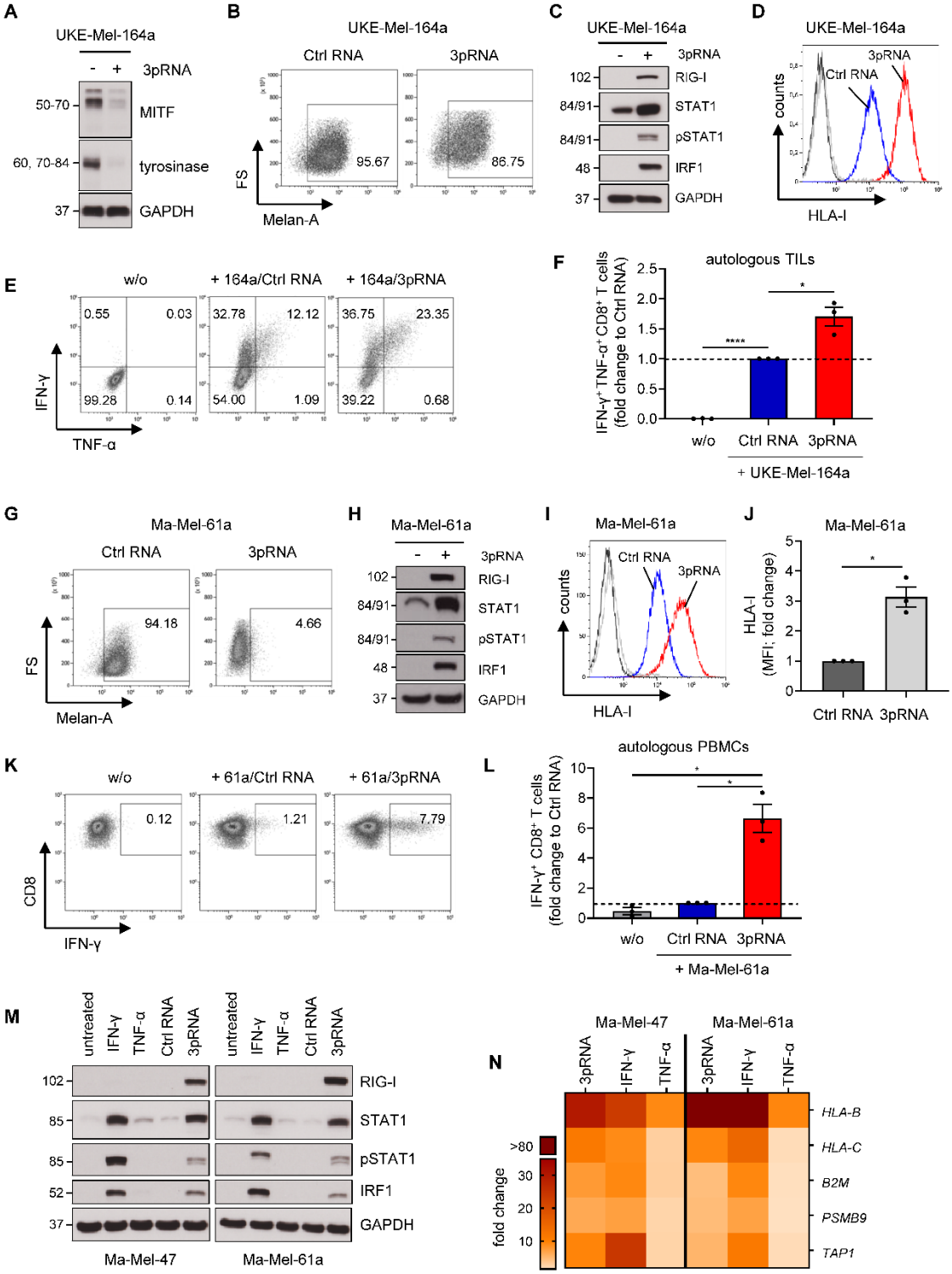
A
UKE-Mel-164a
- +
3pRNA
50-70
MITF
60, 70-84
tyrosinase
37
GAPDH
B
UKE-Mel-164a
Ctrl RNA
3pRNA
95.67
86.75
FS
Melan-A
C
UKE-Mel-164a
- +
3pRNA
102
RIG-I
84/91
STAT1
84/91
pSTAT1
48
IRF1
37
GAPDH
D
UKE-Mel-164a
3pRNA
Ctrl RNA
counts
HLA-I
E
w/o
+ 164a/Ctrl RNA
+ 164a/3pRNA
0.55
0.03
99.28
0.14
32.78
12.12
54.00
1.09
36.75
23.35
39.22
0.68
IFN-γ
TNF-α
F
autologous TILs
IFN-γ+ TNF-α+ CD8+ T cells (fold change to Ctrl RNA)
2.5
2.0
1.5
1.0
0.5
0.0
****
*
w/o
Ctrl RNA
3pRNA
+ UKE-Mel-164a
G
Ma-Mel-61a
Ctrl RNA
3pRNA
94.18
4.66
FS
Melan-A
H
Ma-Mel-61a
- +
3pRNA
102
RIG-I
84/91
STAT1
84/91
pSTAT1
48
IRF1
37
GAPDH
I
Ma-Mel-61a
Ctrl RNA
3pRNA
counts
HLA-I
J
Ma-Mel-61a
HLA-I (MFI; fold change)
5
4
3
2
1
0
*
Ctrl RNA
3pRNA
K
w/o
+ 61a/Ctrl RNA
+ 61a/3pRNA
0.12
1.21
7.79
CD8
IFN-γ
L
autologous PBMCs
IFN-γ+ CD8+ T cells (fold change to Ctrl RNA)
10
8
6
4
2
0
*
*
w/o
Ctrl RNA
3pRNA
+ Ma-Mel-61a
M
untreated
IFN-γ
TNF-α
Ctrl RNA
3pRNA
102
RIG-I
85
STAT1
85
pSTAT1
52
IRF1
37
GAPDH
Ma-Mel-47
Ma-Mel-61a
N
Ma-Mel-47
Ma-Mel-61a
3pRNA
IFN-γ
TNF-α
HLA-B
HLA-C
B2M
PSMB9
TAP1
>80
30
20
10
fold change

Figure 7

Thier et al., Supplementary file 1 – supplementary figures

Innate immune receptor signaling induces transient melanoma dedifferentiation while preserving immunogenicity

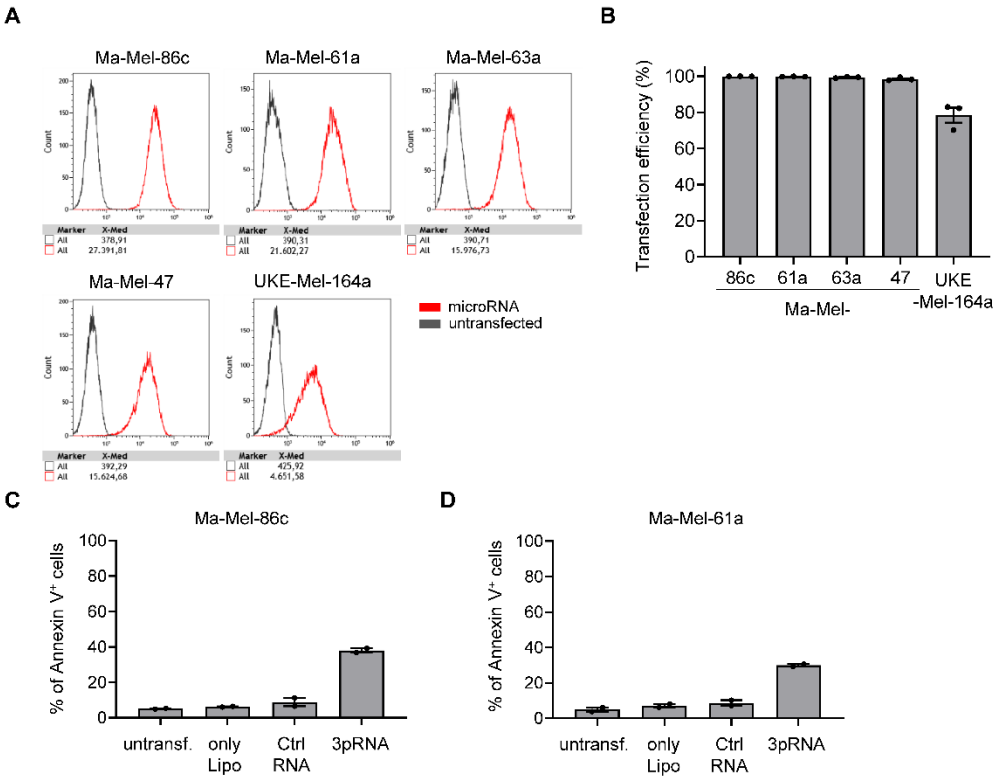

Supplementary figure S1: Control of transfection. (A,B) Melanoma cell lines were transfected with miRNA-Cy3 (red) or left untransfected (grey). After 24 h, transfection efficiency was determined by flow cytometry. (A) Representative histograms and (B) percentage of Cy3-positive cells given as mean±SEM from three independent experiments. (C,D) Transfection procedure does not alter apoptosis induction. Ma-Mel-86c (C) and Ma-Mel-61a (D) were transfected with 3pRNA or Ctrl RNA. As additional controls, cells were left untransfected (untransf.) or only treated with the transfection reagent Lipofectamine (only Lipo). Apoptosis was measured by flow cytometry on day 3 post-transfection. Percentage of Annexin V^+ cells depicted as mean±SEM of two independent experiments.

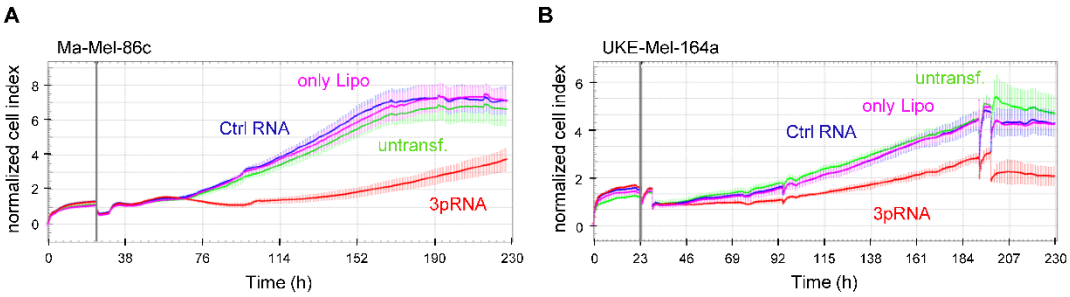

Supplementary figure S2: Transfection does not alter cell proliferation. (A,B) Real-time proliferation of Ctrl RNA (blue)- and 3pRNA (red)-transfected Ma-Mel-86c (A) and UKE-Mel-164a (B) cells, and of controls left untransfected (green) or only treated with Lipofectamine (purple). Vertical grey lines indicate time point of transfection. Representative data from three independent experiments.

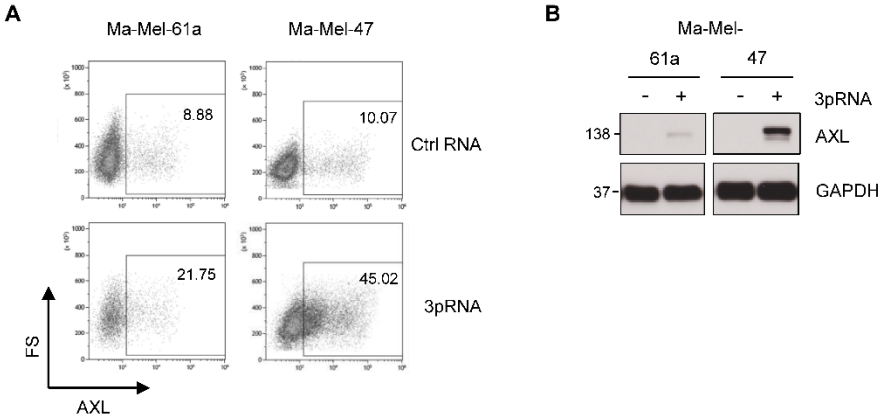

Supplementary figure S3: AXL expression upon RIG-I activation in Ma-Mel-61a and Ma-Mel-47. (A,B) Ma-Mel-61a and Ma-Mel-47 were transfected with 3pRNA or Ctrl RNA. AXL expression analyzed at single cell and bulk levels by flow cytometry (A) and Western Blot (B), respectively, on day 3 post-transfection. GAPDH, loading control. Representative data from one of three independent experiments.

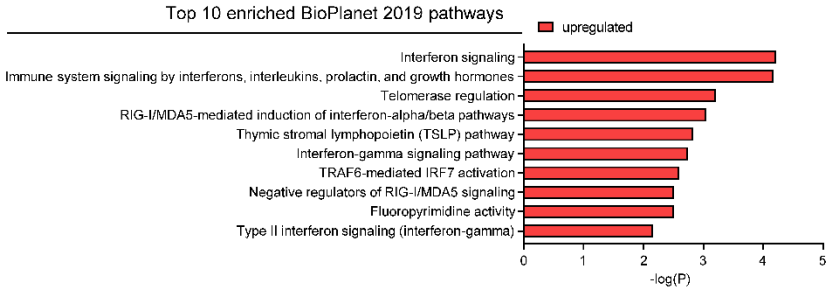

Supplementary figure S4: Significantly upregulated pathways in *RIG-I/DDX58*^{high} melanoma cell lines. BioPlanet database pathways enriched for genes co-regulated with *DDX58* mRNA in the Tsoi transcriptomic data set [27].

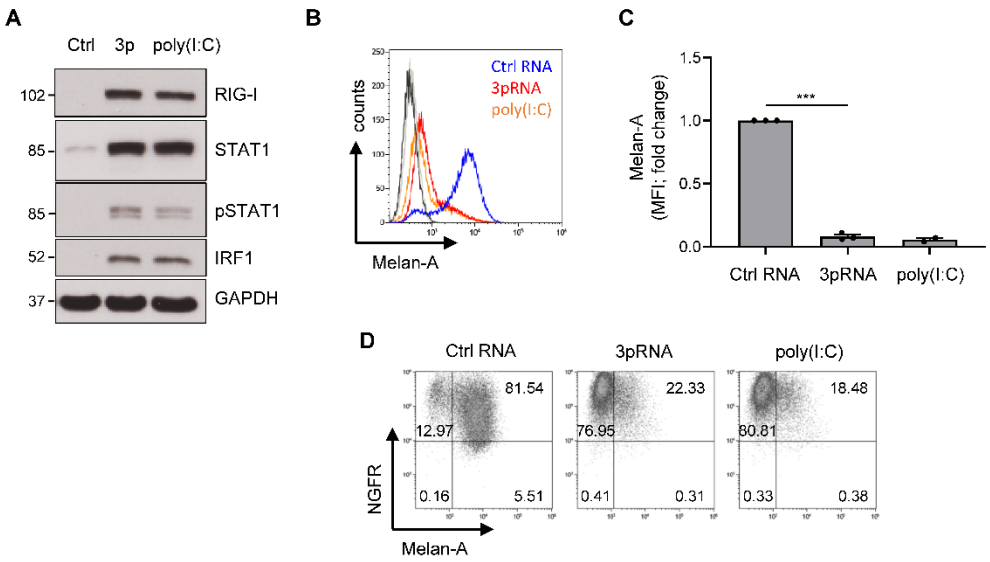

Supplementary figure S5: Dedifferentiation of Ma-Mel-47 cells upon poly(I:C) transfection. Ma-Mel-47 were transfected with 3pRNA, poly(I:C) or Ctrl RNA and subjected to further analyses on day 3 post-transfection. (A) RIG-I expression and signaling pathway activation analyzed by Western blot. GAPDH, loading control. Representative data of two independent experiments. (B,C) Melan-A expression determined by flow cytometry. (B) Representative histograms and (C) fold change of MFI given as mean±SEM of two or three independent experiments. (D) Melan-A and NGFR co-expression in Ma-Mel-47 cells analyzed by flow cytometry. Representative dot plots from two or three independent experiments, numbers indicate percentage of cells. Significantly different experimental groups: *** $p < 0.005$ by two-tailed paired t-test.

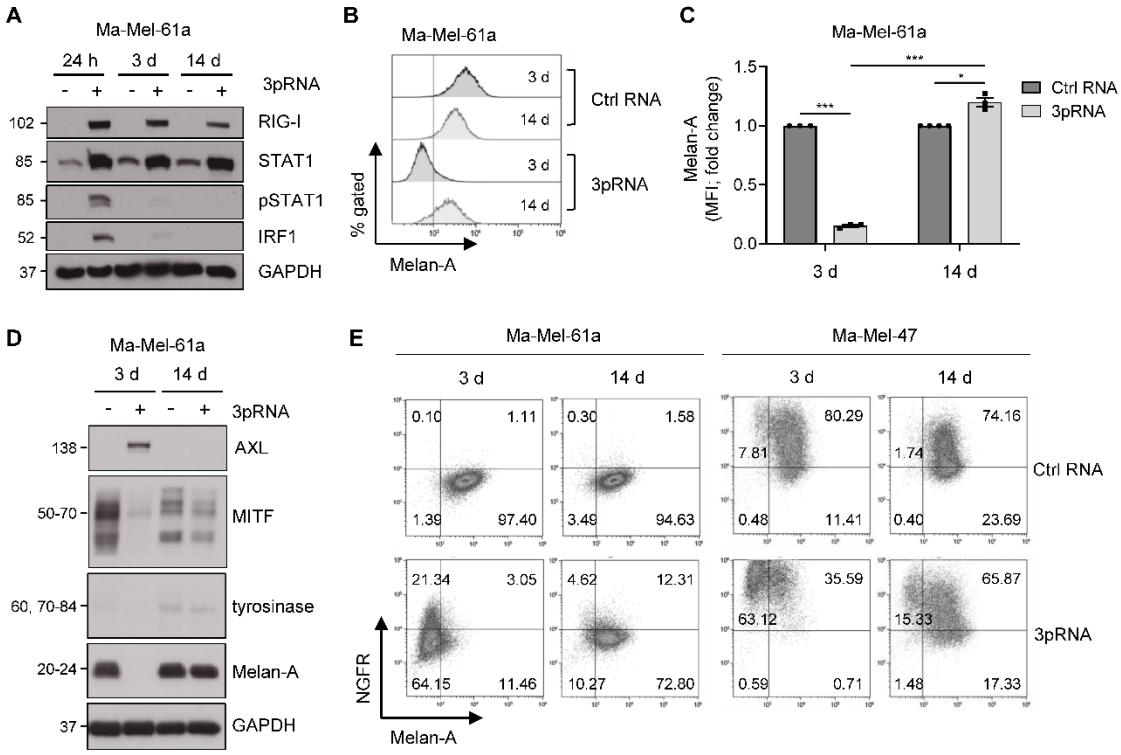

Supplementary figure S6: Transient dedifferentiation upon RIG-I activation. Ma-Mel-61a cells were transfected once with 3pRNA or Ctrl RNA and analyzed on day 3 (3 d) and 14 (14 d) post-transfection. (A) RIG-I expression and JAK-STAT pathway activation analyzed by Western Blot. GAPDH, loading control. Representative data of three independent experiments. (B,C) Melan-A expression determined by flow cytometry. (B) Representative histograms with dotted line representing unstained control and (C) fold change of MFI given as mean±SEM of three independent experiments. (D) Differentiation status of Ma-Mel-61a cells determined by expression of indicated proteins. GAPDH, loading control. Representative data of three independent experiments. (E) Melan-A and NGFR co-expression in Ma-Mel-61a and Ma-Mel-47 cells analyzed by flow cytometry. Representative dot plots of three independent experiments, numbers indicate percentage of cells. Significantly different experimental groups: * $p < 0.05$; *** $p < 0.005$ by two-tailed paired t-test.

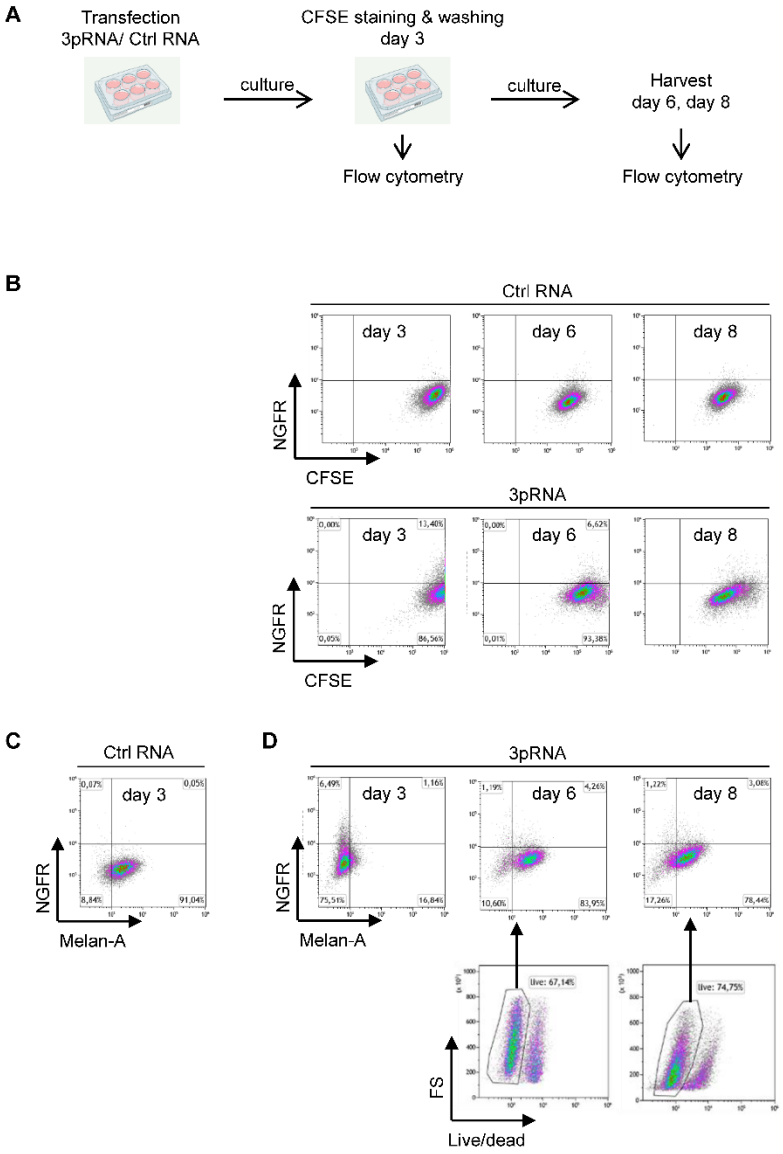

Supplementary figure S7: Monitoring reproliferation of 3pRNA-induced persisters. (A) Scheme of workflow. Ma-Mel-61a cells were transfected with Ctrl RNA or 3pRNA. On day 3 post-transfection, adherent cells were stained with CFSE, washed and directly analysed by flow cytometry or cultured until analysis at indicated time points. (B) Loss in CFSE signal intensity upon proliferation. CFSE-labeled cells co-stained for intracellular NGFR. Note, Ctrl RNA-treated cells: day 6/8 – high cell density, arrest in proliferation. (C, D) Differentiation status of viable Ctrl RNA- and 3pRNA-treated Ma-Mel-61a cells measured by co-staining for intracellular NGFR and Melan-A, in parallel to proliferation. (C) Differentiation status of control cells on day 3 post-transfection. (D) Differentiation status of viable persisters on day 3, day 6 and day 8 post-transfection. Cell death determined by live/dead staining.

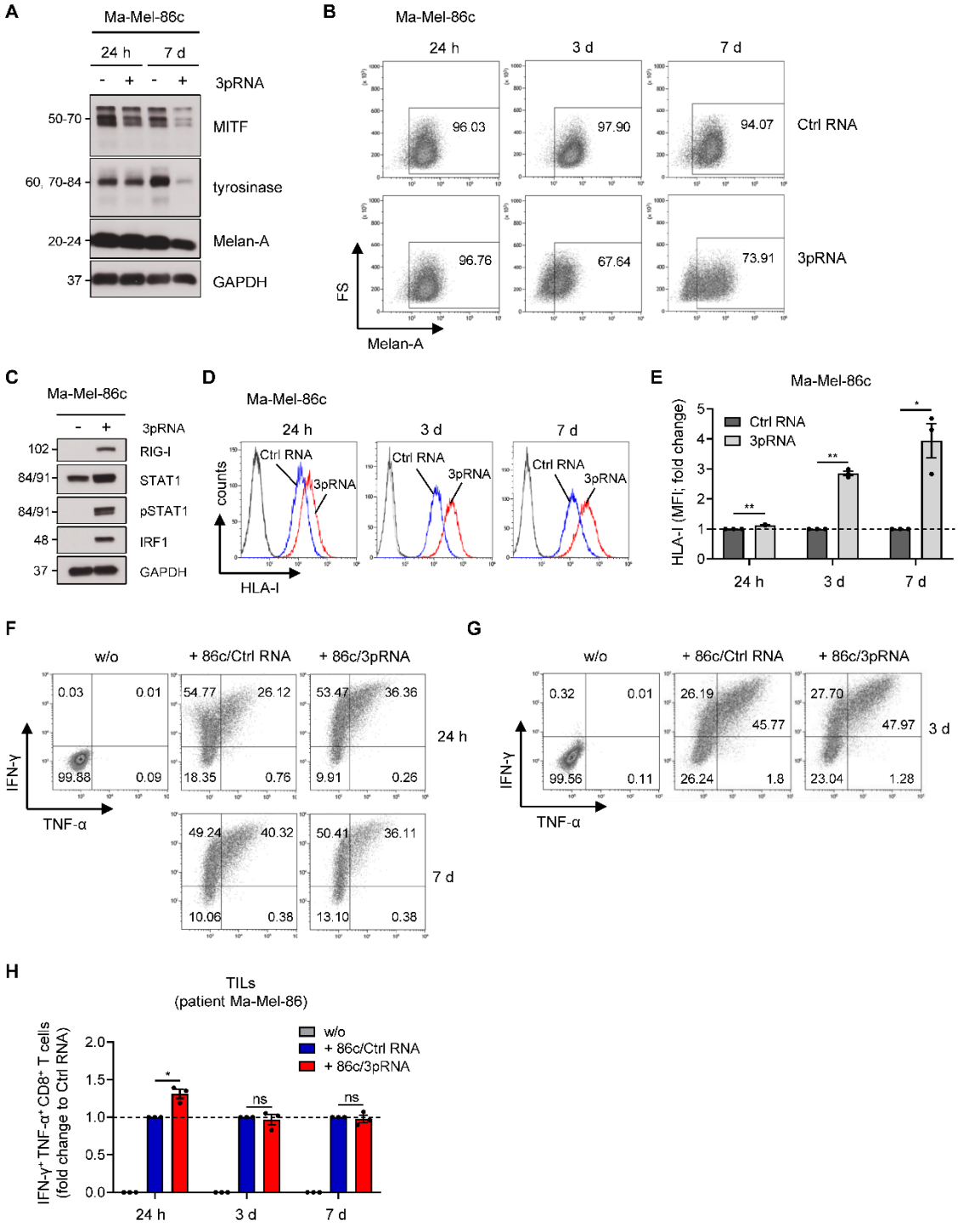

Supplementary figure S8

Supplementary figure S8: CD8 T-cell reactivity toward 3pRNA-induced dedifferentiated Ma-Mel-86c persisters. (A-F) Melanoma cells Ma-Mel-86c were transfected with 3pRNA (+) or Ctrl RNA (-) and subjected to further analyses. Cells analyzed at 24 h post-transfection or on day 3 post-transfection were transfected once (day 0), cells analyzed on day 7 post-transfection were transfected twice (day 0 and 6). (A) Differentiation status of Ma-Mel-86c cells determined by expression of indicated proteins. GAPDH, loading control. Representative data from three independent experiments. (B) Melan-A expression analyzed by flow cytometry. Representative data from three independent experiments. (C) RIG-I expression and JAK-STAT pathway activation analyzed 24 h post-transfection by Western Blot. GAPDH, loading control. Representative data from three independent experiments. (D,E) HLA-I cell surface expression measured by flow cytometry. (D) Representative histogram and (E) fold change of MFI given as mean±SEM from three independent experiments. (F-H) Activation of autologous TILs by melanoma cells transfected with 3pRNA or Ctrl RNA. TIL activation analyzed by intracellular cytokine staining via flow cytometry. (F,G) Representative dot plots, (F) 24 h and day 7, (G) day 3. (H) Quantification of IFN-γ^+ TNF-α^+ $CD8^+$ T cells. Fold change given as mean±SEM from three independent experiments. Significantly different experimental groups: * $p < 0.05$; ** $p < 0.01$ by two-tailed paired t-test.

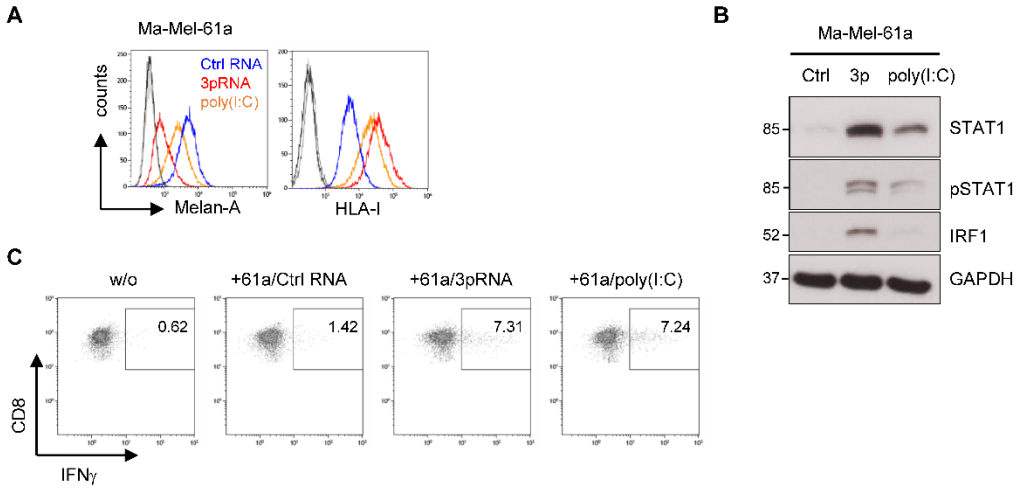

Supplementary figure S9: CD8 T-cell reactivity toward poly(I:C)-induced Ma-Mel-61a persisters. Ma-Mel-61a melanoma cells were transfected with 3pRNA, poly(I:C) or Ctrl RNA and subjected to further analyses. (A) Melan-A and HLA-I expression determined by flow cytometry on day 3 post-transfection. Representative histograms from two independent experiments. (B) JAK/STAT signaling pathway activation analyzed 24 h post-transfection by Western Blot. GAPDH, loading control. Representative data from two independent experiments. (C) Activation of autologous CD8 T cells (PBMCs) by Ma-Mel-61a cells on day 3 post-transfection with 3pRNA, poly(I:C) or Ctrl RNA. T cell activation analyzed by intracellular cytokine staining via flow cytometry. w/o: spontaneous cytokine release in the absence of tumor cells. Representative dot plots from two independent experiments.

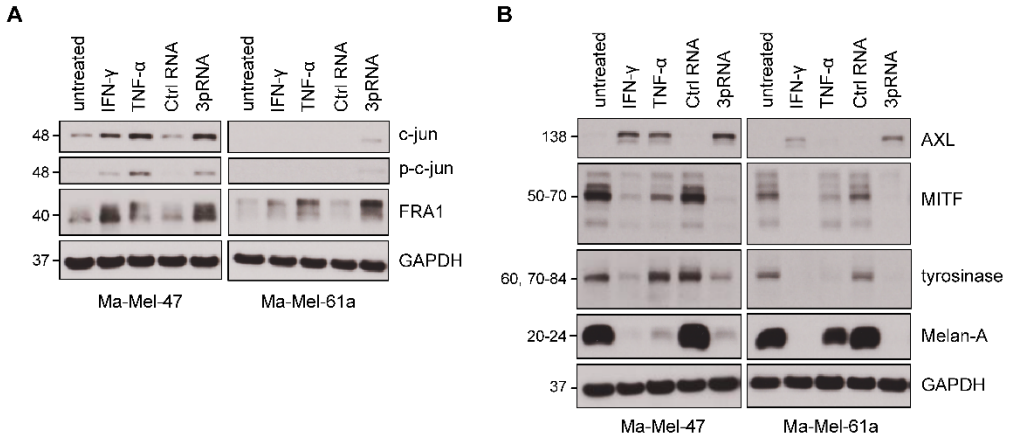

Supplementary figure S10: Signaling pathway activation and differentiation status of melanoma cells upon 3pRNA and cytokine treatment. Ma-Mel-47 and Ma-Mel-61a cells were treated with IFN-γ or TNF-α, or transfected with 3pRNA or Ctrl RNA and subjected to further analyses. (A) Signaling pathway activation analyzed 24 h post-treatment/post-transfection, and (B) differentiation status determined on day 3 post-treatment/post-transfection by Western Blot. Representative data from two independent experiments.

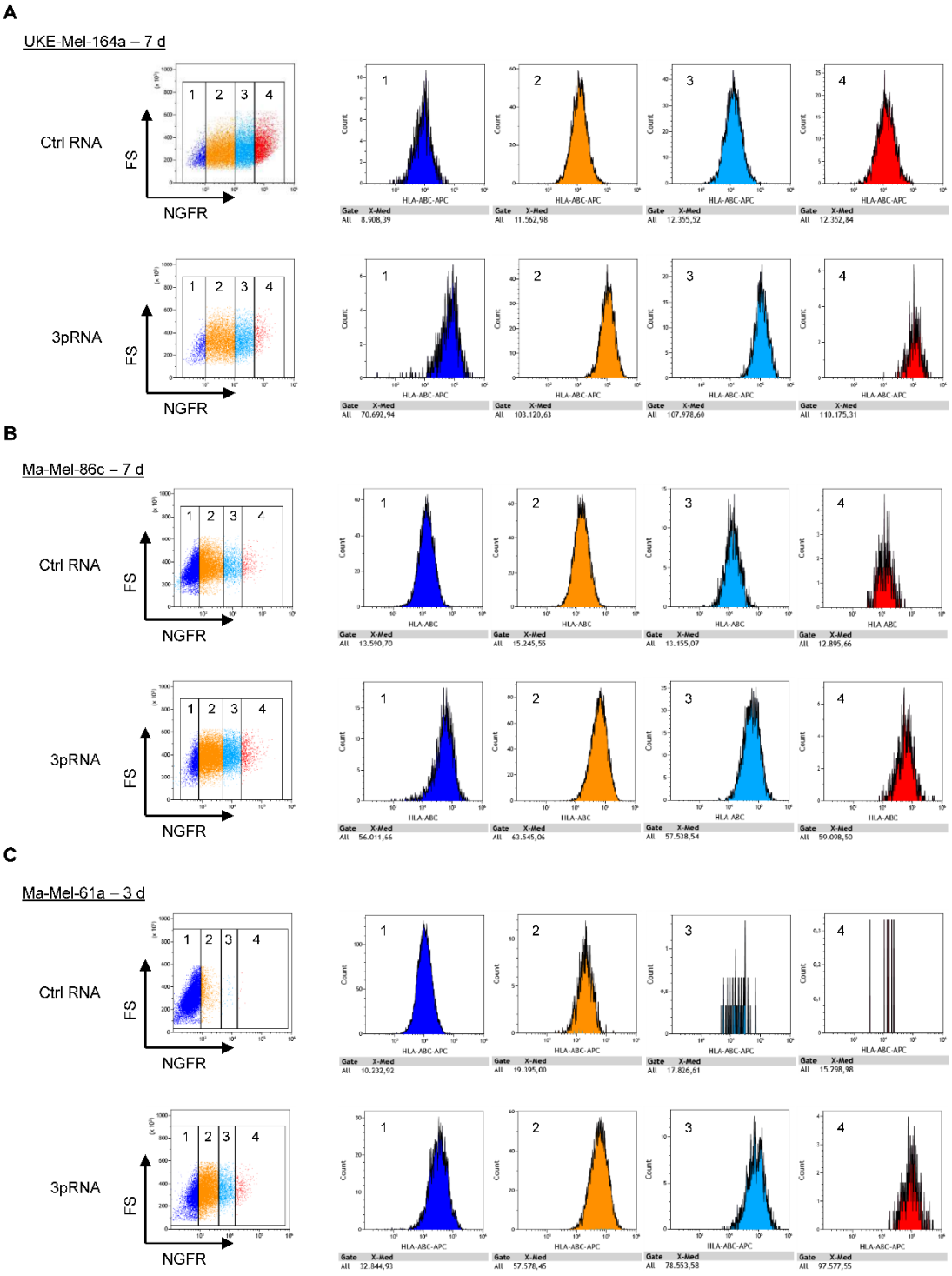

Supplementary figure S11

Supplementary figure S11: Correlation of HLA-I and NGFR expression. (A,B) UKE-Mel-164a (A) Ma-Mel-86c (B) were transfected twice (day 0 and day 6) with 3pRNA or Ctrl RNA and subjected to further analyses on day 7. (C) Ma-Mel-61a cells were transfected once with 3pRNA or Ctrl RNA and subjected to further analyses on day 3 post-transfection. (A-C) Surface expression of NGFR and HLA-I measured by flow cytometry. Left panel, melanoma cells were divided into subpopulations (1-4) according to NGFR expression intensity (1: lowest; highest: 4). Right panel, histograms of HLA-I surface expression in NGFR subpopulations with median MFI.

Supplementary table S1A. Gene expression correlated with *DDX58* in Spearman correlations (p<0.05) in the Tsoi cell lines cohort. Q_Bonf: conservative Bonferroni correction for the number of tests. q_FDR: FDR-corrected p-values applying p.adjust() in R using the fdr method. The top 50 genes were the queried for enrichment analysis in Enrichr (https://maayanlab.cloud/Enrichr/)

List of approx. 4700 genes (digital available)

Supplementary table S1B. Enrichment analyses based on the top 50 co-regulated genes with DDX58 mRNA expression in the Tsoi data set.

Tsoi data set (top 50 genes)

BioPlanet 2019

Index	Name	P-value	Adjusted p-value	Odds Ratio	Combined score
1	Interferon signaling	0,00006149	0,006356	13,49	130,79
2	Immune system signaling by interferons, interleukins, prolactin, and growth hormones	0,00006762	0,006356	9,79	94,02
3	Telomerase regulation	0,0006293	0,03943	19,83	146,19
4	RIG-I/MDA5-mediated induction of interferon-alpha/beta pathways	0,000909	0,04272	17,38	121,72
5	Thymic stromal lymphopoietin (TSLP) pathway	0,001482	0,05573	14,57	94,93
6	Interferon-gamma signaling pathway	0,001838	0,05758	13,48	84,93
7	TRAF6-mediated IRF7 activation	0,002548	0,06429	29,65	177,06
8	Negative regulators of RIG-I/MDA5 signaling	0,003078	0,06429	26,77	154,84
9	Fluoropyrimidine activity	0,003078	0,06429	26,77	154,84
10	Type II interferon signaling (interferon-gamma)	0,00695	0,1287	17,28	85,84

KEGG 2021 Human

Index	Name	P-value	Adjusted p-value	Odds Ratio	Combined score
1	JAK-STAT signaling pathway	0,007738	0,3538	7,95	38,63
2	RIG-I-like receptor signaling pathway	0,01327	0,3538	12,18	52,65
3	Vitamin B6 metabolism	0,01491	0,3538	81,41	342,39
4	Coronavirus disease	0,02024	0,3538	5,5	21,44
5	NF-kappa B signaling pathway	0,0279	0,3538	8,11	29,02
6	Drug metabolism	0,02991	0,3538	7,8	27,38
7	Cytokine-cytokine receptor interaction	0,03743	0,3538	4,3	14,12
8	FoxO signaling pathway	0,04252	0,3538	6,4	20,22
9	Human papillomavirus infection	0,04977	0,3538	3,82	11,46
10	Pantothenate and CoA biosynthesis	0,05123	0,3538	20,34	60,43

WikiPathway 2021 Human

Index	Name	P-value	Adjusted p-value	Odds Ratio	Combined score
1	Fluoropyrimidine Activity WP1601	0,003078	0,183	26,77	154,84
2	Type II interferon signaling (IFNG) WP619	0,003858	0,183	23,71	131,76
3	Novel intracellular components of RIG-I-like receptor (RLR) pathway WP3865	0,009884	0,183	14,29	65,98
4	TCA Cycle Nutrient Utilization and Invasiveness of Ovarian Cancer WP2868	0,01244	0,183	101,77	446,44
5	WP3299	0,01491	0,183	81,41	342,39
6	Nicotine Metabolism WP1600	0,01491	0,183	81,41	342,39
7	Robo4 and VEGF Signaling Pathways Crosstalk WP3943	0,01491	0,183	81,41	342,39
8	Cytosolic DNA-sensing pathway WP4655	0,01513	0,183	11,35	47,55
9	Regulatory circuits of the STAT3 signaling pathway WP4538	0,0163	0,183	10,9	44,85
10	Molybdenum cofactor (Moco) biosynthesis WP4507	0,01737	0,183	67,84	274,94

GO Biological Process 2021

Index	Name	P-value	Adjusted p-value	Odds Ratio	Combined score
1	positive regulation of interferon-beta production (GO:0032728)	0,00009904	0,04788	38,52	355,19
2	response to type I interferon (GO:0034340)	0,000218	0,04788	118,71	1000,81
3	regulation of interferon-beta production (GO:0032648)	0,0002498	0,04788	27,62	229,1
4	(GO:0071357)	0,0005758	0,06622	20,47	152,74
5	(GO:0060337)	0,0005758	0,06622	20,47	152,74
6	positive regulation of type I interferon production (GO:0032481)	0,0009442	0,09048	17,14	119,41
7	regulation of response to cytokine stimulus (GO:0060759)	0,00137	0,1032	41,52	273,73
8	regulation of type I interferon production (GO:0032479)	0,001435	0,1032	14,74	96,51
9	(GO:0071276)	0,002066	0,132	33,21	205,3
10	response to cadmium ion (GO:0046686)	0,002382	0,1322	30,75	185,7

7 Discussion

7.1 Genetic and non-genetic resistance mechanisms in melanoma

A major obstacle in treating melanoma is disease progression due to acquired resistance. Under selective pressure, a reservoir of drug-tolerant or early resistant cells can persist and undergo an adaptation process that shapes their immunogenicity.[13] The genetic and non-genetic intratumoral heterogeneity favors the selection of cell clones with survival advantages. In this thesis, different resistance mechanisms in melanoma were elucidated that led to insensitivity to CD8 T cells.

In the first presented study, we analyzed cell lines established from longitudinal metastases of melanoma patient Ma-Mel-61, an illustrating immunoediting in stage IV disease.[227] Tumor cells from late metastasis Ma-Mel-61g acquired IFN resistance under IFN-α2b immunotherapy by JAK1 inactivation. JAK1 deficiency evolved by an allelic loss and a subsequent inactivation mutation in the second allele. Interestingly, IFN resistance due to the same mechanism was observed for the following metastasis Ma-Mel-61h, clearly indicating the survival advantage of IFN insensitive melanoma cells in this patient.[43,227] Recently, genetic loss of function of JAK1/2 in melanoma has also been shown to drive resistance to different T cell-based immunotherapies.[43,211,223,226] An concomitant advantage of defective IFN signaling for tumor cells is the loss of IFN-induced HLA-I expression, enabling melanoma cells to maintain an HLA-I-low or even HLA-I-negative phenotype in an IFN-γ-rich microenvironment.[43] We and others have intensively studied the strong interdependency of intact IFN signaling and antigen presentation.[43,227–229] Neither HLA-I nor the intercellular adhesion molecule ICAM-1 could be upregulated in cells lacking distinct IFN pathway components.[227] Of note, reduced expression of ICAM-1 has been shown to diminish the tumor-T cell interaction and thus T-cell recognition.[226,230]

Loss of HLA-I surface expression is another vital escape mechanism to T cell-based immunotherapies and was found in melanoma cells from metastasis Ma-Mel-61h, displaying the JAK1 inactivation.[43,227] In this case, the HLA-I-negative phenotype resulted from a coordinated downregulation of distinct components of the HLA-I antigen processing and presentation machinery (APM).[227] The reversibility of the HLA-I APM gene silencing was proven by JAK1 reconstitution in these cells, leading to *de novo* HLA-I restoration upon IFN-γ treatment.[227] Former studies discovered HLA-I-negative tumor-cell variants generated by coordinated downregulation of APM components under immune-selective pressure of

T cells.[231,232] In summary, patient model Ma-Mel-61 represents the paradigm of T cell-based immunoediting. Additionally, it exemplifies intra-patient heterogeneity, hence the diverse genetic and phenotypic makeup among different metastases from the same patient. The continuous evolution of metastases within individual patients was recently outlined by gene-expression profiling and targeted deep sequencing of treatment-naive melanoma metastases, which pointed out the phenotypic and genetic divergency of different tumor lesions within the same patient.[233]

The highly plastic nature of melanoma cells enables them to phenotypically adapt to cellular stresses in response to drug exposure and inflammatory signaling. Phenotypic plasticity and subsequent dedifferentiation have been described as hallmarks of cancer progression in melanoma.[234] Especially melanoma dedifferentiation has repeatedly been observed in melanoma patient biopsies and is associated with resistance to targeted therapy and immunotherapies.[203,219,222] Recently, Rambow and colleagues revised the rheostat model of different melanoma cell states, according to MITF activity levels and distinct cell-state specific marker expression that can promote tumor progression.[135] The articles II (Harbers et al., JID, 2021) and III (Thier et al., JITC, 2022) presented in this thesis investigated phenotype switching in melanoma cells that persisted MAPKi and RIG-I agonist treatment. Both treatments reduced cell viability and induced cell death; however, some melanoma cells survived and remained in a non-proliferative cell state.[235,236] As described in Harbers et al., continuous treatment of four different melanoma cell lines with either single BRAFi or combined BRAFi/MEKi induced a drug-tolerant cell state until resistance was established.[235] During this transition phase, all treated cells exhibited a hyperdifferentiated phenotype until day 7 or 14 of treatment. Several studies have shown that MITF-mediated survival signaling promotes early drug tolerance in the initial MAPKi response phase leading to a $MITF^{high}$ hyperdifferentiated cell state.[127,129,204,237] In two of four tested melanoma models, prolonged MAPKi exposure led to a stabilization of a hyperdifferentiated BRAFi-resistant cell state, while the combined BRAFi/MEKi treatment induced a dedifferentiated $NGFR^{high}$ resistance phenotype.[235] Recently, single-cell RNA-sequencing of MAPKi-treated melanomas uncovered diverse differentiation trajectories that melanomas can follow to acquire drug resistance. The trajectory towards a dedifferentiated and neural-crest stem cell-like cell state is strongly driven by retinoid X receptor γ (RXRγ).[127] Underpinning these observations, our findings demonstrate that tumor cells from the same bulk population can dynamically transit along distinct differentiation trajectories, eventually acquiring discordant resistance cell states in a treatment-dependent manner. Furthermore, the

cellular heterogeneity of the bulk cell population may promote therapy-mediated phenotype selection.

Melanoma phenotype switching can also be induced by inflammatory stimuli. Cytokine-induced melanoma dedifferentiation has been deeply studied for TNF-α.[133,219,238] In the third presented study (Thier et al., JITC, 2022), we elucidate melanoma phenotype switching upon activation of the innate immune receptor RIG-I.[236] Activation of RIG-I by its ligand 3pRNA results in a robust immune response, including the production and secretion of pro-inflammatory cytokines, such as IFN-β, IL-1β, IL-6, and TNF-α, and chemokines, such as CCL5 and CXCL10.[173,174,176,227] We discovered a transient cell state switch towards a non-proliferative and dedifferentiated melanoma cell phenotype upon RIG-I activation.[236] Interestingly, the duration of treatment seems to be critical in the process of dedifferentiation, as we and others did not detect changes in the differentiation status after 24 hours of short-term 3pRNA-treatment.[236,239] Furthermore, we found evidence for the engagement of the JAK-STAT signaling pathway in RIG-I-mediated dedifferentiation by pathway analysis of transcriptomic data and partial blockade of 3pRNA-induced dedifferentiation by the JAK1/2 inhibitor ruxolitinib.[236] Ohanna and colleagues have found evidence of an impact of JAK-STAT signaling in melanoma dedifferentiation. They showed that the secretome of senescent melanoma cells induces STAT3 activation and increases a $MITF^{low}$ cell subpopulation harboring stemness-like features.[240] Still, the specific mechanism of how RIG-I induces this cell state remains unknown. Therefore, it needs to be investigated whether phenotype switching is induced directly by RIG-I-driven gene expression or indirectly by cytokines from 3pRNA-treated cells. Supporting the latter, our observations of RIG-I-mediated dedifferentiation resemble in several aspects cytokine-induced dedifferentiation by TNF-α and IFN-γ. For instance, both TNF-α and IFN-γ altered melanoma cell phenotype by decreasing melanocytic and increasing neural crest markers.[133,219,220] Two independent studies described inflammation-induced dedifferentiation by TNF-α in the context of T cell-derived inflammatory signaling to be reversible when the immune stimulation is removed.[133,219] Similarly, as the RIG-I and IFN signaling declines, dedifferentiated 3pRNA-persisters escaped from the quiescent dedifferentiated cell state by regaining their proliferative capacity and switching towards a more differentiated phenotype. These findings indicate a transient cell state switch upon RIG-I activation.[236] Although we found similarities of 3pRNA-induced phenotypic dedifferentiation to IFN-γ and TNF-α, it is still unclear whether the RIG-I-mediated cell state switch follows identical mechanistic tracts. Kim et al. reported by chromatin landscape analysis that IFN-γ and

TNF-α have divergent effects on epigenomic reprogramming, despite their similar phenotypic dedifferentiation.[220]

The three presented studies of this thesis (Such et al., JCI, 2020; Harbers et al., JID, 2021; Thier et al., JITC, 2022) demonstrated that melanoma cells escaped from the selective pressures of either the immune system or therapeutic interventions via genetic alterations or phenotypic plasticity. Thus, there is an urgent need to unravel persister-directed strategies to overcome therapy resistance.

7.2 Therapy-mediated sculpting of melanoma cell immunogenicity

The immunogenicity of melanoma cells, which comprises a cell's capacity to initiate anti-tumor immune responses, can be shaped by different stimuli. Major events contributing to enhanced immunogenicity are the expression of antigens and their presentation towards immune cells.[241] Therefore, adequate levels of tumor-specific antigens presented on HLA-I molecules on the cell surface of melanoma cells are required to elicit activation of cytotoxic CD8 T cells. In the studies presented here (Such et al., JCI, 2020; Harbers et al., JID, 2021; Thier et al., JITC, 2022), we observed shaping of melanoma cell immunogenicity by distinct molecular events upon treatment with 3pRNA or MAPKi.

We found loss of immunogenicity in Ma-Mel-61h cells due to HLA-I APM downregulation establishing an HLA-I-negative melanoma cell phenotype, which was reversible upon targeted RIG-I activation.[227] In general, HLA-I downregulation can result from epigenetic silencing, transcriptional or post-transcriptional/translational modifications of the HLA-I genes or genes involved in the processing of antigens into peptides, transport of peptides and their loading on HLA-I molecules.[242] Recently, different histone modifiers have been shown to epigenetically downregulate HLA-I APM gene transcription in melanoma and Merkel cell carcinoma.[214,217] Inhibition of these modifiers could restore HLA-I antigen presentation in epigenetically silenced HLA-I-negative tumor cells.[214,217] In our studies, we detected enhanced antigen presentation in several 3pRNA-treated patient-derived melanoma cell lines, which increased over time.[227,236] Interestingly, RIG-I signaling led to *de novo* HLA-I expression in Ma-Mel-61h cells. The HLA-I reexpression was IFN-independent and restored the CD8 T-cell sensitivity of Ma-Mel-61h cells. The fundamental mechanism of RIG-I-mediated upregulation of HLA-I molecules and APM components involves IRF1 and IRF3 via an IFN-independent salvage pathway, as silencing of IRF1 and IRF3 diminished RIG-I-mediated antigen presentation. Importantly, all tested melanoma cell lines induced IRF1 upon 3pRNA

transfection, regardless of their IFN sensitivity.[227] IRF1 is known to bind to regulatory elements of APM component genes. Together with NFκB p65, it has been shown to restore HLA-I-restricted tumor antigen processing and presentation in neuroblastoma cells, supporting our observations upon RIG-I activation.[243,244] Recently, it was demonstrated that induction of immunoproteasome subunits in melanoma cells could result in a distinct HLA-I-bound tumor-antigen repertoire with a more robust T-cell stimulatory capacity.[245] Here, we found evidence for the constitution of immunoproteasomes upon RIG-I activation, which might further improve HLA-I antigen presentation by multiplying and selectively generating immune-relevant peptides.[227,246] In fact, we observed enhanced T-cell activation by short-term 3pRNA-treated melanoma cells, and anti-HLA-I blocking antibodies completely impeded T-cell activation.[227] Overall, these results imply that targeted activation of RIG-I can overcome T-cell resistance, as it restored HLA-I antigen processing and presentation in an IFN-independent manner.[227]

In the second paper of this thesis (Harbers et al., JID, 2021), we demonstrated that melanoma cell immunogenicity upon MAPK pathway inhibition was strongly modulated over time. In general, MAPK signaling is a potent suppressor of HLA-I expression. Bradley et al. uncovered that BRAF-mutant melanomas exhibit downregulated HLA-I expression resulting from rapid and constitutive internalization and subsequent sequestration of HLA-I molecules from the cell surface. Inhibition of the MAPK pathway counteracts this process, thus, recovering HLA-I surface expression and augmenting melanoma recognition by CD8 T cells.[247] This is in line with our observation that short-term BRAFi single or combined BRAFi/MEKi treatment upregulated HLA-I surface expression.[204,235] Furthermore, a recent RNA sequencing analysis of short-term MAPKi-treated tumor cells revealed an inflammatory reprogramming, comprising genes involved in antigen presentation.[248] Moreover, short-term inhibitor treatment altered the melanoma cell phenotype towards a hyperdifferentiated cell state with increased differentiation antigen expression. Therefore, short-term treated melanoma cells exhibit enhanced immunogenicity by upregulated HLA-I expression and high levels of differentiation antigens that led to improved CD8 T-cell responses.[235] However, the duration of MAPK inhibition seems to be highly critical as prolonged treatment reverts the initial tumor-immunogenicity-increasing effects and established resistance to CD8 T cells and T-cell-based immunotherapies.[204,235,249,250] We and others observed that prolonged MAPKi treatment reduces HLA-I expression in drug-resistant tumors and melanoma cell lines.[203,235,251] Furthermore, continued MAPK inhibition induced a dedifferentiated phenotype of BRAFi/MEKi-resistant melanoma cell lines, indicating that targeted therapy impacts the antigen repertoire.[235] An association of a dedifferentiated melanoma cell phenotype with

resistance to targeted therapies has repeatedly been observed by us and others.[125,126,129,203,204,235] Moreover, our group showed that the presentation of tumor antigens others than differentiation antigens can be altered upon MAPK inhibition, including shared and neoantigens.[204] We observed a link between the dynamic in melanoma cell differentiation under prolonged MAPK inhibition and their capability to stimulate CD8 T-cell responses. The dedifferentiation of MAPKi-resistant melanoma cells was associated with a decrease in their T cell-stimulatory capacity.[235] Previously, it has been shown that differentiation antigens play a critical role in the immunogenicity of melanoma, as HLA-A-restricted CD8 TILs from 123 patient-derived cultures recognized predominantly melanocytic-lineage antigens.[252] This underpins our observation that loss of differentiation antigens in drug-treated melanoma cells diminished T-cell activation.[235] Nevertheless, we could exclude the contribution of HLA-I and PD-L1 levels on drug-resistant melanoma cells to the differences in their T-cell stimulatory capacity due to similar expression patterns among BRAFi- and BRAFi/MEKi-resistant melanoma cell lines.[235]

In summary, both targeted RIG-I activation and MAPK inhibitors could powerfully shape melanoma cell immunogenicity by altering the expression of HLA-I molecules and tumor antigens. These results deepen the knowledge of the tight connection between therapy-induced melanoma phenotypes and their CD8 T cell-stimulatory capacity paving the way for novel therapeutic strategies to counteract the evolution of T-cell resistance.

7.3 RIG-I agonists: potent immunity booster in melanoma treatment

Targeting the innate immunoreceptor RIG-I emerged as a promising approach to orchestrate adaptive immunity by activating innate immune responses. The dual effects of RIG-I activation on tumor cells and the tumor microenvironment have been intensively investigated in the last decade. Besides the previously mentioned inflammatory responses, RIG-I signaling induced mitochondrial apoptosis in cancer cells.[172–174,253,254] Our study (Thier et al., JITC, 2022) demonstrated the induction of apoptosis upon 3pRNA transfection in some melanoma cells, supporting the tumoricidal activity of RIG-I signaling.[236] According to our data on IFN-independent HLA-I upregulation, the pro-apoptotic signaling mediated by RIG-I activation also occurs in a type I IFN-independent manner, suggesting that RIG-I signaling could direct IFN-resistant melanoma cells towards cell death.[172] Furthermore, RIG-I-induced apoptotic tumor cells contribute to adaptive immune responses, as dendritic cells in the tumor microenvironment engulf them and cross-present tumor antigens to CD8 T cells.[173] The tumor

itself turns into a vaccine since apoptotic tumor cells release their entire antigenic repertoire. A polyclonal anti-tumor response is elicited, directed towards a broad repertoire of tumor antigens derived from heterogeneous tumor cells.[166] In glioblastoma 3pRNA was able to counteract cellular heterogeneity. Primary glioblastoma populations responded to RIG-I activation by inducing apoptosis and anti-tumor activity, regardless of their diverse phenotypes.[254] Similar effects are achieved by the intralesional application of the FDA-approved oncolytic virus talimogene laherparepvec (T-VEC), a genetically modified herpes simplex virus-1 (HSV-1) expressing human granulocyte-macrophage colony-stimulating factor (GM-CSF). Unlike RIG-I agonists, T-VEC selectively replicates in and destroys tumor cells but likewise targets cellular heterogeneity by releasing tumor antigens that set off local innate and systemic adaptive immune responses.[255,256] As previously mentioned, RIG-I activation in melanoma cells elicits *de novo* pro-inflammatory stimuli orchestrating adaptive immunity. We and others detected elevated release of chemokines, such as CCL5 and CXCL10, by different cancer cell lines upon 3pRNA application.[173,174,227,239,254] Importantly, our study (Such et al., JCI, 2020) underlined the IFN-independency of chemokine expression upon RIG-I activation in JAK-deficient melanoma cells. Furthermore, in a chicken chorioallantoic membrane (CAM) model we demonstrated that 3pRNA-induced chemokine secretion by melanoma cells enhanced their T-cell chemoattractive capacity.[227] According to our experimental findings, we reported a positive correlation of increased levels of CD8 T-cell infiltrates in patients with RIG-I^{high} expression in two different patient cohorts.[236] Our results indicate the capability of targeting the receptor RIG-I to foster immune-cell infiltration into the tumor lesion and, thus, potentially converting immune-cold into immune-hot tumors. Data from a phase Ib clinical trial combining T-VEC and anti-PD-1 blocking antibody indicated enhanced immune-cell infiltration into injected lesions with low CD8 baseline levels and partially into non-injected tumors.[257] The abscopal effects of RIG-I-induced immunity on regression of distant metastases were only observed in the context of immune cell-mediated anti-tumor activity.[178] Importantly, Torrejon et al. demonstrated that targeting the innate TLR9 counteracted locally injected and non-injected IFN-resistant melanomas and improved host survival. In line with our data (Such et al., JCI, 2020), JAK-deficient melanomas showed increased immune-cell infiltration upon innate immune receptor stimulation *in vivo*.[258]

In addition to the experimental data on RIG-I activation, we and others also highlighted the critical role of tumor cell-intrinsic RIG-I expression in therapeutic efficacy and melanoma patient outcome.[178,227,259] High expression of RIG-I (*DDX58*) in human melanomas correlates with improved patient outcome, also in response to ICB therapy.[178,227] Experimental *in vivo*

data support these findings as tumor control and host survival were impeded in RIG-I-deficient B16 melanoma-bearing mice.[259] Moreover, tumor-cell intrinsic RIG-I expression was reported to be indispensable for the efficacy of chemo- and radiation therapy.[259,260] Both treatments induced genotoxic stress in cancer cells resulting in endogenous RNA leakage into the cytoplasm, thus activating RIG-I.[260]

Taken together, both presented RIG-I studies (Such et al., JCI, 2020; Thier et al., JITC, 2022) strongly support the immune-stimulatory capacity of targeting this innate immune receptor that orchestrates innate and adaptive immunity and strongly underpins the implementation of RIG-I agonists in melanoma therapy.

7.4 Dedifferentiation: A marker for T-cell and therapy resistance in melanoma?

The emergence of a dedifferentiated phenotypic cell state is frequently associated with resistance to CD8 T cells and targeted therapy.[133,204,235,250,261] Dedifferentiated melanoma cells are characterized by downregulation of melanocytic-lineage markers. Distinct dedifferentiated cell states can be distinguished showing expression of either AXL or NGFR and have been associated with invasiveness and resistance to MAPK inhibitors.[129,130,199,206] Specifically, NGFR was described to be a key effector in melanoma phenotype switching.[130] Furthermore, Boshuizen and colleagues demonstrated that pre-existing NGFR^{high} cell populations confer resistance to the cytotoxic effector mechanisms of CD8 T cells.[221] Accordingly, dedifferentiated MAPKi-resistant melanoma cells with loss of differentiation antigen showed concomitant increased NGFR expression and reduced T cell-stimulatory capacity.[204,235] Similarly, these inversely correlated expression patterns of Melan-A/MART-1 and NGFR have been reported to arise in response to T cell-derived inflammatory stimuli.[133,219,220,238] Subsequently, we observed dedifferentiation upon RIG-I stimulation with 3pRNA in different melanoma cell lines, which occurred in a JAK-dependent manner.[236] However, in contrast to dedifferentiated drug-resistant cells, we found RIG-I-mediated dedifferentiated melanoma cells being still efficiently recognized by CD8 TILs.[236] The differences in recognition of dedifferentiated melanoma cells by CD8 T cells could be due to the duration and frequency of the different treatments and the activation of distinct signaling pathways involved in the MAPKi- or RIG-I-mediated phenotypic switch. In fact, RIG-I activation strongly induced JAK-STAT signaling and concomitant HLA-I APM upregulation that is associated with a strong enhancement in melanoma cell immunogenicity.[227,235,236] However, our study cannot exclude that for melanoma patients with high frequencies of differentiation antigen-specific CD8 T cells a RIG-I-induced

dedifferentiated melanoma cell phenotype might negatively affect T-cell sensitivity and function. Landsberg and colleagues exemplified that melanoma dedifferentiation can confer T-cell resistance in a genetically engineered mouse model, in which therapy was exclusively directed towards differentiation tumor antigens.[133]

The therapeutic context driving melanoma phenotype switching is intensively investigated and pointed out decisive differences in treatment-induced melanoma dedifferentiation. Recently, melanoma biopsies from ICB-responding patients showed decreased levels of melanocytic markers, suggesting that in this context dedifferentiation could be an indicator of initial responses to immunotherapy.[220] In accordance, we demonstrated that a dedifferentiated melanoma cell phenotype is not necessarily associated with T-cell resistance.[236] In sum, our results challenge the prevalent association between melanoma dedifferentiation and therapy resistance and suggest that the impact of therapy-induced phenotypic plasticity on immunotherapy efficacy depends on the type of therapy and the duration of treatment.

7.5 Exploiting combinational treatment to overcome therapy resistance

A significant obstacle in melanoma treatment is acquired therapy resistance after initial response resulting in disease progression. Combination therapies can target different melanoma subpopulations potentially delaying or even preventing resistance development and prolonging patient survival. In the treatment management of patients with advanced BRAF-mutant melanomas, two pillars exist. Targeted therapy and immune checkpoint blockade can be applied in combination, either as first- or subsequent-line treatment or concomitant administration.[262] So far, no guideline for the sequential administration is fully validated to date. Several studies by us and others uncovered the drug-induced shaping of melanoma immunogenicity bearing the urgent need to refine treatment protocols to achieve the most clinical benefit.[203,204,222,235,247,263] The majority of patients treated with BRAFi monotherapy rapidly progress, while the combination of BRAFi and MEKi has been shown to improve patient survival by delaying therapy resistance.[147,264] Although single BRAFi- and double-drug BRAFi/MEKi-resistant melanoma cells acquire resistance due to MAPK pathway reactivation,[265] we found only BRAFi/MEKi-resistant melanoma cell lines being drug-addicted. Thus, drug-addicted cells were resensitized to the combinational treatment after a drug holiday, providing a rationale for intermittent therapy.[235,266] However, recent results from a randomized phase II clinical trial comparing continuous or intermittent dosing of dual MAPK pathway

inhibitors showed that the promising drug-withdrawal effects, potentially avoiding tumor cell adaptation, were absent in melanoma patients receiving intermittent drug dosing.[267] Besides reduced tumor-cell immunogenicity as shown by us and others,[204,235,251] drug-resistant melanomas possess an altered immune landscape, including T-cell exclusion and exhaustion, as well as the absence of functional antigen-presenting dendritic cells, which can confer cross-resistance to immunotherapy.[203,250] Finally, MAPKi treatment should be considered short-term before drug resistance is established. Moreover, short-term MAPKi treatment transiently increases melanoma cell immunogenicity,[204,235] potentially favoring ICB therapy efficacy. Clinical trials of triple-combined anti-PD-1 inhibitors and BRAFi plus MEKi gave evidence of durable anti-tumor responses suggesting that triple treatment reduces primary ICB and acquired MAPKi resistance.[268–270] Evaluating different sequences of both single and combined ICB and MAPKi application, a recent *in vivo* pre-clinical study proposed a sequential regimen of brief ICB lead-in before additional MAPKi co-treatment. Furthermore, this strategy has been shown to suppress melanoma brain metastases that significantly limit patient survival.[271] Nevertheless, clinical trials are needed to validate these beneficial effects in human beings. Recently, transcriptomic analyses of oncogene-driven tumors, including BRAF-mutant melanoma, uncovered a MAPK/IRF-1 inflammatory response upon kinase inhibitor treatment, which sensitizes xenografted tumors to tumoricidal effects of RIG-I agonists in humanized mouse models.[248] The synergistic effects of combined short-term MAPKi and RIG-I agonist treatment should be considered for further investigations.

Clinical application of immune checkpoint blocking antibodies, such as anti-PD-1 monotherapy or combinational treatment with CTLA-4 inhibitors, are today's standard of care in melanoma therapy. Response to ICB therapy is dependent on a T cell-inflamed tumor microenvironment. Therefore, treating patients with poorly immune-infiltrated melanoma emerges as a major clinical challenge, which PRR agonists could overcome. We and others demonstrated the chemoattractive effects of targeting PRR to recruit immune cells to the tumor site.[59,178,227,258] Accordingly and in line with the previously discussed immune-stimulatory potential, lead-in RIG-I agonist treatment of low immune-inflamed melanomas could provide an optimal immune contexture for following anti-PD-1 co-treatment. Essentially, in our study, we could show the synergistic effects on T-cell activation of combinational treatment of the RIG-I agonist 3pRNA with anti-PD-1 or anti-TIGIT blocking antibodies in melanoma.[227] But even in T cell-inflamed melanomas primary and acquired ICB resistance limits therapeutic efficacy to only a minority of patients. Our group and others showed that primary and acquired resistance to anti-PD-1 therapy is often accompanied by genetic or non-genetic defects in

components involved in IFN-γ signaling or antigen presentation.[43,211,223,224] In the first presented study (Such et al., JCI, 2020), we could demonstrate that targeting RIG-I can, on the one hand, restore silenced HLA-I expression and, on the other, overcome genetic IFN resistance.[227] These findings were simultaneously validated by Kalbasi et al. in pre-clinical melanoma models. The PRR agonist BO-112 resensitized anti-PD-1 resistant JAK-deficient melanomas towards adoptive T-cell transfer therapy.[228] Furthermore, the synergistic effects that we observed on T-cell activity by 3pRNA and ICB were enlarged on tumor control in JAK-deficient mice that received combinational treatment of a TLR9 agonist and anti-PD-1 blocking antibodies.[258]

8 Perspective

In cancer therapy, the responsiveness of a patient towards a selected treatment is largely uncertain. Currently, molecular profiling of oncogenic driver mutations in patient biopsies assists in therapeutic decision-making, for instance, in stratifying melanoma patients according to their BRAF status for targeted therapy. Nevertheless, genomic and phenotypic heterogeneity are highly dynamic. As previously outlined for patient Ma-Mel-61, lesional and cellular heterogeneity evolves under selective pressure. Melanoma cells acquired genetic defects in the IFN signaling pathway and silenced antigen presentation over time, as the alterations were absent in early lesions.[43,227] These observations imply the need for longitudinal monitoring of melanoma patients before and on treatment to guide further treatment decisions. To detect therapy resistance before patients relapse, precision medicine approaches using integrative analysis of multi-omic data could be expedient. With this intention, liquid biopsy from blood or cerebrospinal fluid can provide non- or minimal-invasive sequential analysis of circulating tumor cells (CTC), cell-free tumor DNA (ctDNA), or tumor-derived extracellular vesicles. Advantageously, this approach can be used for early tumor detection, therapy response prediction, and patient follow-up.[272] Since melanoma immunogenicity is dynamically influenced by therapeutic intervention as presented in this thesis,[227,235,236] profiling of the genomic and phenotypic diversity of CTCs might reveal an ideal time point for ICB application when melanoma cells are highly immunogenic.

Based on the results of this thesis, the application of a RIG-I agonist is a promising therapeutic tool to induce tumor cell death, enhance melanoma immunogenicity and recruit immune cells to lesions with an immune-desert phenotype. The high inflammatory response of melanoma upon innate immune receptor stimulation makes the tumor highly receptive to

following ICB treatment. Accordingly, we found synergistic effects of combined RIG-I agonists and immune checkpoint inhibitor treatment on CD8 T-cell responses. A major challenge in melanoma management is refractory tumors that acquired therapy resistance. Even in these cases, administration of PRR agonists could serve as a promising therapeutic option to resensitize tumors from ICB-non-responders as we demonstrated the potential of RIG-I activation by 3pRNA to overcome T-cell resistance in melanoma.

In conclusion, the results obtained within this thesis support combinational treatment for melanoma therapy. However, further investigations are needed to optimize treatment protocols to counteract therapy resistance and reinforce patient benefit.

9 Reference

1. Burnet M. Cancer-A Biological Approach I. The Processes Of Control. Br. Med. J. 1957;1(5022):779–786. doi:10.1136/bmj.1.5022.779

2. Thomas L. “Discussion.” Hoeber-Harper [New York]. 1959;(Cellular and Humoral Aspects of the Hypersensitive States. H.S. Lawrence (Ed.)):529–532.

3. Shankaran V, Ikeda H, Bruce AT, White JM, Swanson PE, Old LJ, Schreiber RD. IFNγ, and lymphocytes prevent primary tumour development and shape tumour immunogenicity. Nature. 2001;410(6832):1107–1111. doi:10.1038/35074122

4. Moloney FJ, Comber H, O’Lorcain P, O’Kelly P, Conlon PJ, Murphy GM. A population-based study of skin cancer incidence and prevalence in renal transplant recipients. Br. J. Dermatol. 2006;154(3):498–504. doi:10.1111/j.1365-2133.2005.07021.x

5. Vajdic CM, McDonald SP, McCredie MRE, van Leeuwen MT, Stewart JH, Law M, Chapman JR, Webster AC, Kaldor JM, Grulich AE. Cancer incidence before and after kidney transplantation. JAMA. 2006;296(23):2823–31. doi:10.1001/jama.296.23.2823

6. Chaturvedi AK, Pfeiffer RM, Chang L, Goedert JJ, Biggar RJ, Engels EA. Elevated risk of lung cancer among people with AIDS. AIDS. 2007;21(2):207–13. doi:10.1097/QAD.0b013e3280118fca

7. Salman T. Spontaneous tumor regression. J. Oncol. Sci. 2016;2(1):1–4. doi:10.1016/j.jons.2016.04.008

8. Galon J, Costes A, Sanchez-Cabo F, Kirilovsky A, Mlecnik B, Lagorce-Pagès C, Tosolini M, Camus M, Berger A, Wind P, et al. Type, Density, and Location of Immune Cells Within Human Colorectal Tumors Predict Clinical Outcome. Science (80-.). 2006;313(5795):1960–1964. doi:10.1126/science.1129139

9. Fridman WH, Pagès F, Sauts-Fridman C, Galon J. The immune contexture in human tumours: Impact on clinical outcome. Nat. Rev. Cancer. 2012;12(4):298–306. doi:10.1038/nrc3245

10. Clemente CG, Mihm MC, Bufalino R, Zurrida S, Collini P, Cascinelli N. Prognostic value of tumor infiltrating lymphocytes in the vertical growth phase of primary cutaneous melanoma. Cancer. 1996;77(7):1303–1310. doi:10.1002/(SICI)1097-0142(19960401)77:7<1303::AID-CNCR12>3.0.CO;2-5

11. Dunn GP, Bruce AT, Ikeda H, Old LJ, Schreiber RD. Cancer immunoediting: from immunosurveillance to tumor escape. Nat. Immunol. 2002;3(11):991–998. doi:10.1038/ni1102-991

12. Dunn GP, Old LJ, Schreiber RD. The three Es of cancer immunoediting. Annu. Rev. Immunol. 2004;22(4):329–360. doi:10.1146/annurev.immunol.22.012703.104803

13. Schreiber RD, Old LJ, Smyth MJ. Cancer immunoediting: Integrating immunity’s roles in cancer

suppression and promotion. Science (80-.). 2011;331(6024):1565–1570. doi:10.1126/science.1203486

14. Vesely MD, Kershaw MH, Schreiber RD, Smyth MJ. Natural innate and adaptive immunity to cancer. Annu. Rev. Immunol. 2011;29:235–271. doi:10.1146/annurev-immunol-031210-101324

15. Aguirre-Ghiso JA. Models, mechanisms and clinical evidence for cancer dormancy. Nat. Rev. Cancer. 2007;7(11):834–846. doi:10.1038/nrc2256

16. Hanahan D, Weinberg RA. Hallmarks of cancer: The next generation. Cell. 2011;144(5):646–674. doi:10.1016/j.cell.2011.02.013

17. Koebel CM, Vermi W, Swann JB, Zerafa N, Rodig SJ, Old LJ, Smyth MJ, Schreiber RD. Adaptive immunity maintains occult cancer in an equilibrium state. Nature. 2007;450(7171):903–907. doi:10.1038/nature06309

18. Smyth MJ, Thia KYT, Street SEA, MacGregor D, Godfrey DI, Trapani JA. Perforin-mediated cytotoxicity is critical for surveillance of spontaneous lymphoma. J. Exp. Med. 2000;192(5):755–760. doi:10.1084/jem.192.5.755

19. Bretscher P, Cohn M. A theory of self-nonself discrimination. Science. 1970;169(3950):1042–9. doi:10.1126/science.169.3950.1042

20. Mueller DL, Jenkins MK, Schwartz RH. Clonal expansion versus functional clonal inactivation: a costimulatory signalling pathway determines the outcome of T cell antigen receptor occupancy. Annu. Rev. Immunol. 1989;7:445–80. doi:10.1146/annurev.iy.07.040189.002305

21. Driessens G, Kline J, Gajewski TF. Costimulatory and coinhibitory receptors in anti-tumor immunity. Immunol. Rev. 2009;229(1):126–144. doi:10.1111/j.1600-065X.2009.00771.x

22. Xiao Z, Mayer AT, Nobashi TW, Gambhir SS. ICOS Is an Indicator of T-cell–Mediated Response to Cancer Immunotherapy. Cancer Res. 2020;80(14):3023–3032. doi:10.1158/0008-5472.CAN-19-3265

23. von Leoprechting A, van der Bruggen P, Pahl HL, Aruffo A, Simon JC. Stimulation of CD40 on immunogenic human malignant melanomas augments their cytotoxic T lymphocyte-mediated lysis and induces apoptosis. Cancer Res. 1999;59(6):1287–94.

24. Pirozzi G, Lombari V, Zanzi D, Ionna F, Lombardi ML, Errico S, Ruggiero G, Manzo C. CD40 expressed on human melanoma cells mediates T cell co-stimulation and tumor cell growth. Int. Immunol. 2000;12(6):787–95. doi:10.1093/intimm/12.6.787

25. Salih HR, Kosowski SG, Haluska VF, Starling GC, Loo DT, Lee F, Aruffo AA, Trail PA, Kiener PA. Constitutive expression of functional 4-1BB (CD137) ligand on carcinoma cells. J. Immunol. 2000;165(5):2903–10. doi:10.4049/jimmunol.165.5.2903

26. Brunet J-F, Denizot F, Luciani M-F, Roux-Dosseto M, Suzan M, Mattei M-G, Golstein P. A new member of the immunoglobulin superfamily—CTLA-4. Nature. 1987;328(6127):267–270. doi:10.1038/328267a0

27. Ishida Y, Agata Y, Shibahara K, Honjo T. Induced expression of PD-1, a novel member of the immunoglobulin gene superfamily, upon programmed cell death. EMBO J. 1992;11(11):3887–95.

28. Pardoll DM. The blockade of immune checkpoints in cancer immunotherapy. Nat. Rev. Cancer. 2012;12(4):252–264. doi:10.1038/nrc3239

29. Boon T, Coulie PG, Van Den Eynde BJ, Van Der Bruggen P. Human T cell responses against melanoma. Annu. Rev. Immunol. 2006;24:175–208. doi:10.1146/annurev.immunol.24.021605.090733

30. van der Bruggen P, Traversari C, Chomez P, Lurquin C, De Plaen E, Van den Eynde B, Knuth A, Boon T. A gene encoding an antigen recognized by cytolytic T lymphocytes on a human melanoma. Science (80-.). 1991;254(5038):1643–1647. doi:10.1126/science.1840703

31. Chávez-Galán L, Arenas-Del Angel MC, Zenteno E, Chávez R, Lascurain R. Cell death mechanisms induced by cytotoxic lymphocytes. Cell. Mol. Immunol. 2009;6(1):15–25. doi:10.1038/cmi.2009.3

32. Liu C-C, Walsh CM, Young JD-E. Perforin: structure and function. Immunol. Today. 1995;16(4):194–201. doi:10.1016/0167-5699(95)80121-9

33. Waterhouse NJ, Sedelies KA, Trapani JA. Role of Bid-induced mitochondrial outer membrane permeabilization in granzyme B-induced apoptosis. Immunol. Cell Biol. 2006;84(1):72–78. doi:10.1111/j.1440-1711.2005.01416.x

34. Shen DT, Ma JSY, Mather J, Vukmanovic S, Radoja S. Activation of primary T lymphocytes results in lysosome development and polarized granule exocytosis in CD4+ and CD8+ subsets, whereas expression of lytic molecules confers cytotoxicity to CD8+ T cells. J. Leukoc. Biol. 2006;80(4):827–37. doi:10.1189/jlb.0603298

35. Strasser A, Jost PJ, Nagata S. The many roles of FAS receptor signaling in the immune system. Immunity. 2009;30(2):180–92. doi:10.1016/j.immuni.2009.01.001

36. Carrington PE, Sandu C, Wei Y, Hill JM, Morisawa G, Huang T, Gavathiotis E, Wei Y, Werner MH. The structure of FADD and its mode of interaction with procaspase-8. Mol. Cell. 2006;22(5):599–610. doi:10.1016/j.molcel.2006.04.018

37. Luo X, Budihardjo I, Zou H, Slaughter C, Wang X. Bid, a Bcl2 interacting protein, mediates cytochrome c release from mitochondria in response to activation of cell surface death receptors. Cell. 1998;94(4):481–90. doi:10.1016/s0092-8674(00)81589-5

38. Wajant H, Pfizenmaier K, Scheurich P. Tumor necrosis factor signaling. Cell Death Differ.

2003;10(1):45–65. doi:10.1038/sj.cdd.4401189

39. Zhang X, Vallabhaneni R, Loughran PA, Shapiro R, Yin X-M, Yuan Y, Billiar TR. Changes in FADD levels, distribution, and phosphorylation in TNFalpha-induced apoptosis in hepatocytes is caspase-3, caspase-8 and BID dependent. Apoptosis. 2008;13(8):983–92. doi:10.1007/s10495-008-0228-3

40. Ikeda H, Old LJ, Schreiber RD. The roles of IFN gamma in protection against tumor development and cancer immunoediting. Cytokine Growth Factor Rev. 2002;13(2):95–109. doi:10.1016/s1359-6101(01)00038-7

41. Chawla-Sarkar M, Lindner DJ, Liu Y-F, Williams BR, Sen GC, Silverman RH, Borden EC. Apoptosis and interferons: role of interferon-stimulated genes as mediators of apoptosis. Apoptosis. 2003;8(3):237–49. doi:10.1023/a:1023668705040

42. Refaeli Y, Van Parijs L, Alexander SI, Abbas AK. Interferon γ Is Required for Activation-induced Death of T Lymphocytes. J. Exp. Med. 2002;196(7):999–1005. doi:10.1084/jem.20020666

43. Sucker A, Zhao F, Pieper N, Heeke C, Maltaner R, Stadtler N, Real B, Bielefeld N, Howe S, Weide B, et al. Acquired IFNγ resistance impairs anti-tumor immunity and gives rise to T-cell-resistant melanoma lesions. Nat. Commun. 2017;8(1):15440. doi:10.1038/ncomms15440

44. Beck RJ, Slagter M, Beltman JB. Contact-dependent killing by cytotoxic T lymphocytes is insufficient for EL4 tumor regression in vivo. Cancer Res. 2019;79(13):3406–3416. doi:10.1158/0008-5472.CAN-18-3147

45. Sanderson NSR, Puntel M, Kroeger KM, Bondale NS, Swerdlow M, Iranmanesh N, Yagita H, Ibrahim A, Castro MG, Lowenstein PR. Cytotoxic immunological synapses do not restrict the action of interferon-γ to antigenic target cells. Proc. Natl. Acad. Sci. U. S. A. 2012;109(20):7835–40. doi:10.1073/pnas.1116058109

46. Hoekstra ME, Bornes L, Dijkgraaf FE, Philips D, Pardieck IN, Toebes M, Thommen DS, van Rheenen J, Schumacher TNM. Long-distance modulation of bystander tumor cells by CD8+ T-cell-secreted IFN-γ. Nat. Cancer. 2020;1(3):291–301. doi:10.1038/s43018-020-0036-4

47. Franco S Di, Turdo A, Todaro M, Stassi G. Role of Type I and II interferons in colorectal cancer and melanoma. Front. Immunol. 2017;8(JUL). doi:10.3389/fimmu.2017.00878

48. Budhwani M, Mazzieri R, Dolcetti R. Plasticity of type I interferon-mediated responses in cancer therapy: From anti-tumor immunity to resistance. Front. Oncol. 2018;8(AUG). doi:10.3389/fonc.2018.00322

49. Dunn GP, Koebel CM, Schreiber RD. Interferons, immunity and cancer immunoediting. Nat. Rev. Immunol. 2006;6(11):836–848. doi:10.1038/nri1961

50. Schroder K, Hertzog PJ, Ravasi T, Hume DA. Interferon-γ: an overview of signals, mechanisms and functions. J. Leukoc. Biol. 2004;75(2):163–189. doi:10.1189/jlb.0603252

51. Jorgovanovic D, Song M, Wang L, Zhang Y. Roles of IFN-γ in tumor progression and regression: a review. Biomark. Res. 2020;8(1):49. doi:10.1186/s40364-020-00228-x

52. Platanias LC. Mechanisms of type-I- and type-II-interferon-mediated signalling. Nat. Rev. Immunol. 2005;5(5):375–386. doi:10.1038/nri1604

53. Gocher AM, Workman CJ, Vignali DAA. Interferon-γ: teammate or opponent in the tumour microenvironment? Nat. Rev. Immunol. 2021;0123456789. doi:10.1038/s41577-021-00566-3

54. Keskinen P, Ronni T, Matikainen S, Lehtonen A, Julkunen I. Regulation of HLA class I and II expression by interferons and influenza A virus in human peripheral blood mononuclear cells. Immunology. 1997;91(3):421–9. doi:10.1046/j.1365-2567.1997.00258.x

55. Shin EC, Seifert U, Kato T, Rice CM, Feinstone SM, Kloetzel PM, Rehermann B. Virus-induced type I IFN stimulates generation of immunoproteasomes at the site of infection. J. Clin. Invest. 2006;116(11):3006–3014. doi:10.1172/JCI29832

56. Meissner TB, Li A, Biswas A, Lee KH, Liu YJ, Bayir E, Iliopoulos D, Van Den Elsen PJ, Kobayashi KS. NLR family member NLRC5 is a transcriptional regulator of MHC class I genes. Proc. Natl. Acad. Sci. U. S. A. 2010;107(31):13794–13799. doi:10.1073/pnas.1008684107

57. Garrido F, Aptsiauri N, Doorduijn EM, Garcia Lora AM, van Hall T. The urgent need to recover MHC class I in cancers for effective immunotherapy. Curr. Opin. Immunol. 2016;39:44–51. doi:10.1016/j.coi.2015.12.007

58. Hervas-Stubbs S, Perez-Gracia JL, Rouzaut A, Sanmamed MF, Le Bon A, Melero I. Direct effects of type I interferons on cells of the immune system. Clin. Cancer Res. 2011;17(9):2619–2627. doi:10.1158/1078-0432.CCR-10-1114

59. Bald T, Landsberg J, Lopez-Ramos D, Renn M, Glodde N, Jansen P, Gaffal E, Steitz J, Tolba R, Kalinke U, et al. Immune cell-poor melanomas benefit from PD-1 blockade after targeted type I IFN activation. Cancer Discov. 2014;4(6):674–687. doi:10.1158/2159-8290.CD-13-0458

60. Grasso CS, Tsoi J, Onyshchenko M, Abril-Rodriguez G, Ross-Macdonald P, Wind-Rotolo M, Champhekar A, Medina E, Torrejon DY, Shin DS, et al. Conserved Interferon-γ Signaling Drives Clinical Response to Immune Checkpoint Blockade Therapy in Melanoma. Cancer Cell. 2020;38(4):500-515.e3. doi:10.1016/j.ccell.2020.08.005

61. Ayers M, Lunceford J, Nebozhyn M, Murphy E, Loboda A, Kaufman DR, Albright A, Cheng JD, Kang SP, Shankaran V, et al. IFN-γ-related mRNA profile predicts clinical response to PD-1 blockade. J. Clin. Invest. 2017;127(8):2930–2940. doi:10.1172/JCI91190

62. Garcia-Diaz A, Shin DS, Moreno BH, Saco J, Escuin-Ordinas H, Rodriguez GA, Zaretsky JM, Sun L, Hugo W, Wang X, et al. Interferon Receptor Signaling Pathways Regulating PD-L1 and PD-L2 Expression. Cell Rep. 2017;19(6):1189–1201. doi:10.1016/j.celrep.2017.04.031

63. Katz JB, Muller AJ, Prendergast GC. Indoleamine 2,3-dioxygenase in T-cell tolerance and tumoral immune escape. Immunol. Rev. 2008;222(1):206–221. doi:10.1111/j.1600-065X.2008.00610.x

64. DeMartino GN, Slaughter CA. The proteasome, a novel protease regulated by multiple mechanisms. J. Biol. Chem. 1999;274(32):22123–22126. doi:10.1074/jbc.274.32.22123

65. Ortiz-Navarrete V, Seelig A, Gernold M, Frentzel S, Kloetzel PM, Hämmerling GJ. Subunit of the "20S" proteasome (multicatalytic proteinase) encoded by the major histocompatibility complex. Nature. 1991;353(6345):662–4. doi:10.1038/353662a0

66. Kimura H, Caturegli P, Takahashi M, Suzuki K. New Insights into the Function of the Immunoproteasome in Immune and Nonimmune Cells. J. Immunol. Res. 2015;2015. doi:10.1155/2015/541984

67. Martinez-Fonts K, Davis C, Tomita T, Elsasser S, Nager AR, Shi Y, Finley D, Matouschek A. The proteasome 19S cap and its ubiquitin receptors provide a versatile recognition platform for substrates. Nat. Commun. 2020;11(1). doi:10.1038/s41467-019-13906-8

68. Tanaka K. Role of proteasomes modified by interferon-gamma in antigen processing. J. Leukoc. Biol. 1994;56(5):571–5. doi:10.1002/jlb.56.5.571

69. van Hall T, Sijts A, Camps M, Offringa R, Melief C, Kloetzel PM, Ossendorp F. Differential influence on cytotoxic T lymphocyte epitope presentation by controlled expression of either proteasome immunosubunits or PA28. J. Exp. Med. 2000;192(4):483–94. doi:10.1084/jem.192.4.483

70. Schwarz K, van Den Broek M, Kostka S, Kraft R, Soza A, Schmidtke G, Kloetzel PM, Groettrup M. Overexpression of the proteasome subunits LMP2, LMP7, and MECL-1, but not PA28 alpha/beta, enhances the presentation of an immunodominant lymphocytic choriomeningitis virus T cell epitope. J. Immunol. 2000;165(2):768–78. doi:10.4049/jimmunol.165.2.768

71. Nandi D, Jiang H, Monaco JJ. Identification of MECL-1 (LMP-10) as the third IFN-gamma-inducible proteasome subunit. J. Immunol. 1996;156(7):2361–4.

72. van Endert PM, Tampé R, Meyer TH, Tisch R, Bach J-F, McDevitt HO. A sequential model for peptide binding and transport by the transporters associated with antigen processing. Immunity. 1994;1(6):491–500. doi:10.1016/1074-7613(94)90091-4

73. Yan J, Parekh V V., Mendez-Fernandez Y, Olivares-Villagómez D, Dragovic S, Hill T, Roopenian DC, Joyce S, Van Kaer L. In vivo role of ER-associated peptidase activity in tailoring peptides for presentation by MHC class Ia and class Ib molecules. J. Exp. Med. 2006;203(3):647–659.

doi:10.1084/jem.20052271

74. Singh-Jasuja H, Emmerich NPN, Rammensee H-G. The T�bingen approach: identification, selection, and validation of tumor-associated HLA peptides for cancer therapy. Cancer Immunol. Immunother. 2004;53(3):187–195. doi:10.1007/s00262-003-0480-x

75. Pamer E, Cresswell P. Mechanisms of MHC class I-restricted antigen processing. Annu. Rev. Immunol. 1998;16:323–358. doi:10.1146/annurev.immunol.16.1.323

76. Nössner E, Parham P. Species-specific differences in chaperone interaction of human and mouse major histocompatibility complex class I molecules. J. Exp. Med. 1995;181(1):327–37. doi:10.1084/jem.181.1.327

77. Diedrich G, Bangia N, Pan M, Cresswell P. A Role for Calnexin in the Assembly of the MHC Class I Loading Complex in the Endoplasmic Reticulum. J. Immunol. 2001;166(3):1703–1709. doi:10.4049/jimmunol.166.3.1703

78. Ortmann B, Androlewicz MJ, Cresswell P. MHC class I/beta 2-microglobulin complexes associate with TAP transporters before peptide binding. Nature. 1994;368(6474):864–7. doi:10.1038/368864a0

79. Grandea AG, Van Kaer L. Tapasin: An ER chaperone that controls MHC class I assembly with peptide. Trends Immunol. 2001;22(4):194–199. doi:10.1016/S1471-4906(01)01861-0

80. Hughes EA, Cresswell P. The thiol oxidoreductase ERp57 is a component of the MHC class I peptide-loading complex. Curr. Biol. 1998;8(12):709–12. doi:10.1016/s0960-9822(98)70278-7

81. Knittler MR, Alberts P, Deverson E V, Howard JC. Nucleotide binding by TAP mediates association with peptide and release of assembled MHC class I molecules. Curr. Biol. 1999;9(18):999–1008. doi:10.1016/s0960-9822(99)80448-5

82. Suh WK, Cohen-Doyle MF, Fruh K, Wang K, Peterson PA, Williams DB. Interaction of MHC class I molecules with the transporter associated with antigen processing. Science (80-.). 1994;264(5163):1322–1326. doi:10.1126/science.8191286

83. Van den Eynde B, Peeters O, De Backer O, Gaugler B, Lucas S, Boon T. A new family of genes coding for an antigen recognized by autologous cytolytic T lymphocytes on a human melanoma. J. Exp. Med. 1995;182(3):689–98. doi:10.1084/jem.182.3.689

84. Chen YT, Scanlan MJ, Sahin U, Türeci O, Gure AO, Tsang S, Williamson B, Stockert E, Pfreundschuh M, Old LJ. A testicular antigen aberrantly expressed in human cancers detected by autologous antibody screening. Proc. Natl. Acad. Sci. U. S. A. 1997;94(5):1914–8. doi:10.1073/pnas.94.5.1914

85. Vigneron N. Human Tumor Antigens and Cancer Immunotherapy. Biomed Res. Int. 2015;2015.

doi:10.1155/2015/948501

86. Kawakami Y, Robbins PF, Wang RF, Parkhurst M, Kang X, Rosenberg SA. The use of melanosomal proteins in the immunotherapy of melanoma. J. Immunother. 1998;21(4):237–46. doi:10.1097/00002371-199807000-00001

87. Van der Bruggen P, Zhang Y, Chaux P, Stroobant V, Panichelli C, Schultz ES, Chapiro J, Van den Eynde BJ, Brasseur F, Boon T. Tumor-specific shared antigenic peptides recognized by human T cells. Immunol. Rev. 2002;188:51–64. doi:10.1034/j.1600-065X.2002.18806.x

88. Jäger E, Ringhoffer M, Karbach J, Arand M, Oesch F, Knuth A. Inverse relationship of melanocyte differentiation antigen expression in melanoma tissues and CD8+ cytotoxic-T-cell responses: Evidence for immunoselection of antigen-loss variants in vivo. Int. J. Cancer. 1996;66(4):470–476. doi:10.1002/(SICI)1097-0215(19960516)66:4<470::AID-IJC10>3.0.CO;2-C

89. Yee C, Thompson JA, Roche P, Byrd DR, Lee PP, Piepkorn M, Kenyon K, Davis MM, Riddell SR, Greenberg PD. Melanocyte destruction after antigen-specific immunotherapy of melanoma: direct evidence of t cell-mediated vitiligo. J. Exp. Med. 2000;192(11):1637–44. doi:10.1084/jem.192.11.1637

90. Hacohen N, Fritsch EF, Carter TA, Lander ES, Wu CJ. Getting personal with neoantigen-based therapeutic cancer vaccines. Cancer Immunol. Res. 2013;1(1):11–5. doi:10.1158/2326-6066.CIR-13-0022

91. Smith CC, Selitsky SR, Chai S, Armistead PM, Vincent BG, Serody JS. Alternative tumour-specific antigens. Nat. Rev. Cancer. 2019;19(8):465–478. doi:10.1038/s41568-019-0162-4

92. Coulie PG, Van Den Eynde BJ, Van Der Bruggen P, Boon T. Tumour antigens recognized by T lymphocytes: At the core of cancer immunotherapy. Nat. Rev. Cancer. 2014;14(2):135–146. doi:10.1038/nrc3670

93. Alexandrov LB, Nik-Zainal S, Wedge DC, Aparicio SAJR, Behjati S, Biankin A V., Bignell GR, Bolli N, Borg A, Børresen-Dale AL, et al. Signatures of mutational processes in human cancer. Nature. 2013;500(7463):415–421. doi:10.1038/nature12477

94. Pfeifer GP. Environmental exposures and mutational patterns of cancer genomes. Genome Med. 2010;2(8):54. doi:10.1186/gm175

95. Gandini S, Sera F, Cattaruzza MS, Pasquini P, Abeni D, Boyle P, Melchi CF. Meta-analysis of risk factors for cutaneous melanoma: I. Common and atypical naevi. Eur. J. Cancer. 2005;41(1):28–44. doi:10.1016/j.ejca.2004.10.015

96. Shain AH, Bastian BC. From melanocytes to melanomas. Nat. Rev. Cancer. 2016;16(6):345–358. doi:10.1038/nrc.2016.37

97. Kaidbey KH, Agin PP, Sayre RM, Kligman AM. Photoprotection by melanin--a comparison of black and Caucasian skin. J. Am. Acad. Dermatol. 1979;1(3):249–60. doi:10.1016/s0190-9622(79)70018-1

98. Whiteman DC, Whiteman CA, Green AC. Childhood sun exposure as a risk factor for melanoma: a systematic review of epidemiologic studies. Cancer Causes Control. 2001;12(1):69–82. doi:10.1023/a:1008980919928

99. Schadendorf D, van Akkooi ACJ, Berking C, Griewank KG, Gutzmer R, Hauschild A, Stang A, Roesch A, Ugurel S. Melanoma. Lancet. 2018;392(10151):971–984. doi:10.1016/S0140-6736(18)31559-9

100. Jiang AJ, Rambhatla P V., Eide MJ. Socioeconomic and lifestyle factors and melanoma: A systematic review. Br. J. Dermatol. 2015;172(4):885–915. doi:10.1111/bjd.13500

101. International Agency for Research on Cancer; WHO. GLOBOCAN 2020: estimated cancer incidence, mortality, and prevalence worldwide in 2020. 2020:https://gco.iarc.fr.

102. International Agency for Research on Cancer; WHO. Melanoma of skin, Source: Globocan 2020. 2020:https://gco.iarc.fr. [accessed July 27, 2021]. https://gco.iarc.fr/today/data/factsheets/cancers/16-Melanoma-of-skin-fact-sheet.pdf

103. Sung H, Ferlay J, Siegel RL, Laversanne M, Soerjomataram I, Jemal A, Bray F. Global Cancer Statistics 2020: GLOBOCAN Estimates of Incidence and Mortality Worldwide for 36 Cancers in 185 Countries. CA. Cancer J. Clin. 2021;71(3):209–249. doi:10.3322/caac.21660

104. Matthews NH, Li W-Q, Qureshi AA, Weinstock MA, Cho E. Epidemiology of Melanoma. 2017.

105. Morton DL, Thompson JF, Cochran AJ, Mozzillo N, Nieweg OE, Roses DF, Hoekstra HJ, Karakousis CP, Puleo CA, Coventry BJ, et al. Final Trial Report of Sentinel-Node Biopsy versus Nodal Observation in Melanoma. N. Engl. J. Med. 2014;370(7):599–609. doi:10.1056/nejmoa1310460

106. Sanborn JZ, Chung J, Purdom E, Wang NJ, Kakavand H, Wilmott JS, Butler T, Thompson JF, Mann GJ, Haydu LE, et al. Phylogenetic analyses of melanoma reveal complex patterns of metastatic dissemination. Proc. Natl. Acad. Sci. U. S. A. 2015;112(35):10995–1000. doi:10.1073/pnas.1508074112

107. Jimbow K, Roth SI, Fitzpatrick TB, Szabo G. Mitotic activity in non-neoplastic melanocytes in vivo as determined by histochemical, autoradiographic, and electron microscope studies. J. Cell Biol. 1975;66(3):663–70. doi:10.1083/jcb.66.3.663

108. Teixido C, Castillo P, Martinez-Vila C, Arance A, Alos L. Molecular markers and targets in melanoma. Cells. 2021;10(9):1–31. doi:10.3390/cells10092320

109. Cancer Genome Atlas Network. Genomic Classification of Cutaneous Melanoma. Cell. 2015;161(7):1681–96. doi:10.1016/j.cell.2015.05.044

110. Davis LE, Shalin SC, Tackett AJ. Current state of melanoma diagnosis and treatment. Cancer Biol. Ther. 2019;20(11):1366–1379. doi:10.1080/15384047.2019.1640032

111. Mort RL, Jackson IJ, Patton EE, Mort RL, Jackson IJ, Patton EE. Erratum to: The melanocyte lineage in development and disease (Development (Cambridge) 142, (620–632)). Dev. 2015;142(7):620–632. doi:10.1242/dev.123729

112. Hoek KS, Goding CR. Cancer stem cells versus phenotype-switching in melanoma. Pigment Cell Melanoma Res. 2010;23(6):746–759. doi:10.1111/j.1755-148X.2010.00757.x

113. Arozarena I, Wellbrock C. Targeting invasive properties of melanoma cells. FEBS J. 2017;284(14):2148–2162. doi:10.1111/febs.14040

114. Hodgkinson CA, Moore KJ, Nakayama A, Steingrímsson E, Copeland NG, Jenkins NA, Arnheiter H. Mutations at the mouse microphthalmia locus are associated with defects in a gene encoding a novel basic-helix-loop-helix-zipper protein. Cell. 1993;74(2):395–404. doi:10.1016/0092-8674(93)90429-t

115. Du J, Widlund HR, Horstmann MA, Ramaswamy S, Ross K, Huber WE, Nishimura EK, Golub TR, Fisher DE. Critical role of CDK2 for melanoma growth linked to its melanocyte-specific transcriptional regulation by MITF. Cancer Cell. 2004;6(6):565–76. doi:10.1016/j.ccr.2004.10.014

116. Wellbrock C, Rana S, Paterson H, Pickersgill H, Brummelkamp T, Marais R. Oncogenic BRAF regulates melanoma proliferation through the lineage specific factor MITF. PLoS One. 2008;3(7):e2734. doi:10.1371/journal.pone.0002734

117. Carreira S, Goodall J, Denat L, Rodriguez M, Nuciforo P, Hoek KS, Testori A, Larue L, Goding CR. Mitf regulation of Dia1 controls melanoma proliferation and invasiveness. Genes Dev. 2006;20(24):3426–3439. doi:10.1101/gad.406406

118. McGill GG, Horstmann M, Widlund HR, Du J, Motyckova G, Nishimura EK, Lin Y-L, Ramaswamy S, Avery W, Ding H-F, et al. Bcl2 regulation by the melanocyte master regulator Mitf modulates lineage survival and melanoma cell viability. Cell. 2002;109(6):707–18. doi:10.1016/s0092-8674(02)00762-6

119. Du J, Miller AJ, Widlund HR, Horstmann MA, Ramaswamy S, Fisher DE. MLANA/MART1 and SILV/PMEL17/GP100 are transcriptionally regulated by MITF in melanocytes and melanoma. Am. J. Pathol. 2003;163(1):333–43. doi:10.1016/S0002-9440(10)63657-7

120. Yasumoto K, Yokoyama K, Shibata K, Tomita Y, Shibahara S. Microphthalmia-associated transcription factor as a regulator for melanocyte-specific transcription of the human tyrosinase gene. Mol. Cell. Biol. 1994;14(12):8058–70. doi:10.1128/mcb.14.12.8058-8070.1994

121. McGill GG, Haq R, Nishimura EK, Fisher DE. c-Met expression is regulated by Mitf in the melanocyte lineage. J. Biol. Chem. 2006;281(15):10365–73. doi:10.1074/jbc.M513094200

122. Hoek KS, Schlegel NC, Brafford P, Sucker A, Ugurel S, Kumar R, Weber BL, Nathanson KL, Phillips DJ, Herlyn M, et al. Metastatic potential of melanomas defined by specific gene expression profiles with no BRAF signature. Pigment Cell Res. 2006;19(4):290–302. doi:10.1111/j.1600-0749.2006.00322.x

123. Goding CR. A picture of Mitf in melanoma immortality. Oncogene. 2011;30(20):2304–2306. doi:10.1038/onc.2010.641

124. Kim IS, Heilmann S, Kansler ER, Zhang Y, Zimmer M, Ratnakumar K, Bowman RL, Simon-Vermot T, Fennell M, Garippa R, et al. Microenvironment-derived factors driving metastatic plasticity in melanoma. Nat. Commun. 2017;8(1):14343. doi:10.1038/ncomms14343

125. Tsoi J, Robert L, Paraiso K, Galvan C, Sheu KM, Lay J, Wong DJL, Atefi M, Shirazi R, Wang X, et al. Multi-stage Differentiation Defines Melanoma Subtypes with Differential Vulnerability to Drug-Induced Iron-Dependent Oxidative Stress. Cancer Cell. 2018;33(5):890-904.e5. doi:10.1016/j.ccell.2018.03.017

126. Tirosh I, Izar B, Prakadan SM, Wadsworth MH, Treacy D, Trombetta JJ, Rotem A, Rodman C, Lian C, Murphy G, et al. Dissecting the multicellular ecosystem of metastatic melanoma by single-cell RNA-seq. Science (80-.). 2016;352(6282):189–196. doi:10.1126/science.aad0501

127. Rambow F, Rogiers A, Marin-Bejar O, Aibar S, Femel J, Dewaele M, Karras P, Brown D, Chang YH, Debiec-Rychter M, et al. Toward Minimal Residual Disease-Directed Therapy in Melanoma. Cell. 2018;174(4):843-855.e19. doi:10.1016/j.cell.2018.06.025

128. Wouters J, Kalender-Atak Z, Minnoye L, Spanier KI, De Waegeneer M, Bravo González-Blas C, Mauduit D, Davie K, Hulselmans G, Najem A, et al. Robust gene expression programs underlie recurrent cell states and phenotype switching in melanoma. Nat. Cell Biol. 2020;22(8):986–998. doi:10.1038/s41556-020-0547-3

129. Müller J, Krijgsman O, Tsoi J, Robert L, Hugo W, Song C, Kong X, Possik PA, Cornelissen-Steijger PDM, Foppen MHG, et al. Low MITF/AXL ratio predicts early resistance to multiple targeted drugs in melanoma. Nat. Commun. 2014;5. doi:10.1038/ncomms6712

130. Restivo G, Diener J, Cheng PF, Kiowski G, Bonalli M, Biedermann T, Reichmann E, Levesque MP, Dummer R, Sommer L. Low Neurotrophin receptor CD271 regulates phenotype switching in Melanoma. Nat. Commun. 2017;8(1). doi:10.1038/s41467-017-01573-6

131. O'Connell MP, Marchbank K, Webster MR, Valiga AA, Kaur A, Vultur A, Li L, Herlyn M, Villanueva J, Liu Q, et al. Hypoxia induces phenotypic plasticity and therapy resistance in melanoma via the tyrosine kinase receptors ROR1 and ROR2. Cancer Discov. 2013;3(12):1378–

93. doi:10.1158/2159-8290.CD-13-0005

132. García-Jiménez C, Goding CR. Starvation and Pseudo-Starvation as Drivers of Cancer Metastasis through Translation Reprogramming. Cell Metab. 2019;29(2):254–267. doi:10.1016/j.cmet.2018.11.018

133. Landsberg J, Kohlmeyer J, Renn M, Bald T, Rogava M, Cron M, Fatho M, Lennerz V, Wölfel T, Hölzel M, et al. Melanomas resist T-cell therapy through inflammation-induced reversible dedifferentiation. Nature. 2012;490(7420):412–416. doi:10.1038/nature11538

134. Roesch A, Paschen A, Landsberg J, Helfrich I, Becker JC, Schadendorf D. Phenotypic tumour cell plasticity as a resistance mechanism and therapeutic target in melanoma. Eur. J. Cancer. 2016;59:109–112. doi:10.1016/j.ejca.2016.02.023

135. Rambow F, Marine JC, Goding CR. Melanoma plasticity and phenotypic diversity: Therapeutic barriers and opportunities. Genes Dev. 2019;33(19–20):1295–1318. doi:10.1101/gad.329771.119

136. Miller KD, Nogueira L, Mariotto AB, Rowland JH, Yabroff KR, Alfano CM, Jemal A, Kramer JL, Siegel RL. Cancer treatment and survivorship statistics, 2019. CA. Cancer J. Clin. 2019;69(5):363–385. doi:10.3322/caac.21565

137. Serrone L, Zeuli M, Sega FM, Cognetti F. Dacarbazine-based chemotherapy for metastatic melanoma: thirty-year experience overview. J. Exp. Clin. Cancer Res. 2000;19(1):21–34.

138. Soengas MS, Lowe SW. Apoptosis and melanoma chemoresistance. Oncogene. 2003;22(20):3138–3151. doi:10.1038/sj.onc.1206454

139. Davies H, Bignell GR, Cox C, Stephens P, Edkins S, Clegg S, Teague J, Woffendin H, Garnett MJ, Bottomley W, et al. Mutations of the BRAF gene in human cancer. Nature. 2002;417(6892):949–54. doi:10.1038/nature00766

140. Tsai J, Lee JT, Wang W, Zhang J, Cho H, Mamo S, Bremer R, Gillette S, Kong J, Haass NK, et al. Discovery of a selective inhibitor of oncogenic B-Raf kinase with potent antimelanoma activity. Proc. Natl. Acad. Sci. U. S. A. 2008;105(8):3041–6. doi:10.1073/pnas.0711741105

141. Flaherty KT, Yasothan U, Kirkpatrick P. Vemurafenib. Nat. Rev. Drug Discov. 2011;10(11):811–2. doi:10.1038/nrd3579

142. Ballantyne AD, Garnock-Jones KP. Dabrafenib: First global approval. Drugs. 2013;73(12):1367–1376. doi:10.1007/s40265-013-0095-2

143. Chapman PB, Hauschild A, Robert C, Haanen JB, Ascierto P, Larkin J, Dummer R, Garbe C, Testori A, Maio M, et al. Improved Survival with Vemurafenib in Melanoma with BRAF V600E Mutation. N. Engl. J. Med. 2011;364(26):2507–2516. doi:10.1056/nejmoa1103782

144. Hauschild A, Grob JJ, Demidov L V., Jouary T, Gutzmer R, Millward M, Rutkowski P, Blank CU,

Miller WH, Kaempgen E, et al. Dabrafenib in BRAF-mutated metastatic melanoma: A multicentre, open-label, phase 3 randomised controlled trial. Lancet. 2012;380(9839):358–365. doi:10.1016/S0140-6736(12)60868-X

145. Shi H, Hugo W, Kong X, Hong A, Koya RC, Moriceau G, Chodon T, Guo R, Johnson DB, Dahlman KB, et al. Acquired resistance and clonal evolution in melanoma during BRAF inhibitor therapy. Cancer Discov. 2014;4(1):80–93. doi:10.1158/2159-8290.CD-13-0642

146. Eroglu Z, Ribas A. Combination therapy with BRAF and MEK inhibitors for melanoma: Latest evidence and place in therapy. Ther. Adv. Med. Oncol. 2016;8(1):48–56. doi:10.1177/1758834015616934

147. Long G V, Stroyakovskiy D, Gogas H, Levchenko E, de Braud F, Larkin J, Garbe C, Jouary T, Hauschild A, Grob JJ, et al. Combined BRAF and MEK inhibition versus BRAF inhibition alone in melanoma. N. Engl. J. Med. 2014;371(20):1877–88. doi:10.1056/NEJMoa1406037

148. Long G V, Stroyakovskiy D, Gogas H, Levchenko E, de Braud F, Larkin J, Garbe C, Jouary T, Hauschild A, Grob J-J, et al. Dabrafenib and trametinib versus dabrafenib and placebo for Val600 BRAF-mutant melanoma: a multicentre, double-blind, phase 3 randomised controlled trial. Lancet (London, England). 2015;386(9992):444–51. doi:10.1016/S0140-6736(15)60898-4

149. Shirley M. Encorafenib and Binimetinib: First Global Approvals. Drugs. 2018;78(12):1277–1284. doi:10.1007/s40265-018-0963-x

150. Koelblinger P, Thuerigen O, Dummer R. Development of encorafenib for BRAF-mutated advanced melanoma. Curr. Opin. Oncol. 2018;30(2):125–133. doi:10.1097/CCO.0000000000000426

151. Dummer R, Ascierto PA, Gogas HJ, Arance A, Mandala M, Liszkay G, Garbe C, Schadendorf D, Krajsova I, Gutzmer R, et al. Encorafenib plus binimetinib versus vemurafenib or encorafenib in patients with BRAF-mutant melanoma (COLUMBUS): a multicentre, open-label, randomised phase 3 trial. Lancet Oncol. 2018;19(5):603–615. doi:10.1016/S1470-2045(18)30142-6

152. Ascierto PA, Dummer R, Gogas HJ, Flaherty KT, Arance A, Mandala M, Liszkay G, Garbe C, Schadendorf D, Krajsova I, et al. Update on tolerability and overall survival in COLUMBUS: landmark analysis of a randomised phase 3 trial of encorafenib plus binimetinib vs vemurafenib or encorafenib in patients with BRAF V600–mutant melanoma. Eur. J. Cancer. 2020;126:33–44. doi:10.1016/j.ejca.2019.11.016

153. Eddy K, Shah R, Chen S. Decoding Melanoma Development and Progression: Identification of Therapeutic Vulnerabilities. Front. Oncol. 2021;10(February):1–13. doi:10.3389/fonc.2020.626129

154. Kirkwood JM, Strawderman MH, Ernstoff MS, Smith TJ, Borden EC, Blum RH. Interferon alfa-2b adjuvant therapy of high-risk resected cutaneous melanoma: the Eastern Cooperative Oncology

Group Trial EST 1684. J. Clin. Oncol. 1996;14(1):7–17. doi:10.1200/JCO.1996.14.1.7

155. Lugowska I, Teterycz P, Rutkowski P. Immunotherapy of melanoma. Contemp. Oncol. (Poznan, Poland). 2018;22(1A):61–67. doi:10.5114/wo.2018.73889

156. Leonardi GC, Candido S, Falzone L, Spandidos DA, Libra M. Cutaneous melanoma and the immunotherapy revolution (Review). Int. J. Oncol. 2020;57(3):609–618. doi:10.3892/ijo.2020.5088

157. Buchbinder EI, Desai A. CTLA-4 and PD-1 pathways similarities, differences, and implications of their inhibition. Am. J. Clin. Oncol. Cancer Clin. Trials. 2016;39(1):98–106. doi:10.1097/COC.0000000000000239

158. Lee HT, Lee SH, Heo Y-S. Molecular Interactions of Antibody Drugs Targeting PD-1, PD-L1, and CTLA-4 in Immuno-Oncology. Molecules. 2019;24(6). doi:10.3390/molecules24061190

159. Larkin J, Chiarion-Sileni V, Gonzalez R, Grob JJ, Cowey CL, Lao CD, Schadendorf D, Dummer R, Smylie M, Rutkowski P, et al. Combined Nivolumab and Ipilimumab or Monotherapy in Untreated Melanoma. N. Engl. J. Med. 2015;373(1):23–34. doi:10.1056/nejmoa1504030

160. Wolchok JD, Chiarion-Sileni V, Gonzalez R, Rutkowski P, Grob J-J, Cowey CL, Lao CD, Wagstaff J, Schadendorf D, Ferrucci PF, et al. Overall Survival with Combined Nivolumab and Ipilimumab in Advanced Melanoma. N. Engl. J. Med. 2017;377(14):1345–1356. doi:10.1056/nejmoa1709684

161. Larkin J, Chiarion-Sileni V, Gonzalez R, Grob J-J, Rutkowski P, Lao CD, Cowey CL, Schadendorf D, Wagstaff J, Dummer R, et al. Five-Year Survival with Combined Nivolumab and Ipilimumab in Advanced Melanoma. N. Engl. J. Med. 2019;381(16):1535–1546. doi:10.1056/nejmoa1910836

162. Schadendorf D, Wolchok JD, Stephen Hodi F, Chiarion-Sileni V, Gonzalez R, Rutkowski P, Grob JJ, Lance Cowey C, Lao CD, Chesney J, et al. Efficacy and safety outcomes in patients with advanced melanoma who discontinued treatment with nivolumab and ipilimumab because of adverse events: A pooled analysis of randomized phase II and III trials. J. Clin. Oncol. 2017;35(34):3807–3814. doi:10.1200/JCO.2017.73.2289

163. Sharma P, Hu-Lieskovan S, Wargo JA, Ribas A. Primary, Adaptive, and Acquired Resistance to Cancer Immunotherapy. Cell. 2017;168(4):707–723. doi:10.1016/j.cell.2017.01.017

164. Paik J. Nivolumab Plus Relatlimab: First Approval. Drugs. 2022 May 11. doi:10.1007/s40265-022-01723-1

165. Qin S, Xu L, Yi M, Yu S, Wu K, Luo S. Novel immune checkpoint targets: Moving beyond PD-1 and CTLA-4. Mol. Cancer. 2019;18(1):1–14. doi:10.1186/s12943-019-1091-2

166. Hong WX, Haebe S, Lee AS, Benedikt Westphalen C, Norton JA, Jiang W, Levy R. Intratumoral immunotherapy for early-stage solid tumors. Clin. Cancer Res. 2020;26(13):3091–3099.

doi:10.1158/1078-0432.CCR-19-3642

167. De Lombaerde E, De Wever O, De Geest BG. Delivery routes matter: Safety and efficacy of intratumoral immunotherapy. Biochim. Biophys. Acta - Rev. Cancer. 2021;1875(2). doi:10.1016/j.bbcan.2021.188526

168. Loo YM, Gale M. Immune Signaling by RIG-I-like Receptors. Immunity. 2011;34(5):680–692. doi:10.1016/j.immuni.2011.05.003

169. Refolo G, Vescovo T, Piacentini M, Fimia GM, Ciccosanti F. Mitochondrial Interactome: A Focus on Antiviral Signaling Pathways. Front. Cell Dev. Biol. 2020;8(February):1–14. doi:10.3389/fcell.2020.00008

170. Xu L, Wang W, Li Y, Zhou X, Yin Y, Wang Y, de Man RA, van der Laan LJW, Huang F, Kamar N, et al. RIG-I is a key antiviral interferon-stimulated gene against hepatitis E virus regardless of interferon production. Hepatology. 2017;65(6):1823–1839. doi:10.1002/hep.29105

171. Hornung V, Ellegast J, Kim S, Brzózka K, Jung A, Kato H, Poeck H, Akira S, Conzelmann K-K, Schlee M, et al. 5'-Triphosphate RNA is the ligand for RIG-I. Science. 2006;314(5801):994–7. doi:10.1126/science.1132505

172. Besch R, Poeck H, Hohenauer T, Senft D, Häcker G, Berking C, Hornung V, Endres S, Ruzicka T, Rothenfusser S, et al. Proapoptotic signaling induced by RIG-I and MDA-5 results in type I interferon-independent apoptosis in human melanoma cells. J. Clin. Invest. 2009;119(8):2399–2411. doi:10.1172/JCI37155

173. Duewell P, Steger A, Lohr H, Bourhis H, Hoelz H, Kirchleitner S V., Stieg MR, Grassmann S, Kobold S, Siveke JT, et al. RIG-I-like helicases induce immunogenic cell death of pancreatic cancer cells and sensitize tumors toward killing by CD8(+) T cells. Cell Death Differ. 2014;21(12):1825–1837. doi:10.1038/cdd.2014.96

174. Kübler K, Gehrke N, Riemann S, Böhnert V, Zillinger T, Hartmann E, Pölcher M, Rudlowski C, Kuhn W, Hartmann G, et al. Targeted activation of RNA helicase retinoic acid - Inducible gene-I induces proimmunogenic apoptosis of human ovarian cancer cells. Cancer Res. 2010;70(13):5293–5304. doi:10.1158/0008-5472.CAN-10-0825

175. Elion DL, Cook RS. Harnessing RIG-I and intrinsic immunity in the tumor microenvironment for therapeutic cancer treatment. Oncotarget. 2018;9(48):29007–29017. doi:10.18632/oncotarget.25626

176. Poeck H, Bscheider M, Gross O, Finger K, Roth S, Rebsamen M, Hannesschläger N, Schlee M, Rothenfusser S, Barchet W, et al. Recognition of RNA virus by RIG-I results in activation of CARD9 and inflammasome signaling for interleukin 1B production. Nat. Immunol. 2010;11(1):63–69. doi:10.1038/ni.1824

177. Gatti G, Nuñez NG, Nocera DA, Dejager L, Libert C, Giraudo C, Maccioni M. Direct effect of dsRNA mimetics on cancer cells induces endogenous IFN-β production capable of improving dendritic cell function. Eur. J. Immunol. 2013;43(7):1849–1861. doi:10.1002/eji.201242902

178. Heidegger S, Wintges A, Stritzke F, Bek S, Steiger K, Koenig PA, Göttert S, Engleitner T, Öllinger R, Nedelko T, et al. RIG-I activation is critical for responsiveness to checkpoint blockade. Sci. Immunol. 2019;4(39). doi:10.1126/sciimmunol.aau8943

179. Jiang X, Muthusamy V, Fedorova O, Kong Y, Kim DJ, Bosenberg M, Pyle AM, Iwasaki A. Intratumoral delivery of RIG-I agonist SLR14 induces robust antitumor responses. J. Exp. Med. 2019;216(12):2854–2868. doi:10.1084/jem.20190801

180. Daßler-Plenker J, Paschen A, Putschli B, Rattay S, Schmitz S, Goldeck M, Bartok E, Hartmann G, Coch C. Direct RIG-I activation in human NK cells induces TRAIL-dependent cytotoxicity toward autologous melanoma cells. Int. J. Cancer. 2019;144(7):1645–1656. doi:10.1002/ijc.31874

181. Middleton MR, Wermke M, Calvo E, Chartash E, Zhou H, Zhao X, Niewel M, Dobrenkov K, Moreno V. Phase I/II, multicenter, open-label study of intratumoral/intralesional administration of the retinoic acid–inducible gene I (RIG-I) activator MK-4621 in patients with advanced or recurrent tumors. Ann. Oncol. 2018;29(October):viii712. doi:10.1093/annonc/mdy424.016

182. Iurescia S, Fioretti D, Rinaldi M. The innate immune signalling pathways: Turning RIG-I sensor activation against cancer. Cancers (Basel). 2020;12(11):1–26. doi:10.3390/cancers12113158

183. Moreno V, Gaudy-Marqueste C, Wermke M, Italiano A, Romano E, Marabelle A, Connors E, Zhou H, Dobrenkov K, Chartash E, et al. 794 Safety and efficacy results from a phase 1/1b study of intratumoral MK-4621, a retinoic acid-inducible gene I (RIG-I) agonist, plus intravenous pembrolizumab in patients with advanced solid tumors. J. Immunother. Cancer. 2020;8(Suppl 3):A842–A842. doi:10.1136/jitc-2020-SITC2020.0794

184. Doener F, Hong HS, Meyer I, Tadjalli-Mehr K, Daehling A, Heidenreich R, Koch SD, Fotin-Mleczek M, Gnad-Vogt U. RNA-based adjuvant CV8102 enhances the immunogenicity of a licensed rabies vaccine in a first-in-human trial. Vaccine. 2019;37(13):1819–1826. doi:10.1016/j.vaccine.2019.02.024

185. Eigentler T, Krauss J, Schreiber J, Weishaupt C, Terheyden P, Heinzerling L, Mohr P, Weide B, Gutzmer R, Becker JC, et al. Abstract LB-021: Intratumoral RNA-based TLR-7/-8 and RIG-I agonist CV8102 alone and in combination with anti-PD-1 in a Phase I dose-escalation and expansion trial in patients with advanced solid tumors. In: Clinical Research (Excluding Clinical Trials). American Association for Cancer Research; 2019. p. LB-021-LB-021.

186. Ziegler A, Soldner C, Lienenklaus S, Spanier J, Trittel S, Riese P, Kramps T, Weiss S, Heidenreich R, Jasny E, et al. A New RNA-Based Adjuvant Enhances Virus-Specific Vaccine Responses by

Locally Triggering TLR- and RLH-Dependent Effects. J. Immunol. 2017;198(4):1595–1605. doi:10.4049/jimmunol.1601129

187. McGranahan N, Swanton C. Biological and therapeutic impact of intratumor heterogeneity in cancer evolution. Cancer Cell. 2015;27(1):15–26. doi:10.1016/j.ccell.2014.12.001

188. Boumahdi S, de Sauvage FJ. The great escape: tumour cell plasticity in resistance to targeted therapy. Nat. Rev. Drug Discov. 2020;19(1):39–56. doi:10.1038/s41573-019-0044-1

189. Long G V., Fung C, Menzies AM, Pupo GM, Carlino MS, Hyman J, Shahheydari H, Tembe V, Thompson JF, Saw RP, et al. Increased MAPK reactivation in early resistance to dabrafenib/trametinib combination therapy of BRAF-mutant metastatic melanoma. Nat. Commun. 2014;5(1):5694. doi:10.1038/ncomms6694

190. Shi H, Moriceau G, Kong X, Lee MK, Lee H, Koya RC, Ng C, Chodon T, Scolyer RA, Dahlman KB, et al. Melanoma whole-exome sequencing identifies V600E B-RAF amplification-mediated acquired B-RAF inhibitor resistance. Nat. Commun. 2012;3. doi:10.1038/ncomms1727

191. Villanueva J, Infante JR, Krepler C, Reyes-Uribe P, Samanta M, Chen H-Y, Li B, Swoboda RK, Wilson M, Vultur A, et al. Concurrent MEK2 Mutation and BRAF Amplification Confer Resistance to BRAF and MEK Inhibitors in Melanoma. Cell Rep. 2013;4(6):1090–1099. doi:10.1016/j.celrep.2013.08.023

192. Nazarian R, Shi H, Wang Q, Kong X, Koya RC, Lee H, Chen Z, Lee MK, Attar N, Sazegar H, et al. Melanomas acquire resistance to B-RAF(V600E) inhibition by RTK or N-RAS upregulation. Nature. 2010;468(7326):973–977. doi:10.1038/nature09626

193. Wagle N, Emery C, Berger MF, Davis MJ, Sawyer A, Pochanard P, Kehoe SM, Johannessen CM, MacConaill LE, Hahn WC, et al. Dissecting therapeutic resistance to RAF inhibition in melanoma by tumor genomic profiling. J. Clin. Oncol. 2011;29(22):3085–3096. doi:10.1200/JCO.2010.33.2312

194. Whittaker SR, Theurillat JP, Van Allen E, Wagle N, Hsiao J, Cowley GS, Schadendorf D, Root DE, Garraway LA. A genome-Scale RNA interference screen implicates NF1 loss in resistance to RAF inhibition. Cancer Discov. 2013;3(3):351–362. doi:10.1158/2159-8290.CD-12-0470

195. Poulikakos PI, Persaud Y, Janakiraman M, Kong X, Ng C, Moriceau G, Shi H, Atefi M, Titz B, Gabay MT, et al. RAF inhibitor resistance is mediated by dimerization of aberrantly spliced BRAF(V600E). Nature. 2011;480(7377):387–390. doi:10.1038/nature10662

196. Montagut C, Sharma S V., Shioda T, McDermott U, Ulman M, Ulkus LE, Dias-Santagata D, Stubbs H, Lee DY, Singh A, et al. Elevated CRAF as a potential mechanism of acquired resistance to BRAF inhibition in melanoma. Cancer Res. 2008;68(12):4853–4861. doi:10.1158/0008-5472.CAN-07-6787

197. Johannessen CM, Boehm JS, Kim SY, Thomas SR, Wardwell L, Johnson LA, Emery CM, Stransky N, Cogdill AP, Barretina J, et al. COT drives resistance to RAF inhibition through MAP kinase pathway reactivation. Nature. 2010;468(7326):968–972. doi:10.1038/nature09627

198. Paraiso KHT, Xiang Y, Rebecca VW, Abel E V., Chen YA, Munko AC, Wood E, Fedorenko I V., Sondak VK, Anderson ARA, et al. PTEN loss confers BRAF inhibitor resistance to melanoma cells through the suppression of BIM expression. Cancer Res. 2011;71(7):2750–2760. doi:10.1158/0008-5472.CAN-10-2954

199. Konieczkowski DJ, Johannessen CM, Abudayyeh O, Kim JW, Cooper ZA, Piris A, Frederick DT, Barzily-Rokni M, Straussman R, Haq R, et al. A melanoma cell state distinction influences sensitivity to MAPK pathway inhibitors. Cancer Discov. 2014;4(7):816–827. doi:10.1158/2159-8290.CD-13-0424

200. Villanueva J, Vultur A, Lee JT, Somasundaram R, Fukunaga-Kalabis M, Cipolla AK, Wubbenhorst B, Xu X, Gimotty PA, Kee D, et al. Acquired Resistance to BRAF Inhibitors Mediated by a RAF Kinase Switch in Melanoma Can Be Overcome by Cotargeting MEK and IGF-1R/PI3K. Cancer Cell. 2010;18(6):683–695. doi:10.1016/j.ccr.2010.11.023

201. Miller MA, Oudin MJ, Sullivan RJ, Wang SJ, Meyer AS, Im H, Frederick DT, Tadros J, Griffith LG, Lee H, et al. Reduced proteolytic shedding of receptor tyrosine kinases is a post-translational mechanism of kinase inhibitor resistance. Cancer Discov. 2016;6(4):383–399. doi:10.1158/2159-8290.CD-15-0933

202. Roesch A. Tumor heterogeneity and plasticity as elusive drivers for resistance to MAPK pathway inhibition in melanoma. Oncogene. 2015;34(23):2951–2957. doi:10.1038/onc.2014.249

203. Hugo W, Shi H, Sun L, Piva M, Song C, Kong X, Moriceau G, Hong A, Dahlman KB, Johnson DB, et al. Non-genomic and Immune Evolution of Melanoma Acquiring MAPKi Resistance. Cell. 2015;162(6):1271–1285. doi:10.1016/j.cell.2015.07.061

204. Pieper N, Zaremba A, Leonardelli S, Harbers FN, Schwamborn M, Lübcke S, Schrörs B, Baingo J, Schramm A, Haferkamp S, et al. Evolution of melanoma cross-resistance to CD8+ T cells and MAPK inhibition in the course of BRAFi treatment. Oncoimmunology. 2018;7(8):1–9. doi:10.1080/2162402X.2018.1450127

205. Fallahi-Sichani M, Becker V, Izar B, Baker GJ, Lin J, Boswell SA, Shah P, Rotem A, Garraway LA, Sorger PK. Adaptive resistance of melanoma cells to RAF inhibition via reversible induction of a slowly dividing de-differentiated state . Mol. Syst. Biol. 2017;13(1):905. doi:10.15252/msb.20166796

206. Shaffer SM, Dunagin MC, Torborg SR, Torre EA, Emert B, Krepler C, Beqiri M, Sproesser K, Brafford PA, Xiao M, et al. Rare cell variability and drug-induced reprogramming as a mode of

cancer drug resistance. Nature. 2017;546(7658):431–435. doi:10.1038/nature22794

207. Su Y, Wei W, Robert L, Xue M, Tsoi J, Garcia-Diaz A, Homet Moreno B, Kim J, Ng RH, Lee JW, et al. Single-cell analysis resolves the cell state transition and signaling dynamics associated with melanoma drug-induced resistance. Proc. Natl. Acad. Sci. U. S. A. 2017;114(52):13679–13684. doi:10.1073/pnas.1712064115

208. Paschen A, Arens N, Sucker A, Greulich-Bode KM, Fonsatti E, Gloghini A, Striegel S, Schwinn N, Carbone A, Hildenbrand R, et al. The coincidence of chromosome 15 aberrations and β2-microglobulin gene mutations is causative for the total loss of human leukocyte antigen class I expression in melanoma. Clin. Cancer Res. 2006;12(11 I):3297–3305. doi:10.1158/1078-0432.CCR-05-2174

209. Sucker A, Zhao F, Real B, Heeke C, Bielefeld N, Maßen S, Horn S, Moll I, Maltaner R, Horn PA, et al. Genetic evolution of T-cell resistance in the course of melanoma progression. Clin. Cancer Res. 2014;20(24):6593–6604. doi:10.1158/1078-0432.CCR-14-0567

210. Zhao F, Sucker A, Horn S, Heeke C, Bielefeld N, Schrörs B, Bicker A, Lindemann M, Roesch A, Gaudernack G, et al. Melanoma lesions independently acquire t-cell resistance during metastatic latency. Cancer Res. 2016;76(15):4347–4358. doi:10.1158/0008-5472.CAN-16-0008

211. Zaretsky JM, Garcia-Diaz A, Shin DS, Escuin-Ordinas H, Hugo W, Hu-Lieskovan S, Torrejon DY, Abril-Rodriguez G, Sandoval S, Barthly L, et al. Mutations Associated with Acquired Resistance to PD-1 Blockade in Melanoma. N. Engl. J. Med. 2016;375(9):819–829. doi:10.1056/nejmoa1604958

212. Sade-Feldman M, Jiao YJ, Chen JH, Rooney MS, Barzily-Rokni M, Eliane JP, Bjorgaard SL, Hammond MR, Vitzthum H, Blackmon SM, et al. Resistance to checkpoint blockade therapy through inactivation of antigen presentation. Nat. Commun. 2017;8(1). doi:10.1038/s41467-017-01062-w

213. Schrörs B, Lübcke S, Lennerz V, Fatho M, Bicker A, Wölfel C, Derigs P, Hankeln T, Schadendorf D, Paschen A, et al. HLA class I loss in metachronous metastases prevents continuous T cell recognition of mutated neoantigens in a human melanoma model. Oncotarget. 2017;8(17):28312–28327. doi:10.18632/oncotarget.16048

214. Ritter C, Fan K, Paschen A, Reker Hardrup S, Ferrone S, Nghiem P, Ugurel S, Schrama D, Becker JC. Epigenetic priming restores the HLA class-I antigen processing machinery expression in Merkel cell carcinoma. Sci. Rep. 2017;7(1):1–11. doi:10.1038/s41598-017-02608-0

215. Lee JH, Shklovskaya E, Lim SY, Carlino MS, Menzies AM, Stewart A, Pedersen B, Irvine M, Alavi S, Yang JYH, et al. Transcriptional downregulation of MHC class I and melanoma de-differentiation in resistance to PD-1 inhibition. Nat. Commun. 2020;11(1):1–12.

doi:10.1038/s41467-020-15726-7

216. Serrano A, Tanzarella S, Lionello I, Mendez R, Traversari C, Ruiz-Cabello F, Garrido F. Expression of HLA class I antigens and restoration of antigen-specific CTL response in melanoma cells following 5-aza-2′-deoxycytidine treatment. Int. J. Cancer. 2001;94(2):243–251. doi:10.1002/ijc.1452

217. Zingg D, Arenas-Ramirez N, Sahin D, Rosalia RA, Antunes AT, Haeusel J, Sommer L, Boyman O. The Histone Methyltransferase Ezh2 Controls Mechanisms of Adaptive Resistance to Tumor Immunotherapy. Cell Rep. 2017;20(4):854–867. doi:10.1016/j.celrep.2017.07.007

218. Ennishi D, Takata K, Béguelin W, Duns G, Mottok A, Farinha P, Bashashati A, Saberi S, Boyle M, Meissner B, et al. Molecular and genetic characterization of MHC deficiency identifies ezh2 as therapeutic target for enhancing immune recognition. Cancer Discov. 2019;9(4):546–563. doi:10.1158/2159-8290.CD-18-1090

219. Mehta A, Kim YJ, Robert L, Tsoi J, Comin-Anduix B, Berent-Maoz B, Cochran AJ, Economou JS, Tumeh PC, Puig-Saus C, et al. Immunotherapy resistance by inflammation-induced dedifferentiation. Cancer Discov. 2018;8(8):935–943. doi:10.1158/2159-8290.CD-17-1178

220. Kim YJ, Sheu KM, Tsoi J, Abril-Rodriguez G, Medina E, Grasso CS, Torrejon DY, Champhekar AS, Litchfield K, Swanton C, et al. Melanoma dedifferentiation induced by IFN-γ epigenetic remodeling in response to anti–PD-1 therapy. J. Clin. Invest. 2021;131(12). doi:10.1172/jci145859

221. Boshuizen J, Vredevoogd DW, Krijgsman O, Ligtenberg MA, Blankenstein S, de Bruijn B, Frederick DT, Kenski JCN, Parren M, Brüggemann M, et al. Reversal of pre-existing NGFR-driven tumor and immune therapy resistance. Nat. Commun. 2020;11(1):1–13. doi:10.1038/s41467-020-17739-8

222. Hugo W, Zaretsky JM, Sun L, Song C, Moreno BH, Hu-Lieskovan S, Berent-Maoz B, Pang J, Chmielowski B, Cherry G, et al. Genomic and Transcriptomic Features of Response to Anti-PD-1 Therapy in Metastatic Melanoma. Cell. 2016;165(1):35–44. doi:10.1016/j.cell.2016.02.065

223. Shin DS, Zaretsky JM, Escuin-Ordinas H, Garcia-Diaz A, Hu-Lieskovan S, Kalbasi A, Grasso CS, Hugo W, Sandoval S, Torrejon DY, et al. Primary resistance to PD-1 blockade mediated by JAK1/2 mutations. Cancer Discov. 2017;7(2):188–201. doi:10.1158/2159-8290.CD-16-1223

224. Gao J, Shi LZ, Zhao H, Chen J, Xiong L, He Q, Chen T, Roszik J, Bernatchez C, Woodman SE, et al. Loss of IFN-γ Pathway Genes in Tumor Cells as a Mechanism of Resistance to Anti-CTLA-4 Therapy. Cell. 2016;167(2):397-404.e9. doi:10.1016/j.cell.2016.08.069

225. Manguso RT, Pope HW, Zimmer MD, Brown FD, Yates KB, Miller BC, Collins NB, Bi K, La Fleur MW, Juneja VR, et al. In vivo CRISPR screening identifies Ptpn2 as a cancer immunotherapy target. Nature. 2017;547(7664):413–418. doi:10.1038/nature23270

226. Patel SJ, Sanjana NE, Kishton RJ, Eidizadeh A, Vodnala SK, Cam M, Gartner JJ, Jia L, Steinberg SM, Yamamoto TN, et al. Identification of essential genes for cancer immunotherapy. Nature. 2017;548(7669):537–542. doi:10.1038/nature23477

227. Such L, Zhao F, Liu D, Thier B, Khanh Le-Trilling VT, Sucker A, Coch C, Pieper N, Howe S, Bhat H, et al. Targeting the innate immunoreceptor RIG-I overcomes melanoma-intrinsic resistance to T cell immunotherapy. J. Clin. Invest. 2020;140(8):4266–4281. doi:10.1172/JCI131572

228. Kalbasi A, Tariveranmoshabad M, Hakimi K, Kremer S, Campbell KM, Funes JM, Vega-Crespo A, Parisi G, Champekar A, Nguyen C, et al. Uncoupling interferon signaling and antigen presentation to overcome immunotherapy resistance due to JAK1 loss in melanoma. Sci. Transl. Med. 2020;12(565). doi:10.1126/scitranslmed.abb0152

229. Respa A, Bukur J, Ferrone S, Pawelec G, Zhao Y, Wang E, Marincola FM, Seliger B. Association of IFN-γ signal transduction defects with impaired HLA class I antigen processing in melanoma cell lines. Clin. Cancer Res. 2011;17(9):2668–2678. doi:10.1158/1078-0432.CCR-10-2114

230. Liu Z, Guo B, Lopez RD. Expression of intercellular adhesion molecule (ICAM)-1 or ICAM-2 is critical in determining sensitivity of pancreatic cancer cells to cytolysis by human γδ-T cells: Implications in the design of γδ-T- cell-based immunotherapies for pancreatic cancer. J. Gastroenterol. Hepatol. 2009;24(5):900–911. doi:10.1111/j.1440-1746.2008.05668.x

231. Garcia-Lora A, Martinez M, Algarra I, Gaforio JJ, Garrido F. MHC class I-deficient metastatic tumor variants immunoselected by T lymphocytes originate from the coordinated downregulation of APM components. Int. J. Cancer. 2003;106(4):521–527. doi:10.1002/ijc.11241

232. Garcia-Lora A, Algarra I, Gaforio JJ, Ruiz-Cabello F, Garrido F. Immunoselection by T lymphocytes generates repeated MHC class I-deficient metastatic tumor variants. Int. J. Cancer. 2001;91(1):109–119. doi:10.1002/1097-0215(20010101)91:1<109::AID-IJC1017>3.0.CO;2-E

233. Harbst K, Lauss M, Cirenajwis H, Winter C, Howlin J, Törngren T, Kvist A, Nodin B, Olsson E, Häkkinen J, et al. Molecular and genetic diversity in the metastatic process of melanoma. J. Pathol. 2014;233(1):39–50. doi:10.1002/path.4318

234. Hanahan D. Hallmarks of Cancer: New Dimensions. Cancer Discov. 2022;12(1):31–46. doi:10.1158/2159-8290.CD-21-1059

235. Harbers FN, Thier B, Stupia S, Zhu S, Schwamborn M, Peller V, Chauvistré H, Crivello P, Fleischhauer K, Roesch A, et al. Melanoma Differentiation Trajectories Determine Sensitivity toward Pre-Existing CD8+ Tumor-Infiltrating Lymphocytes. J. Invest. Dermatol. 2021;141(10):2480–2489. doi:10.1016/j.jid.2021.03.013

236. Thier B, Zhao F, Stupia S, Brüggemann A, Koch J, Schulze N, Horn S, Coch C, Hartmann G, Sucker A, et al. Innate immune receptor signaling induces transient melanoma dedifferentiation

while preserving immunogenicity. J. Immunother. Cancer. 2022;In press.

237. Smith MP, Brunton H, Rowling EJ, Ferguson J, Arozarena I, Miskolczi Z, Lee JL, Girotti MR, Marais R, Levesque MP, et al. Inhibiting Drivers of Non-mutational Drug Tolerance Is a Salvage Strategy for Targeted Melanoma Therapy. Cancer Cell. 2016;29(3):270–284. doi:10.1016/j.ccell.2016.02.003

238. Riesenberg S, Groetchen A, Siddaway R, Bald T, Reinhardt J, Smorra D, Kohlmeyer J, Renn M, Phung B, Aymans P, et al. MITF and c-Jun antagonism interconnects melanoma dedifferentiation with pro-inflammatory cytokine responsiveness and myeloid cell recruitment. Nat. Commun. 2015;6. doi:10.1038/ncomms9755

239. Engel C, Brügmann G, Lambing S, Mühlenbeck LH, Marx S, Hagen C, Horv D, Goldeck M, Ludwig J, Herzne AM, et al. RIG-I Resists Hypoxia-Induced Immunosuppression and Dedifferentiation. Cancer Immunol. Res. 2017;5(6):455–467. doi:10.1158/2326-6066.CIR-16-0129-T

240. Ohanna M, Cheli Y, Bonet C, Bonazzi VF, Allegra M, Giuliano S, Bille K, Bahadoran P, Giacchero D, Lacour JP, et al. Secretome from senescent melanoma engages the STAT3 pathway to favor reprogramming of naive melanoma towards a tumor-initiating cell phenotype. Oncotarget. 2013;4(12):2212–2224. doi:10.18632/oncotarget.1143

241. Passarelli A, Mannavola F, Stucci LS, Tucci M, Silvestris F. Immune system and melanoma biology: A balance between immunosurveillance and immune escape. Oncotarget. 2017;8(62):106132–106142. doi:10.18632/oncotarget.22190

242. Hazini A, Fisher K, Seymour L. Deregulation of HLA-I in cancer and its central importance for immunotherapy. J. Immunother. Cancer. 2021;9(8):1–17. doi:10.1136/jitc-2021-002899

243. Drew PD, Franzoso G, Becker KG, Bours V, Carlson LM, Siebenlist U, Ozato K. NF kappa B and interferon regulatory factor 1 physically interact and synergistically induce major histocompatibility class I gene expression. J. Interferon Cytokine Res. 1995;15(12):1037–45. doi:10.1089/jir.1995.15.1037

244. Lorenzi S, Forloni M, Cifaldi L, Antonucci C, Citti A, Boldrini R, Pezzullo M, Castellano A, Russo V, van der Bruggen P, et al. IRF1 and NF-kB Restore MHC Class I-Restricted Tumor Antigen Processing and Presentation to Cytotoxic T Cells in Aggressive Neuroblastoma. PLoS One. 2012;7(10):1–8. doi:10.1371/journal.pone.0046928

245. Kalaora S, Nagler A, Wargo JA, Samuels Y. Mechanisms of immune activation and regulation: lessons from melanoma. Nat. Rev. Cancer. 2022;0123456789. doi:10.1038/s41568-022-00442-9

246. Neefjes J, Jongsma MLM, Paul P, Bakke O. Towards a systems understanding of MHC class i and MHC class II antigen presentation. Nat. Rev. Immunol. 2011;11(12):823–836. doi:10.1038/nri3084

247. Bradley SD, Chen Z, Melendez B, Talukder A, Khalili JS, Rodriguez-Cruz T, Liu S, Whittington M, Deng W, Li F, et al. BRAFV600E co-opts a conserved MHC class I internalization pathway to diminish antigen presentation and CD8+ T-cell recognition of melanoma. Cancer Immunol. Res. 2015;3(6):602–609. doi:10.1158/2326-6066.CIR-15-0030

248. Brägelmann J, Lorenz C, Borchmann S, Nishii K, Wegner J, Meder L, Ostendorp J, Ast DF, Heimsoeth A, Nakasuka T, et al. MAPK-pathway inhibition mediates inflammatory reprogramming and sensitizes tumors to targeted activation of innate immunity sensor RIG-I. Nat. Commun. 2021;12(1):1–15. doi:10.1038/s41467-021-25728-8

249. Deken MA, Gadiot J, Jordanova ES, Lacroix R, van Gool M, Kroon P, Pineda C, Geukes Foppen MH, Scolyer R, Song JY, et al. Targeting the MAPK and PI3K pathways in combination with PD1 blockade in melanoma. Oncoimmunology. 2016;5(12):1–12. doi:10.1080/2162402X.2016.1238557

250. Haas L, Elewaut A, Gerard CL, Umkehrer C, Leiendecker L, Pedersen M, Krecioch I, Hoffmann D, Novatchkova M, Kuttke M, et al. Acquired resistance to anti-MAPK targeted therapy confers an immune-evasive tumor microenvironment and cross-resistance to immunotherapy in melanoma. Nat. Cancer. 2021;2(7):693–708. doi:10.1038/s43018-021-00221-9

251. Sottile R, Pangigadde PN, Tan T, Anichini A, Sabbatino F, Trecroci F, Favoino E, Orgiano L, Roberts J, Ferrone S, et al. HLA class I downregulation is associated with enhanced NK-cell killing of melanoma cells with acquired drug resistance to BRAF inhibitors. Eur. J. Immunol. 2016;46(2):409–419. doi:10.1002/eji.201445289

252. Kawakami Y, Dang N, Wang X, Tupesis J, Robbins PF, Wang RF, Wunderlich JR, Yannelli JR, Rosenberg SA. Recognition of shared melanoma antigens in association with major HLA-A alleles by tumor infiltrating T lymphocytes from 123 patients with melanoma. J. Immunother. 2000;23(1):17–27. doi:10.1097/00002371-200001000-00004

253. Elion DL, Jacobson ME, Hicks DJ, Rahman B, Sanchez V, Gonzales-Ericsson PI, Fedorova O, Pyle AM, Wilson JT, Cook RS. Therapeutically active RIG-I agonist induces immunogenic tumor cell killing in breast cancers. Cancer Res. 2018;78(21):6183–6195. doi:10.1158/0008-5472.CAN-18-0730

254. Glas M, Coch C, Trageser D, Daßler J, Simon M, Koch P, Mertens J, Quandel T, Gorris R, Reinartz R, et al. Targeting the cytosolic innate immune receptors RIG-I and MDA5 effectively counteracts cancer cell heterogeneity in glioblastoma. Stem Cells. 2013;31(6):1064–1074. doi:10.1002/stem.1350

255. Liu BL, Robinson M, Han Z-Q, Branston RH, English C, Reay P, McGrath Y, Thomas SK, Thornton M, Bullock P, et al. ICP34.5 deleted herpes simplex virus with enhanced oncolytic, immune stimulating, and anti-tumour properties. Gene Ther. 2003;10(4):292–303.

doi:10.1038/sj.gt.3301885

256. Malvehy J, Samoylenko I, Schadendorf D, Gutzmer R, Grob JJ, Sacco JJ, Gorski KS, Anderson A, Pickett CA, Liu K, et al. Talimogene laherparepvec upregulates immune-cell populations in non-injected lesions: Findings from a phase II, multicenter, open-label study in patients with stage IIIB-IVM1c melanoma. J. Immunother. Cancer. 2021;9(3):1–14. doi:10.1136/jitc-2020-001621

257. Ribas A, Dummer R, Puzanov I, VanderWalde A, Andtbacka RHI, Michielin O, Olszanski AJ, Malvehy J, Cebon J, Fernandez E, et al. Oncolytic Virotherapy Promotes Intratumoral T Cell Infiltration and Improves Anti-PD-1 Immunotherapy. Cell. 2017;170(6):1109-1119.e10. doi:10.1016/j.cell.2017.08.027

258. Torrejon DY, Abril-Rodriguez G, Champhekar AS, Tsoi J, Campbell KM, Kalbasi A, Parisi G, Zaretsky JM, Garcia-Diaz A, Puig-Saus C, et al. Overcoming Genetically Based Resistance Mechanisms to PD-1 Blockade. Cancer Discov. 2020;10(8):1140–1157. doi:10.1158/2159-8290.CD-19-1409

259. Poeck H, Wintges A, Dahl S, Bassermann F, Haas T, Heidegger S. Tumor cell-intrinsic RIG-I signaling governs synergistic effects of immunogenic cancer therapies and checkpoint inhibitors in mice. Eur. J. Immunol. 2021:1–4. doi:10.1002/eji.202049158

260. Ranoa DRE, Parekh AD, Pitroda SP, Huang X, Darga T, Wong AC, Huang L, Andrade J, Staley JP, Satoh T, et al. Cancer therapies activate RIG-I-like receptor pathway through endogenous non-coding RNAs. Oncotarget. 2016;7(18):26496–26515. doi:10.18632/oncotarget.8420

261. Massi D, Mihic-Probst D, Schadendorf D, Dummer R, Mandalà M. Dedifferentiated melanomas: Morpho-phenotypic profile, genetic reprogramming and clinical implications. Cancer Treat. Rev. 2020;88(April). doi:10.1016/j.ctrv.2020.102060

262. Bai X, Flaherty KT. Targeted and immunotherapies in BRAF mutant melanoma: where we stand and what to expect. Br. J. Dermatol. 2021;185(2):253–262. doi:10.1111/bjd.19394

263. Frederick DT, Piris A, Cogdill AP, Cooper ZA, Lezcano C, Ferrone CR, Mitra D, Boni A, Newton LP, Liu C, et al. BRAF inhibition is associated with enhanced melanoma antigen expression and a more favorable tumor microenvironment in patients with metastatic melanoma. Clin. Cancer Res. 2013;19(5):1225–1231. doi:10.1158/1078-0432.CCR-12-1630

264. Larkin J, Ascierto PA, Dréno B, Atkinson V, Liszkay G, Maio M, Mandalà M, Demidov L, Stroyakovskiy D, Thomas L, et al. Combined Vemurafenib and Cobimetinib in BRAF -Mutated Melanoma . N. Engl. J. Med. 2014;371(20):1867–1876. doi:10.1056/nejmoa1408868

265. Moriceau G, Hugo W, Hong A, Shi H, Kong X, Yu CC, Koya RC, Samatar AA, Khanlou N, Braun J, et al. Tunable-Combinatorial Mechanisms of Acquired Resistance Limit the Efficacy of BRAF/MEK Cotargeting but Result in Melanoma Drug Addiction. Cancer Cell. 2015;27(2):240–

256. doi:10.1016/j.ccell.2014.11.018

266. Hong A, Moriceau G, Sun L, Lomeli S, Piva M, Damoiseaux R, Holmen SL, Sharpless NE, Hugo W, Lo RS. Exploiting drug addiction mechanisms to select against mapki-resistant melanoma. Cancer Discov. 2018;8(1):74–93. doi:10.1158/2159-8290.CD-17-0682

267. Algazi AP, Othus M, Daud AI, Lo RS, Mehnert JM, Truong TG, Conry R, Kendra K, Doolittle GC, Clark JI, et al. Continuous versus intermittent BRAF and MEK inhibition in patients with BRAF-mutated melanoma: a randomized phase 2 trial. Nat. Med. 2020;26(10):1564–1568. doi:10.1038/s41591-020-1060-8

268. Gutzmer R, Stroyakovskiy D, Gogas H, Robert C, Lewis K, Protsenko S, Pereira RP, Eigentler T, Rutkowski P, Demidov L, et al. Atezolizumab, vemurafenib, and cobimetinib as first-line treatment for unresectable advanced BRAFV600 mutation-positive melanoma (IMspire150): primary analysis of the randomised, double-blind, placebo-controlled, phase 3 trial. Lancet (London, England). 2020;395(10240):1835–1844. doi:10.1016/S0140-6736(20)30934-X

269. Ribas A, Lawrence D, Atkinson V, Agarwal S, Miller WH, Carlino MS, Fisher R, Long G V., Hodi FS, Tsoi J, et al. Combined BRAF and MEK inhibition with PD-1 blockade immunotherapy in BRAF-mutant melanoma. Nat. Med. 2019;25(6):936–940. doi:10.1038/s41591-019-0476-5

270. Ascierto PA, Ferrucci PF, Fisher R, Del Vecchio M, Atkinson V, Schmidt H, Schachter J, Queirolo P, Long G V., Di Giacomo AM, et al. Dabrafenib, trametinib and pembrolizumab or placebo in BRAF-mutant melanoma. Nat. Med. 2019;25(6):941–946. doi:10.1038/s41591-019-0448-9

271. Wang Y, Liu S, Yang Z, Algazi AP, Lomeli SH, Wang Y, Othus M, Hong A, Wang X, Randolph CE, et al. Anti-PD-1/L1 lead-in before MAPK inhibitor combination maximizes antitumor immunity and efficacy. Cancer Cell. 2021:1–13. doi:10.1016/j.ccell.2021.07.023

272. Boyer M, Cayrefourcq L, Dereure O, Meunier L, Becquart O, Alix-Panabières C. Clinical relevance of liquid biopsy in melanoma and merkel cell carcinoma. Cancers (Basel). 2020;12(4):1–25. doi:10.3390/cancers12040960

10 List of Figures

11 List of Abbreviations

3pRNA	5‘Triphosphate double-stranded RNA
ACT	Adoptive T-cell transfer
AIDS	Acquired immune deficiency syndrome
AKT (PKB)	Protein kinase B
APCs	Antigen-presenting cells
APM	Antigen processing and presentation machinery
ATPase	Adenosintriphosphatase
BCL2	B-cell lymphoma 2
BIM	B-cell lymphoma 2 interacting mediator of cell death
BiP	Binding of immunoglobulin protein
BRAF	v-Raf murine sarcoma viral oncogene homolog B
BRAFi	BRAF inhibitor
CAM	Chicken chorioallantoic membrane
CARD	Caspase activation and recruitment domain
Cardif	Caspase activation recruitment domain adaptor inducing interferon-beta
CCL5	Chemokine (C-C motif) ligand 5
CD28/40/271	Cluster of differentiation 28/40/271
CDK2/4	Cyclin-dependent kinase 2/4
c-Met	Mesenchymal-epithelial transition factor
COT/ MAP3K8	Mitogen-activated protein kinase kinase kinase 8
CTC	Circulating tumor cells
ctDNA	Cell-free tumor DNA

CTLA-4	Cytotoxic T lymphocyte antigen-4
CXCL10	C-X-C motif chemokine ligand 10
DAMPs	Damage-associated molecular patterns
Dia1	Diaphanous-related formin 1
DNA	Deoxyribonucleic acid
ds	Double-stranded
EGFR	Epithelial growth factor receptor
EMA	European Medicine Agency
ER	Endoplasmic reticulum
ERAP1/2	ER-resident aminopeptidase ½
ERK	Extracellular-signal regulated kinases
EZH2	Enhancer of zeste homolog 2
FADD	Fas-associated death domain
FasL	Fas ligand
FDA	Food and Drug Administration
GM-CSF	Granulocyte-macrophage colony-stimulating factor
gp100	Glycoprotein 100
HLA-I	Human leukocyte antigen class I
HSV-1	Herpes simplex virus-1
ICAM-1	Intercellular Adhesion Molecule 1
ICB	Immune checkpoint blockade
IDO1	Indoleamine 2,3-dioxygenase
IFNAR1/2	Interferon-alpha/beta receptor
IFNGR1/2	Interferon-gamma receptor
IFN-I/-II	Type I/II interferon
IFN-α/-γ	Interferon-alpha/-gamma
IGF-1R	Insulin growth factor-1 receptor
IL	Interleukin
IPS-1	Interferon-beta promoter stimulator I
IRF1/3/7	Interferon-regulatory factor 1/3/7
ISGs	Interferon-stimulated genes

ITIM	Immunoreceptor tyrosine-based inhibitory motif
JAK	Janus kinase
LAG-3	Lymphocyte activation gene-3
LGP2	Laboratory of genetics and physiology 2
LMP2/7	Large multifunctional peptidase 2/7
MAGE	Melanoma-associated antigen gene
MAPK	Mitogen-activated protein kinase
MAPKi	Mitogen-activated protein kinase inhibitor
MART-1	Melanoma-associated antigen recognized by T cells
MAVS	Mitochondrial antiviral signaling protein
MDA5	Melanoma differentiation-associated factor 5
MECL-1	Multicatalytic endopeptidase complex-like 1
MEK	Mitogen-activated protein kinase kinase
MEKi	MEK inhibitor
MHC-I	Major histocompatibility complex class I
MITF	Microphthalmia-associated transcription factor
mRNA	Messenger ribonucleic acid
mTOR	Mammalian target of rapamycin
NF1	Neurofibromatosis type
NFκB	Nuclear factor 'kappa-light-chain-enhancer' of activated B-cells
NGFR	Neural growth factor receptor
NK cells	Natural killer cells
NRAS	Neuroblastoma RAS viral oncogene homolog
NY-ESO-1	New York esophageal squamous cell carcinoma-1
$p27^{Kip}$/CDKN1B	Cyclin-dependent kinase inhibitor 1B
PA28	Proteasome activator 28
PAMPs	Pathogen-associated molecular patterns
PD-1	Programmed cell death-1
PDGFRβ	Platelet-derived growth factor receptors
PD-L1/2	Programmed cell death ligand ½
PI3K	Phosphoinositide 3-kinases

PLC	Protein loading complex
PRR	Pattern recognition receptor
PSMB8/9	Proteosome subunit beta 8/9
PTEN	Phosphatase and Tensin homolog
RAS	Rat sarcoma
RIG-I	Retinoid acid-inducible gene I
RLR	RIG-I-like receptor
RNA	Ribonucleic acid
RTK	Receptor tyrosine kinase
RXR-γ	Retinoid X receptor-gamma
STAT	Signal transducer and activator of transcription
T cells	T lymphocytes
TAP1/2	Transporter associated with antigen processing
TAPBP	TAP-binding protein
TCR	T-cell receptor
TIGIT	T cell immunoglobulin and ITIM domain
TILs	Tumor-infiltrating lymphocytes
TIM-3	T cell immunoglobulin and mucin-domain containing-3
TLR	Toll-like receptor
TNF-α	Tumor necrosis factor-alpha
TRAF	Tumor necrosis factor receptor-associated factor
TRP1/2	Tyrosinase-related protein ½
T-VEC	Talimogen laherparepvec
TYK2	Tyrosine kinase 2
UV	Ultraviolet
VISA	Virus induced signaling adaptor
β2m	Beta-2-microglobulin

12 Licenses

12.1 License for Article I

CCC Marketplace™

This is a License Agreement between Beatrice Thier, University Duisburg-Essen ("You") and American Society for Clinical Investigation ("Publisher") provided by Copyright Clearance Center ("CCC"). The license consists of your order details, the terms and conditions provided by American Society for Clinical Investigation, and the CCC terms and conditions.

All payments must be made in full to CCC.

Order Date	21-May-2021	**Type of Use**	Republish in a thesis/dissertation
Order License ID	1120680-1		
ISSN	0021-9738	**Publisher**	AMERICAN SOCIETY FOR CLINICAL INVESTIGATION
		Portion	Chapter/article

LICENSED CONTENT

Publication Title	The journal of clinical investigation	**Country**	United States of America
		Rightsholder	American Society for Clinical Investigation
Author/Editor	AMERICAN SOCIETY FOR CLINICAL INVESTIGATION., Robinson, George Canby	**Publication Type**	Journal
Date	01/01/1924		
Language	English		

REQUEST DETAILS

Portion Type	Chapter/article	**Rights Requested**	Main product, any product related to main product, and other compilations/derivative products
Page range(s)	4266-4281		
Total number of pages	17		
Format (select all that apply)	Print, Electronic	**Distribution**	Worldwide
Who will republish the content?	Academic institution	**Translation**	Original language of publication
Duration of Use	Life of current and all future editions	**Copies for the disabled?**	Yes
		Minor editing privileges?	No
Lifetime Unit Quantity	More than 2,000,000	**Incidental promotional use?**	Yes
		Currency	EUR

NEW WORK DETAILS

Title	NA	**Institution name**	University Duisburg-Essen
Instructor name	Beatrice Thier	**Expected presentation date**	2022-01-31

ADDITIONAL DETAILS

Order reference number	N/A

The requesting person / organization to appear on the license	Beatrice Thier, University Duisburg-Essen

REUSE CONTENT DETAILS

Title, description or numeric reference of the portion(s)	doi.org/10.1172/JCI131572	**Title of the article/chapter the portion is from**	Targeting the innate immunoreceptor RIG-I overcomes melanoma-intrinsic resistance to T cell immunotherapy
Editor of portion(s)	NA	**Author of portion(s)**	AMERICAN SOCIETY FOR CLINICAL INVESTIGATION.; Robinson, George Canby
Volume of serial or monograph	NA	**Issue, if republishing an article from a serial**	N/A
Page or page range of portion	whole PDF file	**Publication date of portion**	2020-05-19

CCC Terms and Conditions

1. Description of Service; Defined Terms. This Republication License enables the User to obtain licenses for republication of one or more copyrighted works as described in detail on the relevant Order Confirmation (the "Work(s)"). Copyright Clearance Center, Inc. ("CCC") grants licenses through the Service on behalf of the rightsholder identified on the Order Confirmation (the "Rightsholder"). "Republication", as used herein, generally means the inclusion of a Work, in whole or in part, in a new work or works, also as described on the Order Confirmation. "User", as used herein, means the person or entity making such republication.

2. The terms set forth in the relevant Order Confirmation, and any terms set by the Rightsholder with respect to a particular Work, govern the terms of use of Works in connection with the Service. By using the Service, the person transacting for a republication license on behalf of the User represents and warrants that he/she/it (a) has been duly authorized by the User to accept, and hereby does accept, all such terms and conditions on behalf of User, and (b) shall inform User of all such terms and conditions. In the event such person is a "freelancer" or other third party independent of User and CCC, such party shall be deemed jointly a "User" for purposes of these terms and conditions. In any event, User shall be deemed to have accepted and agreed to all such terms and conditions if User republishes the Work in any fashion.

3. Scope of License; Limitations and Obligations.

   3.1. All Works and all rights therein, including copyright rights, remain the sole and exclusive property of the Rightsholder. The license created by the exchange of an Order Confirmation (and/or any invoice) and payment by User of the full amount set forth on that document includes only those rights expressly set forth in the Order Confirmation and in these terms and conditions, and conveys no other rights in the Work(s) to User. All rights not expressly granted are hereby reserved.

   3.2. General Payment Terms: You may pay by credit card or through an account with us payable at the end of the month. If you and we agree that you may establish a standing account with CCC, then the following terms apply: Remit Payment to: Copyright Clearance Center, 29118 Network Place, Chicago, IL 60673-1291. Payments Due: Invoices are payable upon their delivery to you (or upon our notice to you that they are available to you for downloading). After 30 days, outstanding amounts will be subject to a service charge of 1-1/2% per month or, if less, the maximum rate allowed by applicable law. Unless otherwise specifically set forth in the Order Confirmation or in a separate written agreement signed by CCC, invoices are due and payable on "net 30" terms. While User may exercise the rights licensed immediately upon issuance of the Order Confirmation, the license is automatically revoked and is null and void, as if it had never been

issued, if complete payment for the license is not received on a timely basis either from User directly or through a payment agent, such as a credit card company.

3.3. Unless otherwise provided in the Order Confirmation, any grant of rights to User (i) is "one-time" (including the editions and product family specified in the license), (ii) is non-exclusive and non-transferable and (iii) is subject to any and all limitations and restrictions (such as, but not limited to, limitations on duration of use or circulation) included in the Order Confirmation or invoice and/or in these terms and conditions. Upon completion of the licensed use, User shall either secure a new permission for further use of the Work(s) or immediately cease any new use of the Work(s) and shall render inaccessible (such as by deleting or by removing or severing links or other locators) any further copies of the Work (except for copies printed on paper in accordance with this license and still in User's stock at the end of such period).

3.4. In the event that the material for which a republication license is sought includes third party materials (such as photographs, illustrations, graphs, inserts and similar materials) which are identified in such material as having been used by permission, User is responsible for identifying, and seeking separate licenses (under this Service or otherwise) for, any of such third party materials; without a separate license, such third party materials may not be used.

3.5. Use of proper copyright notice for a Work is required as a condition of any license granted under the Service. Unless otherwise provided in the Order Confirmation, a proper copyright notice will read substantially as follows: "Republished with permission of [Rightsholder's name], from [Work's title, author, volume, edition number and year of copyright]; permission conveyed through Copyright Clearance Center, Inc. " Such notice must be provided in a reasonably legible font size and must be placed either immediately adjacent to the Work as used (for example, as part of a by-line or footnote but not as a separate electronic link) or in the place where substantially all other credits or notices for the new work containing the republished Work are located. Failure to include the required notice results in loss to the Rightsholder and CCC, and the User shall be liable to pay liquidated damages for each such failure equal to twice the use fee specified in the Order Confirmation, in addition to the use fee itself and any other fees and charges specified.

3.6. User may only make alterations to the Work if and as expressly set forth in the Order Confirmation. No Work may be used in any way that is defamatory, violates the rights of third parties (including such third parties' rights of copyright, privacy, publicity, or other tangible or intangible property), or is otherwise illegal, sexually explicit or obscene. In addition, User may not conjoin a Work with any other material that may result in damage to the reputation of the Rightsholder. User agrees to inform CCC if it becomes aware of any infringement of any rights in a Work and to cooperate with any reasonable request of CCC or the Rightsholder in connection therewith.

4. Indemnity. User hereby indemnifies and agrees to defend the Rightsholder and CCC, and their respective employees and directors, against all claims, liability, damages, costs and expenses, including legal fees and expenses, arising out of any use of a Work beyond the scope of the rights granted herein, or any use of a Work which has been altered in any unauthorized way by User, including claims of defamation or infringement of rights of copyright, publicity, privacy or other tangible or intangible property.

5. Limitation of Liability. UNDER NO CIRCUMSTANCES WILL CCC OR THE RIGHTSHOLDER BE LIABLE FOR ANY DIRECT, INDIRECT, CONSEQUENTIAL OR INCIDENTAL DAMAGES (INCLUDING WITHOUT LIMITATION DAMAGES FOR LOSS OF BUSINESS PROFITS OR INFORMATION, OR FOR BUSINESS INTERRUPTION) ARISING OUT OF THE USE OR INABILITY TO USE A WORK, EVEN IF ONE OF THEM HAS BEEN ADVISED OF THE POSSIBILITY OF SUCH DAMAGES. In any event, the total liability of the Rightsholder and CCC (including their respective employees and directors) shall not exceed the total amount actually paid by User for this license. User assumes full liability for the actions and omissions of its principals, employees, agents, affiliates, successors and assigns.

6. Limited Warranties. THE WORK(S) AND RIGHT(S) ARE PROVIDED "AS IS". CCC HAS THE RIGHT TO GRANT TO USER THE RIGHTS GRANTED IN THE ORDER CONFIRMATION DOCUMENT. CCC AND THE RIGHTSHOLDER DISCLAIM ALL OTHER WARRANTIES RELATING TO THE WORK(S) AND RIGHT(S), EITHER EXPRESS OR IMPLIED, INCLUDING

WITHOUT LIMITATION IMPLIED WARRANTIES OF MERCHANTABILITY OR FITNESS FOR A PARTICULAR PURPOSE. ADDITIONAL RIGHTS MAY BE REQUIRED TO USE ILLUSTRATIONS, GRAPHS, PHOTOGRAPHS, ABSTRACTS, INSERTS OR OTHER PORTIONS OF THE WORK (AS OPPOSED TO THE ENTIRE WORK) IN A MANNER CONTEMPLATED BY USER; USER UNDERSTANDS AND AGREES THAT NEITHER CCC NOR THE RIGHTSHOLDER MAY HAVE SUCH ADDITIONAL RIGHTS TO GRANT.

7. Effect of Breach. Any failure by User to pay any amount when due, or any use by User of a Work beyond the scope of the license set forth in the Order Confirmation and/or these terms and conditions, shall be a material breach of the license created by the Order Confirmation and these terms and conditions. Any breach not cured within 30 days of written notice thereof shall result in immediate termination of such license without further notice. Any unauthorized (but licensable) use of a Work that is terminated immediately upon notice thereof may be liquidated by payment of the Rightsholder's ordinary license price therefor; any unauthorized (and unlicensable) use that is not terminated immediately for any reason (including, for example, because materials containing the Work cannot reasonably be recalled) will be subject to all remedies available at law or in equity, but in no event to a payment of less than three times the Rightsholder's ordinary license price for the most closely analogous licensable use plus Rightsholder's and/or CCC's costs and expenses incurred in collecting such payment.

8. Miscellaneous.

   8.1. User acknowledges that CCC may, from time to time, make changes or additions to the Service or to these terms and conditions, and CCC reserves the right to send notice to the User by electronic mail or otherwise for the purposes of notifying User of such changes or additions; provided that any such changes or additions shall not apply to permissions already secured and paid for.

   8.2. Use of User-related information collected through the Service is governed by CCC's privacy policy, available online here:https://marketplace.copyright.com/rs-ui-web/mp/privacy-policy

   8.3. The licensing transaction described in the Order Confirmation is personal to User. Therefore, User may not assign or transfer to any other person (whether a natural person or an organization of any kind) the license created by the Order Confirmation and these terms and conditions or any rights granted hereunder; provided, however, that User may assign such license in its entirety on written notice to CCC in the event of a transfer of all or substantially all of User's rights in the new material which includes the Work(s) licensed under this Service.

   8.4. No amendment or waiver of any terms is binding unless set forth in writing and signed by the parties. The Rightsholder and CCC hereby object to any terms contained in any writing prepared by the User or its principals, employees, agents or affiliates and purporting to govern or otherwise relate to the licensing transaction described in the Order Confirmation, which terms are in any way inconsistent with any terms set forth in the Order Confirmation and/or in these terms and conditions or CCC's standard operating procedures, whether such writing is prepared prior to, simultaneously with or subsequent to the Order Confirmation, and whether such writing appears on a copy of the Order Confirmation or in a separate instrument.

   8.5. The licensing transaction described in the Order Confirmation document shall be governed by and construed under the law of the State of New York, USA, without regard to the principles thereof of conflicts of law. Any case, controversy, suit, action, or proceeding arising out of, in connection with, or related to such licensing transaction shall be brought, at CCC's sole discretion, in any federal or state court located in the County of New York, State of New York, USA, or in any federal or state court whose geographical jurisdiction covers the location of the Rightsholder set forth in the Order Confirmation. The parties expressly submit to the personal jurisdiction and venue of each such federal or state court.If you have any comments or questions about the Service or Copyright Clearance Center, please contact us at 978-750-8400 or send an e-mail to support@copyright.com.

v 1.1

12.2 License for Article II

CCC Marketplace™

This is a License Agreement between Beatrice Thier, University Duisburg-Essen ("You") and Elsevier Science & Technology Journals ("Publisher") provided by Copyright Clearance Center ("CCC"). The license consists of your order details, the terms and conditions provided by Elsevier Science & Technology Journals, and the CCC terms and conditions.

All payments must be made in full to CCC.

Order Date	28-May-2021	**Type of Use**	Republish in a thesis/dissertation
Order License ID	1122261-1		
ISSN	0022-202X	**Publisher**	BLACKWELL PUBLISHING, INC.
		Portion	Chapter/article

LICENSED CONTENT

Publication Title	The Journal of investigative dermatology	**Language**	English
		Country	United States of America
Article Title	Melanoma differentiation trajectories determine sensitivity towards pre-existing CD8+ tumor-infiltrating lymphocytes	**Rightsholder**	Elsevier Science & Technology Journals
		Publication Type	Journal
Author/Editor	SOCIETY FOR INVESTIGATIVE DERMATOLOGY., EUROPEAN SOCIETY FOR DERMATOLOGICAL RESEARCH., Sulzberger, Marion B.		
Date	01/01/1938		

REQUEST DETAILS

Portion Type	Chapter/article	**Rights Requested**	Main product, any product related to main product, and other compilations/derivative products
Page range(s)	NA		
Total number of pages	50		
Format (select all that apply)	Print, Electronic	**Distribution**	Worldwide
Who will republish the content?	Academic institution	**Translation**	Original language of publication
Duration of Use	Life of current edition	**Copies for the disabled?**	Yes
Lifetime Unit Quantity	More than 2,000,000	**Minor editing privileges?**	No
		Incidental promotional use?	Yes
		Currency	EUR

NEW WORK DETAILS

Title	NA	**Institution name**	University Duisburg-Essen

Instructor name	Beatrice Thier	**Expected presentation date**	2022-01-31

ADDITIONAL DETAILS

Order reference number	N/A	**The requesting person / organization to appear on the license**	Beatrice Thier, University Duisburg-Essen

REUSE CONTENT DETAILS

Title, description or numeric reference of the portion(s)	doi.org/10.1016/j.jid.2021.03.013	**Title of the article/chapter the portion is from**	Melanoma differentiation trajectories determine sensitivity towards pre-existing CD8+ tumor-infiltrating lymphocytes
Editor of portion(s)	NA		
Volume of serial or monograph	NA	**Author of portion(s)**	Harbers, F.N.; Thier, B.; Stupia, S.; Zhu, S.; Schwamborn, M.; Peller, V.; Chauvistré, H.; Crivello, P.; Fleischhauer, K.; Roesch, A.; Sucker, A.; Schadendorf, D.; Chen, Y.; Paschen, A.; Zhao, F.
Page or page range of portion	NA		
		Issue, if republishing an article from a serial	N/A
		Publication date of portion	2021-03-30

RIGHTSHOLDER TERMS AND CONDITIONS

Elsevier publishes Open Access articles in both its Open Access journals and via its Open Access articles option in subscription journals, for which an author selects a user license permitting certain types of reuse without permission. Before proceeding please check if the article is Open Access on http://www.sciencedirect.com and refer to the user license for the individual article. Any reuse not included in the user license terms will require permission. You must always fully and appropriately credit the author and source. If any part of the material to be used (for example, figures) has appeared in the Elsevier publication for which you are seeking permission, with credit or acknowledgement to another source it is the responsibility of the user to ensure their reuse complies with the terms and conditions determined by the rights holder. Please contact permissions@elsevier.com with any queries.

SPECIAL RIGHTSHOLDER TERMS AND CONDITIONS

Permission is allowed to use the material in Thesis which can be published on DuEPublico of the Univeristy Duisburg-Essen

CCC Terms and Conditions

1. Description of Service; Defined Terms. This Republication License enables the User to obtain licenses for republication of one or more copyrighted works as described in detail on the relevant Order Confirmation (the "Work(s)"). Copyright Clearance Center, Inc. ("CCC") grants licenses through the Service on behalf of the rightsholder identified on the Order Confirmation (the "Rightsholder"). "Republication", as used herein, generally means the inclusion of a Work, in whole or in part, in a new work or works, also as described on the Order Confirmation. "User", as used herein, means the person or entity making such republication.

2. The terms set forth in the relevant Order Confirmation, and any terms set by the Rightsholder with respect to a particular Work, govern the terms of use of Works in connection with the Service. By using the Service, the person

transacting for a republication license on behalf of the User represents and warrants that he/she/it (a) has been duly authorized by the User to accept, and hereby does accept, all such terms and conditions on behalf of User, and (b) shall inform User of all such terms and conditions. In the event such person is a "freelancer" or other third party independent of User and CCC, such party shall be deemed jointly a "User" for purposes of these terms and conditions. In any event, User shall be deemed to have accepted and agreed to all such terms and conditions if User republishes the Work in any fashion.

3. Scope of License; Limitations and Obligations.

3.1. All Works and all rights therein, including copyright rights, remain the sole and exclusive property of the Rightsholder. The license created by the exchange of an Order Confirmation (and/or any invoice) and payment by User of the full amount set forth on that document includes only those rights expressly set forth in the Order Confirmation and in these terms and conditions, and conveys no other rights in the Work(s) to User. All rights not expressly granted are hereby reserved.

3.2. General Payment Terms: You may pay by credit card or through an account with us payable at the end of the month. If you and we agree that you may establish a standing account with CCC, then the following terms apply: Remit Payment to: Copyright Clearance Center, 29118 Network Place, Chicago, IL 60673-1291. Payments Due: Invoices are payable upon their delivery to you (or upon our notice to you that they are available to you for downloading). After 30 days, outstanding amounts will be subject to a service charge of 1-1/2% per month or, if less, the maximum rate allowed by applicable law. Unless otherwise specifically set forth in the Order Confirmation or in a separate written agreement signed by CCC, invoices are due and payable on "net 30" terms. While User may exercise the rights licensed immediately upon issuance of the Order Confirmation, the license is automatically revoked and is null and void, as if it had never been issued, if complete payment for the license is not received on a timely basis either from User directly or through a payment agent, such as a credit card company.

3.3. Unless otherwise provided in the Order Confirmation, any grant of rights to User (i) is "one-time" (including the editions and product family specified in the license), (ii) is non-exclusive and non-transferable and (iii) is subject to any and all limitations and restrictions (such as, but not limited to, limitations on duration of use or circulation) included in the Order Confirmation or invoice and/or in these terms and conditions. Upon completion of the licensed use, User shall either secure a new permission for further use of the Work(s) or immediately cease any new use of the Work(s) and shall render inaccessible (such as by deleting or by removing or severing links or other locators) any further copies of the Work (except for copies printed on paper in accordance with this license and still in User's stock at the end of such period).

3.4. In the event that the material for which a republication license is sought includes third party materials (such as photographs, illustrations, graphs, inserts and similar materials) which are identified in such material as having been used by permission, User is responsible for identifying, and seeking separate licenses (under this Service or otherwise) for, any of such third party materials; without a separate license, such third party materials may not be used.

3.5. Use of proper copyright notice for a Work is required as a condition of any license granted under the Service. Unless otherwise provided in the Order Confirmation, a proper copyright notice will read substantially as follows: "Republished with permission of [Rightsholder's name], from [Work's title, author, volume, edition number and year of copyright]; permission conveyed through Copyright Clearance Center, Inc. " Such notice must be provided in a reasonably legible font size and must be placed either immediately adjacent to the Work as used (for example, as part of a by-line or footnote but not as a separate electronic link) or in the place where substantially all other credits or notices for the new work containing the republished Work are located. Failure to include the required notice results in loss to the Rightsholder and CCC, and the User shall be liable to pay liquidated damages for each such failure equal to twice the use fee specified in the Order Confirmation, in addition to the use fee itself and any other fees and charges specified.

3.6. User may only make alterations to the Work if and as expressly set forth in the Order Confirmation. No Work may be used in any way that is defamatory, violates the rights of third parties (including such third parties' rights of copyright, privacy, publicity, or other tangible or intangible property), or is otherwise

illegal, sexually explicit or obscene. In addition, User may not conjoin a Work with any other material that may result in damage to the reputation of the Rightsholder. User agrees to inform CCC if it becomes aware of any infringement of any rights in a Work and to cooperate with any reasonable request of CCC or the Rightsholder in connection therewith.

4. Indemnity. User hereby indemnifies and agrees to defend the Rightsholder and CCC, and their respective employees and directors, against all claims, liability, damages, costs and expenses, including legal fees and expenses, arising out of any use of a Work beyond the scope of the rights granted herein, or any use of a Work which has been altered in any unauthorized way by User, including claims of defamation or infringement of rights of copyright, publicity, privacy or other tangible or intangible property.

5. Limitation of Liability. UNDER NO CIRCUMSTANCES WILL CCC OR THE RIGHTSHOLDER BE LIABLE FOR ANY DIRECT, INDIRECT, CONSEQUENTIAL OR INCIDENTAL DAMAGES (INCLUDING WITHOUT LIMITATION DAMAGES FOR LOSS OF BUSINESS PROFITS OR INFORMATION, OR FOR BUSINESS INTERRUPTION) ARISING OUT OF THE USE OR INABILITY TO USE A WORK, EVEN IF ONE OF THEM HAS BEEN ADVISED OF THE POSSIBILITY OF SUCH DAMAGES. In any event, the total liability of the Rightsholder and CCC (including their respective employees and directors) shall not exceed the total amount actually paid by User for this license. User assumes full liability for the actions and omissions of its principals, employees, agents, affiliates, successors and assigns.

6. Limited Warranties. THE WORK(S) AND RIGHT(S) ARE PROVIDED "AS IS". CCC HAS THE RIGHT TO GRANT TO USER THE RIGHTS GRANTED IN THE ORDER CONFIRMATION DOCUMENT. CCC AND THE RIGHTSHOLDER DISCLAIM ALL OTHER WARRANTIES RELATING TO THE WORK(S) AND RIGHT(S), EITHER EXPRESS OR IMPLIED, INCLUDING WITHOUT LIMITATION IMPLIED WARRANTIES OF MERCHANTABILITY OR FITNESS FOR A PARTICULAR PURPOSE. ADDITIONAL RIGHTS MAY BE REQUIRED TO USE ILLUSTRATIONS, GRAPHS, PHOTOGRAPHS, ABSTRACTS, INSERTS OR OTHER PORTIONS OF THE WORK (AS OPPOSED TO THE ENTIRE WORK) IN A MANNER CONTEMPLATED BY USER; USER UNDERSTANDS AND AGREES THAT NEITHER CCC NOR THE RIGHTSHOLDER MAY HAVE SUCH ADDITIONAL RIGHTS TO GRANT.

7. Effect of Breach. Any failure by User to pay any amount when due, or any use by User of a Work beyond the scope of the license set forth in the Order Confirmation and/or these terms and conditions, shall be a material breach of the license created by the Order Confirmation and these terms and conditions. Any breach not cured within 30 days of written notice thereof shall result in immediate termination of such license without further notice. Any unauthorized (but licensable) use of a Work that is terminated immediately upon notice thereof may be liquidated by payment of the Rightsholder's ordinary license price therefor; any unauthorized (and unlicensable) use that is not terminated immediately for any reason (including, for example, because materials containing the Work cannot reasonably be recalled) will be subject to all remedies available at law or in equity, but in no event to a payment of less than three times the Rightsholder's ordinary license price for the most closely analogous licensable use plus Rightsholder's and/or CCC's costs and expenses incurred in collecting such payment.

8. Miscellaneous.

   8.1. User acknowledges that CCC may, from time to time, make changes or additions to the Service or to these terms and conditions, and CCC reserves the right to send notice to the User by electronic mail or otherwise for the purposes of notifying User of such changes or additions; provided that any such changes or additions shall not apply to permissions already secured and paid for.

   8.2. Use of User-related information collected through the Service is governed by CCC's privacy policy, available online here:https://marketplace.copyright.com/rs-ui-web/mp/privacy-policy

   8.3. The licensing transaction described in the Order Confirmation is personal to User. Therefore, User may not assign or transfer to any other person (whether a natural person or an organization of any kind) the license created by the Order Confirmation and these terms and conditions or any rights granted hereunder; provided, however, that User may assign such license in its entirety on written notice to CCC in the event of a transfer of all or substantially all of User's rights in the new material which includes the Work(s) licensed under this Service.

8.4. No amendment or waiver of any terms is binding unless set forth in writing and signed by the parties. The Rightsholder and CCC hereby object to any terms contained in any writing prepared by the User or its principals, employees, agents or affiliates and purporting to govern or otherwise relate to the licensing transaction described in the Order Confirmation, which terms are in any way inconsistent with any terms set forth in the Order Confirmation and/or in these terms and conditions or CCC's standard operating procedures, whether such writing is prepared prior to, simultaneously with or subsequent to the Order Confirmation, and whether such writing appears on a copy of the Order Confirmation or in a separate instrument.

8.5. The licensing transaction described in the Order Confirmation document shall be governed by and construed under the law of the State of New York, USA, without regard to the principles thereof of conflicts of law. Any case, controversy, suit, action, or proceeding arising out of, in connection with, or related to such licensing transaction shall be brought, at CCC's sole discretion, in any federal or state court located in the County of New York, State of New York, USA, or in any federal or state court whose geographical jurisdiction covers the location of the Rightsholder set forth in the Order Confirmation. The parties expressly submit to the personal jurisdiction and venue of each such federal or state court.If you have any comments or questions about the Service or Copyright Clearance Center, please contact us at 978-750-8400 or send an e-mail to support@copyright.com.

v 1.1

13 Curriculum vitae

The biography is not included in the online version for reasons of data protection.

The biography is not included in the online version for reasons of data protection.

The biography is not included in the online version for reasons of data protection.

14 List of Publications and scientific activities

Publications

Thier B, Zhao F, Stupia S, Brüggemann A, Koch J, Schulze N, Horn S, Coch C, Hartmann G, Sucker A, Schadendorf D, Paschen A. Innate immune receptor signaling induces transient melanoma dedifferentiation while preserving immunogenicity. J Immunother Cancer. 2022;10:e003863. doi: 10.1136/jitc-2021-003863. PMID: 35697379.

Harbers FN, **Thier B**, Stupia S, Zhu S, Schwamborn M, Peller V, Chauvistré H, Crivello P, Fleischhauer K, Roesch A, Sucker A, Schadendorf D, Chen Y, Paschen A, Zhao F. Melanoma Differentiation Trajectories Determine Sensitivity toward Pre-Existing $CD8^+$ Tumor-Infiltrating Lymphocytes. J Invest Dermatol. 2021 Oct;141(10):2480-2489. DOI: 10.1016/j.jid.2021.03.013. Epub 2021 Mar 30. PMID: 33798535.

Thier B, Paschen A. Innate RIG-I signaling restores antigen presentation in tumors and overcomes T cell resistance. Cell Stress. 2021 Jan 18;5(2):26-28. DOI: 10.15698/cst2021.02.242. PMID: 33554047; PMCID: PMC7841847.

Bhat H, Zaun G, Hamdan TA, Lang J, Adomati T, Schmitz R, Friedrich SK, Bergerhausen M, Cham LB, Li F, Ali M, Zhou F, Khairnar V, Duhan V, Brandenburg T, Machlah YM, Schiller M, Berry A, Xu H, Vollmer J, Häussinger D, **Thier B**, Pandyra AA, Schadendorf D, Paschen A, Schuler M, Lang PA, Lang KS. Arenavirus Induced CCL5 Expression Causes NK Cell-Mediated Melanoma Regression. Front Immunol. 2020 Aug 21;11:1849. doi: 10.3389/fimmu.2020.01849. PMID: 32973762; PMCID: PMC7472885.

Such L, Zhao F, Liu D, **Thier B**, Le-Trilling VTK, Sucker A, Coch C, Pieper N, Howe S, Bhat H, Kalkavan H, Ritter C, Brinkhaus R, Ugurel S, Köster J, Seifert U, Dittmer U, Schuler M, Lang KS, Kufer TA, Hartmann G, Becker JC, Horn S, Ferrone S, Liu D, Van Allen EM, Schadendorf D, Griewank K, Trilling M, Paschen A. Targeting the innate immunoreceptor RIG-I overcomes melanoma-intrinsic resistance to T cell immunotherapy. J Clin Invest. 2020 Aug 3;130(8):4266-4281. doi: 10.1172/JCI131572. PMID: 32427578; PMCID: PMC7410049.

Scientific activities

Oral presentation	Hallmarks of Skin Cancer Conference 2021 (virtual)
Poster	31st German Skin Cancer (ADO) Congress 2021 (virtual)
Oral presentation & Poster	Arbeitsgemeinschaft Dermatologische Forschung (ADF) conference 2021 (virtual)
Poster	4th Essen Translational Oncology Symposium (ETOS) 2021 (virtual)
Poster	19th Day of Research 2020 by the Medical Faculty of the University Duisburg-Essen (virtual)
Oral presentation	7th Immunotherapy of Cancer Conference (ITOC7) 2020 (virtual)
Oral presentation & Poster	3rd Essen Translational Oncology Symposium (ETOS) 2020 at the University Hospital Essen, Germany
Poster	18th Day of Research 2019 by the Medical Faculty of the University Duisburg-Essen, at the University Hospital Essen, Germany
Flash talk & Poster	9th Mildred Scheel Cancer Conference 2019 of German Cancer Aid in Bonn, Germany
Oral Presentation	Tumor immunology meets Oncology Conference (TIMO XV) 2019 in Halle (Saale), Germany
Poster	2nd Essen Translational Oncology Symposium (ETOS) 2019 at the University Hospital Essen, Germany
Poster	17th Day of Research 2018 by the Medical Faculty of the University Duisburg-Essen, at the University Hospital Essen, Germany
Poster	Society of Melanoma Research (SMR) Congress 2018 in Manchester, United Kingdom

15 Statutory declarations

Declaration:

In accordance with § 6 (para. 2, clause g) of the Regulations Governing the Doctoral Proceedings of the Faculty of Biology for awarding the doctoral degree Dr. rer. nat., I hereby declare that I represent the field to which the topic "Treatment-induced sculpting of melanoma phenotype and immunogenicity – Impact on resistance to CD8 T cells*"* is assigned in research and teaching and that I support the application of Beatrice Thier.

Essen, _____	Annette Paschen	_____
	Name of the scientific supervisor/member of the University of Duisburg-Essen	Signature of the supervisor/ member of the University of Duisburg-Essen

Declaration:

In accordance with § 7 (para. 2, clause d and f) of the Regulations Governing the Doctoral Proceedings of the Faculty of Biology for awarding the doctoral degree Dr. rer. nat., I hereby declare that I have written the herewith submitted dissertation independently using only the materials listed, and have cited all sources taken over verbatim or in content as such.

Essen, _____	_____
	Signature of the doctoral candidate

Declaration:

In accordance with § 7 (para. 2, clause e and g) of the Regulations Governing the Doctoral Proceedings of the Faculty of Biology for awarding the doctoral degree Dr. rer. nat., I hereby declare that I have undertaken no previous attempts to attain a doctoral degree, that the current work has not been rejected by any other faculty, and that I am submitting the dissertation only in this procedure.

Essen, _____	_____
	Signature of the doctoral candidate